A Feasibility Study on Weight Saving in Bascule Bridge Design by Implementing an FRP-deck

D.Y. Mouroulis

TUDelft

Movares
consultants & engineers
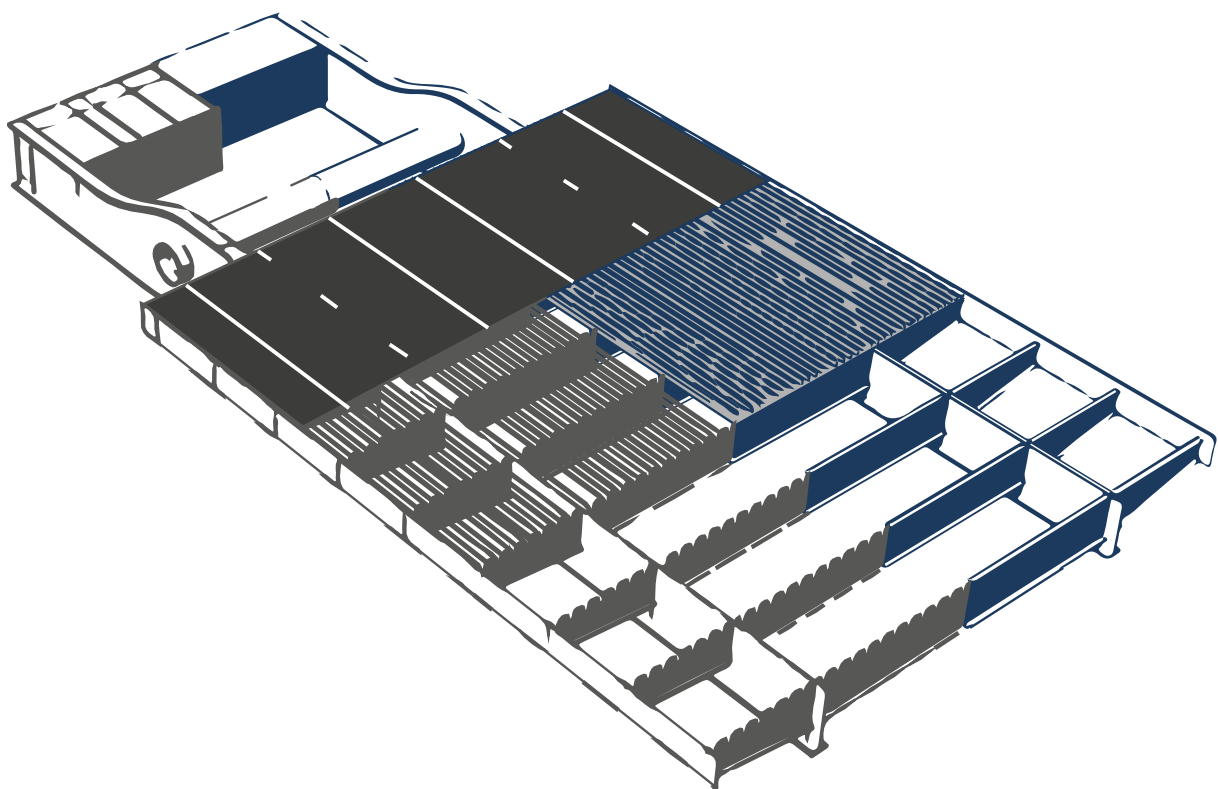
A Feasibility Study on Weight Saving in Bascule Bridge Design by Implementing an FRP-deck

by

D.Y. Mouroulis

in partial fulfilment of the requirements for the degree of

Master of Science

in Civil Engineering

at the Delft University of Technology,
to be defended publicly on Wednesday October 17, 2018 at 10:00 AM.

Supervisor:	Ir. M. Pavlović	TU Delft
Thesis committee:	Prof. Ir R. Nijsse,	TU Delft
	Ir. J. Smits,	TU Delft
	Ir. A. Steenbrink,	Movares

An electronic version of this thesis is available at http://repository.tudelft.nl/.

This thesis has been dedicated to my father

ΓΕΩΡΓΙΟΣ ΜΟΥΡΟΥΛΙΣ

Preface

The following pages contain a master thesis representing the final graduation assignment for Building Engineering, a master track of the Civil Engineering department at the TU Delft. It discusses the implementation of Fibre Reinforced Polymers onto a bascule bridge system, aiming for weight reduction. The purpose here is to illustrate the added value of FRP in Civil Engineering.

This case study-based graduation work on FRP and bridges, has been made in close collaboration with Dutch engineering firm Movares, located in Utrecht. Movares is active in various construction markets, offering a versatile range of services connected to infrastructure. The organisation's interest lies in the application of Fibre Reinforced Polymers (FRP) as a structural material. FRP is a well-known structural material which is getting continuingly more attention in civil construction market. This growing attention helps Movares to safeguard the ability to compete in the field of structural engineering on the civil market and more specifically in the role of design consultancy. Using FRP in structural design requires in depth knowledge on the material properties and practical knowledge on its application. This thesis gives technical feasible outcome on the application of FRP in the construction, with two alternatives for the use of FRP in the construction of the Amalia bridge.

Next, I would like to thank several people for their contribution to this thesis. First, I would like to thank my daily supervisors Arjen Steenbrink (from Movares) and Marko Pavlović (from TU Delft), my committee chair Rob Nijsse (TU Delft) and second supervisor Joris Smits (TU Delft/ RHDHV) for their time and effort, knowledge and guidance, patience and respect during my graduation process. Next, I would like to thank my colleagues Mark van der Burg, Gary Greiner, Roeland van Hof and Jack Kazimier for their involvement. With a special thanks to my co-graduate Arnout Franken and roommate Tristan Quiten for their helpful insights.

Last, I would like to express my gratitude to family and friends, who have supported me throughout this turbulent process.

Stijn Mouroulis

October 2nd, 2018

Abstract

This master thesis contains a study on the implementation of Fibre Reinforced Polymers (FRP) onto a steel bascule bridge, with the aim of weight reduction. As a case study, the Amalia bridge near Waddinxveen (crossing the Gouwe channel) is used. Two alternative design propositions are presented. The thesis has been subdivided into several parts, which are introduced below.

The first part consists of several expositions. It examines the built up of a movable bridge, the material FRP & its properties together with methods of connecting an FRP deck to steel girders and the rules & regulations required for bridge design in the Netherlands.

The second part is the design study, which contains an overview of the original Amalia bridge and the designs created based on adaptions of the original. The designs have been made to have a lower total weight than the Amalia bridge. A lower bound approach has been used, not an optimisation. Thus, leaving room for improvement. Two alternatives are discussed: a **hybrid** and a **non-hybrid** solution. A hybrid solution is defined as a solution with the full interaction between the FRP-deck and steel girders: allowing for shear transfer between the two and enabling the deck to function as the top flange of the steel girders. A non-hybrid solution only allows for the transfer of vertical forces and limits the transfer of shear, resulting in the structural separation between the deck and the girders.

The design study has led to a weight reduction for both the **hybrid** and **non-hybrid solution** of **24** and **16%** respectively. It can be concluded that both alternatives clearly illustrate the potential of FRP in bridge design, given the objective to reduce weight. It should be noted that in the case of a hybrid solution, the temperature influences become significant. This requires close attention to the details for the connection between the deck and girders.

Contents

Introduction

1. General

Bridges have evolved from stone constructs in ancient Greece into the marvels of steel that can be seen today. Today, we approach the start of the use of new materials such as polymers.

Bridges are a means to an end with their purpose to cross an obstacle. These being waters, valleys and/ or roads with a communication route (Pavlovic & Kolstein, 2016). Per the Cambridge dictionary, a bridge is defined as:

A structure that is built over a river, road, or railway to allow
people and vehicles to cross from one side to the other.
(Cambridge University Press, 2017)

This thesis revolves around bridges and a case study of a specific bridge. On the upcoming pages an exposition of a redesign study of a bascule bridge is depicted. To illustrate, a case study bridge is chosen: this being an orthotropic steel bascule bridge, the Amalia bridge. This bridge has been chosen because it is a rather new bridge, up-to-date regarding design and the use of materials. This makes is suitable for a redesign with even more modern materials and techniques as the base construction of the bridge does not need to be redesigned. A detailed description on the thesis' objective can be found in chapter 2 – Problem Definition.

1.1. Location description

The Amalia-bridge is a movable bridge placed across the Gouwe river as a part of a newly created provincial road system. It is located in between Waddinxveen and Gouda in the province of South-Holland in the Netherlands. This is illustrated in Figure 1-2. The bridge was built as a solution to the high traffic flow between The Hague and Gouda due to people commuting from and to work. As imaginable this led to dangerous situations and major traffic-congestions concentrated in and around the existing Gouwe-junction. Thus, a large-scale improvement of this Gouwe-junction and the creation of a network of provincial roads, which includes the Amalia-bridge, was realised. This network is shown in Figure 1-1 with **red lines**.
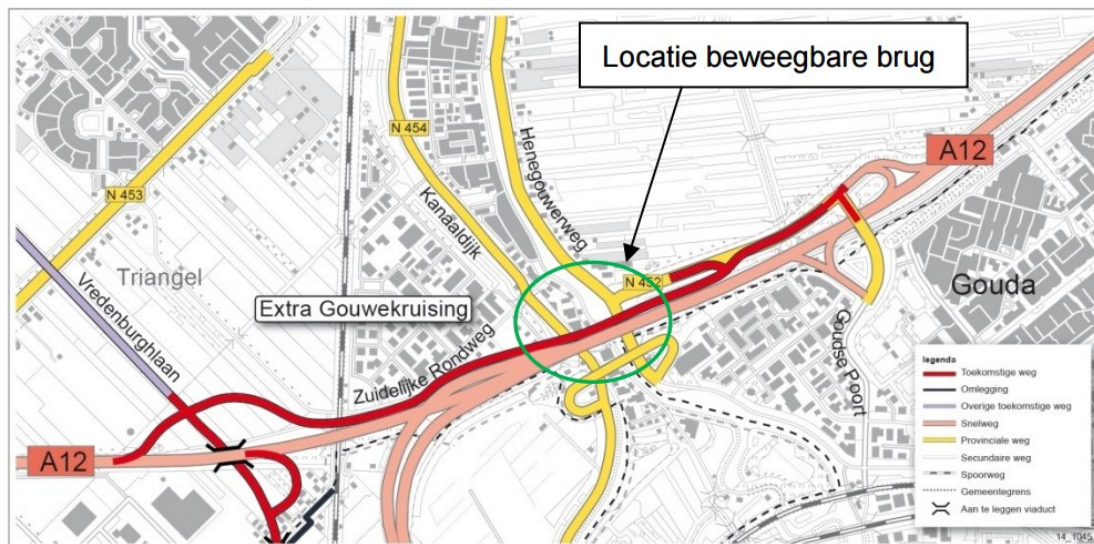
Figure 1-1 Location of the Amalia-bridge (Heijmans, 2015)

This newly created road network has been nicknamed the "parallel structure A12" and it contains a new provincial road: the N457, which has a maximum speed limit of 80km/h and a double lane built-up in both directions. This leads to a connection between the highways A20 and A12. Together with the provincial roads, N207, N452 and N457, this recent upgrade ensures a better traffic flow from and to the rural vicinity into the national connection between Gouda and The Hague.

This thesis focusses on this movable bridge, which is only one small part in this undertaking. The movable bridge is located at the **blue** with **orange** circle in Figure 1-2 and a close-up of the location is displayed in Figure 1-1 inside the **green** circle. In the latter, it is shown that the new road will cross two, lower situated, traffic roads and a waterway. The movable section of the Amalia-bridge is only located above the waterway. By making use of a bascule bridge-system, the waterway will have an infinite headroom (when the bridge is opened) for the crossing boats. When the bridge is closed, the headroom is limited to a mere 7.0 meters. This allows a large variety of boats to pass, without opening the bridge. This headroom allows containerships with up to three layers to pass. (Rijkswaterstaat, 2017)

1.2.　　　Current situation

The creation of the *parallel structure A12* has been fully realised today. From December the 23rd of 2016 the N451 and the N457 has been opened to the public traffic, both on road and the water. (Province of South-Holland, 2016) The boundary conditions as used in this design of the Amalia bridge will be the bases from which the thesis will start. These boundary conditions refer to the traffic flow crossing the bridge; resulting in the deck loading; the aforementioned clearance gauge below the bridge in closed (and opened condition); the structural height of the bridge; and the locations of the abutments of the bridge. From here on the view will be zoomed into the movable section of the Amalia-bridge.

Figure 1-2 Project location

2. Problem Definition

This master thesis focusses on the implementation of FRP (Fibre Reinforced Polymers) onto the movable section of an orthotropic steel deck, bascule bridge. The material FRP has a significantly better strength to weight ratio compared to steel. (As illustrated in Table C-7 of Appendix C) Implementing FRP can result in weight reduction. As mentioned, the Amalia-bridge, has been selected for this project. The functional-aspects of the bridge will remain unchanged. Meaning that, the traffic flow over and under the bridge will have the same capacity and clearance gauge, as is the case for the existing design, both in the just and fully opened conditions, will be maintained. In the process of implementing the FRP onto an existing design, two alternatives will be dealt with. Both of these have a similar built up but differ greatly in their structural behaviour.

1. The first design has a **non-hybrid** built up: an FRP-deck combined with steel load bearing structure. In this design the structural capacity will be provided by the girders, whereas the deck 'simply' placed on top of it. Limiting shear transfer between these two elements is key.
2. The second design has a **hybrid** bridge built up. Here the FRP-deck and the steel girders will work together as one hybrid structure. Thus, allowing for shear interaction between the two.

A more detailed description is given in section 3.1.2 Bridge designs

2.1.   Thesis objective

The objective is to create a feasible structure using FRP in accordance with the guidelines provided in the various design regulations stated in section 3.2.1.4 Rules & regulations. The purpose here is to illustrate the added value of FRP in Civil Engineering. Thus, FRP will be implemented in situations where its properties are most favourable.

2.2.   Research question

The following research question has been set to define the master thesis at hand:

Can the movable section of the Amalia-bridge be re-designed with the use of
FRP to realise a feasible alternative?

2.2.1. Sub-questions

To answer the main research question, several sub-questions will need to be answered to support the choices in the design process:

- *What is currently leading in movable bridge design, regarding material and bridge types?*
- *What are the challenges regarding the production and design of Fibre Reinforced Polymers?*
  - *How are these currently dealt with?*
- *What are the rules and regulations in the Netherlands regarding the design of a movable bridge with the use of Fibre Reinforced Polymers?*
- *What are the boundary conditions of the Amalia-bridge?*
- *How can Fibre Reinforced Polymers be of added value in designing movable bridges similar to the Amalia-bridge?*
  - *Is this added value applicable in a wider range?*

These questions are used as a guideline for this thesis and its theoretical research to create an in-depth view on the combination of FRP and movable bridges.

2.2.2. Definition of feasibility

In project management, the term TELOS is used to define feasibility into five areas (Hoffman, 2013). This gives **technical**, **economic**, **legal**, **operational** and **scheduled** feasibility. This thesis is the graduation project of a technical mast and thus will have its main focus on technical feasibility. This paragraph will shortly discuss the economic feasibility, because in the end projects can only make it beyond the drawing table if they are economically feasible.

The technical or structural feasibility can be measured by answering the question:

Can FRP be used to make a structurally strong and stable bridge, which fulfils the guidelines required in the Netherland, as stated in section3.2.1.4 Rules & regulations?

The 3.2.1.4 Rules & regulations also mention the mechanical properties of the bridge. This is outside of the scope of the thesis, but for the full inclusion this would need to be addressed.

Whereas economic feasibility is more difficult to determine. It is not just about the material- and labour costs, it is also about the costs during operation and for demolition/ replacement. A major factor in economic feasibility is the lifetime expectancy of the bridge. Another is whether the material is recyclable or not. Addressing the question:

Is the bridge designed such that the economic investment over its lifetime is in the same price-range as comparable bridges, when taking the abovementioned aspects in to account?

2.3.   Defined goals

This thesis has four main involved parties, all with different goals. These are the company (Movares), the university (TU-Delft), the collaborating graduate student (A. Franken) and the author of the thesis (Civil Engineering graduate student).

2.3.1. Movares' perspective

The company is interested in the material FRP and whether it would be beneficial to invest man-hours into applying this structural material to their structural designs. Right now, there is a limited knowledge into FRP within Movares. Thus, the research conducted in this thesis will be a test to define whether the interest should be further examined.

This will be measured by, of course, the thesis. To do this effectively and in a comparable manner an overview will be made of the use of FRP as a structural element in movable bridges. In which the benefits, spear points, key aspects, problem areas, etc. will be displayed.

2.3.2. TU-Delft's perspective

The University wants a thesis which clearly shows the graduate student's capability and knowledge of theory at hand. They want the student to add value to the theory and thus contributing to the field of Civil Engineering. The extent to which this has been realised is to be determined using the thesis and in an oral presentation, both of which are at MSc-level.

2.3.3. Franken's perspective

As a graduation student with an adjoining research topic, his goal is to have a beneficial collaboration with the author of the thesis. The collaboration is made so that it will be advantageous to both parties for the betterment of their respective theses.

2.3.4. Graduate's perspective

The goal of this master thesis is to design an innovative movable bridge with FRP. To dive into the material of FRP for reaching more depths than reached thus far. Illustrating that FRP is a good alternative to the exiting structural materials and should be considered as a structural material in Civil Engineering. This will conclude the journey at the TU-Delft and show all the puzzle pieces that have been gathered over these years. In this thesis, these puzzle pieces will come together and complete the puzzle.

2.4.   Relevance

As stated before, the parallel structure A12-project, which includes the Amalia-bridge, has been fully realised. This recent realisation makes the bridge suitable as an example to illustrate the intent of designing a movable bridge with the use of FRP, to verify whether the material is suited for similar situations (e.g. comparable movable bridges).

3. Framework

The questions at hand have resulted in a scope where each design will have its own specific boundaries as mentioned in the Problem Definition. This is summarised in the research scope, whereas the different steps for this scope are explained in the research approach.

3.1.   Research scope

This thesis is divided into a research and design phase. During the design phase there will be a collaboration with another graduate student (A. Franken). What will be done in each of these phases and how this collaboration will function is explained in this section.

3.1.1. Theoretical research

In advance to the actual design several aspects will be addressed. The **first** is the bascule bridge. This is to define what a bascule bridge is and how it functions. The **second** is the material FRP. This is to emphasize how the material behaves and how it should be used. **Third** is connecting FRP with steel, with regard to (non-) hybrid interaction. **Last** is a study on the rules and regulations required for bridge design. This is needed when designing and verifying the movable bridge-section.

3.1.2. Bridge designs

Designing with FRP and illustrating its added value in Civil Engineering, requires knowledge to implement the material in situations where its properties are most advantageous. Since the goal of this thesis is weight reduction, for which the use of FRP is very suitable, it makes sense to only use this at the location this would make sense: the leaf of the bridge. This is illustrated in the drawing below:
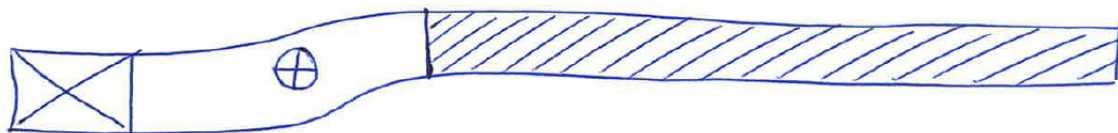
Figure 3-1 Scope regarding the bridge design (Steenbrink, 2017)

A distinction will be made two create two alternatives: one non-hybrid and one hybrid alternative. With this hybrid interaction, full shear capacity between the two 'stacked' elements is meant. The elements to be stacked are the deck and the supporting girders. The interaction between these two, will be either allow for shear transfer or restrict it as much as possible, to consider it non-hybrid.

3.1.3. Collaboration

As mentioned earlier, there will be collaboration between A. Franken and the author of the thesis. This collaboration has been done in such a way that it will be a beneficial two-way street. If it would occur, that party one cannot supply data required to proceed for party two an educated estimate will be made regarding the missing data. This will be done in such a way that once the data arrives it can be implemented (by means of parameters) with relative ease. This ensures that our graduation works are aligned.

3.2. Research approach

In the approach to the design phase a literature study in combination with getting acquainted with the Finite Element Method-program (FEM) will be required. This creates a basis of theoretical knowledge combined with the practical skills to apply this in the FEM-program. A more detailed explanation of each step is depicted next.

3.2.1. Theoretical- & practical- research phase

3.2.1.1. Location

In this section the boundaries for the design will be illustrated. These boundaries are based upon maintaining the current functionality of the bridge and forming this into (physically) measurable boundaries. This is necessary to ensure the alignment of the new bridge-segment into the existing structure. Thus, answering the question:

What are the boundary conditions of the Amalia-bridge?

3.2.1.2. Bascule bridges

The main question to be answered in the research into bascule bridges is:

What is currently leading in movable bridge design, regarding material and bridge types?

The main focus will be on the trunnion bascule bridge. Getting insight into this bridge type and extrapolating this to make use of the knowledge gained in the design-phase.

3.2.1.3. Fibre Reinforced Polymers

The main question to be answered in the research into FRP is:

What are the challenges regarding the production and design of Fibre Reinforced Polymers?

An explanation will be given to explain what FRP is. How it differs from other structural materials and how it should be addressed when making designs with FRP.

3.2.1.4. Rules & regulations

To design a movable bridge-section with FRP it will have to be verified. To do this, research into the required rules and regulations in the Netherlands is necessary. This means answering the question:

What are the rules and regulations in the Netherlands regarding the design of a movable bridge with the use of Fibre Reinforced Polymers?

This will result in a list with all the required checks and values the bridge will have to fulfil.

3.2.2. Design phase

As explained in section 3.1.2: Bridge designs, the design-phase consists of two design alternatives: a hybrid and a non-hybrid option, as has been addressed in the Problem Definition. These alternatives have a similar built up, however have very different structural functions. The goal here is to create feasible alternatives within the composed boundary conditions.

3.2.3. Concluding phase

To illustrate the significance of FRP in the movable bridge design the following question should be answered positively:

How can Fibre Reinforced Polymers be of added
value in designing movable bridges similar to the
Amalia-bridge?

One

Literature Study

4. Movable Bridges

4.1. Different types

Movable bridges are used when fixed bridges are not an option due to for example, under passing boats. A requirement is certain clearance gauge for the underpass, at the crossing with a bridge. If this cannot be achieved with a closed condition, it means that the bridge would have to be moved to allow for the required clearance. This can be done in a variety of different manners:

- Horizontal rotation (remaining perpendicular)
- Vertical rotation (perpendicular to parallel)
- Vertical translation (remaining perpendicular)
- Horizontal translation (remaining perpendicular)

Each of these approaches results in a different type of bridge to be used. This has been illustrated in Table 4-1.

Horizontal rotation	Vertical rotation	Horizontal translation	Vertical translation
Swing bridge	Drawbridge	Rolling bridge	Lifting bridge
Crane bridge	Bascule bridge		Table bridge
Ponton bridge	Folding bridge		
	Tail bridge		

Table 4-1 Bridge tyes (Reusink, 2017)

A combination of these approaches can also be used. This, for instance, has resulted in a specific type of bascule bridge: the rolling bascule bridge. This bridge type uses both vertical rotation as well as horizontal translation. This is illustrated in Figure 4-1, by the Lower Hatea bridge in Whangarei, New Zealand.

Figure 4-1 Lower Hatea bascule bridge (Reynolds, 2013)

When a movable bridge with a vertical rotational system is considered, like the trunnion bascule bridge, the leaf of the bridge will not reach a full 90-degree angle. (The leaf of the bridge is the movable section which spans the crossing and the trunnion is the axle around which the bridge rotates) This results in the leaf remaining above the crossing and effectively reducing the width of the crossing which has an infinite clearance gauge. This is visible in Figure 4-2.

For a rolling bascule bridge this does not have to be the case. In this case the bridge rolls back, while the leaf of the bridge is lifted. This essentially moves the bridge in two directions (both horizontal and vertical) simultaneously. This is illustrated in Figure 4-1.

When comparing the two bascule bridge's types (trunnion & rolling), another advantage is found for the rolling version. Since there is no trunnion, this removes the concentration of stresses around this area. However, extra attention should be given to the area on which the bridge will roll. Likewise, each bridge has its advantages and disadvantages. Since however, this thesis is a case study on the Amalia-bridge, which is a (trunnion) bascule bridge construction, from here on the focus lies on this movable bridge type.[1]

4.2.   Amalia bridge

The Amalia-bridge is a movable bridge with a bascule-construction. This bridge is a perfect example of a state-of-the-art bascule bridge: light, slender and fatigue resistant. Its built-up can be divided into three sections: the western ramp, the crossing of the Gouwe with the movable section and the eastern ramp. The movable section of the Amalia-bridge consists of a movable deck and a basement. It has a drivable surface of 26.5 meters in length and is four lanes (of each 3.1 meters) in width. The whole movable section (from the main axel until the end support) is 29.75 meters long and just over 23.5 meters wide. The end support of the movable section coincides with the intermediate support of the whole bridge while crossing the water (Heijmans, 2015). This can be seen clearly in Figure 4-2.

Figure 4-2 Amalia-bridge; picture is taken in the northern direction (Berk, 2016)

---

[1] When a bascule bridge is mentioned, the trunnion bascule bridge type is meant.

Furthermore, the Amalia bridge is a steel bascule bridge with an orthotropic steel bridge deck construction. This is basically a built-up (top to bottom) of a steel plate, supported by troughs (U-shaped sections), cross and main girders (both are upside down T-shaped sections).
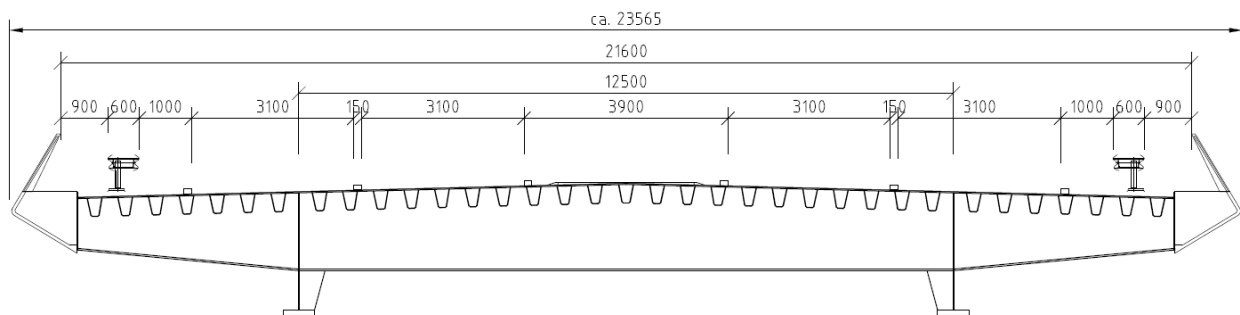

Figure 4-3 Cross section of the Current Amalia-bridge (Heijmans, 2015)

The movable bridge is directed perpendicular to the undergoing waterway, onto which the main axle lies parallel. The counterweight of the bascule-system is 'hidden' underneath the road enclosed in a basement. It is not really hidden, since the walls are mostly built up of glass, thus allowing a view into the mechanics of the bridge. This single bridge-system is based upon two main-girders which support an orthotropic deck with continuous trough-shaped profiles. A cross-section of the deck built-up is illustrated in Figure 4-3. To put the bridge into motion a panama-wheel construction has been used consisting of crack connecting rod with two panama wheels.
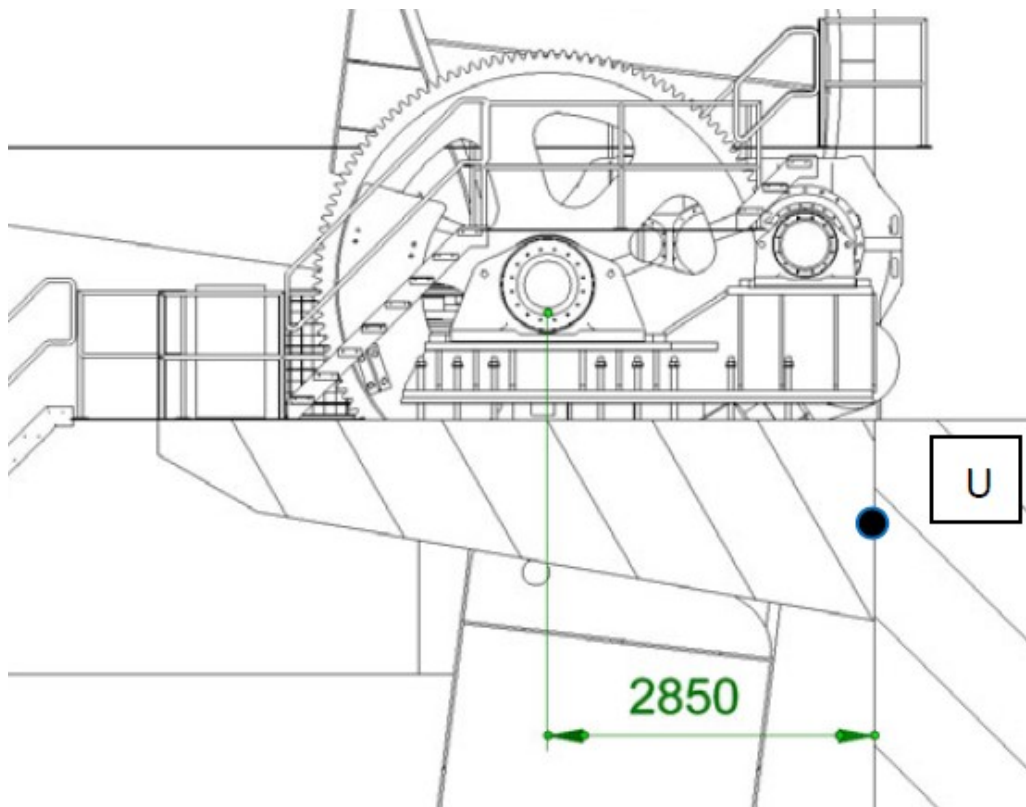

Figure 4-4 Sectional view highlighting the panama wheel construction of the Current Amalia-bridge (Heijmans, 2015)

In the design of the Amalia-bridge, the expertise of Movares (through Heijmans) was implemented for the movable steel bridge-deck, the counterweight basement and the mechanics of the bridge (Heijmans, 2015).

4.3.   General bridge built up

Bridges are complex structures with different components at different levels. These can be divided into a **superstructure**, a **substructure** and other components. The superstructure is the main structural system of the bridge, both in longitudinal and transverse direction. The substructure contains the elements on which the superstructure will rest. The other components vary from bearing and expansion joints to drainage systems and installations. This is illustrated in Figure 4-5.
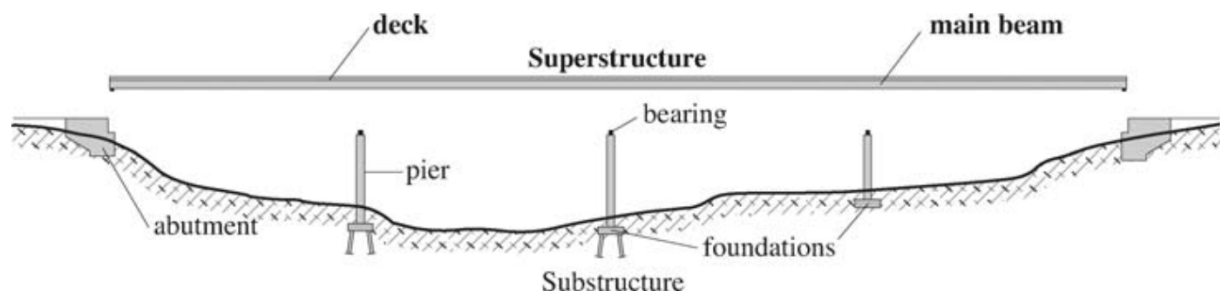

Figure 4-5 Super and substructure of a bridge (Pavlovic & Kolstein, 2016)

For a movable bridge, extra components are required to allow for safety during both movement and fixation:

- Counterweight (in basement of open air)
- Driving gear
- Mechanical locking (for both opened and closed condition)
- Buffer: energy shock absorber
- Front support: hydraulic speed damper

The focus of this thesis is on the movable section. Thus, a limitation of the scope has been made to the superstructure of the bridge. However, one should note, that changes in this part of the bridge design, influence all the other, aforementioned, components. Thus, to balance the bridge properly and execute a fatigue assessment for the main girders, the counterweight has also been taken into the scope of this thesis.

4.3.1. Structural system

Globally, the orthotropic deck acts as the top flange of the main girder. Locally, the bending of the deck is restrained in the longitudinal direction by the stiffeners; in this case aforementioned troughs; whereas in the transverse direction the cross girders handle the load transfer to the main girders. These different elements all work together, resulting in a complex load transfer system. The above illustrated cross section, clearly show the placement of these elements.

NOTE: localised bending of the deck (within or) in between the stiffeners is caused by direct wheel loading.

4.3.1.1.   Deck and main girders

The deck consists of the deck-plate and the stiffeners. Together they function as the top flange of the main girders. Due to shear lag[2] only a section of the deck is used effectively. This effect is illustrated in Figure 4-6. In the case of the Amalia bridge, a thickness of 20 mm is used for the deck plate. This is relatively thick for a deck-plate. This due to the heavy traffic loading which has been considered for the Amalia bridge.
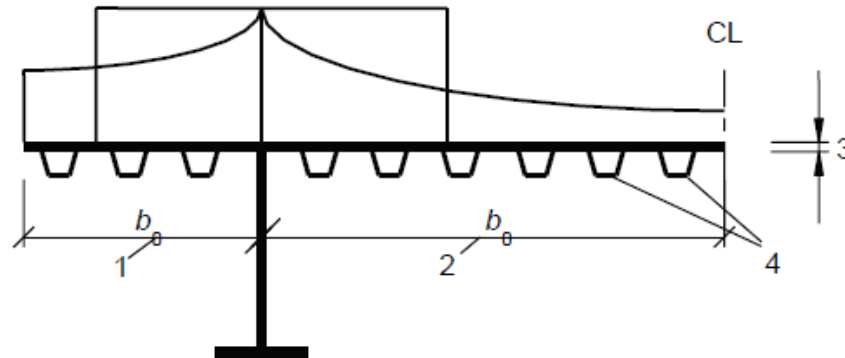

Figure 4-6 Deck and troughs function as top flange (NNI, 2012)

4.3.1.2.   Cross girders

The cross girders can be divided into two sets. The first set consists of the girders located closest to the front and rear of the leaf of the bridge. The second set contains the rest of the cross girders. The first set of girders is stiffer (higher webs) to stay within the deflection limit at the front and the rear of the leaf. At these locations, the bridge transfers onto the main road and it is advised that the deflection at this point should remain within 5 mm.

To support the cross girders on the main girders, consoles are used. These are small webs located underneath the cross girder to connect the bottom flange of the cross girder with the bottom flange of the main girder. In the case of the Amalia bridge, these consoles have an additional flange. This has been applied in case of a collision with crossing waterway traffic. An illustration of these consoles can be found in Figure 4-7. If this flange is not present, the web of this console will give way without virtually any resistance.
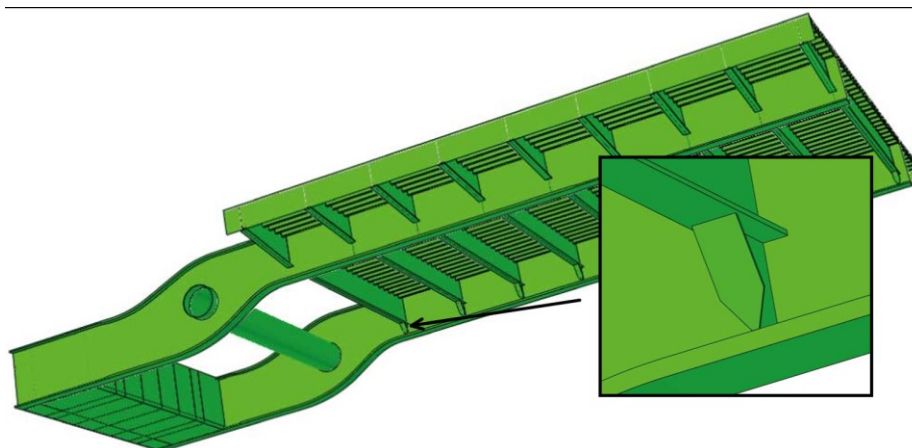

Figure 4-7 Close up of a console in the abaqus model of the Amalia bridge

---

[2] Shear stresses dissipate when the distance to the web increases

4.3.2. Functional aspects of the Amalia bridge

As discussed in the previous section, the current flow applies to the bridge-construction as well. Placing a bridge which serves as a bottleneck to the traffic flow is unwanted. The mentioned flow results into cross sectional measurements for the road and therefore the bridge. A cross section has been depicted in Figure 4-3 to illustrate the cross sectional built-up of the road.

NOTE: this figure is NOT of the final design stage of the current Amalia bridge, slight alterations have been made for the existing bridge. The measurements for the layout of the N451 have been depicted in the table below. (Heijmans, 2015)

Function	Distance	[unit]
Central reservation	3,900	mm
Traffic lanes (2x2)	3,100	mm
Lane separation	150	mm
Roadside reservation	1,235	mm
Total width (excl. edge elements)	**19,070**	**mm**
Guardrail	365	mm
Inspection path	900	mm
Total road width	20.940	mm
Total bridge width (incl. edge elements)	**23,565**	**mm**

Table 4-2 Road layout N451 at Amalia bridge (Heijmans, 2015)

Table 4-2 summarises the measurements from the cross section, as illustrated in Figure 4-3, ensuring a perfect alignment of the design, onto the existing provincial road.

For the bridge not to obstruct the underlaying waterway and its traffic flow the following measurements will be taken into account:

Function		[unit]
Water level (with regard to. N.A.P.)[3]	-600	mm
Ground level (with regard to N.A.P.)	100	mm
Waterway width	70 - 65	m
Passage width (closed condition)	25	m
Passage width (open condition)	22.5	m
Clearance gauge (closed condition)	7,000	mm
Clearance gauge (open condition)	infinite	
Reference height (z_e)[4]	7,610	mm
Construction height	2,500	mm

Table 4-3 Waterway clearance with N451 at Amalia bridge

The objective of this thesis is to obtain a feasible alternative of the existing Amalia bridge. With feasibility in mind, one must take caution into 'maintaining' the costs. If the structural height Is increased, combined with maintaining the abovementioned clearance gauge, this results in raising the level of top of the deck (road level). Which than directly correlates to the raising the level of the existing provincial roads. Since the N451 not only crosses a waterway, but roads on either side as well,

---

[3] The values related to N.A.P. have been determined based on the data received from the AHN (AHN, 2018)
[4] This reference height has been determined to be the distance from the centre of the bridge deck until the lowest ground elevation level. (Heijmans, 2015) (NNI, 2011)

the road is supported by T-shaped concrete columns (Figure 4-8). Increasing their height, to allow for a higher road level, is a very costly endeavour. With this in mind the structural height of the Amalia bridge will be maintained. This results in the following conditions:

- The clearance gauge of the underlying waterway must be maintained.
- The structural height of the bridge must be maintained.

Figure 4-8 Bottom view of N451. Located on the south embankment of the Amalia bridge. Facing in the south direction. (Google Streetview, 2017)

The scope for this thesis is limited to the movable section of the Amalia bridge. To create comparable bridge alternatives additional boundaries are illustrated below in Table 4-4.

Function	Distance	
Centre to centre distance of the main load bearing girders	12,500	mm
Bridge leaf length	26,500	mm
Distance between the supports	29,750	mm

Table 4-4 Boundaries regarding the leaf of the bridge

5. Fibre Reinforced Polymers

Composites contain different components, where the properties are each used favourably. The principle of a composite can be described as the ability to strengthen (or reinforce) a weaker or brittle material, by the addition of another (Kolstein, 2008). A composite made up of a fibre-based reinforcement confined by a polymer matrix is collectively called a Fibre Reinforced Polymer (or FRP for short). These two components have complementary properties (Moen, 2014). This allows an engineer to *tailor* the material efficiently for each new purpose.

5.1.　　　Materials

The fibres in FRP provide the load-bearing function of the material, whereas the resin (aforementioned as the polymer matrix) has four functions:

- Fixing the fibres in the desired geometrical location.
- Transferring the forces to the fibres.
- Preventing buckling of the fibres under compressive action.
- Protecting the fibres from humidity and other weather conditions.

The mechanical properties of FRP are defined by the adhesion, the mechanical interaction between the fibres and the resin and the angle with regard to the direction of the loading. (Kolstein, 2008)

An FRP-composite can be viewed on three different levels: micro-, meso- and macro-scale. In the micro-scale, a distinction can be made between the fibres (reinforcement) and the resin (matrix) to combine into a ply. In the meso-scale the distinction can be made between the different plies to create the laminate. And the laminates are viewed at the macro level. This is illustrated in Figure 5-1.
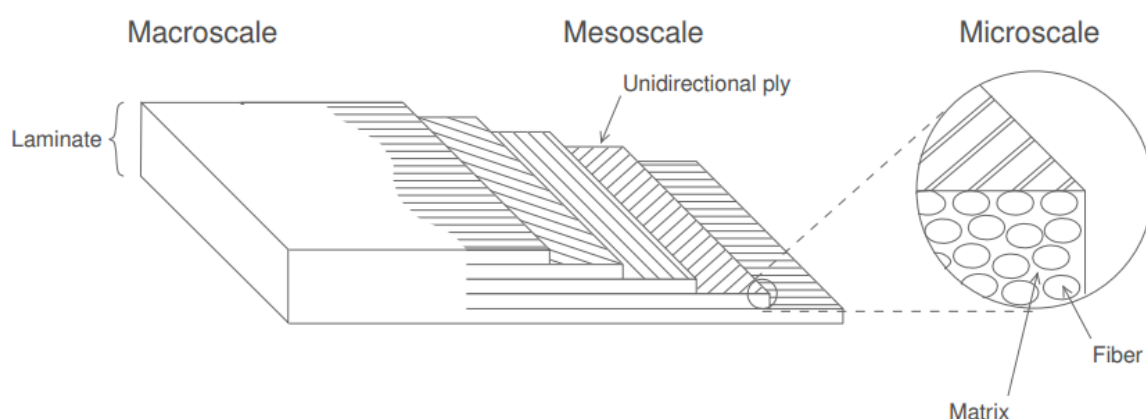

Figure 5-1 FRP-laminate built up (Meer, 2016)

Placing the gross of the material at its most effective location is done conventionally by making I-shaped profiles or by means of sandwich-panels. The components involved and their differences, are discussed in this section.

5.1.1. Fibres

There is a wide range of fibres to be implemented in FRP: glass, carbon, polyaramid, polyester, jute, sisal, nylon and boron. Since this thesis revolves around the structural application of FRP in civil engineering structures only the first three mentioned fibres are discussed next. The other fibre-types are not used in civil engineering.

5.1.1.1.   Glass fibres

Excellent properties and a low price allow glass fibres to be, by far, the most dominant reinforcement material in terms of usage. There are five types of glass fibre. Where A-glass used to be the main material used E-glass has now superseded it, due to its good electrical, mechanical and chemical properties. Then there is C-glass, which has a special chemical resistance and R- and S-glass, which have high strength properties. (Strong, 2008)

To obtain a homogeneous glass composition the blends of inorganic material are fused and reacted together in a furnace at around 1600 °C. The molten glass is drawn through a filament-forming platinum called a "bushing", at a speed of 50 m/s. Resulting in continuous filaments which are coated afterwards and brought together into strands to be wound up onto rolls. The diameter of these filaments has a range of 3.25 to 14 μm. The linear density of glass fibres is measures in 'tex' [grams/ kilometre]. (Kolstein, 2008)

5.1.1.2.   Carbon Fibres

The most expensive of the common reinforcement fibres. Carbon fibres come in a number of precursors: cellulose fibres; polyacrylonite fibres; lignin and hydrocarbon pitch. In all these precursors the carbon fibres are produced by controlled oxidation and carbonization of the precursor fibre at temperatures of 2600°C. An increase to 3000°C leads to polyacrylonite fibres rather than cellulose fibres, which is more efficient, due to a higher carbon-content.

The price of carbon fibres can cost up to forty times that of glass. (Kolstein, 2008)

5.1.1.3.   Aramid fibres

Most widely known by the brand Kevlar®, Polyaramid fibres, is one of the most important man-made type of fibres. Its main features being high tensile strength combined with low density. With the highest in the reinforcement fibres, thus far, these fibres are five times stronger than steel, on a weight for weight basis. Opposed to glass and carbon fibres, the fibre fracture of aramid fibres behaves in a ductile manner and they are more susceptible to fibre breaking in bending by a compressive mode. This compressive fibre breaking would be reached far earlier than the tensile yielding by deformation.

A combination with other fibres to form hybrid fabrics allows an acceptable compromise to take advantage of the aramid fibres' unique properties. One does have to take the cost of aramid fibres into account, mostly because it can cost up to fifteen times that of glass. (Kolstein, 2008)

5.1.1.4.   Comparisons

In the thesis of J.C. Moen, a well based comparison has been made between the different kinds of bare fibres, based on quite a spread of their specified mechanical properties. A quantitative and qualitative comparison in Table 5-1 is based on his work. To illustrate the potential of FRP the strength to weight ratio[5] has been given in the table. The fibres have a strength to weight ratio which is at least 27 times greater than steel. In Appendix C, section C.4, a comparison between FRP and steel is illustrated.

---

[5] Take attention that this indicates the tensile strength to weight ratio of the fibres ONLY, not the FRP as a material. However it clearly indicates the potential of the material.

	Density [kg/m³]	Tensile Modulus [GPa]	Tensile Strength [MPa]	Strength/weight ratio [[MPa*m³/kg]]	Elongation until break [%]	Thermal expansion [10⁻⁶ °C]
E-glass	2500	69	3400	1.36	4.9	5.2
C-glass	2500	72	3450	1.38	5	7.3
S-glass	2500	83	4600	1.84	5.7	5.7
Carbon – HM	1900	440	3450	1.82	0.5	-0.75
Carbon – HS	1800	270	5300	2.94	1.8	-0.6
Aramid – HM	1450	180	3400	2.34	2	-2
Aramid – HS	1450	130	4000	2.76	2.8	-2
Steel (S355)	7800	210	355	**0.05**	0.2	12

Table 5-1 Representative fibre properties (Moen, 2014)

NOTE: Both the carbon and aramid fibres have been divided into two sections where first has high modulus properties (HM) and the second has high strength properties (HS).
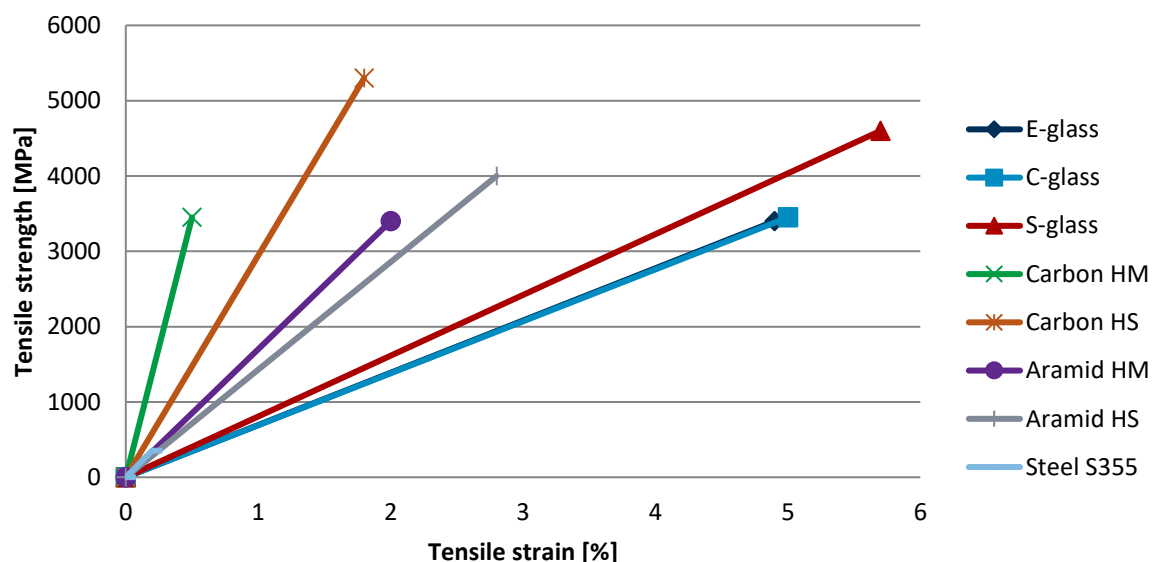

Figure 5-2 Stress-strain diagram of different fibre types (and steel)

In Figure 5-2 the data, as mentioned in Table 5-1, has been visualised in a stress- strain diagram. This clearly shows the behavioural differences between the glass-, carbon- and aramid fibres with regard to elongation. This clearly shows the strength quality of the fibres used in FRP compared to steel (elastic only). However, this does NOT properly show FRP-laminates/plies itself.

	Glass fibre	Carbon fibre	Aramid fibre
Specific strength	Yellow	Green	Yellow
Strength-to-weight ratio	Red	Yellow	Green
Specific stiffness	Red	Green	Yellow
Stiffness-to-weight ratio	Red	Green	Yellow
Density	Red	Yellow	Green
Toughness	Yellow	Red	Green
Creep / fatigue	Yellow	Yellow	Red
Cost	Yellow	Red	Yellow

Table 5-2 Qualitative comparison different fibre types (Moen, 2014)

Green = best property choice;   **Yellow** = middle property choice;   **Red** = worst property choice.

A comparison with regard to difference in their respective properties is shown in Table 5-2. Here different colours are use illustrate which has the most/ least favourable properties, compared to the others.

By means of combining different fibres into one cross section/ element, the fibres can be applied at their best suited location. For example: an element resistant to impact loads, combined with high strength, can be achieved by proper placement of carbon and aramid fibres. These are however more expensive.

5.1.1.5. Variations

The way the fibres are used can be divided into two major categories:

5.1.1.5.1. Continuous fibres

The continuous filaments are wound up, parallel and without twist, onto rolls (a spool) to create a **continuous filament roving**. These can then be woven into fabrics. Fabrics can also be made out of yarn. These, however, will have to be twisted before being woven into so called cloths. This is done to be allow uniform cloths to be woven. The difference between woven cloths and woven rovings is their respective densities, due to difference in thickness of the strands. Different weaves allow for different material behaviour in the principle directions. Some examples are: the plain-, twill-, satin- and weave; as illustrated (from left to right) in Figure 5-3. Using different fibre types inside one hybrid fabric is another option.
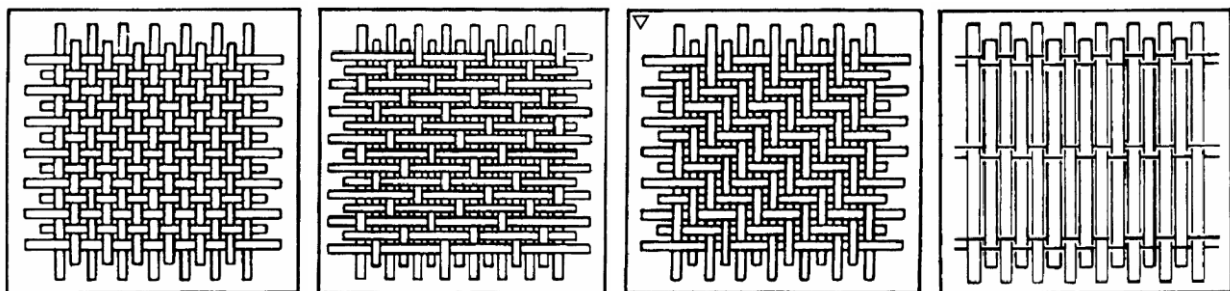

Figure 5-3 Different weaves possibilities (Kolstein, 2008)

Often laminates are made of continuous fibre components. These laminates consist of different plies, where each ply is a unidirectional continuous fibre layer. The plies are stacked in with different orientation to obtain the desired strength- and stiffness properties, as illustrated in Figure 5-1.

The difference between a UD-ply (unidirectional) and a roving is the interaction between the fibres in the different directions. Where UD's perform better in axial loading, the rovings perform better when loaded at 45° to the fibre directions. This is due to their woven nature.

5.1.1.5.2. Non-continuous fibres

This type of fibres behaves differently compared to the continuous fibres. Continuity implies a continuous fibre in one direction. Therefore, non-continuous fibre can be divided into chopped strand mat (CSM) rovings and continuous filament mat (CFM). In a CSM the fibres are chopped and spread out uniformly on a mat, whereas in a CFM the continuous fibres are deposited randomly in a swirl-like pattern. The CSM and CFM have been illustrated in Figure 5-4.
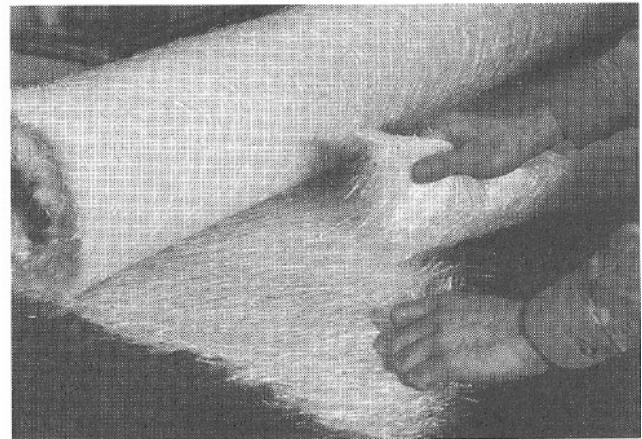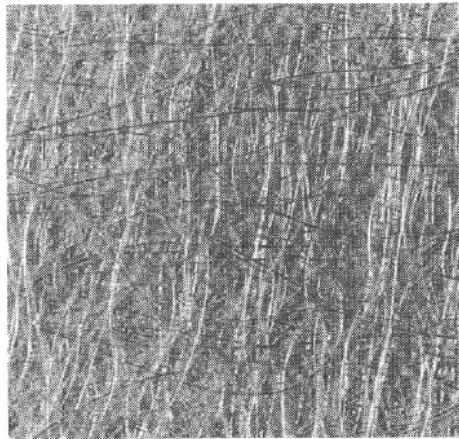
Figure 5-4 Left: CFM; Right: CSM (Pavlovic & Kolstein, 2016)

5.1.2. Resins

Bundles of parallel fibres are useless in a load-bearing function. They may be functional in tension but are incapable of resisting shear and compression forces. Combining the fibres together with a resin matrix, the fibres are capable of carrying most of the stress, while the resin matrix distributes the external loading to all fibres. It also protects the fibres and prevents buckling of the fibres, under compressive action.

In this thesis the matrix part of FRP has been defined by resins, because in this thesis the matrix will be made up of polymeric based (resins). Other possibilities for the matrix can be metallic or ceramic. In this thesis the FRP built-up has been limited to fibres combined with polymeric based resins. Meaning that other options such as latter two mentioned possibilities, fall outside of this scope due to time restrictions. A (polymeric) resin consists of polymers and possible additives to enhance the material properties.

Then there is a clear distinction between thermoset resins and thermoplastic resins. Their behaviour differs greatly. Thermoset resins cannot be melted down to be reused once they have been fully cured: they are set. Thermoplastic resins can be melted down to be reused. Both can be used to make FRP, however currently thermoset resins are alternative used in today's products used in Civil Engineering. This difference is caused by the cross links between the polymers. This is illustrated in Figure 5-5.
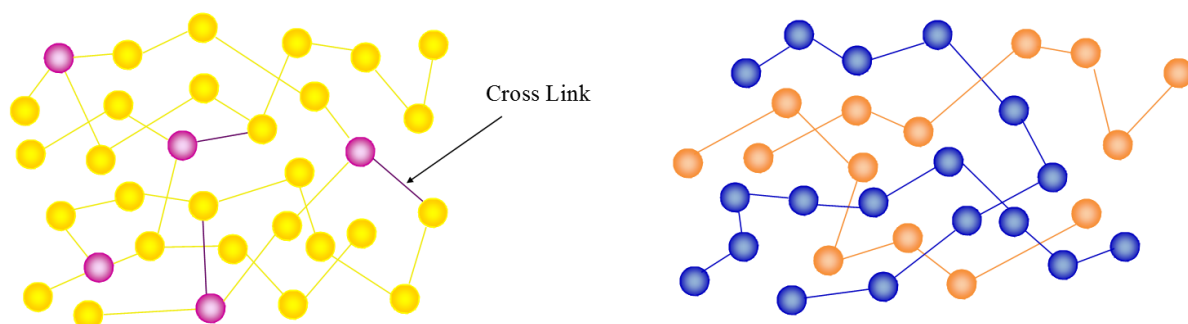

Figure 5-5 Thermoset- (left) vs thermoplastic resins (right) (Star Thermoplastics, 2017)

5.1.2.1. Thermoset

Different thermoset resins are used in FRP. Each has its own structure and curing process. Some examples of these thermoset resins are: **polyester**, **vinyl ester**, and **epoxy** resins. To each of these most used resins, variations can be made such that requested characteristics can be achieved. This

depends on the curing ratio between the component used to manufacture the resin, the curing temperature and/or the curing agent used in the production. (Pavlovic & Kolstein, 2016)

5.1.2.2.   Thermoplastic

Thermoplastics have a great advantage and that is that they are relatively easily retrievable from created products. Their greatest asset is also their greatest downside. They can be reused by elevating the temperature as they would then melt. This temperature elevation, however, is unwanted during the use-phase of the material. Some examples of these polymers are **polycarbonates, nylons, polyethylenes, polypropylene** and **polystyrenes**. (Pavlovic & Kolstein, 2016)

5.1.2.3.   Comparison

Below a table is illustrated displaying a comparison with the current state of affairs comparing thermosets and thermoplastics.

	Thermoplastic polymers		Thermosetting polymers
	Amorphous	Semi-crystalline	
Polymer bond type	Molecular *(reversible)*		Chemical *(irreversible)*
Morphology	Amorphous	Semi-crystalline	Cross-linked
Glass transition T_g	Yes	Yes	No
Specific T_m	No	Yes	No
Modulus retention (heat resistance)	Low (+/- XX° C)	Moderate (+/- XX° C)	Very good (+/- XX° C)
Volumetric shrinkage	Low	High	Low
Wall thickness transitions	Yes *(low in-mould shrinkage)*	No *(in-mould shrinkage)*	Yes *(very low in-mould shrinkage)*
Impact resistance	High	High	Moderate
Manufacturing	High temperature (+/- 200° C)		Room temperature (+/- 20° C)
Surface finish	Excellent		Good
Eco-friendly	Excellent *(recyclable)*		Moderate *(non-recyclable)*
Process complexity	Moderate		Low
Process control	Easy		Complex
Recyclable	Yes		No
Chemical resistance	Poor	Excellent	Excellent
Creep resistance	Poor	Moderate	Good
Cost	Low	High	Moderate
Market share	80%		+/- 20%

Table 5-3 Different polymer properties (Franken, 2017)

Thermoplastics become a suitable alternative to thermosets, when the temperature at which they would melt is high enough for it not to occur during working conditions. Thermoplastics are also suitable when it is certain that the rise of temperature can be prevented during the use-phase of the construction. This latter option results in additional attributes onto the construction to restrict this temperature rise, including a failsafe system.

Currently thermosets are not easily separable once set. This is the downside of the application of thermoset resins. However, research is being done which would allow for easier separation of thermoset resins. Making them much more favourable to be applied.

5.1.2.3.1.   Recycling thermosets

In a workshop on the LCA (life cycle assessment) of composites (Pickering, 2013) on September 25th 2013, Steve Pickering depicted the available options in recycling FRP and reusing it as a structural material, with the goal of creating high grade structural properties with a high fibre volume fraction

and (almost) perfect fibre alignment. Two different types of recycling are discussed: mechanical/ and thermal recycling.

Mechanical recycling is essentially size reduction of the FRP. Resulting in powder (resin rich) recyclate[6] or a coarser fibrous (fibre rich) recyclate. These recyclates contain all the elements used in the FRP (resin, fibres, contaminations, paint, etcetera). Most research has been done on glass fibres. This will not lead to the required goal, due to the contaminations of the recyclate.

Thermal recycling aims to recover clean fibres (both glass and carbon). The polymers are recycled either to recover energy of the mechanical products. For thermal recycling, a shredder of cutter is required for processing.

Pickering mentioned several issues in the recycling process of thermosets:

- There are some technical problems like retrieving long fibres and reducing the amount of contamination. (In other words, ensuring a clean product).
- When creating random mats, high pressure is required to achieve high volume fraction. This however results in fibre damage.
- Aligning the fibres allows higher volume fractions at lower moulding pressure, which has less fibre damage as a result.
- Recyclates are too expensive, making it hard to compete with in the available markets.

He then concluded that at that time, the processes are suitable for manufacturing scrap and some end-of-life materials. However, to recover the true potential of FRP a higher grade of aligned recyclates is needed. First of for the carbon fibre market, due to the expensive nature of the recycling process.

For FRP applied in bridge structures, the above-mentioned recycling process can become a source for materials, however this will not be in the near future due to the high costs accompanied with this process. The costs will have to drop severely and become a well proven alternative in other fields to break ground in the bridge market. Already the base cost for FRP is a reason to choose a steel alternative over a hybrid (steel and FRP) solution. Even higher costs, resulting from using recyclates, is a very unwelcome scenario.

5.1.2.4.   Additives

Improving material properties and lowering the cost or the amount of pure polymer usage can be done by applying additives. Some examples of additives are used as surface finishing; fire retardancy/ resistance and/or thermal degradation resistance. (Franken, 2017)

5.2.   Applying FRP

When using FRP, one can simply place ply upon ply however, this is not structurally efficient. Take an I profile for example. This is a structurally improved shaped compared to a rectangle, containing most of its mass as far as possible from its own centre of gravity. Applying this to FRP and placing the material such that it has larger structural height, without the mass of just stacking ply on ply, **sandwich panels** were created. Placing the material where it counts and introducing height into the element, by having a core to combine the top and bottom facings. The facings can be created, as discussed earlier

---

[6] Wanted product as a result of recycling, however due to recycling it is hard to have this be a clean product. Meaning that is only contains the elements of the required product and nothing else.

in section 5.1.1 regarding Fibres. Next the different possibilities regarding the core are discussed. (Pavlovic & Kolstein, 2016)

5.2.1. Solid

Since the idea of the core is to induce height while not increasing weight, a light solid core is wanted. These properties are found in wood.

5.2.2. Foam

Applying foam as core material can be done in different manners: structural, non-structural and even reinforced. Non-structural implies that the foams sole purpose is to allow for the alignment of the fibres for the production process. This can be seen as a 'lost core'. Depending on the properties desired, a core can be chosen. In this design study, the *lost-core* principal has been used. (Pavlovic & Kolstein, 2016) (FiberCore europe, n.d.)

5.2.3. Honeycomb

This natural shape was found only in the aerospace engineering until 1940's and can be found in a variety of shapes: being hexagonal, over-expanded or flex-core. These thin walled shapes are often made of aluminium or aramid-fibre sheets.
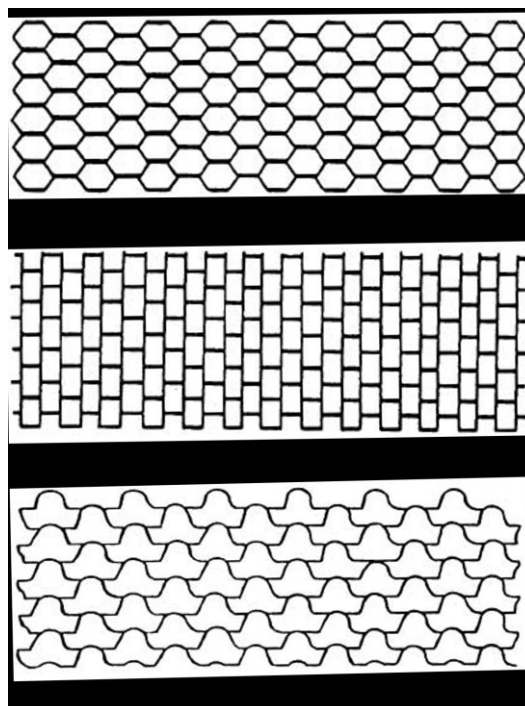
Figure 5-6 Common types of honeycomb (Pavlovic & Kolstein, 2016)

5.3.　　Production

There are two main options in the production systems for FRP: **opened** and **closed** moulding. For each of these categories several methods are available, each has its own advantages and disadvantages. The most important aspects for a quality product rely on the precision in the resin impregnation and the placement of the fibres. This first depends on the viscosity of the resin, the pressure and flow resistance, which are different for each production process. A clear overview of the aforementioned system categories and the different production processes available, have been illustrated in Table 5-4, Table 5-5 and Table 5-6, curtesy of A. Franken:

Closed mould system	Open mould system
✓　Closed system (better management)	✓　Low complexity machinery
✓　Less to no resin vapours (closed system)	✓　Low cost
✓　Faster impregnation (pressure)	✓　Easy to operate
✓　Less bubbles (pressure)	
-　Complex system	-　Low impregnation (no pressure)
-　Sealing (needed due to pressurisation)	-　Air bubbles (no pressure)
-　Pressure leads to backflow (towards the fibre inlet side of the mould)	-　Resin vapours (health concern)

Table 5-4 Closed and open mould process comparison (Franken, 2017)

Process	Process type	Mould type	Pressure		Mould temp.	
			Mould	Injection	T.set	T.plast
Hand lay-up	Open	Single sided	None	None	Low	n.a.
Filament winding		Rotational				
Pultrusion	Closed	Die	None	Medium	Low	High
Compression mld.		2-s	High	None		
Injection mld.				High		
HP-RTM						n.a.
(VA-)RTM		2-s or 1-s + film	Low	Vacuum	n.a.	High
RFI						
Vacuum infusion		1-s + film	None		Low	n.a.

Table 5-5 Production process properties comparison (Franken, 2017)

Process	Production				Product	
	Volumes	Automation	Complexity	Cost	Size	Complexity
Hand lay-up	Low	No	Low	Low	Large	Low
Filament winding	Medium	Yes		Medium	Medium	
Pultrusion	High	Yes	Medium	Medium	S-L	Medium
Compression mld.			High	High	Medium	High
Injection mld.				High		High
HP-RTM	Medium		1-s: low 2-s: high	1-s: low 2-s: high		High
(VA-)RTM	Low	1-s: no 2-s: yes				High
RFI						
Vacuum infusion	Medium				Large	

Table 5-6 Production process properties comparison (Franken, 2017)

NOTE: in the above illustrated tables a short legend is required:

1-s	Single sided mould
2-s	Two-sided mould
S	Smaller than 15 cm
M	Between 15 and 15 cm
L	Larger than 150 cm
HP-RTM	High pressure resin transfer moulding
VA-RTM	Vacuum assisted resin transfer moulding

The production process used frequently, which results in a very high-quality product is VARTM. This is an expensive method, but a large product can be made with a high quality.

6. Connecting FRP and Steel in Critical Elements

As said all materials have their advantages and disadvantages. To compensate for the disadvantages and create better solutions a combination of more materials into one structure (or element) can be made and thus a hybrid structure (or element) is born. A brief dissertation on connecting FRP and steel is given below. The choice to combine these two materials is two sided:

- First extensive research has been done in this combination;
- Secondly due that the Amalia bridge is made of steel.

In this chapter FRP-joints will be discussed, as this differs somewhat from steel connections. Then the connection (and interaction) between the two are discussed.

6.1.   Joint types

There are three methods of connecting FRP: **bonded** and **mechanical fastening** or a **hybrid** form. Each has their own behaviour and application restrictions. For instance, bonded joints can be designed such that the joint is stronger than the composite being joint, whereas mechanically fastened joint are difficult to create such that their strength is greater than 50% of the joint composite, thus, to obtain acceptable efficiency, local reinforcement may be required. Unfortunately, bonded joints cannot solely be used for primary loadbearing connections. This means that the connection between the steel girders and an FRP-deck must be mechanically fastened or with a combination of both, mechanically and bonded. Still the bonded option is to be considered a backup option. This meaning both must be capable of carrying the entire load. (JRC, 2016) (Kolstein, 2008)

The figure below illustrates the different joint types that can be made (either bonded of mechanically fastened):

To avoid bending located at the joint a joint should be carried out double, not single. This not only removes the bending, but also gives a much stronger, resilient connection. A double joint leads to symmetrical loading, thus double shear loading.
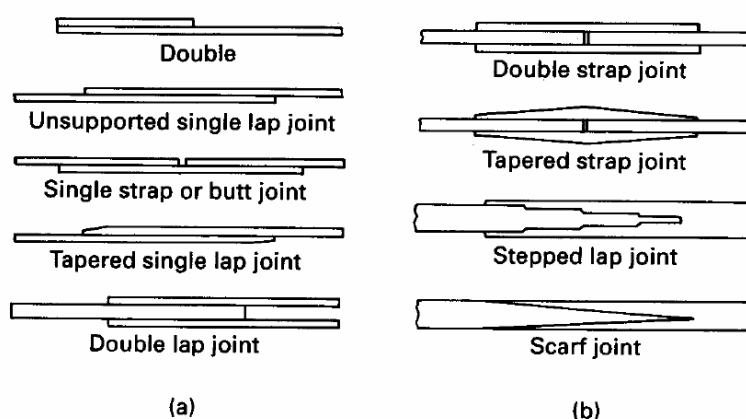

Figure 6-1 Basic join types (Kolstein, 2008)

6.1.1. Composite action

Whether it being a bonded, mechanically fastened or a hybrid joint, when making a composite section, the two composites could work together as one section. This phenomenon is called composite action.

The connection between the two elements, can be described as a degree of composite action (DCA for short).

If the two sections show to have a very low to none DCA, the section functions as two separate entities. Hereby each element (deck and girder), under a positive bending moment, have a top surface under compression and a bottom surface under tension, thus resulting in slippage between the bottom surface of the deck and the top flange of the girder. In case of partial composite action, this slippage will be somewhat reduced and, of course, in the case of full composite action, where the DCA is near to 1, the aforementioned slippage will be prevented from occurring. (Alnahhal, et al., 2007)

6.1.2. Effective flange width

In case of (partial) composite action and a positive bending moment, the deck will function as the compression flange of the steel girder. Then, in the case of large spacing of the steel girders, the compressive, longitudinal, compressive stresses in the flange vary with de distance from the girder web, resulting in beam theory not being applicable anymore. This result in a phenomenon called **shear lag**. "*Due to the action of in-plane shear strain in the flange of the composite girder under flexure, the longitudinal displacements in the parts of the flanges remote from the webs lag behind those near the webs*", is the explanation given by Alnahhal et al. This phenomenon has led to the introduction of the effective width flange, to provide a simple procedure and dealing with the shear lag.

NOTE: A procedure has been made for concrete – steel composite sections, NOT (yet) for FRP – steel composites. Research has been done by Zou on this phenomenon and in the Cur96 the recommendation is made to review the approach of Zou in case the shear lag phenomenon would occur. (Alnahhal, et al., 2007) (Zou, et al., 2010) (CURNET, 2003)

In the current effective width method (concrete) the effective width is influenced by:

- Span length
- Girder spacing
- Degree of composite action
- Loading pattern

6.1.3. Bonded joints

Bonding could be said to be 'natural' way of connecting FRP, since this is the basis of FRP. It is a permanent method of joining two (or more) elements into one. This permanent issue is one to take into account. In case of damages to the structure, how will replacement/ reparation take place? When designing bonded joints, one needs to take into account that an overlap is required and most critical to the strength of the connection. Hereby an optimum ratio between the overlap and the adherent's thickness is about 30 to 1. Furthermore, critical to a bonded joint is the surface preparation of the locations. Bonded joints are very susceptible to moisture. (Kolstein, 2008)
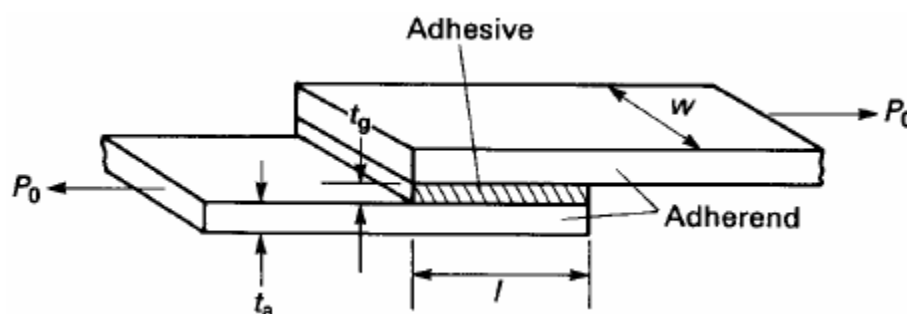

Figure 6-2 Base lay-up of a bonded FRP-connection (Kolstein, 2008)

Different materials are available as bond material (the adhesive). Depending on the material which is to be bonded, a choice in adhesive should be made.

6.1.3.1.   Failure modes
Joint failure can be divided into two types:

- Failure of the actual joint. (in this case the adhesive material)
- Failure of the bonded material. (in this case either steel or FRP)

For bonded joints the joint can fail by five different modes, this being: failure of the adherend, adhesive or cohesive; OR transverse, tensile or interlaminar failure. Where the actual strength of the connection is the lowest of all these possible failure modes. A visual illustration has been depicted in Figure 6-3:
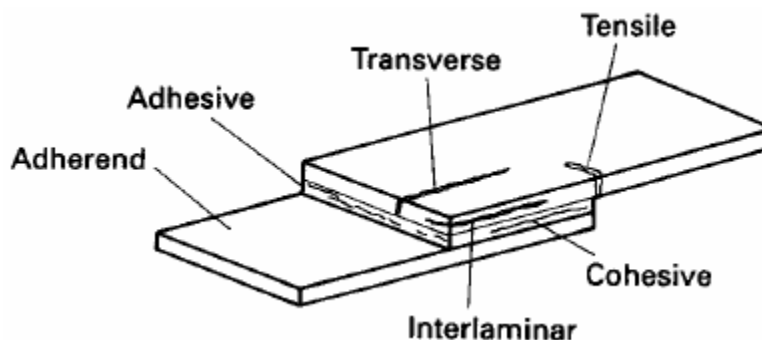
Figure 6-3 Failure modes of a bonded connection (Kolstein, 2008)

6.1.4. Mechanically fastened Joints
Joints which are mechanically fastened are relatively easy to prepare, compared to bonded joints, however extra caution should be taken when drilling the holes. An accurate fit of the fasteners is essential to achieve the required design load. (Kolstein, 2008)

NOTE: Mechanically fasteners CANNOT be as strong as the laminates which are to be connected, thus an increased thickness in the joint region will be required. Here, the weight penalty will be compensated by the increase in overall structural efficiency

The aspects that should be considered when using mechanical fasteners are shown in Table 6-1.

What	Details
General	Essential to fastener loading, in multi-fastener joints is maintenance of the hole tolerance, circularity and position.
Hole tolerance	Holes should have a 'net' fit (0 +/- 0.1 mm), unless otherwise specified.
Drill bit	- The use of high-speed drills is NOT recommended. - Sharper drill points, than compared to steel. **Thin** sheets: 55 – 60° **Thicker** sheets: 90 – 100°
Drilling	- Either use a sacrificial backing sheet or a controlled-feed drill. - Do NOT use lubricant fluids. - Essential is dust extraction. - Cutting speed of around 20 mm per min is advised. - When countersinking makes use of a combined drill/ countersink tool, with initial pilot hole. The countersink depth cannot exceed half of the laminate thickness.
Laminate material	- Glass FRP (GFRP) & Carbon FRP (CFRP) can be treated similarly. Additional for CFRP is to avoid exit surface splitting. - For Kevlar FRP (KFRP) special bits are required. - Improve the hole quality by using a surface layer of 120 style glass cloth.

Table 6-1Considerations regarding mechanical fasteners (Kolstein, 2008)
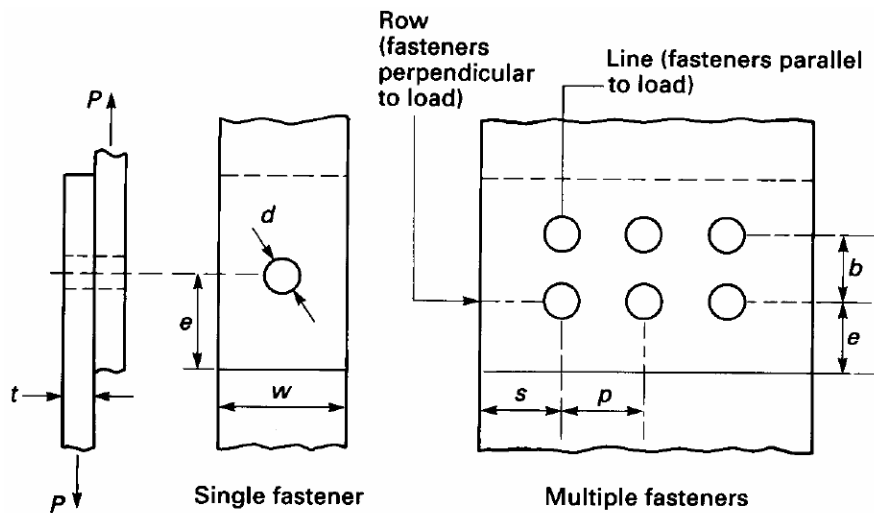
Figure 6-4 Joint dimensions (Kolstein, 2008)

6.1.4.1. Geometry

The joint lay-up types, which have been illustrated in Figure 6-1, combined with the dimensions, as shown in Figure 6-4, define a complete joint lay-up. Depending on the combination a certain failure mode will be governing.

6.1.4.2. Failure modes

Failure can occur in the joint in several different manners (as is illustrated in Figure 6-5). Since FRP does not have the ability to deform plastically, the joints will be critical to the design. The strength of a joint depends on the combination of different factors, it being: geometrical, material, fastener specific design factors and environment and long-term exposure. (Moen, 2014)
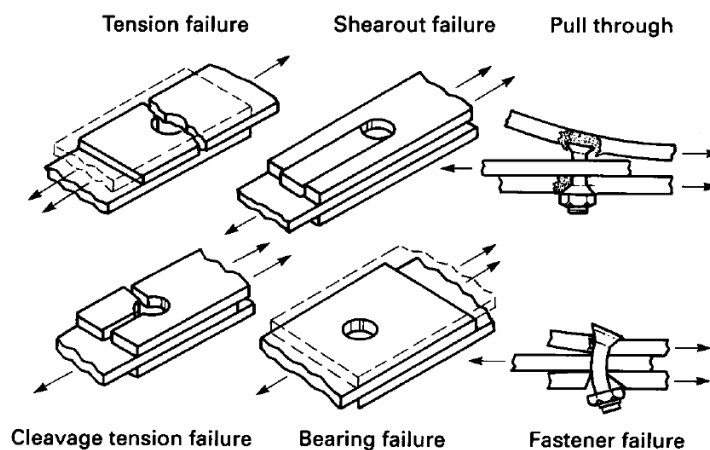
Figure 6-5 Joint failure modes (Kolstein, 2008)

6.1.4.2.1. Tension failure

This is essentially a material dependent failure mechanism and is in general catastrophic, thus it MUST be avoided. This is done by over dimensioning the material such that this failure mode is no longer the governing failure mode. This means, another failure mode will occur before this one does.

6.1.4.2.2. Shear-out failure

Can be avoided by ensuring a large enough end distance ($e > 4d$).

6.1.4.2.3.　　　Pull through failure

Is only likely to occur when countersunk heads have been used. Head angle should not exceed 120 or 130°.

6.1.4.2.4.　　　Cleavage tension failure

To avoid cleavage, one must ensure adequate end distance ($e > 4d$) and width (w).

6.1.4.2.5.　　　Bearing failure

Just as goes for tension failure, bearing failure is material dependent, however it is non-catastrophic.

6.1.4.2.6.　　　Fastener failure

There are two types; shear and bending. A correct diameter avoids shear failure and if $d/t > 1$, bending failure is avoided.

6.1.5.　Different fasteners

Mechanically there are different type of fixings: being screws, rivets, bolts, studs and clamping. **Screws** can be used in load-bearing joints, Self-tapping screws, however, cannot. They can be used in bonded joints as anti-peel fastening. **Rivets**, as used in joining metals, are not recommended. Controlled expansion and clamp-up rivets, with a suitable geometry, should be used for laminates. A combined thickness of 6 to 8 mm can be joined. Conventional (un-countersunk) **bolts** can be used, tightened to standard torque. The nut should be locked, preventing clamping loss. In case of blinds installation or flush-fitting, special purpose bolts are recommended. (Kolstein, 2008) Out of the first three, only bolts seem to be applicable, as well as the latter two, depending on the requirements of the specific project. It depends on whether composite action of the two composite elements is desired. Headed shear **studs** are routinely used in concrete – steel composites and have proven to be well functioning for FRP – steel composites as well; (Davalos, et al., 2011) This is discussed on page 31. A **clamped** connection functions as means to prevent uplifting of the panels. However, it does not provide composite action. NOTE, this is a rather labour-intensive method of connection, since they are to be installed from underneath. (Alnahhal, et al., 2007)

6.1.6.　Laminate material

Besides the mechanical fastener, the to be joined materials have an influence on the structural behaviour of the joint. (Kolstein, 2008)

6.1.6.1.　　　Type of fibre

The fibre type has an influence of the strength level. Other general characteristics are not affected by the fibre type. The strength can be rated in ratios of 1 : 0.8 : 0.5 for carbon, glass and Kevlar fibres respectively.

6.1.6.2.　　　Lay-up of the laminate

A quasi-isotropic laminate lay-up would give the most optimum performance. Here the proportions would lie between 0.125 to 0.375 for any direction. For a (0/±45)-lay-up there is a range of 0.375 to 0.75 proportion in the ±45-layer.

6.1.6.3.　　　Sequence of stacking

Depending on the fastener used, the stacking sequence is of influence. For fully tightened bolts its of minor importance. For rivets, the stacking sequence is of more importance. Having a surface layer in 90 or 45° is recommended (when loaded in 0°). Laminate stacking is preferred over ply-stacking, due to the alternating angles for each ply.

6.2. Shear Connecters (FRP deck to Steel Girder)

In the connection of an FRP-deck to the steel girders one could see similarities with a concrete slab onto steel girders for a composite action. In order for these two elements to work as one composite, they need to be connected sufficiently and effectively. Unfortunately (solely) bonded joints cannot be used for this purpose, as stated earlier, therefore mechanical fasteners become the choice. An example of a (concrete-steel) composite system can be seen in Figure 6-6. Studs are welded onto the steel girders which pultrude into a concrete section, thus creating, after casting, one composite, shear transferring, construction.
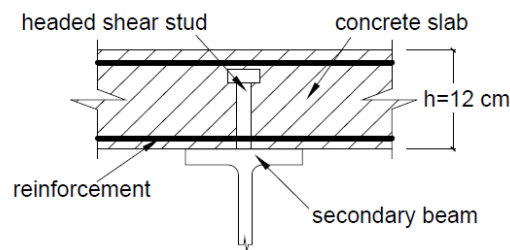
Figure 6-6 Shear stud connection in concrete-steel composite (Dinu , et al., 2013)

Shear transfer and connection constructability are major issues for a system-level connection. In a composite bridge system, one has to take into account the degree of composite action. (As has been done by Davalos in section 6.2.1.2: T-Beam test including results.) This significantly effects the behaviour of the composite section of the bridge. (Alnahhal, et al., 2007)

6.2.1. Davalos' shear connector (mechanical fastener)
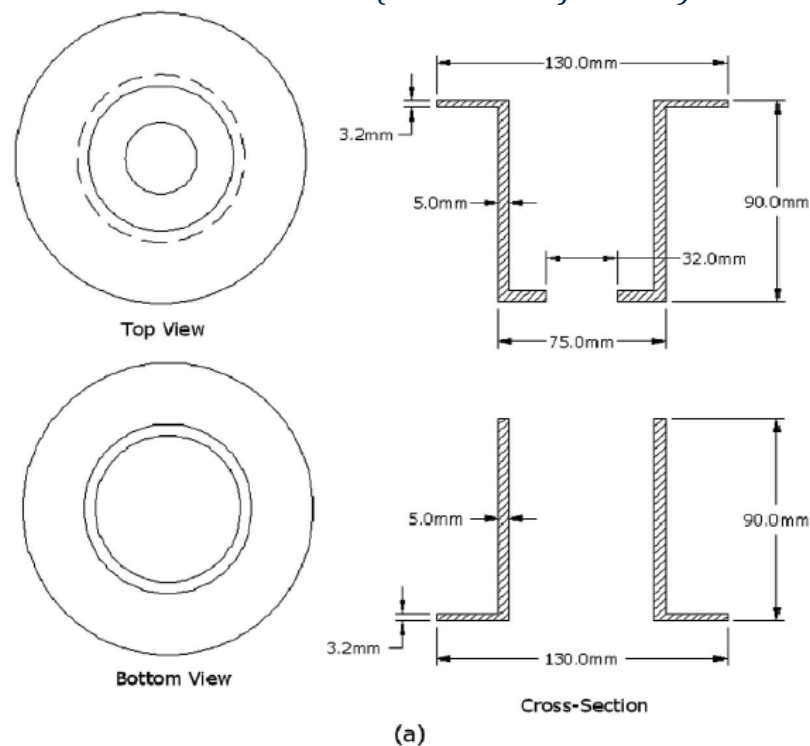
Figure 6-7 Detail shear connection – steel sleeves (Davalos, et al., 2011)

This essence is what (Davalos, et al., 2011) have applied to an FRP-deck connecting it to steel girders in their research. Their method consists of drilling a hole into the FRP-deck, creating a passage for a connection. Here a threaded shear stud (welded onto the supporting girder) pultrudes into the hole of the FRP-deck. The stud is housed in a steel sleeve, which are to be installed in the aforementioned hole. It provides a secure connection, preventing uplifting of the deck, by means of the top washer. Due to the simplicity of this connection, it can be applied to any type of FRP-deck, with a wide range of deck thicknesses. The details of this shear joint have been illustrated in Figure 6-7.

The hole required for the connection is covered by means of granular material (sand) and a polymer binder or a simple cap (for easy access).
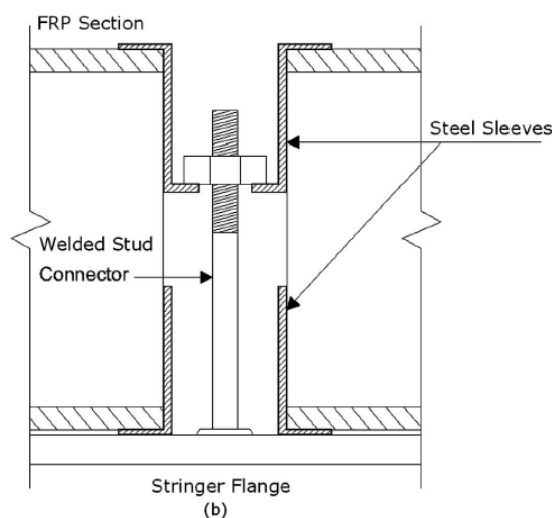
Figure 6-8 Detail shear connection – cross section (Davalos, et al., 2011)

6.2.1.1. Push-out test including results

In their research and testing they subjected the connection to a push-out test, by means of displacement control at a rate of 3 mm per min. up to failure, with a horizontal 245 kN actuator.

The failure mechanism of Davalos' shear connector, after initial slip, the force transfer mechanism was bearing between the FRP-deck and the top sleeve. Both the inside and outside **washer** displayed warping. The bottom sleeve first displayed deformation at approximately 22 kN. The top face sheet of the **FRP-deck** displayed no damage, whereas the bottom face sheet experienced significant deformation. At the third post yielding stage, the specimen displayed a ductile behaviour. This come primarily from the shear studs' yielding.

Resulting in average strengths:

- Yield strength of 114 kN.
- Ultimate strength of 136 kN.

The bolt was tightened as "snug", as done by an ironworker with an ordinary spud wrench. (Davalos, et al., 2011)

6.2.1.2. T-Beam test including results

The section from the Scaled Bridge test was cut and used for the T-Beam test. (This was possible due to no apparent damages.) With this three-point bending test an actuator, of 490 kN, was placed at midspan, acting on a 0.6 by 0.25 m² surface. Hereby research was done on the DCA and this was found to be approximately 25% were:

$$DCA = \frac{N_p - N_0}{N_{10} - N_0}$$

This relative low composite action value is due to the low equivalent modulus of the FRP-deck. Even for full-composite action it would not contribute significantly to the bridge system. Using FRP with steel in a full-composite action (by mean of for instance fully constrained shear connectors) could lead to adverse effects on the bridge system, due to inconsistency in thermal coefficients of expansion between steel and FRP. For the executed test the level of composite action is enough to achieve a proper responds under both static and fatigue loading. (Davalos, et al., 2011)

6.2.1.3.   Implementation

This method is easy to install on different types of FRP-decks, only if the right precautions have been made when using this connection. (One must not risk the integrity of the FRP-deck, when drilling for the connection.) The applied shear connectors display to function sufficiently and allow for a partial DCA, while refraining from a full DCA and having other possible complications.

Thus, a proven system in connecting an FRP-deck to steel girders and a possible solution.

NOTE: tests must be done, when changing the configuration to verify the actual connection. For instance, the FRP-deck used in this case, might differ from the FRP-deck that will be used in this MSc. thesis.

6.2.2. Keller's shear connector (bonded)

Thomas Keller and his team have done research into hybrid bridge girders, with an adhesively bonded connection between a pultruded FRP deck and steel girders. Their research was directed into three different sections: First the in-plane load-carrying performance of the FRP deck, acting as composite top chords of the steel girder. Secondly the static and fatigue behaviour of four, full scale, girders were examined, when subjected to the four-point bending test. Their third objective was establishing a design method for hybrid FRP-steel girders with flexible shear connections. (Keller & Gürtler, 2005)

For the FRP pultruded deck systems the ASSET and the DuraSpan systems were chosen, as is illustrated below, in Figure 6-9, with a) and b), respectively. (Satasiviam, et al., 2013)
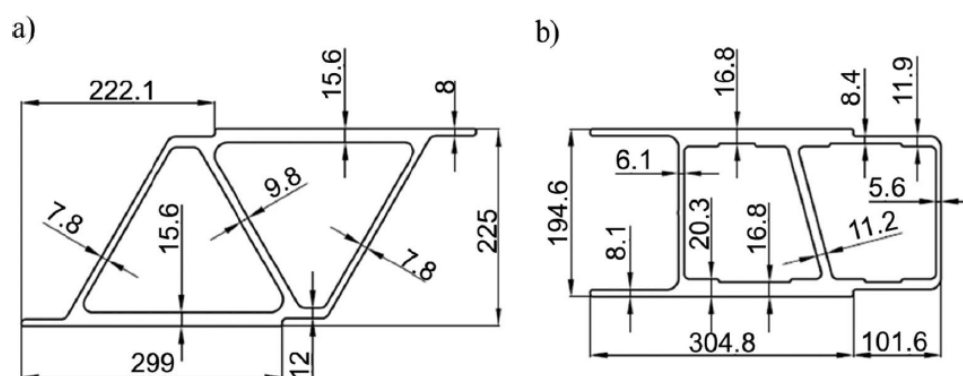

Figure 6-9 Pultruded FRP bridge deck systems (Satasiviam, et al., 2013)

The FRP deck is connected to the steel girders with an adhesive. Here two alternatives were considered. Being a relative stiff epoxy-adhesive (SikaDur 330) and a flexible polyurethane-adhesive (SikeForce 7851). A cross section of the test set-up, as used by Keller, et al. has been depicted in Figure 6-10:
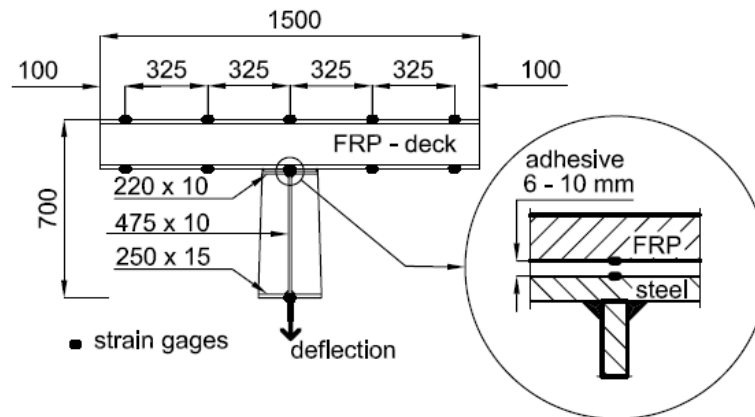
Figure 6-10 Cross section of the test set-up of a hybrid (FRP-steel) girder (Keller & Gürtler, 2005)

6.2.2.1.   Adhesive connection influencing composite action

For both alternatives a full composite action of the cross section has been verified by this research, with a γ-factor ranging from 0.955 up to 0.997. (Keller & Gürtler, 2005)

6.2.2.2.   Long-term behaviour of the adhesive bonding

In the years between '68 and '92, seven composite (concrete-steel) bridges, which span from 15 to 32 meters, were constructed in East-Germany, using epoxy adhesive bonding. Now, more than thirty years of exposure to dynamic loading and environmental attacks later these bridges are still in service. Then, from the tested specimens, two were subjected to a fatigue test, where, after more than 10 million cycles, they did show any signs of damage, nor were any noticeable creep deformations visible. (Keller & Gürtler, 2005)

6.2.2.3.   Keller's conclusion

It was found that, for the selected pultruded FRP-deck system, a full composite action between the FRP-deck and the steel girders was achieved, even with the flexible polyurethane adhesive, with a layer thickness up to 50 mm. However, for the pultruded FRP bridge deck systems, the webs provide only a partial shear connection of the upper face panels in the longitudinal direction.

The transverse behaviour of this system has not been included and MUST be included in the design method. Research on this will have to be done. Also, more research on the long-term behaviour of the deck-girder bond must be conducted. (Keller & Gürtler, 2005)

6.2.2.4.   Implementation

The method used by Keller show great promise in connecting an FRP bridge deck onto a steel girder. One should take into account a couple of things.

First of: according to regulation the connection cannot be solely bonded. Thus, does one want to create both a mechanically fasted and bonded connection? This should provide redundancy and an alternative load path in case of mechanical fastener failure.

Secondly does one wish to have composite action between the deck and the girders? This could beneficial. It has been done between concrete and steel and this is proven to work great and FRP and concrete do show to have similar stiffness properties. However, for FRP these differ in the transverse direction. Thus, for this to become a viable solution, research must be done into this topic. (As was suggested by Keller in their conclusion.)

In short: This method shows promise, but more research into the behaviour of its application will need to be done. Thus, for now, it could be used as an addition to the mechanically fastened connection IF the composite action is taken into account properly.

6.2.3. Satasiviam's shear connector (bonded)

The connection method (as well as the FRP decks) used in this research (Satasiviam, et al., 2013) are very similar to the ones by Keller et al. (Keller & Gürtler, 2005)

In this research a FEM analysis and experimental tests have been done on an FRP-deck bonded onto a steel girder. The results from these experiments match quite closely for most results. To investigate the axial strain distribution and shear lag effects, Satasiviam et al. did a parametric study. Here the conclusion was drawn that shear lag is influenced by loading level effects, the shear stiffness of the adhesive and the b/L ratio. This ratio was found to be a major determinant of shear lag, where an increase in the ratio resulted in a decrease of the effective width. The other aforementioned factors were not as significant. (Satasiviam, et al., 2013)

6.3.   Thermal influences

Temperature induced stresses become governing when applying different materials and connecting them such that each material cannot expand/contract independently. This is the case when allowing shear transfer between an FRP-deck and the steel girders. Shear transfer can only occur when slippage is hindered between these two elements and unfortunately these are the perfect circumstances for temperature induced stresses.

NOTE: this is theoretical. For the actual amount and ensuring that the joints will suffice the loading, calculations will be necessary, along with proper testing.

Since the focus of this thesis is on a large scale, this topic has been dealt with merely theoretically with a solution. For a full inclusion this should be calculated according, however this falls outside of the scope of this thesis.

6.3.1. Thermal expansion coefficients

A bridge is subjected to two kinds of temperature influences:

- The difference in environment temperature. This is the basis of the construction temperature. It increases and decreases during the day/night cycle throughout the year. This results shortening/ lengthening of the elements due to the temperature changes.
- The temperature difference due to external influences. This means a difference in temperature between the top/ bottom of the construction, due to for example harsh sunlight or a fire on top/ below the bridge. This results in a curvature of the bridge.

These can be described using the following formulas: (Hartsuiker, 2007)

$$\varepsilon_i^T = \alpha_i^T \cdot \Delta T^\varepsilon \qquad \qquad \kappa_i^T = \alpha_i^T \cdot \frac{\Delta T^\kappa}{h}$$

Where:

Symbol		Explanation	Unit
$\alpha_i^{T\,7}$	=	Thermal expansion coefficient (material and direction dependent);	[1/°K]
ε_i^{T}	=	Strain resulting from a temperature increase/ decrease;	[-]
ΔT^{ε}	=	Temperature increase/ decrease;	[°K]
κ_i^{T}	=	Curvature resulting from a temperature difference;	[1/m]
ΔT^{κ}	=	Temperature difference;	[°K]
h	=	Structural height of the cross section.	[m]

6.3.2. Bridge application

Since the deck and the girders are made of different materials and are located of different sides of the cross section (top vs bottom), both will be subjected to different strains and curvatures. For a bridge which allows composite action (or hybrid[8] interaction) this becomes an issue, since the elements are hindered from deforming independently. This leads to stress development. These stresses are a result from the difference in **thermal expansion coefficients**, the local **temperatures[9]** and **constrained movement**. The method used to connect the deck and the girders should accommodate for the excess stresses as a result of thermal influences.

When applying a bonded connection, this kind of stresses, will cause failure of the adhesive. To lengthen the duration of this adhesive failure, the type of joint should have a long length and be stepped or scarf like. (As is illustrated in Figure 6-1.) In the aerospace industry bonded joints have prover to function well. However, the lifespan of airplanes is considerably less than of bridges. This raises the question: Will this joint withstand the test of time? Thus, to be absolutely sure the bridge will not fail at this location in a timespan of at least 50 years, also mechanical fasteners should be used. It would catastrophic for FRP in the bridge industry were it to fail at a critical location such as this. In short: with the aim at future endeavours and continuing growth of FRP in the bridge industry, when bonded joint are applied, mechanical fasteners are applied for critical elements. This means if the bonded connection has failed, the bolted connection must take the load, meaning the connection has been made structurally redundant.

6.3.3. Practical solutions

Reviewing the case illustrated above, the failure of the adhesive occurs at the edges. This is where peak stresses occur. Countering this results in strengthening these specific locations. For mechanically fastened joints this principal remains. The highest loaded joints are located at the edges of the connections. Thus, the first to fail are the ones closest to the edge.

6.3.3.1. Mechanically fastened joints

For mechanically fastened joints the solution to counter the peak stresses is simple: apply a high density of joints at the critical locations. Which means more joints at the front and rear (cross) girders, along with both main girders and the cantilevering sides of all cross girders. For the simply centre span of the middle (cross) girders a less dense amount of joint is required.

---

[7] The thermal expansion coefficients used in this thesis can be found in Table C-8 in Appendix C.

[8] In the Design Study when the term **hybrid** (interaction) is mentioned this refers to the **composite action** as mentioned in this this chapter.

[9] The local temperatures are dependent on the location of each element in the cross section with respect to the external environment.

6.3.3.2.   Bonded joints

For bonded joints special attention is to be taken with regard to the edges of the adhesive. (as has been stated in the bottom text of section 0. Critical is that the above mentioned mechanically fastened joints should be applied together with the bonded joints, since the connection here is a critical connection. The bonded joints are applied along the entire connecting surface, whereas the application of the mechanical fasteners has been described above.

6.4.   Summary

When creating an FRP steel composite section an answer to following question should be given:

Should composite action between FRP and
steel be achieved or avoided?

When allowing composite action to occur, the location of the neutral axis (n.a.) shifts such that the bottom fibres of the steel are used much more effectively. (Their distance to the n.a. is greatly increased.) The downside here are the introduction of stresses under temperature influences, which can become significant for the connection between the two elements.

When the choice has been made to avoid composite action, the aforementioned temperature influences are no longer an issue, due to each material being able to extend/ contract on its own. However particular care should be taken to truly ensure that NO composite action occurs.

Depending on the answer, certain conditions must be achieved to allow for the correct outcome. This has been illustrated below:

1. Composite action:
    a. The **connection method** can either be done bonded or bolted. As long as Shear transfer is allowed between the FRP-deck and the steel girders.
    (Currently, in the case of bonding additional bolts need to be applied in the case of critical connections.)
    b. **Thermal induced stresses** are an arising issue. These are critical for the connection and should be dealt with accordingly.
    c. An **effective width** approach should be used on the FRP-deck, when calculating the sectional resistance.
    d. The **degree of composite action** also determines the sectional resistance and should be taken into account, not to overestimate the section.
2. No composite action:
    a. The **connection method** must allow the FRP-deck and steel girders to extend/ contract independently due to temperature changes. Also, it needs to keep the deck in place, both in the opened and closed condition.
    b. **No thermal induced stresses**, due to the above-mentioned connection approach.
    c. The **degree of composite action** should be very low to none.

7. Rules & Regulations regarding bridge design

In the Netherlands, bridge designs are to be verified using the Eurocode. In the codes restrictions and guidelines can be found regarding the imposed loads (and combinations) as well as the material-based resistance. Values regarding strength and deflection can be found in the Eurocode, but for the deflections of a traffic bridge there is no restriction given. For supporting edges (the connection onto the regular road) this is given and should be less than 5 mm. This also goes for a movable bridge (when it is closed). In addition, a movable bridge needs to be designed for both the opened and transfer phases (closed-to-open and open-to-closed). (Pavlovic & Kolstein, 2016)

In case of the open bridge, the wind is a major factor. The bridge acts like a windscreen. Therefore, there are restrictions to the wind-loads during (emergency) operations. This is not only a structural issue but also a mechanical issue. The bridge will need to be locked into place during its fully opened and fully closed condition. During the intermediate phase, the bridge will need to be stable and safe. This is achieved with a proper design of the mechanical- and safety system.

The guidelines used in Dutch movable bridge design are next: (Romeijn, 2006) (Heijmans, 2015)

- **NEN-EN 1990   –   Basis of structural design**
- **NEN-EN 1991   –   Actions on structures**
- **NEN-EN 1993   –   Design of steel structures**
- **NEN 6786   –   Movable bridges**
- **ROK 1.0   –   Design Guideline Civil Works**
- **CUR 96+   –   Dutch Design Guideline for FRP in Infrastructure**

The aforementioned guidelines combined result in design criteria and parameters for the designs. In this chapter the different criteria and parameters have been depicted. First off it should be mentioned that this case contains a movable bridge. This means there are different conditions for the bridge:

- Closed condition, outside the movement cycle.
- Non-closed condition, during the movement cycle.
- Non-closed condition, outside the movement cycle.

This distinction is made to determine the loads on the superstructure of the bridge, both during and outside of the movement cycle. (NNI, 2017) In this design study, the first and the latter conditions have been checked.

7.1.   Loading

According to the *Basis of structural design* of the Eurocode the different kinds of loading can be classified into permanent loading (G), variable loading (Q) and accidental loading (A). When combining loads, a combination factor, ψ, will have to be determined and multiplied to each segment. The different values for this combination factor, can be found in the aforementioned section of the Eurocode NEN-EN-1990; Table NB.9 – A2.1. To obtain design values for each loading, a multiplication with a partial safety factor, γ_f, is applied. The latter factor is applied to account for uncertainties / inaccuracies. (NNI, 2011)

Different load cases/ scenarios have been checked. For a full check, all conceivable worst-case scenarios should be checked. However, due to time constraints, a selection of several checks has been executed. These can be found in the Design Study, section 8.4 – Design verification.

7.2.   Resistance

The resistance of the structure is determined by all materials used. For each material their respective Eurocode section should be consulted. This has been done for steel (Eurocode: NEN-EN-1993). However, since there is no Eurocode for FRP, rather the CUR 96+ is to be consulted.

7.2.1. CUR 96+

In the design of an FRP structure in the Civil industry no Eurocode has been developed. To fill this empty slot the CUR 96+ has been created. The CUR 96+ has been created with the same safety philosophy as the Eurocode itself. The manner of using the CUR 96+ is mimicked unto the Eurocode, thus an implementation of the CUR 96+ into the Eurocode would be possible. The adapted safety philosophy is displayed next.

NOTE: This is an alteration compared to other materials in the Eurocode, by means of a conversion factor. (CURNET, 2003) This section has been translated from the CUR 96+, which is in Dutch. It can be found in Appendix B – CUR 96+.

Two

Design Study

8. General Design Approach

8.1.   Design objective

Weight reduction is the aim of this thesis. However, the goal is not to do a structural optimisation, since the original Amalia bridge itself, has not been structurally optimised. The original Amalia bridge is an economic optimisation. Here some elements/ sections have been made larger on purpose to reduce for instance the costs/ calculation time.

This lead the objective of this thesis to become a lower bound approach: the amount of weight saved, will increase as the design is optimised. The weight reduction values found in this thesis are the **minimal achievable values** for each respectable design.

Each design must fulfil the conditions set by the Eurocode, the Dutch National Annex and the, currently in development, CUR 96+.

Saving weight in the leaf of a movable bridge has many benefits. Several are:

-   The counterweight required for the bridge can also be reduced. Resulting in additional weight saving. If this reduction is significant enough, the counterweight can be moved closer to the rotation centre, allowing for shorter main girders. Possibly even leading to the redundancy of the basement, which composes a considerable part of the costs for a bascule bridge. A length section of the bridge can be seen in Figure 8-1. On the left side of the illustration, the counterweight is lower than the water level, thus the need for a basement.
-   When installing the bridge, less weight will need to be moved into place, thus requiring less energy during shipment and installation.
-   The same applies to the use phase. The weight, which has to be moved by the mechanical system, is reduced. Thus, less engine power is required for the mechanical system to set the bridge into motion. Meaning less energy required during operation.
-   Less weight is resting on the abutments, resulting in lower strength capacity required for these abutments. Meaning fewer piles are required for the foundation, which is a costly expense. And, not to forget, less energy will be necessary during construction.

As has been illustrated above, the benefits can have a beneficial influence on the total financial picture of the bridge. The benefits of weight saving in the leaf, are not restricted to the leaf alone, but have a tremendous influence on the rest of the bridge, both in construction and operation.

Weight reduction is achieved if the mass of the original design is higher when compared to the adapted design:

$$\sum m_{Amalia} > \sum m_{adaption}$$

To achieve weight reduction the material FRP has been used. Its properties (high strength together with, low self-weight) make it a suitable option. In this design study **two alternatives** will be given: a **hybrid** construction and a **non**-**hybrid** construction.[10] To obtain the total mass, the sum of the different elements must be taken. Since each element has a different density and volume:

$$\sum m_{Amalia} > \sum \rho_i \cdot V_i$$

8.2.   Design basis

First of the *technical description of the leaf of the Amalia bridge* has been examined. This document has been supplied (and created) by Movares, commissioned by, Heijmans. Here Mark van der Burg, the lead author, illustrates the entire built up of the movable section, along with all the applied load models, including the governing design criteria. (Heijmans, 2015)

In the calculations made for the original design the different load cases were grouped into the two states (SLS and ULS). For each state an enveloping stress diagram was made and used for the unity checks. Since these enveloping stress diagrams contain a great number of load cases, an engineering approach was used and only load cases, leading to governing stresses, were applied.

8.2.1. Critical load

The most governing section of the Amalia bridge is located at the end girder. At this location the web and the bottom flange, of the main girders, are most critical for **fatigue** loading. This governing criterium of fatigue loading is caused by the opening and closing cycle of the bridge and is the only governing load leading to fatigue damages. (Vibrations of the counterweight and different traffic loads leading to stress alterations are not governing in this case) This can be reviewed in Appendix E, section E.3. To ensure that the designs created for this thesis have the same location of the governing load, the built up of the bottom flanges of the main girders have been made identical. The same assumption has been made as has been done for the original Amalia bridge. Resulting in the same location/ load case as. This is therefore the governing criterium in creating the designs for this thesis.

This results into two different situations. The mechanical schemes for these conditions have been illustrated in Figure 8-3 and Figure 8-4 and an impression of the closed/ opened condition of the bridge, along with the bascule basement can be seen below (Heijmans, 2015). A more detailed explanation on this fatigue calculation, can be reviewed in the aforementioned appendix. Here the differences between SCIA and Abaqus are also addressed.

---

[10] The definition of a (non-) hybrid construction has been defined in section 6.4 of the Literature Study.
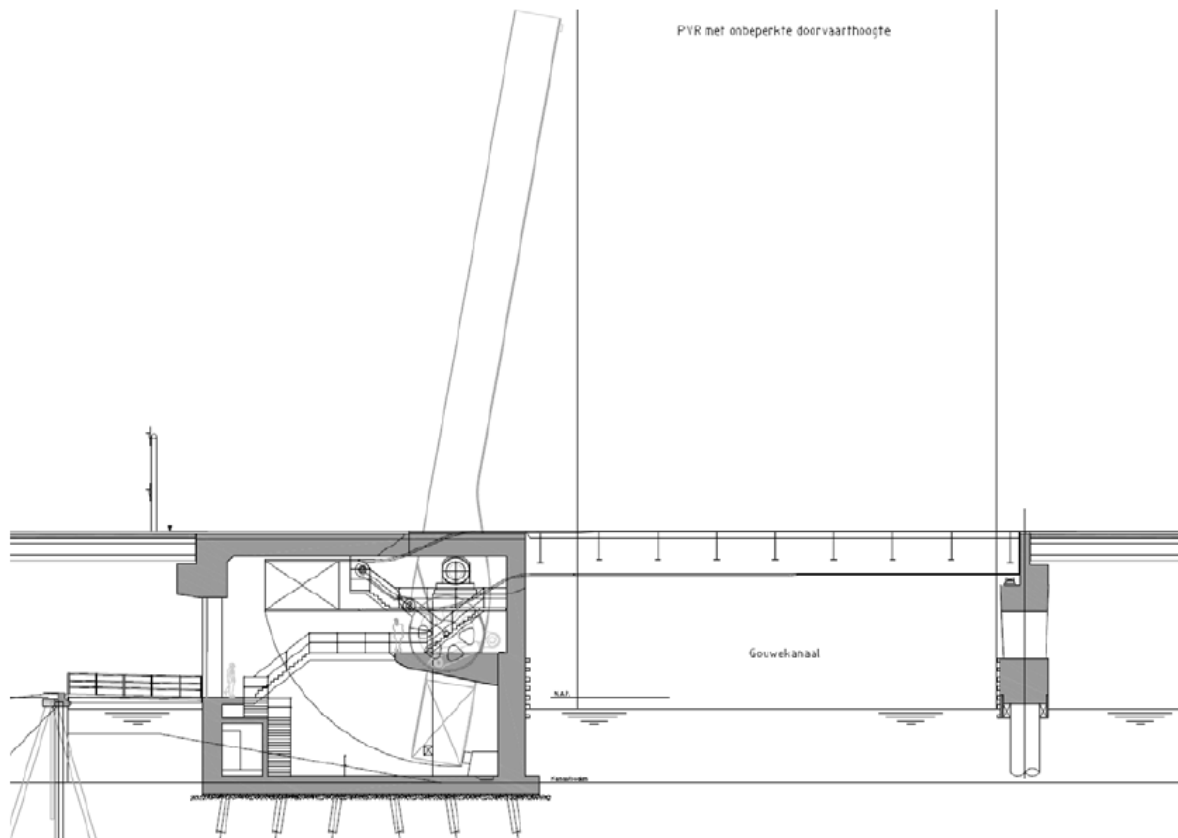
Figure 8-1 Impression opened & closed condition of the bridge (Heijmans, 2015)

The designs created in this thesis, are to be comparable to the current Amalia bridge. It makes sense that, for comparable designs, this location and condition would result in a similar governing criterium. To ensure the location of these governing stresses do not differ from the original and since, the focus of this thesis lies on the implementation of FRP, rather than the optimisation of the steel girders, the choice has been made to maintain the bottom flange of the main girders from the original design. Since these are sufficient in the case of the original Amalia bridge, they will also be sufficient for the designs created for this thesis. Combining this with the reductions in weight in other sections, one can say with certainty

NOTE: for the original Amalia-bridge design an orthotropic steel deck is used with troughs. This has another critical location, governed by fatigue loading. However, the designs discussed in this thesis, will not contain a steel orthotropic deck and troughs, thus this criterium is not governing.

8.3. Modelling in Abaqus

8.3.1. Comparing models

The model made by Mark van der Burg from Movares, has been done in SCIA-Engineer. The models created in this thesis have been made in Simulia Abaqus. To have comparable results, first the original Amalia bridge has been modelled in Abaqus. Thus, in this thesis the comparison will be made between the models created in Abaqus. Only in the first step, when designing the original Amalia bridge in Abaqus, will there be a comparison between models of the different FEM-programs. Thus, unless further specified, when the Amalia bridge is mentioned, the model of the Amalia bridge in **Abaqus** is meant.
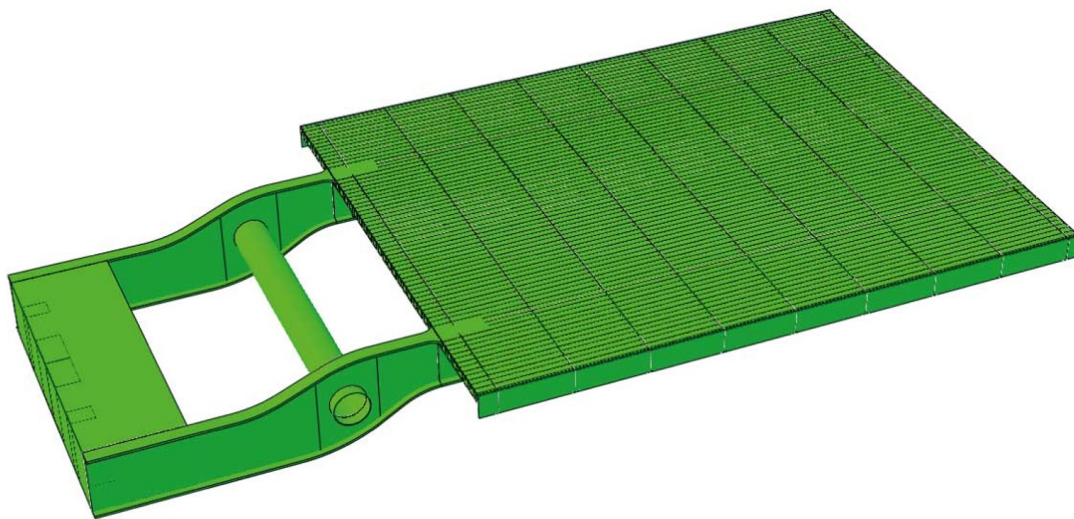
Figure 8-2 Impression original Amalia bridge - Abaqus

The original Amalia bridge in Abaqus has been made such that the stresses related to the aforementioned governing criterium correspond between the design made in SCIA-Engineer and Abaqus.

There are some differences between both models of the original Amalia bridge:

- The SCIA-model is built up of shell elements, whereas the Abaqus-model is composed of solid elements.
  NOTE: In this thesis the choice has to be made between using solid or shell elements, solid have been chosen since the interaction between different elements became much easier and it reduced calculation time drastically. It also resulted in a visually improved representation of reality, due to thicknesses of the plates. Another choice had to be made between the properties of the solid element, meaning 3D-stress or shell (planar) stress. Here, no significant stress differences were found between the two, thus 3D-stress was used. This choice is simply based upon readability of the results.
- The total mass differs slightly, thus the counterweight has been re-determined for the Abaqus-model. This latter calculation can be reviewed in Appendix E– Weight calculation.
- Then it should be noted that each program has its code to model the behaviour of a structural element. In theory these should result in identical results, however. Since there are multiple roads to Rome, slight differences may occur along the road. Especially in calculations which are not as straight forward as for instance force times arm quals moment.

8.3.2. Boundary conditions

In the design verifications, which will be dealt with in the next section, different boundary conditions have been applied. Since this is a movable bridge, also the conditions of an opened bridge must be considered. For fatigue damage calculation, where the self-weight is the governing load, the bridge has been considered in the extremes of the opening and closing cycle. In the other load cases, the closed situation of the bridge has been used. These are illustrated below:

8.3.2.1.   Just opened condition

In the just opened condition , four simple supports have been used. Two are located at the axle and two are located at the counterweight, where the counterweight is supported by the mechanical system to set the bridge into motion. The latter the support is such that movement in longitudinal directed, has not been restricted.

Figure 8-3 Mechanical scheme – just opened condition

8.3.2.2.   Fully opened condition

In the fully opened condition , four simple supports have been used. Two are located at the axle and two are located at the counterweight, where the counterweight is supported by the mechanical system to set the bridge into motion. The latter the support is such that movement in longitudinal directed, has not been restricted. The difference between the just opened condition, is the rotation of the bridge into its opened stage, with a rotation of 78 degrees.
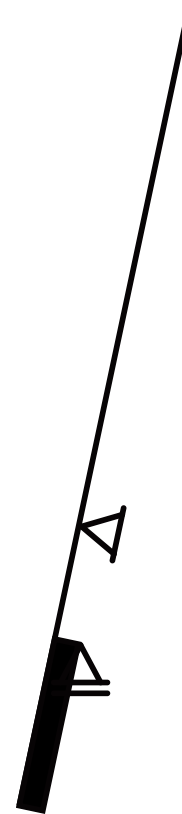
Figure 8-4 Mechanical scheme – fully opened condition

8.3.2.3.   Closed condition

In the closed condition the bridge is simply supported at four locations. Two are located at the axle, whereas the other two are located at the tip of the leaf, below the main girders. At the latter the support is such that movement in longitudinal directed, has not been restricted.

Figure 8-5 Mechanical scheme – closed condition

NOTE: In the closed condition the, counterweight is supported by the axle system which allows for the opening of the bridge. This can be modelled by placing an equivalent force in the required direction. This value is obtained by placing a support at this location. When the bridge opens this load, first helps in keeping the bridge closed, then the bridge is set in motion, this force is reduced and eventually helps opening the bridge. (This is, of course, its function.)

The closed condition has been chosen at the moment where this force can be considered a support, which lies between the above described conditions.

8.4.   Design verification

When designing a bridge, a large amount of load cases and combinations should be checked. To ensure all maximum loads are taken into account, one figure, composed of the extremes of all possible load cases should be made. This is than compared to the allowed maximum stresses.

For this thesis, however, this is to elaborate. The goal is to design two alternatives and make a qualitive comparisons between them and the original. Thus, a restriction to the amount of checks has been made.

As stated earlier, the fatigue load and location from the Amalia bridge are used to design the alternatives. Including this, the following checks will be conducted to check the integrity of the bridge and its deck:

LM1	LM2	LM4	Fatigue (Self-weight)
Deck	Deck	Main girder	Main girder
Main girder		Cross girder	
Cross girder			

Table 8-1 Loads used for different checks

The details for these different checks have been elaborated in Appendix D.

NOTE: For the steel elements, in some cases, the Von Mises stress values can be used, since steel is an isotropic material. For FRP however, a distinction must always be made in the primary stresses and their shear stress.

9. Original Amalia Bridge

9.1.　General description

This moveable bridge section is a bascule system bridge. It consists of an orthotropic steel deck, supported by nine cross and two main girders, balanced by a counterweight around an axle. The edges of the bridge (both the sides, as well as the front and the back) are covered with an additional steel plate. On these side plates covers are added, which includes a railing. Not to be mistaken with the guard rail, which is located more internally. These covers allow for the aesthetics of the bridge deck.

9.2.　Sectional drawings

Below a small illustration of the bridge built up has been given by means of two cross sections. A larger version of these drawings can be seen in Appendix D.
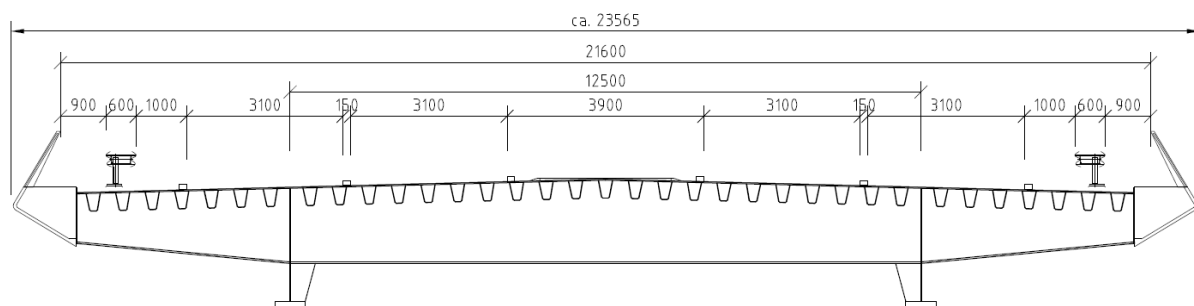
Figure 9-1 Cross section of the orignal Amalia bridge (Heijmans, 2015)
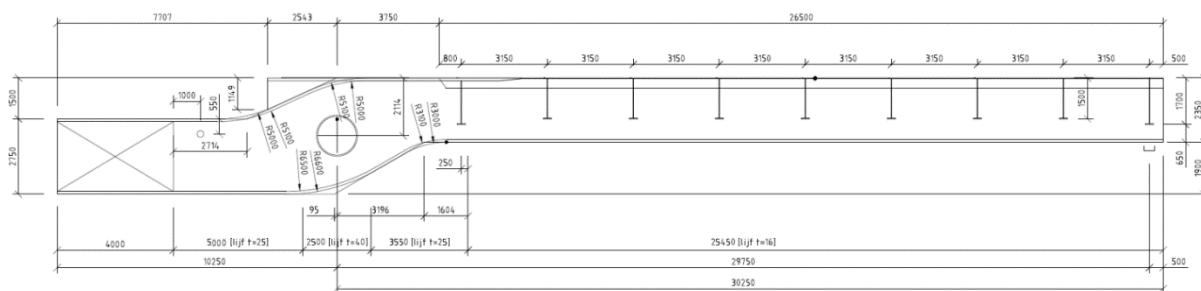
Figure 9-2 Cross section of the orignal Amalia bridge (Heijmans, 2015)

9.3.　Weight and counterweight calculation

When creating the model in Abaqus, a counterweight must be used such that the bridge will have the proper overclose pressure. In the case of the Amalia bridge, according to the documentation of Movares (Heijmans), an overclose pressure of 30 kN is required to ensure that the bridge will remain closed in closed condition, even if winds are present. Thus, since the Abaqus model differs from the SCIA-model, a new counterweight has been designed to ensure this fact. The calculation for the counterweight, along with the balancing of the bridge, can be found in Appendix D – Weight

calculation. Next a brief weight distribution has been given, non-hybrid into the different structural elements.

Whole bridge	Amalia bridge	
	[kN]	
Deck-system	1369	16%
Main girders	783	9%
Cross girders	435	5%
Counterweight	5176	61%
Axle	194	2%
Rest	515	6%
Total bridge	**8472**	**100%**

Table 9-1 Weight distribution Amalia bridge

As Table 9-1 clearly illustrates, the mayor weight is in the counterweight. This means, that weight saved in any other element, will also reflect in this section. The second heaviest element is the bridge deck. This is where the arrow of this thesis is focused at. The other two main elements will have the aim to remain about the same size if possible.

Since the counterweight has been determined to balance the bridge on both sides of the rotation centre (the axle), a slightly more detailed exposition on this weight distribution, has been illustrated below. These are based upon the weight calculations, which can be found in Appendix D – Weight calculation.

The counterweight-side of the bridge

Counterweight	Amalia bridge	
	[kN]	
Main girders	278	5%
Axle	97	2%
CW-box	640	11%
CW-content	4535	81%
Conservation	20	0.4%
Total bridge	**5571**	**100%**

Table 9-2 Weight devision in the countweight section of the Amalia bridge

The leaf-side of the bridge

Leaf-section	Amalia bridge	
	[kN]	
Deck-system	1369	47%
Main girders	505	17%
Cross girders	435	15%
Axle	97	3%
Conservation	24	0.8%
Road equipment	471	16%
Total bridge	**2901**	**100%**

Table 9-3 Weight devision in the leaf section of the Amalia bridge

Table 9-2 shows that the left side of the bridge almost completely contains the counterweight (81%). This makes sense, since this is its function. Which illustrates that any weight saved in the leaf of the bridge directly correlates to weight saving in the counterweight.

Table 9-3 shows that the deck almost provides for half of the weight in the leaf of the bridge (47%), whereas the girders only account for almost a third of the weight (32%). This data supports the goal of this thesis, as to where the weight saving of this bridge type is most beneficial.

9.4.   Fatigue verification

As stated earlier, in chapter 8, fatigue damage is the governing scenario for the original Amalia bridge. The model created in Abaqus is compared to the SCIA model, by means of this scenario. In Appendix E – Fatigue verification, a detailed explanation and verification can be found. Here a brief summary is given.

9.4.1. Brief summary

In the case of fatigue loading, different load cases on the bridge are examined, each case resulting into fatigue damage. Then the sum of these different load cases is taken and a total damage number is found. For the Amalia bridge in the SCIA model, only the load case of the opening and closing cycle, resulted in damage. Thus, this is the section that is compared between the SCIA model and the Abaqus model, for the governing sections.

For the total stress and damages resulting from this load case, the sum of the damage resulting from the longitudinal stress in the bottom flange and the radial stress in the web have to be taken.

	SCIA-model		Abaqus model	
	$\Delta\sigma_c$ [MPa]	Damage [-]	$\Delta\sigma_c$ [MPa]	Damage [-]
Results from stresses in longitudinal direction (S11)	89.85	0.46	84.30	0.377
Results from stress in radial direction (S22)	76.56	0.55	51.65	0.379
SUM		**1.01**		**0.757**

Table 9-4 Comparison fatigue results between SCIA and Abaqus

In the table above, one can see a difference in the values resulting from S11. This difference is deemed to be close enough to be comparable. The values resulting from S22, differ significantly more. This is due to a difference in S22 in the fully opened condition. In the SCIA model a stress of 92 MPa has been found, whereas in the Abaqus model only a stress of 70 MPa has been found.

This difference in stresses is significant, even though the physical measurements of models created in SCIA-engineer and Simulia Abaqus are almost identical. The exception being the use of solids vs shells, resulting in overlapping elements.

9.4.2. Conclusion

The results following from model in SCIA, clearly are different from the ones following from Abaqus. They have been deemed to be comparable enough. However, to compare the adaptation designs for fatigue loading, they will be compared to the Abaqus model, not the SCIA model.

10. Design 1 – Non-hybrid

*Replacing the steel orthotropic plate deck, with an FRP alternative, **without** making use of hybrid interaction between the steel girders and the FRP deck.*

10.1.   General description

This design has the basis of the original Amalia bridge and is based upon an orthotropic steel plate deck, bascule bridge design. The deck plate, along with the troughs have been removed. They have been replaced with an FRP-sandwich deck. This is combined with modifications of the girders to implement the aforementioned deck.

This adaption does **not** include hybrid interaction between the different materials used in the deck and the girders.

10.1.1. Basis of the design

Based on the governing fatigue loading for the original Amalia bridge, this bridge has been designed. (This has been explained in section 9.4 – Fatigue verification.) For this design, the bridge deck is not an integral part of the main load bearing structure, thus balanced main and cross girders have been applied.

10.2.   Design elements

The bridge consists of the following main elements:

10.2.1. Deck built up

The deck is an FRP sandwich deck, consisting of a top and bottom flange, with a large number of slim webs to create the required construction height. In Figure 10-1 an illustration of the applied deck has been shown. Here the different measurements are shown. An essential part of the design is the use of the Z-shaped profile approach of FiberCore. This means that the top facing is connected directly to the bottom facing through the webs. This ensures, in case of damages, that these remain contained and do not spread. This results in a ply of the facings on either side of the webs. This last is clearly visible in the close up view of the aforementioned figure. The facing plies are coloured **blue**, whereas the web plies are coloured **orange**.

In the orthotropic steel bridge deck design, the deck has been 'sunk' in between the girders, this has not been done with the FRP-deck. The main reasoning here is to create a continuous deck, rather than separate sections.

10.2.1.1.   Top/bottom facing

The built-up of the top and bottom facing are similar. These are based on the stacking of several plies of the FiberCore skin laminates, which are also located on either side of the webs. In total reaching the thickness are has been illustrated in Figure 10-2.

10.2.1.2.   Webs

The built-up of the webs is a combination of both FiberCore laminates used: the skin laminates (which the top/bottom facings are composed of and the flutes laminates. More detail on the exact built-up of the layers can be found in section 10.2.1.5.

10.2.1.3.   Front/ back covers

To create a fully closed deck covers are used at the front and the rear of deck, with the same principal as has been used for the webs, thus the properties are the same.
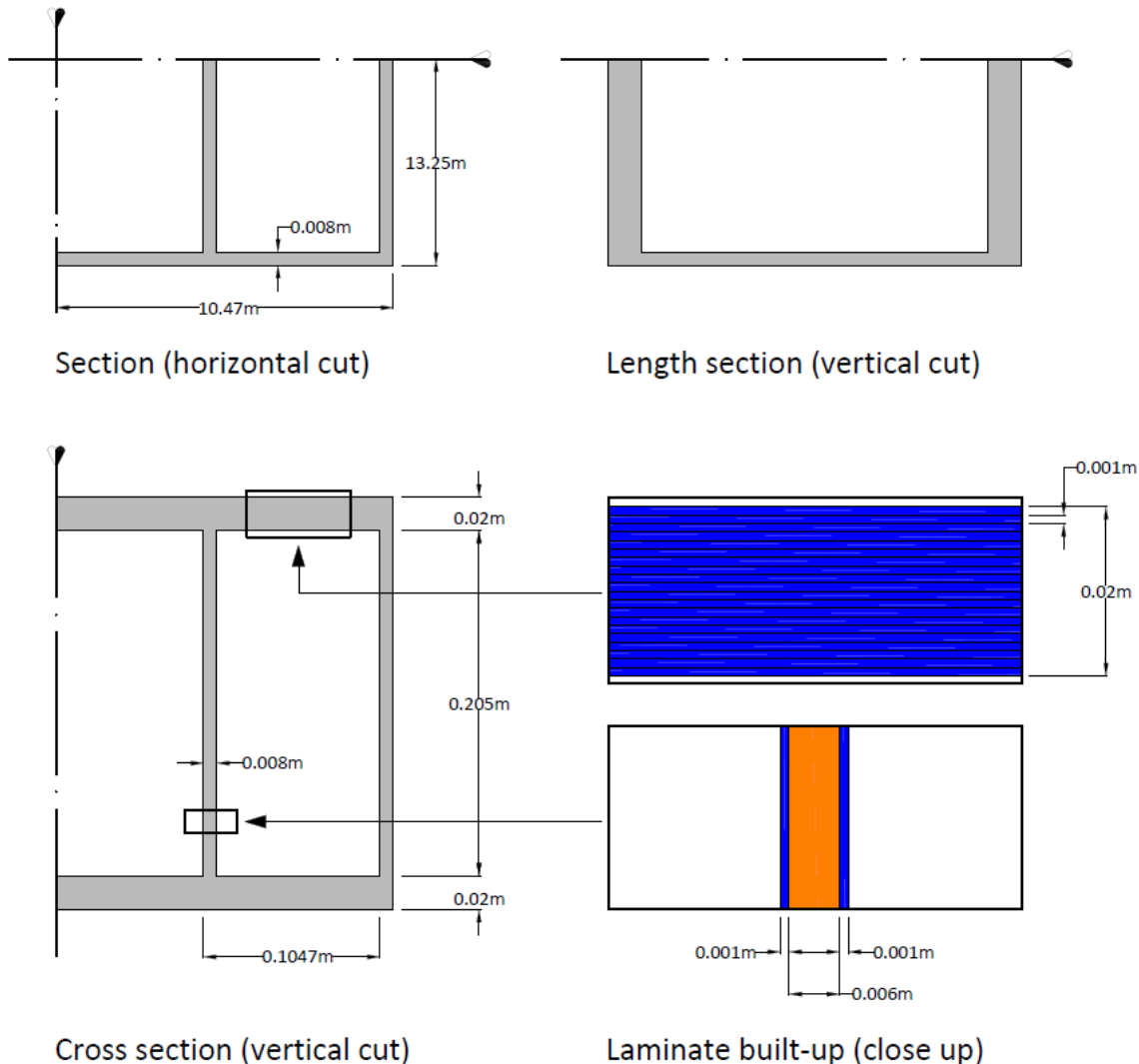
Figure 10-1 Technical drawing of the FRP deck

10.2.1.4.   Production

The product is a VARTM method. The sheets with fibres are laid down on a mould, while using PUR-cores to ensure the correct placement of the sheets, especially the webs and the bottom facing. The latter might seem strange, but to have a smoother top surface, the element is made bottom up. Thus, the bottom facing lies on top. Next the whole element is closed off with a bag, to seal off the vacuumable area.

NOTE: For modelling simplification, the z-shape has not been modelled. The deck has been simplified into a top layer, multiple webs and a bottom layer. The cores have also not been modelled, since they are considered to be 'lost'. This means their sole purpose is to place the fibres for the moulding process. They give no structural strength/ stiffness.

10.2.1.5. Layers

Below three tables are displayed illustrating the ply-composition of each layer; the measurements belonging to the respective layers; and their mechanical properties.

Laminates	Material	Built up	Angles [degrees]			
			0	90	45	-45
Top facing (skin)	GFRP	[0,90]s	75%	25%		
Webs (flutes)	GFRP	[90,+/-45]s		50%	25%	25%
Front/back (flutes)	GFRP	[90,+/-45]s		50%	25%	25%
Bottom (skin)	GFRP	[0,90]s	75%	25%		

Table 10-1 Layer composition – non-hybrid (FiberCore europe, n.d.)

In the close up of Figure 10-1 the FiberCore skin plies are illustrated with a **blue** colour, whereas the FiberCore flutes plies are illustrated with an **orange** colour.

Laminate	Width	Length	Thickness	Amount
	[mm]	[mm]	[mm]	[-]
Top facing	20940	26500	20	1
Webs	205	26500	8[11]	201
Front/back	205	20940	8	2
Bottom facing	20940	26500	20	1

Table 10-2 Layer measurements – non-hybrid

The layers have been calculated to have the following properties. This is based upon test results received from FiberCore, which can be reviewed in section C.3 of Appendix C.

Laminate	E1	E2	Nu12	G12	G13	G23
	[GPa]	[GPa]	[-]	[GPa]	[GPa]	[GPa]
Top facing	28.29	15.48	0.27	5.13	5.13	5.13
Webs[12]	14.08	16.73	0.29	5.20	5.20	5.20
Front/back	14.08	16.73	0.29	5.20	5.20	5.20
Bottom facing	28.29	15.48	0.27	5.13	5.13	5.13

Table 10-3 Layer properties – non-hybrid (FiberCore europe, n.d.)

NOTE: to comply with the CUR 96+, the material must be verified by means of testing. This is due to the fact that not each laminate has 15% of the fibres in each direction. In this case, the values are obtained from FiberCore and are from tests, therefore they are assumed to be applicable with the CUR 96+. However, for full inclusion and in case of execution, they still must be verified by testing specimens. (CURNET, 2003)

---

[11] The web-section contains both laminates. Due to the continuation of the top facing through the webs into the bottom facing. Thus the thickness of 6 mm, represents the total thickness of the webs. This laminate can be divided into **facing plies of 1 mm**, followed by **web plies of 6 mm** and **facing plies of 1 mm**.

[12] The web properties mentioned in Table 10-3, are calculated using classical laminate theory by stacking the different FiberCore laminates used. In Abaqus the properties are calculated using the same approach, which is done by Abaqus itself. The same principle applies to the front/ back covers.

10.2.2. Main girders

The main girders have been designed by creating a balanced I-profile, with the stresses found in governing load cases, comparable to the original Amalia bridge, at the same locations. In essence:

$$\sigma_{gov,Amalia} \cong \sigma_{gov,Adapt}$$

This has been done, to have comparable bridge alternatives. Comparable in the sense that they have similar maximum stresses and fatigue resistance. The latter is truly hard to achieve and comes with a very large uncertainty, due to the influence a slight stress difference has on its resulting fatigue damages.

This comparability has been done for two different locations: the first is the fatigue location, which is located at beneath the rear cross girder and the second is at the max deflection of the main girder.

Another restriction in this design has been the total structural height of the bridge. This must not exceed the total structural height as was the case for the original Amalia bridge:

$$h_{Amalia} = 2350 \, mm \geq h_{adapt} + h_{deck} \rightarrow h_{adapt} \leq 2105 \, mm$$

Where the total thickness of the deck is:

$$h_{deck} = 245 \, mm$$

This is essential at the leaf of the bridge, since the clearance gauge of the waterway, cannot be interfered. For the counterweight section, this should not be increased, since this would result in a basement which would need a larger excavation. This resulted in the following cross sections for the main girder in the leaf of the bridge:
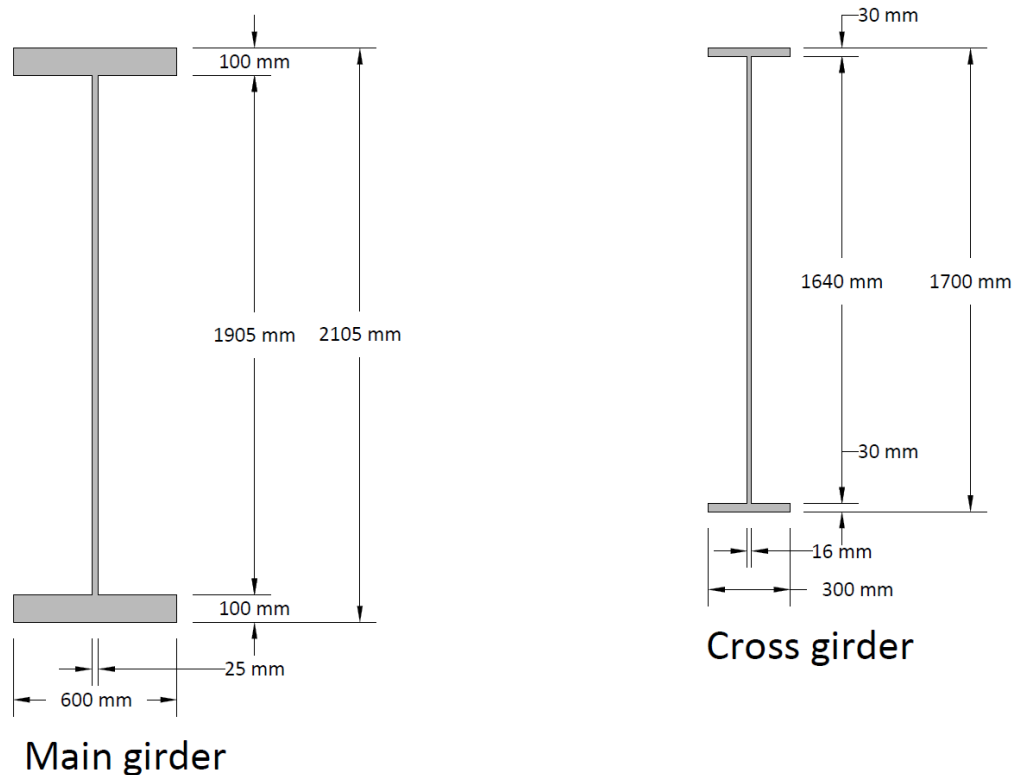
Figure 10-2 Cross sections of the main and cross girders – non-hybrid

10.2.3. Cross girders

For the cross girders, the same approach has been used as for the main girders. The created balanced cross girders come in two different heights; 1500 and 1700 mm. The rest of the measurements remain the same. Here the latter of the two, the one displayed in Figure 10-2, is located closest the front and the back of the leaf.

NOTE: due to the implementation of balanced I-profiles; a significant increase in weight is achieved.

10.2.4. Connecting the elements

All the elements are connected by means of welding. With the exception for the connection between FRP and steel; the deck and the girders. These elements are to function separately. Thus, a partial connection is required and not all movement should be hindered.

10.2.4.1. Reality

To achieve this, a system based upon the Davalos connector is used. This connector allows for the transfer of shear forces, which is needed at a single location to fix the deck onto the girders. This Davalos connector, as can be reviewed in chapter 6.2.1, is a bolted connection. A hole is drilled in the FRP-deck, special steel sleeves are placed at the top and bottom of the deck, with a shear stud passing though. These are then tightened with a bolt, thus clamping the deck together, allowing shear transfer though the stud to the load bearing girders. The rest of the connectors will be adapted versions of the Davalos connector, which allows either translation in one or two directions. This is done by increasing the hole and bolt width size, as well as the steel sleeves. In this manner, the two bridge elements (deck and girders) can expand/ contract individually, while remaining fixed enough, to allow for the opening and closing of the bridge.

10.2.4.2. Modelled

To achieve this in the Abaqus model, while not increasing the work/calculation load due to creating each and every individual connection, an interaction property has been defined. Defining the interaction between the deck and the girders, representing the aforementioned, stud-based, shear transfer system. The behaviour, as used in Abaqus has been defined below:

Normal behaviour   **Tangential behaviour**
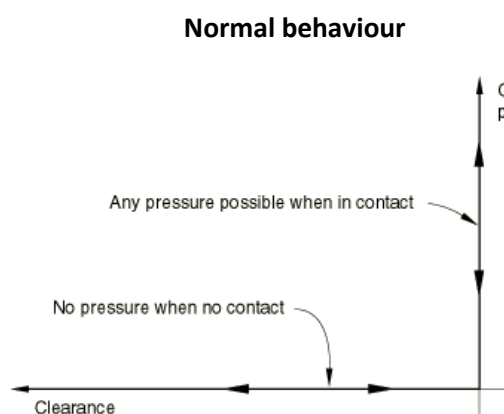
Figure 10-3 Default pressure-overclosure relationship (Simulia - Abaqus, 2018)
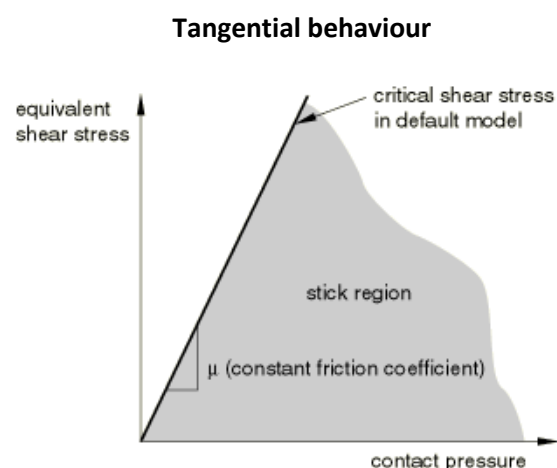
Figure 10-4 Slip regions for the basic Coulomb friction model (Simulia - Abaqus, 2018)

10.2.4.2.1. Normal behaviour

The normal behaviour is defined as '*pressure-overclosure – hard contact*'. According to the Abaqus Analysis User's Guide is defined as:

> *The "hard" contact relationship minimizes the penetration of the slave surface into the master surface at the constraint locations and does not allow the transfer of tensile stress across the interface.* (Simulia - Abaqus, 2018)

This results in transfer of contact pressure when the clearance between surfaces is equal to zero. Surfaces will separate in case the contact pressure is reduced to zero. This behaviour is illustrated in Figure 10-3.

To allow for tensile stresses to occur. The 'no-separation' relationship is used. This allows surfaces that have come into contact to stay in contact, even if this results into tensile stresses. This is only allowed for pure master-slave contact pairs and cannot be used in adaptive meshing. (This is the case in the created models.) To allow this, tangential behaviour properties must be defined.

10.2.4.2.2. Tangential behaviour

The tangential behaviour has been set as a penalty value using an isotropic friction coefficient of 0.05. This frictional behaviour is based on the Coulomb friction model. The default model has been used, which means that the friction is defined as a function of the equivalent slip rate and contact pressure. This behaviour has been illustrated in Figure 10-4.

10.3. Weight and counterweight calculation

Using the same approach as for the original Amalia bridge, the weight and counterweight have been calculated. These calculations can be found in Appendix F – Weight calculation. The table shown below illustrates weight distribution of the non-hybrid design. It can also be found in the aforementioned appendix:

Bridge-section	Amalia bridge		Non-hybrid	
	[kN]		[kN]	
Deck-system	1369	16%	702	10%
Main girders	783	9%	918	13%
Cross girders	435	5%	588	8%
Counterweight	5176	61%	4187	59%
Axle	194	2%	194	3%
Rest	515	6%	503	7%
Total bridge	**8472**	**100%**	**7092**	**100%**

Table 10-4 Absolute weight distribution (Amalia and non-hybrid)

Comparing the non-hybrid design to the original Amalia bridge, related to each bridge's total weight, results in:

- a great reduction in weight contribution of the deck system;
- an increase in weight contribution of the main girders;
- a great increase in weight contribution of the cross girders;
- a slight increase in counterweight contribution;

Comparing the non-hybrid design to the original Amalia bridge, relative to their respective parts from the original Amalia bridge:

Whole bridge	Amalia bridge		Non-hybrid	
	[kN]		[kN]	
Deck-system	1369	100%	702	51%
Main girders	783	100%	918	117%
Cross girders	435	100%	588	135%
Counterweight	5176	100%	4187	81%
Axle	194	100%	194	100%
Rest	515	100%	503	98%
Total bridge	**8472**	**100%**	**7092**	**84%**

Table 10-5 Relative weight distribution (Amalia and non-hybrid)

In Table 10-5 the weight savings have been visualized, compared to the original weight distribution. This clearly shows that weight can be saved in the deck, by applying FRP. However, as a result of the implementation of the balanced girders, an increase of the weight in the main and cross girders is found. Nonetheless the bridge's weight has been reduced with **16%**.

For a visual overview and exposition of the weight comparison between each bridge and their corresponding elements, please review section Appendix H.

10.4. Load cases / verification

The load placements and the approach used in for the different load cases, can be found in Appendix D. For a detailed review of each load cases and their verifications, please view their respective appendices:

10.4.1. LM1

- Appendix F; section F.3.1.1 – Deck, illustrates the verifications made for the deck. This includes the top and bottom facing as well as the webs. The maximum UC-value has been reached for the shear stress (S12) in the webs of the deck:

$$UC = 0.784$$

- Appendix F; section F.3.1.2 – Main girders, illustrates the verifications made for the main girders. The Von Mises stress resulted in the following unity check:

$$UC = 0.836$$

- Appendix F; section F.3.1.3 – Cross girders, illustrates the verifications made for the cross girders. The Von Mises stress resulted in the following unity check:

$$UC = 0.576$$

10.4.2. LM2

Appendix F; section F.3.2, illustrates the verifications made for the webs of the deck. This includes both strength and stability. The stability is governing here, due to the slim webs; resulting in:

$$\alpha_{cr} = 4.2481$$

10.4.3. LM4

- Appendix F; section F.3.3.1 – Main girders, illustrates the verifications made for the main girders. The Von Mises stress resulted in the following unity check:

$$UC = 0.195$$

- Appendix F; section F.3.3.2 – Cross girders (centre span) , illustrates the verifications made for the cross girders. The Von Mises stress resulted in the following unity check:

$$UC = 0.116$$

- Appendix F; section F.3.3.3 – Cross girders (side span), illustrates the verifications made for the cross girders. The Von Mises stress resulted in the following unity check:

$$UC = 0.078$$

10.4.4. Fatigue verification

Appendix F; section F.2.6 – Fatigue verification, illustrates the verifications for the opening and closing cycle of the bridge. As has been stated in the General Design Approach, this loading has been assumed to be the only load leading to fatigue damages.

	Amalia bridge (Abaqus)		Non-hybrid	
	$\Delta\sigma_c$ [MPa]	Damage [-]	$\Delta\sigma_c$ [MPa]	Damage [-]
Results from stresses in longitudinal direction (S11)	84.30	0.377	67.50	0.378
Results from stress in radial direction (S22)	51.65	0.379	43.51	0.161
SUM		**0.757**		**0.539**

Table 10-6 Comparison fatigue results between the original Amalia bridge (Abaqus model) and the non hybrid design.

Table 10-6 illustrates a comparison between the original Amalia bridge and the non-hybrid design. The fatigue damage resulting from the longitudinal stresses are almost identical, even though the stress differences are not. This is due to the calculation method used. For the radial direction, the opposite can be said. (The stresses differences are closer to each other than the fatigue damages.

For this one must conclude that the damages obtained in fatigue calculations are very sensitive to the stress differences used and their magnitude, compared to the *design value of the detail category* and the *constant amplitude limit*.

Nonetheless the non-hybrid design is safe with regard to fatigue design, at this location.

11. Design 2 – Hybrid

*Replacing the steel orthotropic plate deck, with an FRP alternative, **whilst** making use of hybrid interaction between the steel girders and the FRP deck.*

11.1.   General description

This design has the basis of the original Amalia bridge and is based upon an orthotropic steel plate deck, bascule bridge design. The deck plate, along with the troughs have been removed. They have been replaced with an FRP-sandwich deck. This is combined with modifications of the main and cross girders to implement the aforementioned deck.

This adaption **does** include hybrid interaction between the different materials used in the deck and the girders.

11.1.1. Basis of the design

This hybrid alternative for the Amalia bridge is essentially an adaption of the earlier made non-hybrid design. Whereas the previous design does not include the deck to contribute in the total load bearing capacity, this option does. In essence this option is a reduction of the top flanges of both main and cross girders. However, it should be noted, due to stress concentrations in the main girders when nearing the rotation centre of the bridge, less to no reduction of the top steel flange is possible.

11.2.   Design elements

The bridge consists of the following main elements:

11.2.1. Deck built up

The deck built up for this design is identical to the one used for the non-hybrid design. For the details regarding the different elements please review section 10.2.1. Here an impression of this deck can be seen in Figure 10-1, whereas the properties of the different elements in the deck are found in section 10.2.1.5 – Layers.

11.2.2. Main girders

The main girders for this hybrid design are an adaption of the non-hybrid design, with the same basis regarding the stress levels found in the bottom fibres as well as the height limit. In this case, the top flange of the main girders has been reduced only in the sections connected to the FRP-deck. This has been done, since this design has hybrid interaction and the FRP-deck, functions as the top flange of the main (and cross) girders. This resulted in the following cross sections for the main girder in the leaf of the bridge:

NOTE: For a cross sectional view of the bridge, please review Figure G-3 and Figure G-4, located in Appendix G – Bridge built up.
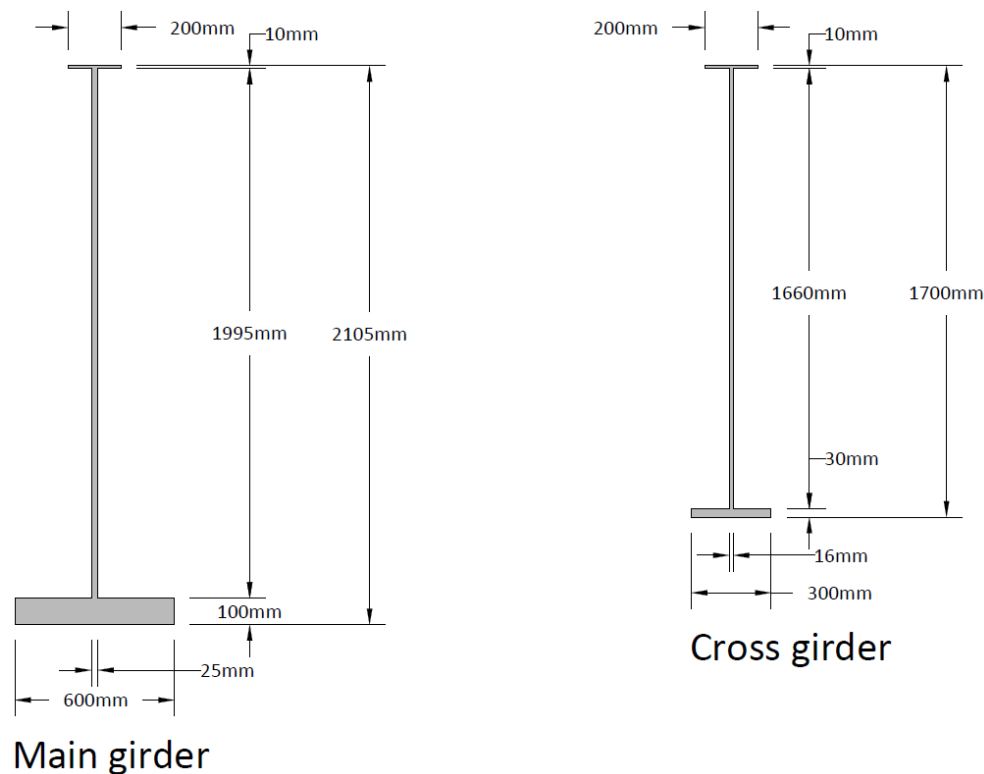
Figure 11-1 Cross sections of the main and cross girders – non-hybrid

NOTE: the girders, as shown in Figure 11-1, seem to be out of balance. (resulting in a neutral axis (n.a.) to be very near the bottom flange) This is true, were it not for the hybrid interaction. The (effective) FRP-deck functions as the top flange of the girders, raising the n.a. such that the outer fibres of the bottom flange are used much more effectively.

11.2.3. Cross girders

For the cross girders, the same approach has been used as for the main girders. The created cross girders come in two different heights; 1500 and 1700 mm. The rest of the measurements remain the same. Here the latter of the two, the one displayed in Figure 11-1, is located closest the front and the back of the leaf.

11.2.4. Connecting the elements

All the elements are connected by means of welding. With the exception for the connection between FRP and steel; the deck and the girders. These elements are to function as one hybrid structure. Thus, a full connection is required and movement should be hindered.

11.2.4.1.　Reality

To achieve full hybrid interaction a bonded connection will be used. However, since applying only bonded connections is NOT allowed for critical elements, a bolted connection should be placed (as a backup system) To achieve this bolted connection, the Davalos' connector is used. This connector allows for the transfer of shear forces, which allows for hybrid interaction. This Davalos connector, as can be reviewed in chapter 6.2.1,

11.2.4.2.　Modelled

To achieve this in the Abaqus model, tie constraints are used between all elements. This allows for both the transfer of all kinds of stresses, resulting in a 'full' hybrid interaction:

NOTE: This is 'perfect' connection. This means that the connection allows for full transfer of the forces across the connected areas. In reality, there will always be some reduction in the degree of hybrid interaction. This is a slight overestimation. This has been considered not to be significant for this design stage. In case of a final design, more research should be done and this must be considered.

11.3. Weight and counterweight calculation

Using the same approach as for the previous designs, the weight and counterweight have been calculated. These calculations can be found in Appendix G – Weight calculation. The table shown below illustrates weight distribution of the hybrid design. It can also be found in the aforementioned appendix:

	Amalia bridge		Hybrid	
	[kN]		[kN]	
Deck-system	1369	16%	702	11%
Main girders	783	9%	859	13%
Cross girders	435	5%	492	8%
Counterweight	5176	61%	3682	57%
Axle	194	2%	194	3%
Rest	515	6%	501	8%
Total bridge	**8472**	**100%**	**6430**	**100%**

Table 11-1 Absolute weight distribution (Amalia and hybrid)

Comparing the hybrid design to the original Amalia bridge, related to each bridge's total weight, results in:

- a great reduction in weight contribution of the deck system;
- an increase in weight contribution of the main girders;
- a great increase in weight contribution of the cross girders;
- a slight reduction in counterweight contribution;

Comparing the hybrid design to the original Amalia bridge, relative to their respective parts from the original Amalia bridge:

	Amalia bridge		Hybrid	
	[kN]		[kN]	
Deck-system	1369	100%	702	51%
Main girders	783	100%	859	110%
Cross girders	435	100%	492	113%
Counterweight	5176	100%	3682	71%
Axle	194	100%	194	100%
Rest	515	100%	501	97%
Total bridge	**8472**	**100%**	**6430**	**76%**

Table 11-2 Relative weight distribution (Amalia and hybrid)

In Table 11-2 the weight savings have been visualized, compared to the original weight distribution. This clearly shows that weight can be saved in the deck, by applying FRP. Weight can even be saved in the main girders. However, an increase of the weight in the cross girders is found due to maintaining

the stability of the bridge in the opened condition. Nonetheless the bridge's weight has been reduced with **24%**.

For a visual overview and exposition of the weight comparison between each bridge and their corresponding elements, please review section Appendix H.

11.4. Load cases / verification

The load placements and the approach used in for the different load cases, can be found in Appendix D. For a detailed review of each load cases and their verifications, please view their respective appendices:

11.4.1. LM1

- Appendix G; section G.4.1.1 – Deck, illustrates the verifications made for the deck. This includes the top and bottom facing as well as the webs. The maximum UC-value has been reached for the shear stress (S12) in the webs of the deck:

$$UC = 0.664$$

- Appendix G; section G.4.1.2 – Main girder, illustrates the verifications made for the main girders. The Von Mises stress resulted in the following unity check:

$$UC = 0.976$$

- Appendix G; section G.4.1.3 – Cross girder, illustrates the verifications made for the cross girders. The Von Mises stress resulted in the following unity check:

$$UC = 0.669$$

11.4.2. LM2

Appendix G; section G.4.2, illustrates the verifications made for the webs of the deck. This includes both strength and stability. The stability is governing here, due to the slim webs; resulting in:

$$\alpha_{cr} = 4.5030$$

11.4.3. LM4

- Appendix G; section G.4.3.1 – Main girders, illustrates the verifications made for the main girders. The Von Mises stress resulted in the following unity check:

$$UC = 0.214$$

- Appendix G; section G.4.3.2 – Cross girders (centre span) , illustrates the verifications made for the cross girders. The Von Mises stress resulted in the following unity check:

$$UC = 0.149$$

- Appendix G; section G.4.3.3 – Cross girders (side span), illustrates the verifications made for the cross girders. The Von Mises stress resulted in the following unity check:

$$UC = 0.099$$

11.4.4. Fatigue verification

Appendix G; section G.3 – Fatigue verification, illustrates the verifications for the opening and closing cycle of the bridge. As has been stated in the General Design Approach, this loading has been assumed to be the only load leading to fatigue damages.

	Amalia bridge (Abaqus)		Hybrid	
	$\Delta\sigma_c$ [MPa]	Damage [-]	$\Delta\sigma_c$ [MPa]	Damage [-]
Results from stresses in longitudinal direction (S11)	84.30	0.377	60.37	0.271
Results from stress in radial direction (S22)	51.65	0.379	37.78	0.079
SUM		**0.757**		**0.351**

Table 11-3 Comparison fatigue results between the original Amalia bridge (Abaqus model) and the hybrid design.

In Table 11-3, illustrates a comparison between the original Amalia bridge and the non-hybrid design. The fatigue damage resulting from the longitudinal stresses are almost identical, even though the stress differences are not. This is due to the calculation method used. For the radial direction, the opposite can be said. (The stresses differences are closer to each other than the fatigue damages.

For this one must conclude that the damages obtained in fatigue calculations are very sensitive to the stress differences used and their magnitude, compared to the *design value of the detail category* and the *constant amplitude limit*.

Nonetheless the non-hybrid design is safe with regard to fatigue design, at this location.

An additional check on fatigue stresses has been done for the opening and closing cycle for the reduced top flange of the main girders. This can be found in the aforementioned appendix in section G.3.3 and G.3.4. It should be noted that the fatigue damages at this location are governed by others load cases than the opening and closing cycle. The damages from the checked load case are non-existent. Thus, it should be checked if traffic and the vibrations of the counterweight result into any damages. This has NOT been done in this thesis but, for the full inclusion, this should be done.

12. Design Comparison

In the previous chapters the different designs have been discussed. This chapter contains a summary of the comparison of the three different alternatives. For a more detailed comparison of the different elements in the bridge, please review Appendix H.

12.1. Design built-up

The **Amalia bridge** has an orthotropic steel bridge deck design combined with a trunnion bascule bridge construction. More details on this design can be found in chapter 9.

The first adaption (the **non-hybrid** design) has an FRP-sandwich deck placed instead of the orthotropic steel deck. To allow for this, additional top flanges have been placed on the main and cross girders. Here, since composite action is avoided, the top flanges have the same dimensions as their corresponding bottom flanges. More details on this design can be found in chapter 10.

The second adaption (the **hybrid** design) has, compared to the first adaption reduced top flanges underneath the FRP-deck. This is since in this design, composite action has been allowed. More details on this design can be found in chapter11.

12.2. Weight reduction

	Amalia bridge		Non-hybrid		Hybrid	
	[kN]		**[kN]**		**[kN]**	
Deck-system	1369	100%	702	51%	702	51%
Main girders	783	100%	918	117%	859	110%
Cross girders	435	100%	588	135%	492	113%
Counterweight	5176	100%	4187	81%	3682	71%
Axle	194	100%	194	100%	194	100%
Rest	515	100%	503	98%	501	97%
Total bridge	**8472**	**100%**	**7092**	**84%**	**6430**	**76%**

Table 12-1 Weights compared to the original Amalia bridge

Applying an FRP-deck reduces the weight of the deck by half. Even though the use of this deck-type requires additions to the main and cross girders, these does not outweigh the weight saved in the deck. The lower bound approach[13] clearly shows the value of applying FRP in bridge design. More details on this design can be found in Appendix H

---

[13] The lower bound approach essentially is maintaining the main and cross girders. This refers to the web and bottom flange built-up. By maintaining this, the only area for weight reduction is in the deck. This goes well with the economic approach on which the original Amalia bridge is also designed, making for a better comparisons compared to two optimised adaptions.

12.3.   Fatigue damage

The load case which truly governs the design is the fatigue damage. Another reason in maintaining the bottom flange of the main girders is the fatigue damage. The bottom flange of the main girders has been designed such that the critical location lies in the region where it is governed by the opening and closing cycle. At other locations, traffic induced fatigue damages together with fatigue damages caused by vibrations of the counterweight are contributing.

	SCIA-model		Abaqus model		Non-hybrid		Hybrid	
	$\Delta\sigma_c$ [MPa]	Damage [-]	$\Delta\sigma_c$ [MPa]	Damage [-]	$\Delta\sigma_c$ [MPa]	Damage [-]	$\Delta\sigma_c$ [MPa]	Damage [-]
S11[14]	89.85	0.46	84.30	0.377	67.50	0.378	60.37	0.271
S22[15]	76.56	0.55	51.65	0.379	43.51	0.161	37.78	0.079
SUM		**1.01**		**0.757**		**0.539**		**0.351**

Table 12-2 Fatigue damages compared to the original Amalia bridge

The goal here is to ensure safety with regard to fatigue damages, which has been achieved with this approach. However, it should be noted that differences occur due to the modelling approach and the calculation sensitivity of the fatigue damage calculation. More details on this design can be found in chapter 8.3.

---

[14] Results from stresses in longitudinal direction found in the flanges.
[15] Results from stress in radial direction found in the webs.

Three

Conclusions &

Recommendations

13. Conclusions

The objective of this thesis has been to create a feasible bascule bridge construction, using FRP to achieve weight reduction, in accordance with the guidelines provided in the various design regulations and the Amalia bridge near Waddinxveen as the case study example. Ultimately, in effort to answer the following question:

Can the movable section of the Amalia-bridge be re-designed with the use of
FRP to realise a feasible alternative?

Chapter 10 and 11 present evidence in favour of the aforementioned question. For this thesis two alternatives have been designed. Each has their own strengths and weaknesses, still both achieve the primary goal of reducing the total weight of the bridge; while retaining construction feasibility.

Upcoming is a brief comparison between the different bridges, which contains a conclusion per option. This is followed by the verification of the designs and their weight savings. Concluding with a point by point summary conclusion.

13.1. Weight saving

The designs created have led to a reduction of the total weight compared to the original Amalia bridge. An overview of the achieved reduction rates is found in Table 13-1.

	Amalia bridge		Non-hybrid		Hybrid	
	[kN]		**[kN]**		**[kN]**	
Deck-system	1369	100%	702	51%	702	51%
Main girders	783	100%	918	117%	859	110%
Cross girders	435	100%	588	135%	492	113%
Counterweight	5176	100%	4187	81%	3682	71%
Axle	194	100%	194	100%	194	100%
Rest	515	100%	503	98%	501	97%
Total bridge	**8472**	**100%**	**7092**	**84%**	**6430**	**76%**

Table 13-1 Weights compared to the original Amalia bridge

It can be inferred that non-hybrid and the hybrid design save 16 and 24 % respectively. The majority of these savings are located at the deck and (by extension) the counterweight. The latter is due to the savings of the first. Meaning all weight saved in the leaf, has an influence on the weight saved in the counterweight. For a detailed exposition on the different elements and their influence, please see Appendix H.

13.2.   Point by point conclusion

- Bascule bridges are excellent for weight reduction purposes. Due to all weight saved in the leaf, has an influence on the weight saved in the counterweight. This makes a bascule bridge an excellent case study for optimisation. This however, is not within the scope of this thesis.
- For bridge cases similar to the Amalia bridge, replacing the orthotropic steel deck with an FRP-deck, can save weight, even when hybrid interaction between the FRP-deck and the steel girders is not considered.
- By extension, when hybrid interaction is considered, additional weight saving can be achieved. However special notice must be made of the temperature induced stresses in this case.
- The weight reduction does not apply for all elements of the bridge. This is due to the following:
    o The cross girders have been mostly maintained as is: same total heights; same bottom flange measurements (both width and thickness). This results in a stable weight.
    o The cross girders have a slightly larger reduction of the height towards the sides of the bridge, due to maintaining the size of the side covers, while implementing a thicker deck. This results in some weight reduction.
    o The original Amalia bridge has troughs, which creates cut-outs through all cross girders. Since these troughs are NOT in the design adaptions, nor are the resulting cut-outs. This results in an increase in weight.
    o The cross girders of the (non-) hybrid design have an additional top flange compared to the original Amalia bridge. This also results in an increase in weight.
- FRP is a very suitable material in cases of bridge renewal. Since FRP has a high strength to weight ratio. The placement of a bridge with a higher strength/weight ratio, has two advantages:
    o First, an increase of the maximum applicable load can be achieved without an increase in weight. A bridge can be placed which will suffice the traffic demands for the years to come, since it can be stronger without becoming heavier.
    o Secondly, if the bridge has an identical/ lighter weight, the foundation will not have to be adapted/ increased. Resulting in a large cost saving, since the existing foundation can be maintained.
- FRP is much less maintenance intense compared to steel, which has to have a decent coat of paint to prevent it from rust formation. Hence reducing the maintenance and its accompanied costs in the long-term view.

14. Recommendations

Applying an FRP-deck to replace an orthotropic steel deck, can result in weight reduction for the whole bridge. However, for future research some notes and recommendations should be made.

- **Additional weight reduction by optimising each design.** The designs are an illustration on the benefits of FRP in bascule bridge design. They are comparable to the original design in terms of the ultimate stresses for the governing load cases at the governing locations. The original Amalia bridge is economically efficient, this does not mean it is the lightest design possible. The same can be said regarding the designs made for this thesis.
- **When designing a hybrid structure with hybrid interaction special care must be taken of thermal induced stresses.** When making a hybrid construction and allowing hybrid interaction, different materials and the limitation for each material to deform separately, since they are fixed to allow for a hybrid interaction. These stress values can become significant which could result, in cases of bonded connections into delamination and therefore special attention must be given to this scenario.
- **Research into the interaction behaviour between FRP deck and steel girders**. In this thesis the interaction between the deck and the girders have been modelled as interaction properties in normal and transvers direction. In reality bolted connections will be used. In the case of hybrid interaction these bolts allow for the transfer of shear forces between the deck and the girders, whereas the bolts used in the non-hybrid design, allow for slippage, such that hybrid interaction is limited. The next step is to do more tests to gain further insight into the behaviour and to be able to model these as the connection would be created.
- **Possibility of removing the bascule basement**. When enough weight is saved in the leaf, there is an option that the reduced length of the main girders eliminates the need for a bascule basement. This scenario has however not been fully explored in the is thesis. Hence it could be an interesting next step, as it can save tremendous costs.
- **Recyclability of FRP**. What happens in the end of life phase of the bridge. Especially since FRP is a plastic based material, the need to recycle/ reuse the material is a priority. The use of FRP is relatively young in the bridge industry, thus not much is known about the long-term behaviour of the material. If the material has not deteriorated, the bridge can be relocated and downgraded as a re-used bridge at a different location. Research is being done on the recyclability of thermoset FRP materials, allowing for the possibility of FRP becoming recyclable in the future. Another option is using thermoplastic FRP. However, this has its own issues which need to be addressed.

Four

References

15. List of Referred Documents

AHN, 2018. *Actueel Hoogtebestand Nederland.* [Online]
Available at: http://www.ahn.nl/common-nlm/viewer.html
[Accessed 30 04 2018].

Alnahhal, W., Aref, A. & Alampalli, S., 2007. *Composite behaviour of hybrid FRP-concrete bridge decks on steel girders,* Toronto: Halcrow Yolles.

Berk, B. v. d., 2016. *Twitter.* [Online]
Available at: https://mobile.twitter.com/heijmansnl/status/750603382042288128/photo/1
[Accessed 08 02 2017].

Cambridge University Press, 2017. *Cambridge University Dictonary.* [Online]
Available at: http://dictionary.cambridge.org/dictionary/english/bridge
[Accessed 08 02 2017].

CUR, 2013. *CONCEPT CUR-Aanbeveling 96 1st revision,* Delft: CUR.

CURNET, 2003. *Vezelversterkte kunststoffen in civiele draagconstructies; Achtergrondrapport bij CUR-aanbeveling 96,* Breda: Civiel Technisch Centrum Uitvoering Research en Regelgeving.

Davalos, J. F., Chen, A. & Zou, B., 2011. *Stiffness and Strength Evaluations of a Shear Connection Stystem for FRP Bridge Decks to Steel Girders,* Morgantown: American Society of Civil Engineering.

Dinu , F., Dubina, D. & Marginean, I., 2013. *Effect of connection between reinforced conrete slab and steel beams in multi-story frames subjected to different column loss scenarios,* Timisoara: Polithehnica University of Timisoara.

FiberCore europe, n.d. *Material properties used in InfraCore structures v02,* Rotterdam: FiberCore.

Franken, A., 2017. *MSc Thesis - Application and environmental evaluation of fibre reinforced polymers in movable bridge design,* Delft: Movares/ TU-Delft.

Google Streetview, 2017. *Wilhelminakade 26. Waddinxveen, Zuid-Holland (september 2017).* [Art] (Google).

Hartsuiker, C., 2007. *Toegepaste Mechanica.* 4e oplage september 2007 ed. Den Haag: Sdu Uitgevers.

Heijmans, M. v. d. B. -., 2015. *Technische Beschrijving Kunstwerk KG Stalen val - Parallelstructuur A12: Moordrechtboog en Extra Gouwekruising,* Rosmalen: Heijmans Intergrale Projecten B.V..

Hoffman, A., 2013. *What are Feasibility Studies.* [Online]
Available at: http://www.godfreyhoffman.com/Civil-Engineering-Blog/bid/258756/What-are-Feasibility-Studies
[Accessed 02 03 2017].

JRC, 2016. *Prospect for new guidance in the design of FRP - support for the implementation, harmonization and further development of the Eurocodes,* Ispra (VA), Italy: Joint Research Centre - Insitute for the Protection and Security of the Citizen.

Keller, T. & Gürtler, H., 2005. *Design of hybrid bridge girders with adhesively bonded and compositely acting FRP deck,* Lausanne, Switserland: Swiss Federal Institute of Technology.

Kolstein, D. M., 2008. *Lecture CT5128: Fibre Reinforced Polymer (FRP) Structures.* Delft: Faculty of Civil Engineering and Geosciences, TU-Delft.

Meer, F. v. d., 2016. *Materials and Failure Analysis (of FRP).* Delft: Faculty of Civil Engineering and Geosciences, TU Delft.

Moen, J., 2014. *Feasibility Study on Heav-Traffic Bascule Bridges,* Delft: Faculty of Civil Engineering and Geosciences, TU-Delft.

NNI, 2011. *NEN-EN 1990,* Delft: Nederlands Normalisatie-instituut.

NNI, 2011. *NEN-EN 1991-1-4,* delft: Nederlands Normalisatie-instituut.

NNI, 2011. *NEN-EN 1991-2 NB,* Delft: Nederlands Normalisatie-instituut.

NNI, 2012. *NEN-EN-1993-1-5,* Delft: Nederlands Normalisatie-istituut.

NNI, 2012. *NEN-EN-1993-1-9,* Delft: Nederlands Normalisatie-istituut.

NNI, 2015. *NEN-EN 1991-2,* Delft: Nederlands Normalisatie-instituut.

NNI, 2017. *NEN 6786-1 ,* Delft: Nederlands Normalisatie-instituut.

Pavlovic, M. & Kolstein, H., 2016. *Course: CIE5125 Steel Bridges (lecture slides).* Delft: Faculty of Civil Engineering at the TU-Delft.

Pickering, S., 2013. *Recycling and Disposal of Thermoset Composites,* Dartington Hall (Dartington): University of Nottingham.

Province of South-Holland, 2016. *Nieuwsbrief Parallelstructuur A12.* [Online]
Available at: https://www.zuid-holland.nl/publish/pages/14951/nieuwsbriefparallelstructuura1208december2016.pdf
[Accessed 20 02 2017].

Reusink, J., 2017. *Guest Lecture: Steel Bridges - Movable bridges,* Delft: TU-Delft.

Reynolds, P., 2013. *Lower Hatea bascule bridge.* [Art] (Novare Design).

Rijkswaterstaat, 2017. *Richtlijnen Vaarwegen 2017,* Rijswijk: Rijkswaterstaat Water, Verkeer en Leefomgeving.

Romeijn, D. A., 2006. *Steel Bridges, part 1.* Delft: Faculty of Civil Engineering and Geosciences, TU-Delft.

Satasiviam, S., Bai, Y. & Zhao, X. L., 2013. *Evaluation of effective width of GFRP-steel composite beams for struutral construction.* London, Taylor & Francis Group.

Simulia - Abaqus, 2018. *Abaqus Analysis User's Guide (6.13).* [Online]
Available at: http://abaqus.software.polimi.it/v6.13/books/usb/default.htm?startat=book01.html
[Accessed 11 06 2018].

Star Thermoplastics, I., 2017. *Thermoset-vs-Thermoplastic.* [Art] (Star Thermoplastics Alloys & Rubbers, Inc.).

Steenbrink, A., 2017. *Sideview, structural system Amalia-bridge, Scope 1st design.* [Art] (Movares / TU-Delft).

Strong, A. B., 2008. *Fundamentals of Composites Manufacturing - Materials, Methods, and Applications.* 2nd ed. Dearborn, Michigan: Society of Manufacturing Engineers (SME).

Zou, B., Chen, A., Davalos, J. F. & Salim, H. A., 2010. *Evaluation of effective flange width by shear lag model for orthotropic FRP bridge decks,* Morgantown: West Virginia University.

16. List of Figures

17. List of Tables

Five

Appendices

Appendix A. Eurocode

An extensive research has been done on the different load scenarios the Eurocode guides to be done and for a full enclosure it must be noted, that the best solution is given, when all conceivable governing load scenarios are taken into account. However, due to time constraints, this has not been done and aa selection has been made. This selection is based upon the load governing scenarios of the original Amalia bridge, to be able to compare designs and load scenarios which should be governing when placed accordingly. This has been done in collaboration with mister Steenbrink of Movares.

A brief exposition of the applied load cases is depicted below:

A.1.   Self-weight

When regarding the self-weight of a bridge, this means a summation of the total mass of the permanent elements, both load bearing and non-load bearing. Traditional construction materials have their nominal densities in the Eurocode. Since FRP is not, yet, in the Eurocode. For FRP, the density varies on the ratio of fibres and resin. When ordering from a manufacturer, the density/ weight has been specified by them, if this is not the case, the rule of mixtures can be applied:

$$\rho_i = V_f \cdot \rho_f + V_m \cdot \rho_m$$

Where:

ρ_i is the total density (for increment i)
V_f is the fibre volume ratio
ρ_f is the fibre density
V_m is the matrix volume ratio
ρ_m is the resin density

The next step is using the found density to calculate total weight, which is the sum of all elements:

$$M_{bridge} = \sum M_{elements} = \sum V_i \cdot \rho_i$$

Where:

V_i is the volume for element i.
ρ_i is the density for element i.

This has been used in the different weight calculations. For example, in the determination of the counterweight size and, by extension, for the fatigue calculations. Details on these calculations can be found in the following sections:

- Verification approach:
  - o **Boundary conditions**: section 8.3 (Modelling in Abaqus)
- Weight balancing calculations:
  - o **Amalia bridge**: Appendix E (Weight calculation)
  - o **Non-hybrid design**: Appendix F (Weight calculation)
  - o **Hybrid design**: Appendix G (Weight calculation)
- Fatigue calculations:
  - o **Amalia bridge**: chapter 9.4 and Appendix E (Fatigue verification)
  - o **Non-hybrid design**: chapter 10.4.4 and Appendix F (Fatigue verification)
  - o **Hybrid design**: chapter 10.4.4 and Appendix G (Fatigue verification)

A.2.   Traffic

According to the Eurocode traffic loading can be divided into several load models (LM's). Each LM contains different kinds of loading, ranging from general to occasional and exceptional load cases.

A.2.1.   Load Model 1

LM1 is a combination of both concentrated and distributed load, which covers most of the effects of traffic (both heavy and light). This model is used for both global and local checks. The concentrated loads are double axel loads, representing heavy traffic. These loads are the concentrated load $\alpha_{Qi}Q_{i,k}$ and the distributed load $\alpha_{qi}q_{i,k}$. They act on a surface to 0.4 times 0.4 m², non-hybrid c.t.c. 1.2 m in x-direction and 2.0 m in y-direction. Here α_{Qi} and α_{qi} are correction factors, depending on the expected traffic and the category of the road (NNI, 2011). The application and values are shown in Figure A-1 and Table A-1 respectively. The table also displays the values obtained by Movares. These have been used in the design calculations.
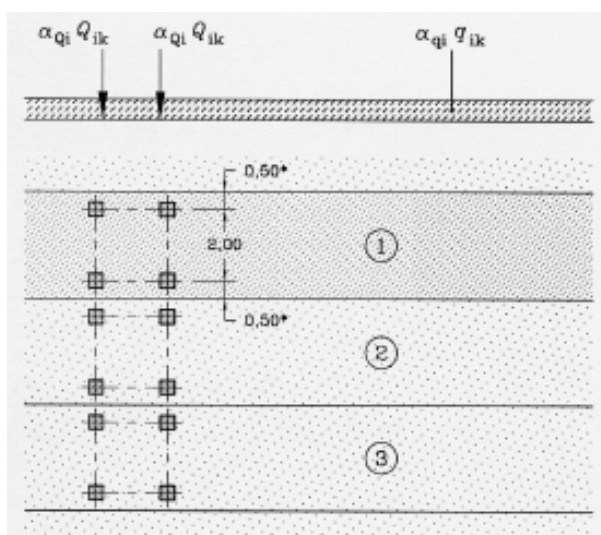
Figure A-1 Load definition of LM1 (NNI, 2015)
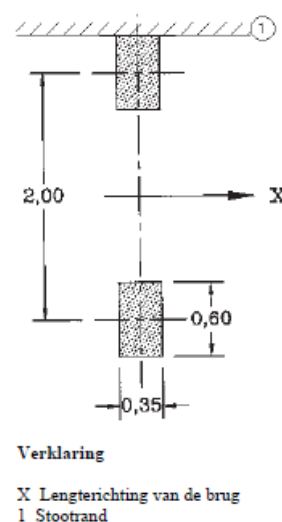
Figure A-2 Load definition of LM2 (NNI, 2015) (Heijmans, 2015)

NOTE: the area of the loads will be slightly larger than is illustrated in the figures above, due to the spread of the loads through the material. The load should be applied on to the centre line of the material; whereas the illustrations above show the area on top of the road. The spread is 45 degrees in all directions.

Correction factor	[-]	Tandem load*	[kN]	Correction factor	[-]	Distributed load	[kN/m2]
$\alpha_{Q,1}$	1.00	$Q_{k,1}$	300	$\alpha_{q,1}$	1.15	$q_{k,1}$	9
$\alpha_{Q,2}$	1.00	$Q_{k,2}$	200	$\alpha_{q,2}$	1.40	$q_{k,2}$	2.5
$\alpha_{Q,3}$	1.00	$Q_{k,3}$	100	$\alpha_{q,3}$	1.40	$q_{k,3}$	2.5
				$\alpha_{q,r}$	1.00	$q_{k,r}$	2.5

Table A-1 Characteristic values for LM1, according to the Eurocode (NNI, 2015) (Heijmans, 2015)

* The tandem load is spread out over two wheels, thus the load per wheel is halved.

A.2.2. Load Model 2

LM2 is single axel load in which a dynamic amplification factor, β_Q, is taken into account. It is advised to take this factor with the same value as α_{Q1} (NNI, 2011). The load is to be applied at any random position of the road. As can be seen in Figure A-2, the area for the applied load, differs from LM1.

$$Q_{1,k} = 400 \, kN$$

NOTE: since the load used in LM2 is a single axle load, which is used fully and is not halved. This differs from LM1.

A.2.3. Load Model 4

LM4 corresponds with a crowd of people. In case this is relevant, it is applied as a load of 5 kN/m². This load already contains a dynamic amplification factor. It is to be applied on ALL relevant areas: total length, width, including the central partition if it were to be present. The relevance for LM4 is to be determined per project.

A.3. Fatigue

For fatigue loading a total of 5 different load models are given in the Eurocode. (NNI, 2015) However, as can be viewed in the section regarding Fatigue loading of Appendix D, these has not led to damages. The opening and closing cycles have led to damages and therefore this scenario has been used as the governing load scenario, for the new designs. To review the executed fatigue calculations, below an overview has been given for each design:

-     Amalia bridge: Chapter 9.4 and E.3.
-     Non-hybrid design: Chapter 10.4.4 and F.2.6.
-     Hybrid design: Chapter 11.4.4 and G.3.

Appendix B. CUR 96+

This appendix contains a brief exposition of the CUR 96+ which has been used in verifications.

B.1.   Safety philosophy

$$S \cdot \gamma_f \leq R/(\gamma_m \cdot \gamma_c)$$

Where:

S	is the effect of the representative (= characteristic or nominal) applied load (**Solicitation**)
R	is the representative (=characteristic or nominal) load bearing capacity; e.g. strength of the construction (**Resistance**)
γ_f	is a load factor
γ_m	is a material factor
γ_c	is a conversion factor

The conversion factor varies for different load cases (either short of long term).In load combinations where different conversion factors would be applied, the principal of superposition is applied to the strongest one. Hereby it must comply such that:

$$S_1 \cdot \gamma_{f1} \leq R_1/(\gamma_m \cdot \gamma_{c1}) \qquad \text{and} \qquad S_2 \cdot \gamma_{f2} \leq R_2/(\gamma_m \cdot \gamma_{c2}) \qquad \text{and} \qquad R_1 + R_2 \leq R$$

NOTE: The conversion factor in CUR 96+ (γ_{c1}) differs from the conversion factor in the JRC2016 (η_{c1}). In the JRC the conversion factor η, is a reduction factor, used in multiplication, thus smaller than 1.0, whereas in the CUR the conversion factor γ, is a reduction factor larger, used by division, thus larger than 1.0. The implementation of the factors remains unchanged, the execution, however, is different.

B.1.1. Elasticity theory

FRP based materials show behaviour corresponding with elastic behaviour until fracture, thus ONLY elasticity theory can be applied in cases FRP is used. NO redistribution of stresses by plastic behaviour can be applied.

B.1.2. Material and construction modelling

In the calculation of orthotropic material properties, for panels of laminates, classical laminate theory must be used. The stacking order, orientation and thickness of the plies influences this. The orthotropic material properties (E_1, E_2, G_{12} and υ_{12}) must be known. Using this theory, these property values for the laminate will be known and can be expressed in the laminate stiffness matrix: the ABD-matrix.

A brief intermezzo regarding classical laminate theory and the ABD-matrix has been illustrated on the next page:

B.1.2.1.   Classical laminate theory

The ABD-matrix shows the relations between internal forces (normal forces N and moments M) and deformations (strains ε₀ and curvature κ) of the laminate.

$$\begin{pmatrix} N \\ M \end{pmatrix} = \begin{pmatrix} A & B \\ B & D \end{pmatrix} \cdot \begin{pmatrix} \varepsilon_0 \\ \kappa \end{pmatrix}$$

Normal forces: $N = \begin{pmatrix} N_x \\ N_y \\ N_{xy} \end{pmatrix}$ Strains at neutral axis: $\varepsilon_0 = \begin{pmatrix} \varepsilon_{0x} \\ \varepsilon_{0y} \\ \varepsilon_{0xy} \end{pmatrix}$

Moments: $M = \begin{pmatrix} M_x \\ M_y \\ M_{xy} \end{pmatrix}$ Curvatures: $\kappa = \begin{pmatrix} \kappa_x \\ \kappa_y \\ \kappa_{xy} \end{pmatrix}$

Normal forces stiffness matrix: $A = \begin{pmatrix} A_{11} & & \\ A_{12} & A_{22} & \\ A_{13} & A_{23} & A_{33} \end{pmatrix}$

Moments stiffness matrix: $D = \begin{pmatrix} D_{11} & & \\ D_{12} & D_{22} & \\ D_{13} & D_{23} & D_{33} \end{pmatrix}$

(Normal forces to Moments) Coupling matrix: $B = \begin{pmatrix} B_{11} & & \\ B_{12} & B_{22} & \\ B_{13} & B_{23} & B_{33} \end{pmatrix}$

For symmetrical ply lay-up the coupling matrix equals zero, thus meaning that no normal force can result into curvature, nor a moment can result into strain. (CURNET, 2003)

B.1.3. Testing the limit states

- ULS   Maximum load bearing capacity taking into account **strength**, **stability** and **fatigue**.
- SLS   **Deformation** and **vibration** behaviour and, in some cases, **first ply failure**.

When verifying the strength of FRP, laminate illustrates two stages:

- The first ply failure. Here, under tensile stress, the first ply of the laminate is exceeded.
- Ultimate tensile strength. This is the limit of the laminate. Causing failure of the whole laminate.

The strength checks are done using this **ultimate tensile strength**. (Or in case of compression, the compression strength.) In general, the first ply failure leads to a very slight reduction in strength and stiffness.

The behaviour described above, has been illustrated in Figure B-1.
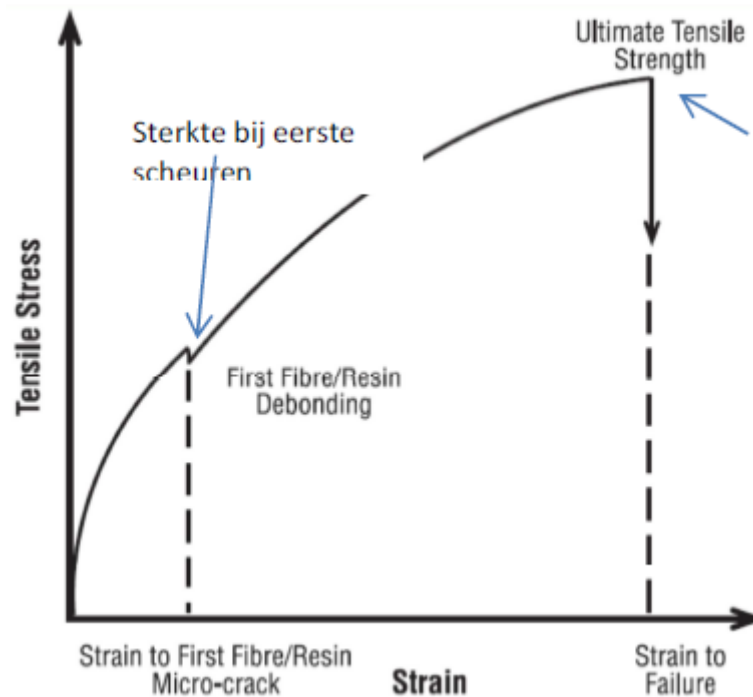
Figure B-1 Ultimate Tensile Strength FRP

B.2.   Material factors

This factor takes into account uncertainties in the material properties. The material factor consists of two partial material factors:

$$\gamma_m = \gamma_{m,1} \cdot \gamma_{m,2}$$

The first partial material factor takes into account the method of achieving the material properties. To compensate for the difference between the properties during testing, within calculating and in the actual construction.

$$\gamma_{m,1} = 1.35$$

The lather material factor takes into account the production process and the uncertainties due to the type of production, including geometrical deviations due to production tolerances the value of $\gamma_{m,2}$ differs depending on the method and whether or not the laminate has been cured. This is displayed in the next table:

Production method	Cured laminate	Not cured laminate
Spray-up	1.6	1.9
Hand lay-up	1.4	1.7
VA-RTM of RTM	1.2	1.4
Filament winding	1.1	1.3
Prepreg	1.1	1.3
Pultrusion	1.1	1.3

Table B-1 Partial material factor γm,2 (CURNET, 2003)

B.2.1. Material factor and ULS

When checking **strength** in **ULS** the material factor must be at least 1.5:

$$\gamma_m \geq 1.5$$

When checking stability in ULS the material factor multiplied with the load factor must be at least 2.5:

$$\gamma_m \cdot \gamma_f \geq 2.5$$

B.3.   Conversion factors

These factors make FRP unique from other building materials. They take into account the foreseen effects due to temperature, time, environmental influence, duration of the loading and cycling loading on the material properties.

For each limit state (LS) different (combinations of) conversion factors apply. A total conversion factor is achieved by multiplication of each applicable conversion factor.

$$\gamma_c = \gamma_{ct} \cdot \gamma_{cv} \cdot \gamma_{ck} \cdot \gamma_{cf}$$

B.3.1. Temperature

Temperature can have a negative influence on the material properties of FRP, especially in case of moisture and long-term loading. The HDT (Heat Distortion Temperature) must be at least 30 °C, but preferably 40 °C higher than the maximum use temperature of the construction. The conversion factor for temperature influences is:

$$\gamma_{ct} = 1.1$$

It is used in checking the ULS for strength and stability and the SLS for deformation, vibration and first ply failure. For the SLS-vibration check both with and without conversion factor should be checked.

B.3.2. Environmental influence – moisture

In time the properties of the resin and the resin-fibre interface changes by means of condensing of the molecular structure, post curing and leaching. These effects are beneficial for the properties of FRP. Sunlight; temperature; moisture; weather changes and wind gusts; and chemical aging / attack. These influences have a negative effect on the properties of FRP. By means of the proper coating / additives to the resin, the FRP can be protected to these influences.

There are three different cases to be distinguished for moisture influence:

1. In case the FRP structure is constantly located in dry circumstances:

$$\gamma_{cv} = 1.0$$

2. In case the FRP structure is exposed to both dry and wet conditions, where these alternate:

$$\gamma_{cv} = 1.1$$

3. In case the FRP structure is constantly located in wet circumstances (surface water, groundwater, seawater, storage silo's):

$$\gamma_{cv} = 1.25$$

Regardless the case, it is used in checking the ULS for strength and stability and the SLS for deformation, vibration and first ply failure. For the SLS-vibration check both with and without conversion factor should be checked.

B.3.3. Load duration – creep

When an FRP structure undergoes long term loading, a conversion factor for creep effects will need to be taken into account:

$$\gamma_{ck} = t^n$$

Where:

t is the duration of the load(s) in hours
n is dependent on the type of fibre reinforcement

UD:	n	=	0.01
Woven:	n	=	0.04
Mat:	n = 0.1		

Reinforcement	t = 1 year	t = 10 years	t = 20 years	t = 50 years
Uni directional	1.10	3.12	1.13	1.14
Woven	1.44	1.58	1.62	1.68
Mat	2.48	3.12	3.34	3.67

Table B-2 Creep conversion factor γ_{ck} (CURNET, 2003)

It is used in checking the ULS for strength and stability and the SLS for deformation and first ply failure. In all cases **only for the long-term loading**, the conversion factor should be used.

B.3.4. Cyclic loading – fatigue

If an FRP structure undergoes cyclic loading and a strength-fatigue analysis will need to be done, a conversion factor is required:

$$\gamma_{cf} = 1.1$$

It is used in checking the ULS for stability and the SLS for deformation, vibration and first ply failure. For the SLS-vibration check both with and without conversion factor should be checked.

B.3.5. Summary conversion factors

In the following table an overview on applying the conversion factors is placed:

	Ultimate Limit State			Serviceability Limit State		
Conversion factor	Strength	Stability	Fatigue	Deformation	Vibration[3]	First ply failure
Temperature (ct)	X	X	X	X	X	X
Moisture (cv)	X	X	X	X	X	X
Creep[1] (ck)	X	X		X		X
Fatigue[2] (cf)		X		X	X	X

Table B-3 Combining the conversion factorsfor different checks (CURNET, 2003)

Appendix A.   The creep conversion factor only applies to the long-term load.
Appendix B.   The fatigue conversion factor only applies to stiffness related limit states.
Appendix C.   When checking for vibrations a check must be done both with and without the temperature, moisture and fatigue conversion factor.

B.4.   Stiffness

Hereby the CUR 96+ references the Dutch code (NEN 6702). In this code the deflection of a structure or structural element is as follows:

$$u_{tot} = u_{el} + u_{kr}$$

$$u_{add} = u_{tot} - u_{on}$$

$$u_{fin} = u_{tot} - u_c$$

Where:

u_{tot}	Total deflection
u_{el}	Time independent deflection. Determined due to load combinations as is defined in NEN 670 section 6.4.3.1 2
u_{kr}	Time dependent deflection. Determined due to load combinations as is defined in NEN 670 section 6.4.3.1 2
u_{add}	Additional deflection (u_{bij})
u_{on}	Time independent deflection, due to permanent loading of the structure of structural element.
u_{fin}	Deflection in the final situation (u_{ein})
u_c	Precamber (u_{ze})

B.4.1. Determining the different deflections:

When determining the, u_{el}, the conversion factor for moisture, γ_{cv}, has to be taken into account, according to the section Environmental influence – moisture.

When determining the, u_{kr} and the u_{on}, the modulus of elasticity is multiplied with both the conversion factor for moisture, γ_{cv}, and the conversion factor for moisture, γ_{ck}, according to the section Environmental influence – moisture and Load duration – creep.

Appendix C. Material Properties

Based upon the different recourses (guidelines/ companies) consulted, below a summary of the material properties has been displayed.

C.1. Steel (Eurocode)

The steel grades used for the main load bearing structural elements are:

- S355J2+N
- S355M

Steel has different values regarding the yield and ultimate limit strength, depending on the thickness applied. The table below illustrates these for different thicknesses applied.

Nominal thickness [mm]	f_y [N/mm²]	f_u [N/mm²]	Source
$t \leq 40\ mm$	355	490	Table 3.1 of the NEN-EN 1993-1-1
$40\ mm < t \leq 80\ mm$	355	470	Table 3.1 of the NEN-EN 1993-1-1
$80\ mm < t \leq 100\ mm$	315	470	Table 7 of the NEN-EN 10025-2:2004
$100\ mm < t \leq 150\ mm$	295	450	Table 7 of the NEN-EN 10025-2:2004

Table C-1 Stiffness properties of steel

C.2. Standard laminate properties (CUR 96+)

The table below illustrates the properties belonging to a quasi-isotropic and an anisotropic laminate, Both with a Vf of 50%. Where the first has 25% of the fibres in each (0,90,45,-45°) direction and the latter 55% in the 0°-direction and 15% in the remaining three. (CURNET, 2003)

Stiffness properties		Quasi-isotropic laminate (Vf=50%)	Anisotropic laminate (Vf= 50%)
E_1	[GPa]	18.6	25.8
E_2	[GPa]	18.6	15.9
G_{12}	[GPa]	7.0	5.6
$υ_{12}$	[-]	0.33	0.32

Table C-2 Stiffness properties of standard FRP laminates according to the CUR 96+ (CURNET, 2003)

Strength properties		Quasi-isotropic laminate (Vf=50%)	Anisotropic laminate (Vf= 50%)
σ_{1tR}	[MPa]	223	310
σ_{1cR}	[MPa]	223	310
σ_{2tR}	[MPa]	223	191
σ_{2cR}	[MPa]	223	191
τ_{12R}	[MPa]	168	134

Table C-3 Strength properties of standard FRP laminates according to the CUR 96+ (CURNET, 2003)

IMPORTANT: According to the CUR 96+ at least 15% of the fibres must be used in **all** directions (0,90,45,-45°) and have a volume fraction of at least 20%. Only then are the rules and guidelines, set

by the CUR 96+, applicable. If the first is not the case, CUR 96+ can still be used, however, the material must be verified by tests.

C.3.   Laminate properties FiberCore

In this section the properties have been given of the laminates provided by FiberCore. **Skin laminates** have been used for the **top** and **bottom facings** and **Flutes laminate** has been used for **webs**. These laminates are built up of layered UD-plies and are made by means of VARTM.

FiberCore laminate	Material	Built up	Volume fraction	Angles [degrees]			
			Vf	0	90	45	-45
Skin laminate	GFRP	[0,90]s	0.45	75%	25%		
Flutes laminate	GFRP	[90,+/-45]s	0.30		50%	25%	25%

Table C-4 FiberCore laminate composition (FiberCore europe, n.d.)

FiberCore laminate	E1	E2	Nu12	G12	G13	G23
	[GPa]	[GPa]	[-]	[GPa]	[GPa]	[GPa]
Skin laminate	28.29	15.48	0.27	5.13	5.13	5.13
Flutes laminate	8.88	17.22	0.29	5.22	5.22	5.22

Table C-5 FiberCore laminate stiffness properties (FiberCore europe, n.d.)

FiberCore laminate	S11,k		S22,k		S12,k
	Stxx	Scxx	Styy	Scyy	Txy
	[MPa]	[MPa]	[MPa]	[MPa]	[MPa]
Skin laminate	558.00	-515.00	172.00	-218.00	44.00
Flutes laminate	130.00	-99.00	315.00	-181.00	64.00

Table C-6 FiberCore laminate characteristic strength properties (FiberCore europe, n.d.)

Combining this with the CUR 96+ guidelines (as can be reviewed in Appendix B), lead to the design strength properties for different checks, as has been stated in the aforementioned appendix in Table B-3. These have been illustrated on the next page.

C.4.   Strength to weight comparison

Since FRP is light weight and really strong, the strength to weight ratio truly illustrates the added value of FRP. This can be reviewed in Table C-7 below:

	Density	Tensile Strength		Strength/weight ratio	
		S11	S22	S11	S22
	[kg/m³]	[MPa]	[MPa]	[MPa*m³/kg]	[MPa*m³/kg]
Steel (S355)	7800	355	355	**0.05**	**0.05**
Skin laminate (FiberCore)	1670	558	172	**0.33**	**0.10**
Flutes laminate (FiberCore)	1460	130	315	**0.09**	**0.22**

Table C-7 Strength to weight ratio's for steel and FiberCore laminates

In Table C-7 a higher value for the strength/ weight ratio means a more strength per unit of weight. This is the case for FRP with a value of at least twice of that of steel. In terms of strength this means a clear improvement, thus illustrating the potential of FRP.

C.5.   Thermal expansion coefficients

In section 6.3 the stresses induced by thermal influences are addressed. Here the values belonging to the materials used in this thesis are given:

	α^T_{xx}	α^T_{yy}	E1	E2
	[1/°K]	[1/°K]	[GPa]	[GPa]
Steel (S355)	1.00E-05	1.00E-05	28.29	15.48
Skin laminate (FiberCore)	1.33E-05	3.04E-05	8.88	17.22
Flutes laminate (FiberCore)	4.89E-05	1.68E-05		

Table C-8 Thermal expansion coefficents for steel and FiberCore laminates

The values for FRP differ in each direction and are all different from the steel value.

C.6.   Laminate properties deck components

The properties of the modelled elements differ from the properties of the products used in reality. This is due to a modelling simplification for the implementation in Abaqus. The values below are calculated by applying the material factors and conversion factors, as stated in the CUR 96+. The materials used have been illustrated in section C.3, whereas the design of built up of these components has been described in section F.1.1.

NOTE: the values for the webs are lower bound values. Since the webs are composed of the aforementioned skin and flutes laminates, the, absolute, minimum values for each type of stress are used.

C.6.1. Strength

	S11,d		S22,d		S12,d
	Stxx	**Scxx**	**Styy**	**Scyy**	**Txy**
	[MPa]	**[MPa]**	**[MPa]**	**[MPa]**	**[MPa]**
Top/bottom facing	249.71	-230.46	76.97	-97.56	19.69
Webs	63.99	-48.73	84.67	-89.10	21.66

Table C-9 Deck components; design strength properties in case of strength checks

C.6.2. Stability

	S11,d		S22,d		S12,d
	Stxx	**Scxx**	**Styy**	**Scyy**	**Txy**
	[MPa]	**[MPa]**	**[MPa]**	**[MPa]**	**[MPa]**
Top/bottom facing	227.01	-209.51	69.97	-88.69	17.90
Webs	58.18	-44.30	76.97	-81.00	19.69

Table C-10 Deck components; design strength properties in case of stabililty checks

C.6.3. Fatigue

	S11,d		S22,d		S12,d
	Stxx	**Scxx**	**Styy**	**Scyy**	**Txy**
	[MPa]	**[MPa]**	**[MPa]**	**[MPa]**	**[MPa]**
Top/bottom facing	284.66	-262.73	87.75	-111.21	22.45
Webs	72.95	-55.56	96.52	-101.57	24.69

Table C-11 Deck components; design strength properties in case of fatigue checks

C.6.4. Deformation

	S11,d		S22,d		S12,d
	Stxx	**Scxx**	**Styy**	**Scyy**	**Txy**
	[MPa]	**[MPa]**	**[MPa]**	**[MPa]**	**[MPa]**
Top/bottom facing	227.01	-209.51	69.97	-88.69	17.90
Webs	58.18	-44.30	76.97	-81.00	19.69

Table C-12 Deck components; design strength properties in case of deformation checks

Appendix D. Design Verification – Approach

This appendix contains more detailed information regarding the verification checks that have been made for the designs. It contains the following load cases; each adapted such that a particular element can be checked:

LM1	LM2	LM4	Self-weight
Deck	Deck (webs)	Main girder	Main girder
Main girder		Cross girder	
Cross girder			

Table D-1 Loads used for different checks

NOTE: for the original Amalia bridge, the latter load case has been executed to compare the model made in Abaqus to the model created in SCIA-Engineer.

D.1.   LM1

The three main structural elements have been checked to fulfil loading caused by LM1. First the loads applied at the different sections have been illustrated in Table D-2 and Table D-3.

Symbol	Load-definition	Lane	Magnitude (SLS) [kN/m²]	
$\alpha_{Q,1}Q_{k,1}$	Concentrated load, lane 1	1	789.07	150 kN
$\alpha_{Q,2}Q_{k,2}$	Concentrated load, lane 2	2	526.05	100 kN
$\alpha_{Q,3}Q_{k,3}$	Concentrated load, lane 3	3	263.02	50 kN
$\alpha_{q,1}q_{k,1}$	Distributed load, lane 1	1	10.35	(-)
$\alpha_{q,2}q_{k,2}$	Distributed load, lane 2	2	3.5	(-)
$\alpha_{q,3}q_{k,3}$	Distributed load, lane 3	3	3.5	(-)
$\alpha_{q,r}q_{k,rest}$	Distributed load, rest applied area	rest	2.5	(-)

Table D-2 LM1; load definition (SLS) (Heijmans, 2015)

Symbol	Load-definition	Lane	Magnitude (ULS) [kN/m²]	
$\alpha_{Q,1}Q_{d,1}$	Concentrated load, lane 1	1	1183.61	225 kN
$\alpha_{Q,2}Q_{d,2}$	Concentrated load, lane 2	2	789.07	150 kN
$\alpha_{Q,3}Q_{d,3}$	Concentrated load, lane 3	3	394.54	75 kN
$\alpha_{q,1}q_{d,1}$	Distributed load, lane 1	1	15.525	(-)
$\alpha_{q,2}q_{d,2}$	Distributed load, lane 2	2	5.25	(-)
$\alpha_{q,3}q_{d,3}$	Distributed load, lane 3	3	5.25	(-)
$\alpha_{q,r}q_{d,rest}$	Distributed load, rest applied area	rest	3.75	(-)

Table D-3 LM1; load definition (ULS) (Heijmans, 2015)

NOTE: the far-right column illustrates the magnitude of the force as a concentrated load. These are based upon the Eurocode NEN-EN 1991-2.

The location and the magnitude of these loads differs per check. This will be explained per check respectively:

D.1.1. Deck

The material FRP is governed by deflection. Nonetheless it has been checked for the fibre directions. This results in different checks for the faces & the webs of the deck: The faces should be within a **5 mm deflection limit** and the webs must not **buckle**.

D.1.1.1. Vertical deflection

Regarding the vertical deflection of the deck at the front and back of the leaf a recommendation has been stated in the Eurocode (NEN-EN 1993-2 +C1 NB). It is NOT stated which load combination should be taken into account, nonetheless a maximum recommended height difference of 5 mm is stated.

First off, the situation of an unloaded bridge, in closed condition, will have a height difference, at the aforementioned locations of 0 mm.

D.1.1.1.1. Amalia bridge

Since this is a recommendation and not a strict rule, there is some leeway here. Thus, in the design of the original Amalia bridge, this has been taken advantage of. Resulting in the following (Heijmans, 2015):

Heavy traffic has been applied, on a theoretical lane, in the centre of the midspan (corresponding with lane 1, as illustrated in Figure D-2) & on the **rear edge** of the bridge (corresponding with lane 1, as illustrated in Figure D-1). Please note, the concentrated load varies compared to the illustrations mentioned and for the latter, also the longitudinal location of the concentrated load differs. Resulting in the following deflections:

- Located at the rear girder – 12.7 and – 13.3 mm.
- Located at the front girder – 6.4 mm.

Both exceed, however, since this concerns heavy traffic and these vehicles have larger wheels, this vehicle will not receive the same burden as regular vehicles. Directly outside of the vicinity of the heavy traffic, the displacement dissipates quite rapidly. Thus, it is deemed acceptable.

D.1.1.1.2. Design adaptions

To make valid comparisons between the adaptions and the original design, not the Eurocode values will be kept, but rather the actual values found for the Amalia bridge. If the Eurocode would be used, this would result into an over-dimensioning of the adaption designs.

D.1.1.2. Buckling of the webs

To check this a buckling simulation has been done in Abaqus for a web of the deck. The obtained critical stress is then compared to the values found in the aforementioned load scenario.

D.1.2. Main girder

In the case of the main girder, the loads have been applied onto the bridge deck, as is illustrated in Figure D-1.

Figure D-1 LM1 - main girder; load placement

The built up of this load model is conform NEN-EN 1991-2. The most effective position of the location of the loading has been determined with a small hand-calculation. This has been illustrated in Figure D-3.

D.1.2.1. Deflection (SLS)

The limit for deflection has been set on L/500. There are no real limitations for this deflection, thus this limit has been used. However, the clearance gauge must be maintained. This results in a max deflection of **59.5 mm**.

D.1.2.2. Strength (ULS)

The largest stresses (both in compression and tension) should be below the material allowed stresses.

D.1.3. Cross girder

In the case of the cross girder, the loads have been applied onto the bridge deck, as is illustrated in Figure D-2.
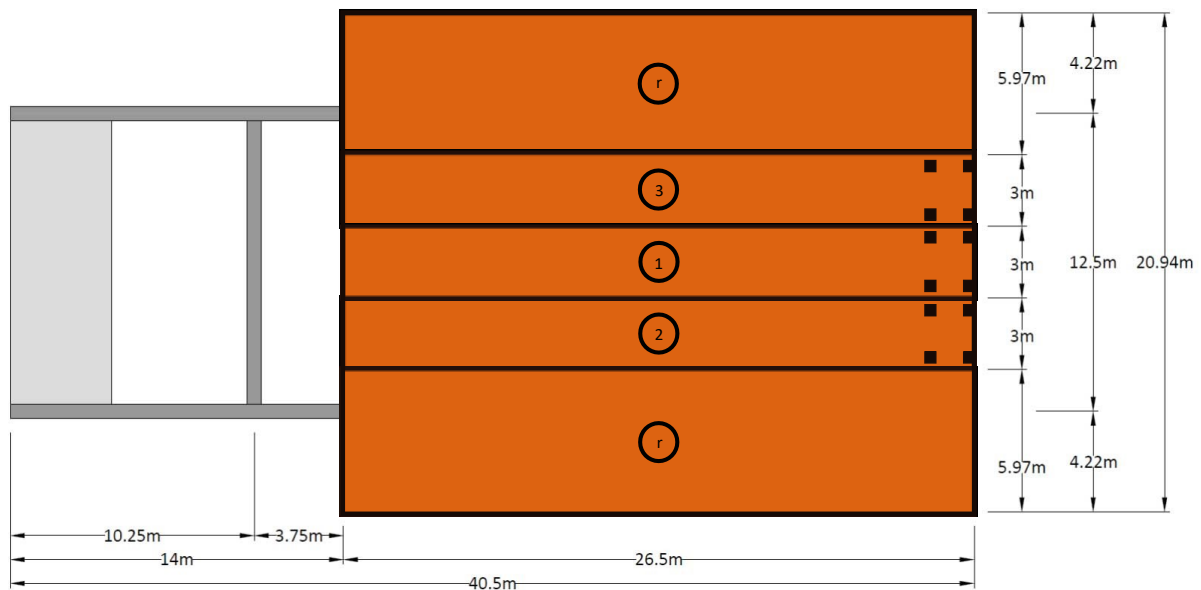
Figure D-2 LM1 - cross girder; load placement

D.1.3.1. Deflection (SLS)

The limit for deflection has been set on L/500. There are no real limitations for this deflection, thus this limit has been used. This results in a max deflection of **25.0 mm**.

D.1.3.2. Strength (ULS)

The largest stresses (both in compression and tension) should be below the material allowed stresses.

The differential equations shown below, have the bridge simplified to a simply supported beam, split into two sections (deck and beam) with boundary equations (moments) at either end and transition equations in between. Only a distributed load is applied at the deck. The location with the largest deflection is then used as the centre of the location for the concentrated loads.

```
restart;
Q := 1010.304 :
q := 288.75 :
a := 8.14 :
F := 5036 :
EI := 1e6 :
l1 := 0.5 :
l2 := 26.5 :
l3 := 29.75 :
```

$$w1 := C1 + C2 \cdot x + C3 \cdot x^2 + C4 \cdot x^3 + \frac{1}{24 \cdot EI} \cdot q \cdot x^4 :$$

$$w2 := C5 + C6 \cdot x + C7 \cdot x^2 + C8 \cdot x^3 :$$

```
phi1 := -diff(w1, x) : phi2 := -diff(w2, x) :
M1 := EI·diff(phi1, x) : M2 := EI·diff(phi2, x) :
V1 := diff(M1, x) : V2 := diff(M2, x) :
x := 0 :
eq1 := w1 = 0 :
```

$$eq2 := M1 = + \frac{1}{2} \cdot q \cdot l1^2 :$$

```
x := l2 - l1 :
eq3 := w1 = w2 :
eq4 := phi1 = phi2 :
eq5 := M1 = M2 :
eq6 := V1 = V2 :
x := l3 - l1 :
eq7 := w2 = 0 :
eq8 := M2 = F·a :
sol1 := solve({eq1, eq2, eq3, eq4, eq5, eq6, eq7, eq8}, {C1, C2, C3, C4, C5, C6, C7, C8}) :
assign(sol1) : x := 'x':
with(plots) :
A := plot(-w1, x = 0 ..(l2 - l1)) :
B := plot(-w2, x = (l2 - l1) ..(l3 - l1)) :
display((A, B));
```
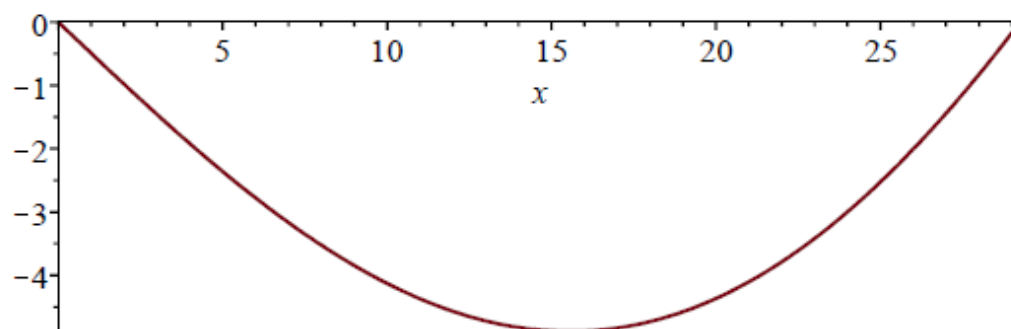


```
sol2 := solve({phi1 = 0, x ≮ 0, x ≯ l3 - l1}, {x}) :
assign(sol2) :
```
Horizontal distance from the rear of the deck to the location of max deflection, due to the distributed load on the deck.
```
xcrit := (l1 + x);
```

$$xcrit := 16.06410009 \tag{1}$$

Figure D-3 LM1 - differential equations w.r.t. load placement; main girder

D.2.   LM2

Load model 2 (NEN-EN 1991-2 section 4.3.3) contains a single axle load and is used for local analysis. This load is placed at random positions on the bridge. In this case study it is used to check the webs of the deck, thus the load is placed dead centre of the deck. This can be seen below in
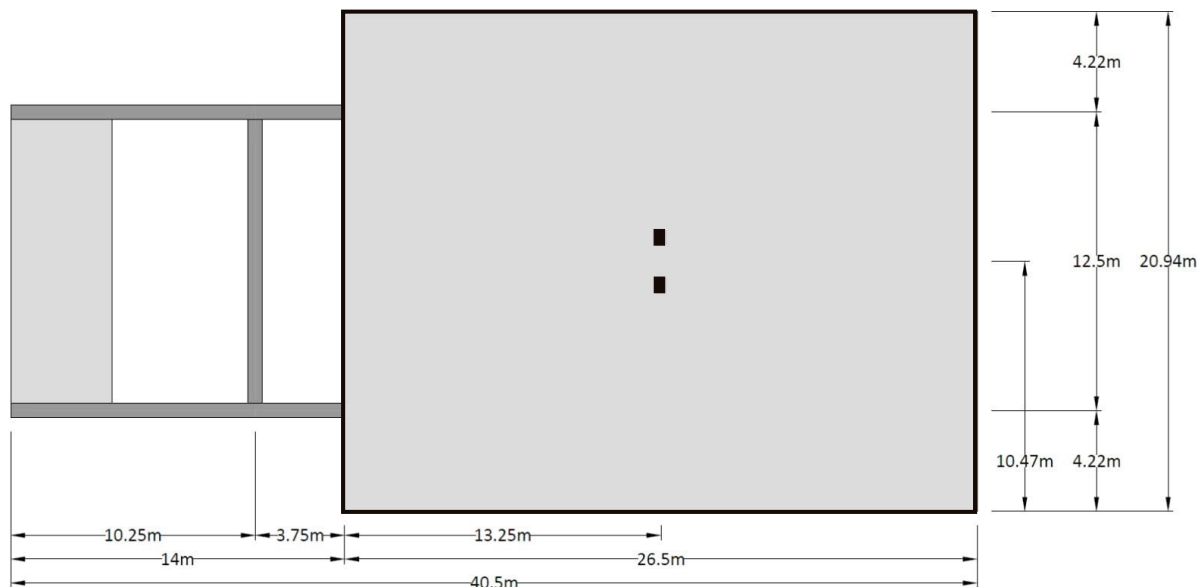
Figure D-4.
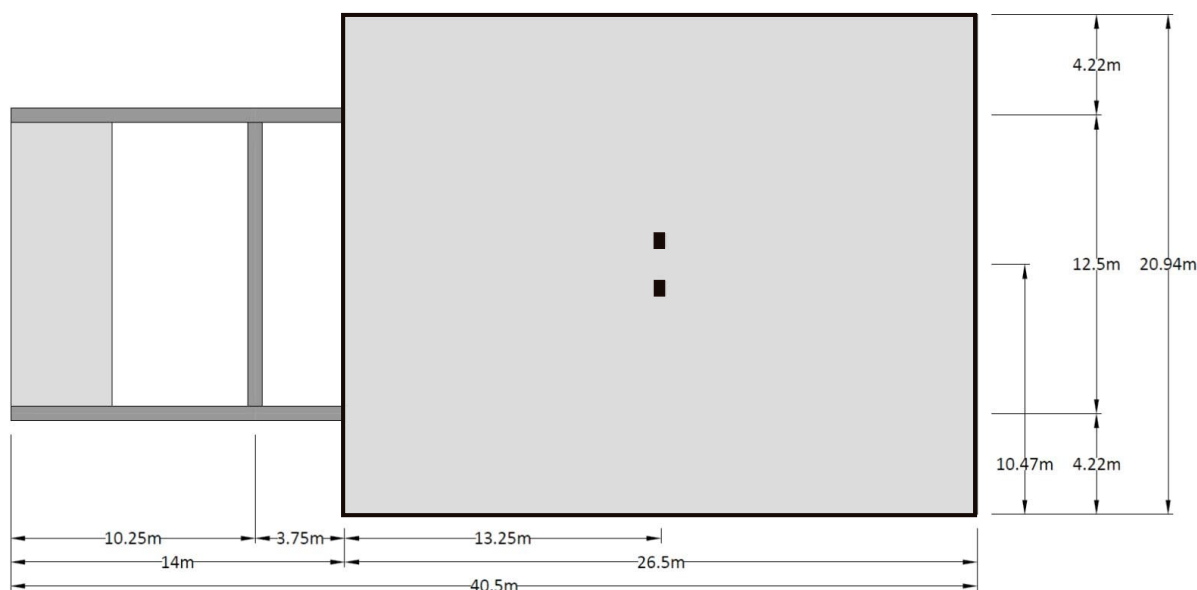
Figure D-4 LM2 -webs of the deck; load placement

The load used for the calculations in LM2 is defined in Table D-4.

Symbol	Load-definition	Magnitude (ULS) [kN/m²]	
$\beta Q_{d,1}$	Concentrated load	2444.03	400 kN

Table D-4 LM2; load definition (ULS) (Heijmans, 2015)

NOTE: the far-right column illustrates the magnitude of the force as a concentrated load. These are based upon the Eurocode NEN-EN 1991-2.

D.3.   LM4

Load model 4 contains a distributed load of 5 kN/m². This has been done for three different options. In the first scenario, where the area between the main girder has been loaded, the deflection of the deck and cross girder in the centre span will be checked. In the latter, the same checks will be done, only now for the sections located at the sides of the bridge. The third is a combination of the first two. This is used to check the main girders. These are illustrated in Figure D-5 until Figure D-7.

D.3.1. Centre span
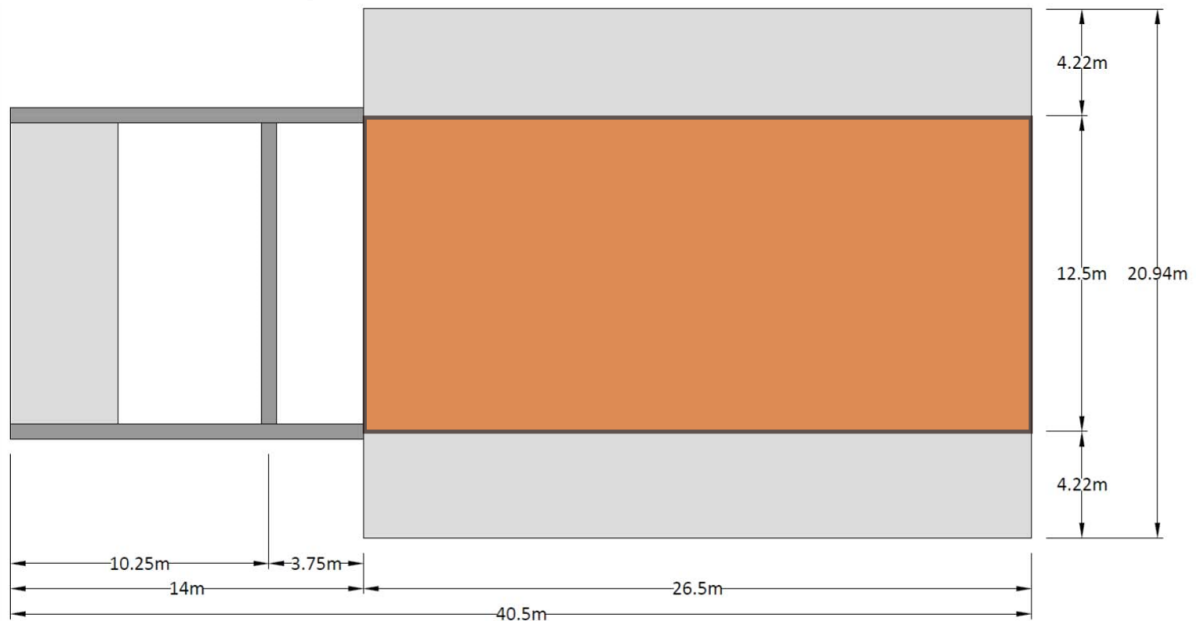
Figure D-5 LM4 - centre span; load placement for cross girders at centre span

D.3.2. Side span
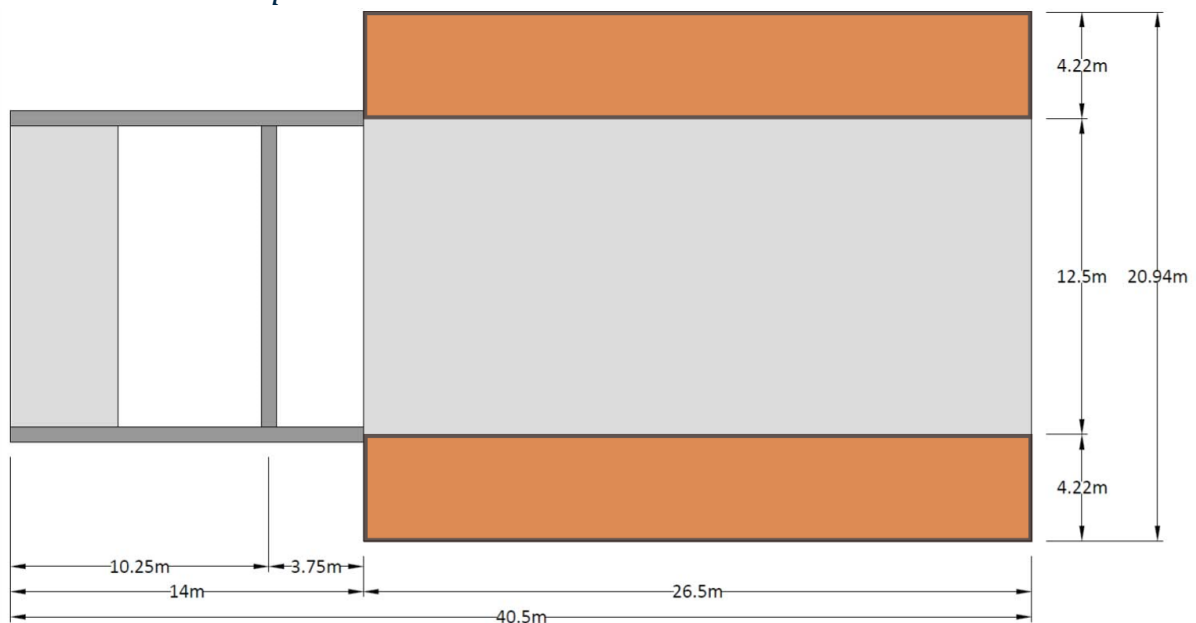
Figure D-6 LM4 - side span; load placement for cross girders at side span

D.3.3. Full span
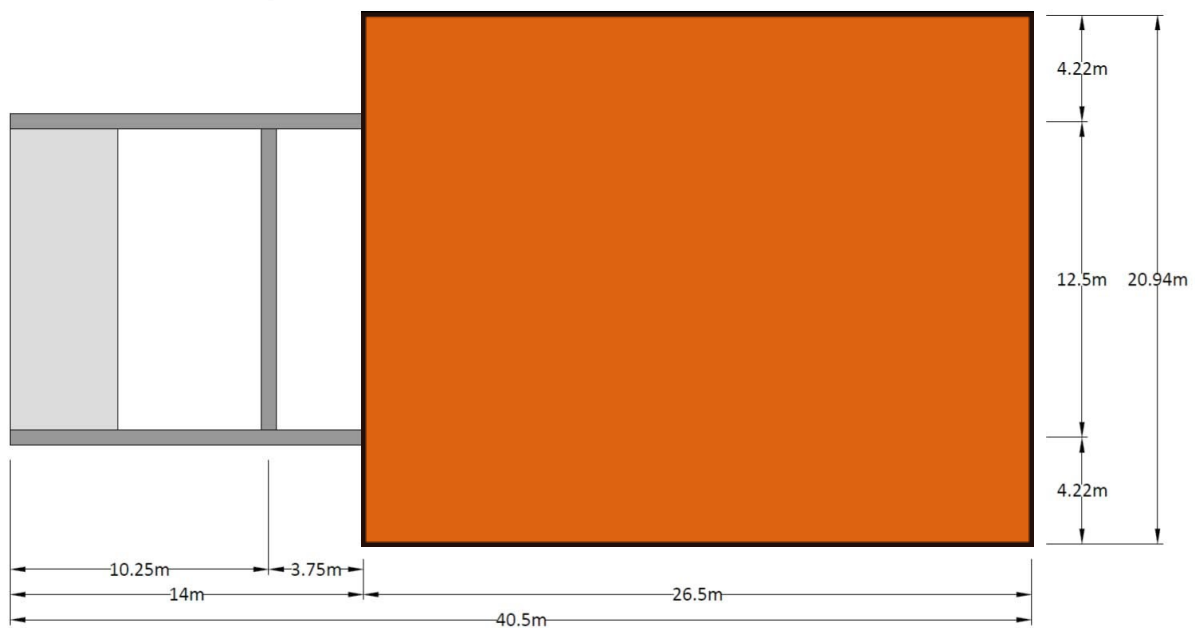
Figure D-7 LM4 - full span; load placement for the main girders

D.4. Fatigue loading

Fatigue damages can be caused by vehicles, the opening & closing cycle of the bridge and vibrations of the counterweight. For the most governing element, the main girder, the second scenario is the governing scenario. This is, therefore, become the load scenario which has been used in this thesis. For a complete check, the others should be enclosed as well, however due to time constraints these have not been done.

The thickness of the bottom flange of the Amalia bridge is determined by fatigue loading. This has led to the application of a 100 mm thick flange, rather than a slimmer alternative. This has been done to move the governing location from lying underneath the deck section towards the rotation centre of the bridge.

Since the built-up of the bottom flange as well as the webs of the main girders of the original Amalia bridge have been used in the adaption designs, the assumption has been made that the governing location of the adaption designs will be located just like the one from the Amalia bridge, as stated just before.

In essence, the stresses found in the different calculations should be comparable to the ones found in the original Amalia bridge's design. This leads to comparable bridge alternatives.

The fatigue calculations for each bridge can be found in their respective chapter/ appendix:

- Amalia bridge: chapter 9.4 and Appendix E (Fatigue verification)
- Non-hybrid design: chapter 10.4.4 and Appendix F (Fatigue verification)
- Hybrid design: chapter 10.4.4 and Appendix G (Fatigue verification)

The essence of the fatigue calculation for opening & closing cycle:

The bridge is taken at its two extremes, regarding stresses. Meaning the lowest and the highest stress values at the same location, result in a stress difference. For the examined girders, this means a **fully opened condition** (the bridge is lifted up to 78 degrees) and a **just opened condition** (the bridge just misses it's supports at the tip of the bridge's leaf. Fatigue damage is tolerated if the sum, of the different elements considered, which would result in a similar cracking pattern, stays below 1.0. The opening and closing cycle has the self-weight of the bridge as the used loading. Next a table has been made illustrating the self-weight of the different components.

Material	Name	Density [kN/m3]
Steel (S355)	[-]	78.0
FRP-facing	FiberCore: skin laminate (FiberCore europe, n.d.)	16.7
FRP-webs	FiberCore: laminate of flat webs (FiberCore europe, n.d.)	14.6
Concrete (light)	Counterweight filling	40.5
Concrete (heavy)	Counterweight filling	50

Table D-5 Material densities used in the self-weight calculations

NOTE: The concrete used in the counterweight, as illustrated above, are heavier than regular concrete. They contain additions of heavy metals to increase the volumetric weight, thus decreasing the total amount of volume required. This allows for smaller counterweights. In this case, two variations on the volumetric weight have been used.

D.5.   Temperature

Temperature influences can cause significant stresses in the construction, especially when using different materials and not allowing for enough clearance for each material to deform on its own (within reason).

For the vertical displacement of deck of the original Amalia bridge design this has resulted in the following:

- Located at the rear girder – 3.6 and + 10.7 mm.
- Located at the front girder – 3.0 and + 1.9 mm.

With the addition that the juncture at this location can be adjusted in the centre of the found displacement, one reaches a maximum displacement of 7.2 mm, differing only 2 mm from the recommended value. (Heijmans, 2015)

NOTE: due to time constraints the calculations required for the determination of he temperature influence, have not been executed. Rather the behaviour due to the influence of temperature differences has been addressed in the literature study in section 6.3.

Appendix E. Details of the Amalia bridge

This appendix contains more detailed information regarding the original Amalia bridge, recreated in Abaqus. It contains the following topics:

- Sectional drawings
- Weight calculation
- Fatigue verification

This model has been based upon the work done by Movares (and Heijmans). Their documents have been used to create this model. The information in this section is, partially derived directly from there.
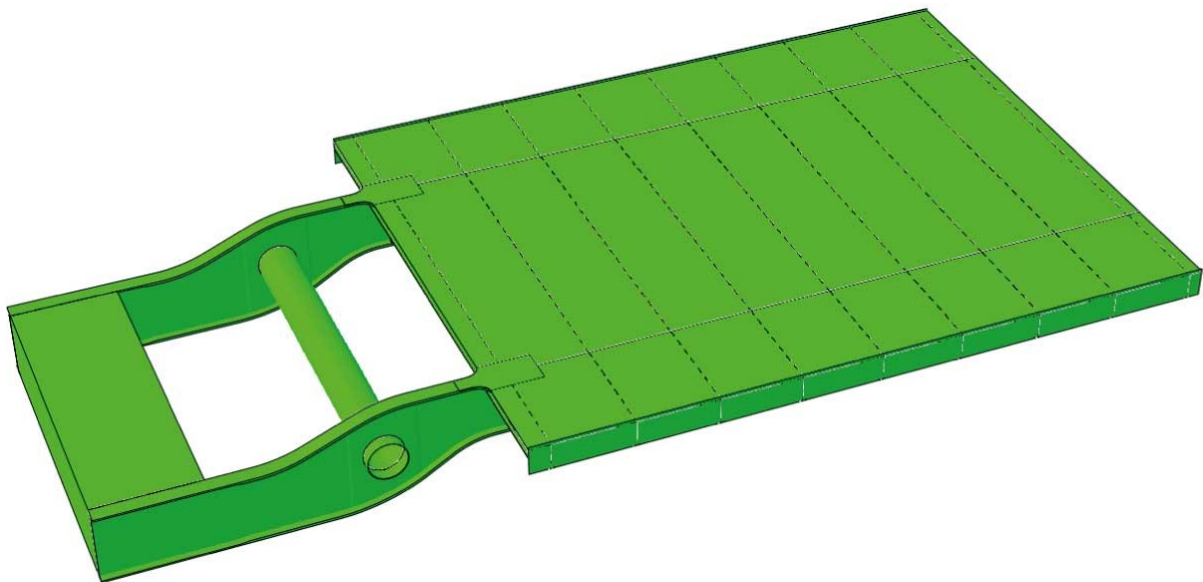
Figure E-1 3D-impression of the original Amalia Bridge; made in Abaqus

E.1.   Sectional drawings

The sections of the original Amalia bridge have been depicted on a larger scale, as has been explained in chapter 9.

E.1.1. Cross section of the movable bridge section
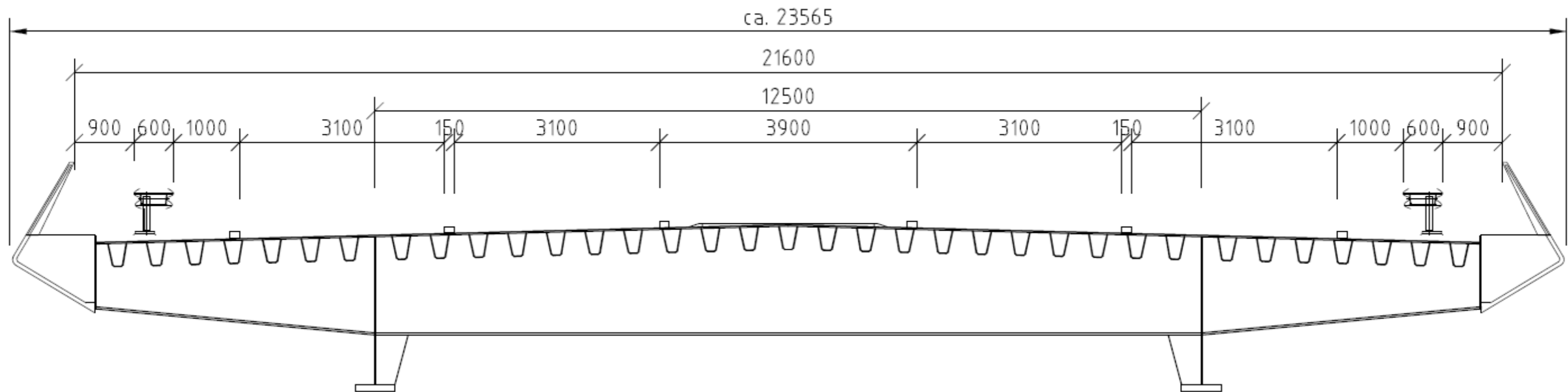
Figure E-2 Cross section original Amalia bridge (Heijmans, 2015)

E.1.2. Length section of the movable bridge section
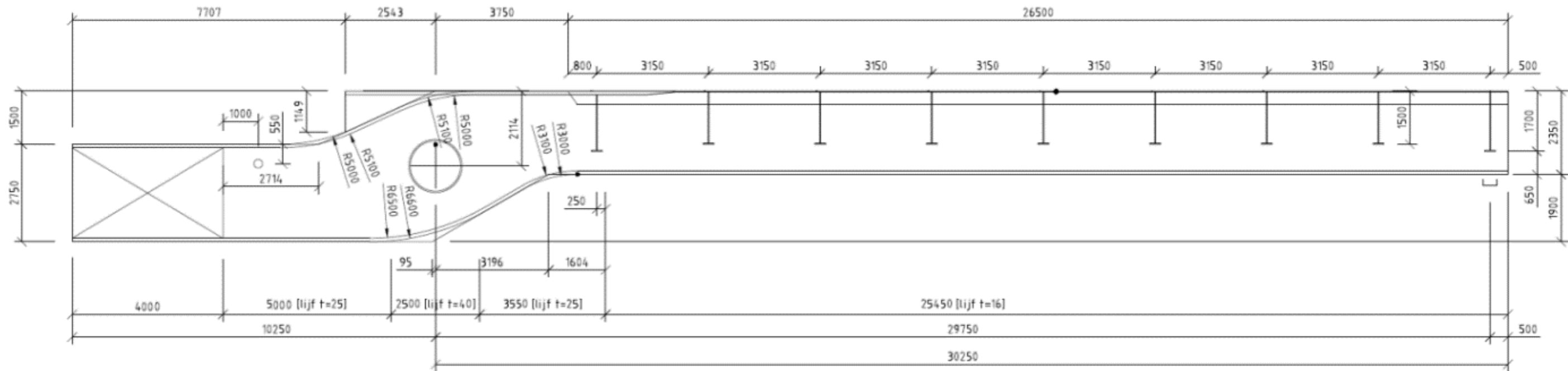
Figure E-3 Length section original Amalia bridge (Heijmans, 2015)

E.2. Weight calculation

In this section the calculation, mentioned in chapter 9.3, has been shown. In essence the bridge's length section is split into two; one left and one right section. For all the existing elements an approximation of the volume, combined with the location of the centre of gravity and the modelled counterweight, using only steel.

E.2.1. Input parameters

Here the different parameters used in these calculations have been displayed.

General		
width deck	20940	mm
length deck	26500	mm
distance rotation centre - start deck	3750	mm
c.t.c. main girders	12500	mm
number of cross girders	9	[-]
distance rotation centre - top deck	2100	mm

Table E-2 General input parameters defining the original Amalia bridge

Densities		
rho,steel	78.5	kN/m3
rho, conc.l	40.5	kN/m3
rho, conc.h	50	kN/m3

Table E-1 Desity definitions regarding the materials of the original Amalia bridge

Deck			Troughs			Main girder			Cross girder		
t,deck	20	mm	t,trough	6	mm	h,girder	2330	mm	h,girder-1,9	1700	mm
			b,top	285	mm	t,w	16	mm	h,girder-2-8	1500	mm
Front/ back cover			b,bot	150	mm	t,f,1	100	mm	t,w	16	mm
t,w	20	mm	h,trough	350	mm	t,f,2	60	mm	t,f	30	mm
h,w	380	mm	c.t.c.	585	mm	b,bot	600	mm	b,bot	300	mm
						c.t.c.	12.5	m	c.t.c.	3.15	m
Side cover			Developed width			l,thin	11950	mm	offset,l	800	mm
t,w	20	mm		863mm	mm	tr,offset	400	mm	offset,r	500	mm
h,w	1150	mm							h,side	1030	mm

Table E-3 Detailled input parameters, per component, defining the original Amalia bridge

E.2.2. Leaf calculation

Below is the table containing the values used for the weight calculation. This is regarding the section on the right side of the rotation centre, as is shown in Figure E-3.

| Description	b1	b2	t	L	Horizontal centre of gravity X	Vertical centre of gravity Y (above is +)	Amount	Volume	Weight	Moment X	Centre of Gravity X	Moment Y	Centre of Gravity Y
Deck system									**1369 kN**	**23270 kNm**	**17. m**	**2792 kNm**	**2.04 m**
Main deck	20940mm	20940mm	20mm	26500mm	17000mm	2090mm	1	11.1 m3	871kN	14811 kNm		1821 kNm	
Side cover	1150mm	1150mm	20mm	26500mm	17000mm	1825mm	2	1.22 m3	96kN	1627 kNm		175 kNm	
Troughs	863mm	863mm	6mm	26500mm	17000mm	1985mm	35	4.8 m3	377kN	6408 kNm		748 kNm	
Front cover (tip leaf)	20940mm	20940mm	20mm	380mm	30250mm	1910mm	1	.16 m3	12kN	378 kNm		24 kNm	
Back cover (base leaf)	20940mm	20940mm	20mm	380mm	3750mm	1910mm	1	.16 m3	12kN	47 kNm		24 kNm	
Main girder									**505 kN**	**6683 kNm**	**13.23 m**	**236 kNm**	**.47 m**
Web-1 (t=40mm)	4050mm	3338mm	40mm	1250mm	980mm	63mm	2	.3 m3	23kN	23 kNm		1 kNm	
Web-2 (t= 25mm)	3338mm	2230mm	25mm	1946mm	2158mm	515mm	2	.27 m3	21kN	46 kNm		11 kNm	
Web-3 (t=25mm)	2230mm	2230mm	25mm	1604mm	3998mm	885mm	2	.18 m3	14kN	56 kNm		12 kNm	
Web-4 (t=16mm)	2230mm	2230mm	16mm	950mm	5275mm	965mm	2	.07 m3	5kN	28 kNm		5 kNm	
Web-5 (t=16mm)	2230mm	2230mm	16mm	12550mm	12025mm	965mm	2	.9 m3	70kN	845 kNm		68 kNm	
Web-6 (t=16mm)	2230mm	2230mm	16mm	11950mm	24275mm	965mm	2	.85 m3	67kN	1625 kNm		65 kNm	
Flange-1 (t=100mm)	600mm	600mm	100mm	3196mm	1598mm	-1090mm	2	.38 m3	30kN	48 kNm		-33 kNm	
Flange-2 (t=60mm)	600mm	600mm	60mm	11950mm	27471mm	-160mm	2	.86 m3	68kN	1855 kNm		-11 kNm	
Flange-3 (t=100mm)	600mm	600mm	100mm	14550mm	14221mm	-180mm	2	1.75 m3	137kN	1949 kNm		-25 kNm	
Top-flange-1	600mm	600mm	100mm	2596mm	1298mm	2050mm	2	.31 m3	24kN	32 kNm		50 kNm	
Top-flange-2	600mm	1400mm	100mm	600mm	2896mm	2050mm	2	.12 m3	9kN	27 kNm		19 kNm	
Top-flange-3	1400mm	1400mm	80mm	2000mm	4196mm	2060mm	2	.45 m3	35kN	148 kNm		72 kNm	

Cross girder-1 (front girder)									**51 kN**	**1524 kNm**	**29.75 m**	**55 kNm**	**1.08 m**
Web-centre	1650mm	1650mm	16mm	12484mm	29750mm	1275mm	1	.3 m3	23kN	691 kNm		30 kNm	
Web-side	1650mm	980mm	16mm	4212mm	29750mm	1443mm	2	.15 m3	12kN	362 kNm		18 kNm	
Flange-centre	300mm	300mm	30mm	12484mm	29750mm	415mm	1	.11 m3	9kN	262 kNm		4 kNm	
Flange-side	300mm	300mm	30mm	4265mm	29750mm	750mm	2	.08 m3	6kN	179 kNm		5 kNm	
Support-web	292mm	610mm	16mm	550mm	29750mm	125mm	2	.01 m3	1kN	19 kNm		kNm	
Support-flange	250mm	30mm	16mm	635mm	29750mm	82mm	2	. m3	kN	11 kNm		kNm	
Cross girder-9 (rear girder)									**51 kN**	**233 kNm**	**4.55 m**	**55 kNm**	**1.08 m**
Web-centre	1650mm	1650mm	16mm	12475mm	4550mm	1275mm	1	.3 m3	23kN	106 kNm		30 kNm	
Web-side	1650mm	980mm	16mm	4208mm	4550mm	1443mm	2	.15 m3	12kN	55 kNm		18 kNm	
Flange-centre	300mm	300mm	30mm	12484mm	4550mm	415mm	1	.11 m3	9kN	40 kNm		4 kNm	
Flange-side	300mm	300mm	30mm	4265mm	4550mm	750mm	2	.08 m3	6kN	27 kNm		5 kNm	
Support-web	292mm	610mm	16mm	550mm	4550mm	125mm	2	.01 m3	1kN	3 kNm		kNm	
Support-flange	250mm	30mm	16mm	635mm	4550mm	82mm	2	. m3	kN	2 kNm		kNm	
Cross girder-2-4 (h=1500mm)									**142 kN**	**2893 kNm**	**20.3 m**	**165 kNm**	**1.16 m**
Web-centre	1450mm	1450mm	16mm	12484mm	20300mm	1375mm	3	.77 m3	60kN	1224 kNm		83 kNm	
Web-side	1450mm	980mm	16mm	4212mm	20300mm	1493mm	6	.42 m3	33kN	676 kNm		50 kNm	
Flange-centre	300mm	300mm	30mm	12484mm	20300mm	615mm	3	.34 m3	26kN	537 kNm		16 kNm	
Flange-side	300mm	300mm	30mm	4265mm	20300mm	850mm	6	.23 m3	18kN	367 kNm		15 kNm	
Support-web	292mm	725mm	16mm	750mm	20300mm	225mm	6	.04 m3	3kN	58 kNm		1 kNm	
Support-flange	250mm	30mm	16mm	866mm	20300mm	167mm	6	.02 m3	1kN	30 kNm		kNm	
Cross girder-5-8 (h=1500mm)									**190 kN**	**1761 kNm**	**9.28 m**	**220 kNm**	**1.16 m**
Web-centre	1450mm	1450mm	16mm	12475mm	9275mm	1375mm	4	1.02 m3	80kN	745 kNm		110 kNm	
Web-side	1450mm	980mm	16mm	4208mm	9275mm	1493mm	8	.56 m3	44kN	411 kNm		66 kNm	
Flange-centre	300mm	300mm	30mm	12484mm	9275mm	615mm	4	.45 m3	35kN	327 kNm		22 kNm	
Flange-side	300mm	300mm	30mm	4265mm	9275mm	850mm	8	.31 m3	24kN	224 kNm		20 kNm	
Support-web	292mm	725mm	16mm	750mm	9275mm	225mm	8	.05 m3	4kN	36 kNm		1 kNm	
Support-flange	250mm	30mm	16mm	866mm	9275mm	167mm	8	.02 m3	2kN	18 kNm		kNm	
Axle									**97 kN**	**kNm**	**. m**	**kNm**	**. m**
Axle (R=750mm)		750mm	40mm	13500mm	mm	mm	1	1.24 m3	97kN	kNm		kNm	
Addition									**24 kN**	**346 kNm**	**14.38 m**	**33 kNm**	**1.37 m**
Welding/ conservation				1.00%					24kN	346kN		33kN	
Road equipment & wear layer									**471 kN**	**8005 kNm**	**17. m**	**967 kNm**	**2.05 m**
Wear layer 22,5 kN/m³	20940mm	20940mm	8mm	26500mm	17000mm	2104mm	1	4.44 m3	100kN	1698 kNm		210 kNm	
Edge elements 4,0 kN/m				26500mm	17000mm	1804mm	2		212kN	3604 kNm		382 kNm	
Midsection 3,0 kN/m				26500mm	17000mm	2104mm	1		80kN	1352 kNm		167 kNm	
Road equipment 1,5 kN/m				26500mm	17000mm	2600mm	2		80kN	1352 kNm		207 kNm	
Total									**2901 kN**	**44715 kNm**	**15414 mm**	**4523 kNm**	**1559 mm**

Table E-4 Weight calculation of the right side of the original Amalia bridge

E.2.3. Counterweight calculation

Below is the table containing the values used for the weight calculation. This is regarding the section on the left side of the rotation centre, as is shown in Figure E-3.

Description	b1	b2	t	L	Horizontal centre of gravity X	Vertical centre of gravity Y (below is +)	Amount	Volume	Weight	Moment X	Centre of Gravity X	Moment Y	Centre of Gravity Y
Main girder									**278 kN**	**1271 kNm**	**4.57 m**	**32 kNm**	**.12 m**
Web-1 (t=40mm)	4050mm	3520mm	40mm	1250mm	974mm	-35mm	2	.31 m3	24kN	24 kNm		-1 kNm	
Web-2 (t= 25mm)	2550mm	3520mm	25mm	2286mm	2454mm	-709mm	2	.35 m3	27kN	67 kNm		-19 kNm	
Web-3 (t=25mm)	2550mm	2550mm	25mm	1664mm	4368mm	675mm	2	.21 m3	17kN	73 kNm		11 kNm	
Web-4 (t=25mm)	2630mm	2630mm	25mm	5050mm	7725mm	-865mm	2	.66 m3	52kN	403 kNm		-45 kNm	
Bottom-flange-1 (60mm)	600mm	600mm	60mm	5050mm	7725mm	2120mm	2	.36 m3	29kN	220 kNm		61 kNm	
Bottom-flange-2 (100mm)	600mm	600mm	100mm	5200mm	2600mm	2100mm	2	.62 m3	49kN	127 kNm		103 kNm	
Top-flange-1 (100mm)	600mm	600mm	100mm	3841mm	1768mm	-1350mm	2	.46 m3	36kN	64 kNm		-49 kNm	
Top-flange-2 (60mm)	600mm	600mm	60mm	5050mm	7725mm	-630mm	2	.36 m3	29kN	220 kNm		-18 kNm	
Top-flange-3(100mm)	600mm	600mm	100mm	1664mm	4673mm	-650mm	2	.2 m3	16kN	73 kNm		-10 kNm	
Axle									**97 kN**	**kNm**	**. m**	**kNm**	**. m**
Axle (R=750)		750mm	40mm	13500mm	mm	mm	1	1.24 m3	97kN	kNm		kNm	
Counterweight (steel box)									**640 kN**	**5600 kNm**	**8.74 m**	**496 kNm**	**.78 m**
Top cover	12500mm	12500mm	25mm	4000mm	8250mm	-600mm	1	1.25 m3	98kN	810 kNm		-59 kNm	
Bottom cover	12500mm	12500mm	25mm	4000mm	8250mm	2150mm	1	1.25 m3	98kN	810 kNm		211 kNm	
Front cover	12500mm	12500mm	25mm	2750mm	6263mm	775mm	1	.86 m3	67kN	422 kNm		52 kNm	
Back cover	12500mm	12500mm	25mm	2750mm	10238mm	775mm	1	.86 m3	67kN	691 kNm		52 kNm	
Width separators	12500mm	12500mm	25mm	2750mm	9275mm	775mm	1	.86 m3	67kN	626 kNm		52 kNm	
Length separators	4000mm	4000mm	40mm	2750mm	9275mm	775mm	7	3.08 m3	242kN	2243 kNm		187 kNm	
Addition									**20 kN**	**137 kNm**	**6.77 m**	**11 kNm**	**.52 m**
Welding/ conservation				2.00%					20kN	137kN		11kN	
Counterweight (content)									**4535 kN**	**36813 kNm**	**8.12 m**	**3490 kNm**	**.77 m**
Front counterweight (40.5 kN/m3)	12195mm	12195mm	2520mm	2975mm	7750mm	710mm	1	91.43 m3	3703kN	28696 kNm		2629 kNm	
Rear counterweight (40.5 kN/m3)	1625mm	1625mm	2700mm	975mm	9750mm	800mm	2	8.56 m3	347kN	3378 kNm		277 kNm	
Rear counterweight (40.5 kN/m3)	760mm	760mm	2700mm	975mm	9750mm	800mm	2	4. m3	162kN	1580 kNm		130 kNm	
Adjustable (50 kN/m3)	1600mm	1600mm	1125mm	900mm	9750mm	1403mm	2	3.24 m3	162kN	1579 kNm		227 kNm	
Adjustable (50 kN/m3)	1600mm	1600mm	1125mm	900mm	9750mm	1403mm	2	3.24 m3	162kN	1579 kNm		227 kNm	
Total									**5571 kN**	**43822 kNm**	**-7866 mm**	**4029 kNm**	**-723 mm**

Table E-5 Weight calculation of the left side of the original Amalia bridge

E.2.4. Balance calculation

According to the Dutch code (NEN6787 VOBB:2001 article 8.4.2.5.2) to prevent the bridge from opening an overpressure is required at the tip of the leaf of the bridge. This pressure (of 30kN) has resulted in the below mentioned **moment X** in the closed condition; The same principle is to be used in the fully opened condition, resulting in a moment which is 1/3 of the aforementioned closed condition counterpart.

Description	Element angle [°]	Distance between total & elemental Centre of Gravity	Horizontal centre of gravity X	Vertical centre of gravity Y (above is +)		Weight	Moment X	Centre of Gravity X	Moment Y	Centre of Gravity Y
Closed condition						8472 kN	892.5 kNm	105 mm	494 kNm	58 mm
Leaf section	5.78	15493 mm	15414 mm	1559 mm		2901 kN	44715 kNm		4523 kNm	
Counterweight section	5.25	7899 mm	-7866 mm	-723 mm		5571 kN	-43822 kNm		-4029 kNm	
Opened condition						8472 kN	-297.5 kNm	-35 mm	-976 kNm	-115 mm
Leaf section	83.78	15493 mm	1680 mm	15402 mm		2901 kN	4872 kNm		-44678 kNm	
Counterweight section	83.25	7899 mm	928 mm	7844 mm		5571 kN	-5170 kNm		43702 kNm	

Table E-6 Balancing calculation of the original Amalia bridge

NOTE: In the opened condition the rotation angle of the bridge is set at 78 degrees.

E.2.5. Weight division

Below insight is given into the weight division of the Amalia bridge and its sections. This is illustrated in three tables; each illustration their respective components with their corresponding contribution to the total weight.

	Whole bridge	
	[kN]	
Deck-system	1369	16%
Main girders	783	9%
Cross girders	435	5%
Counterweight	5176	61%
Axle	194	2%
Rest	515	6%
Total bridge	**8472**	**100%**

Table E-8 Weight division of the original Amalia bridge

	Leaf	
	[kN]	
Deck-system	1369	47%
Main girders	505	17%
Cross girders	435	15%
Axle	97	3%
Conservation	24	0.8%
Road equipment	471	16%
Total bridge	**2901**	**100%**

Table E-9 Weight division of the leaf of the original Amalia bridge

	Counterweight	
	[kN]	
Main girders	278	5%
Axle	97	2%
CW-box	640	11%
CW-content	4535	81%
Conservation	20	0.4%
Total bridge	**5571**	**100%**

Table E-7 Weight division of the counterweight of the original Amalia bridge

E.3.   Fatigue verification

E.3.1. SCIA-Engineer model

E.3.1.1.   Governing location

In table 8.5 of the *technical description of the leaf of the Amalia bridge* (Heijmans, 2015) the results of the fatigue calculations for the main load bearing construction has been made. Below the governing section has been displayed. This is located in the main girder, below the heal girder.

Appendix	Description	Detail	Category [$\Delta\sigma_c$]	Damage [-]
D.2	Main girder, rounding radius (r=3100) below heel girder, stress in length direction.	Table 8.2, detail 1	125	**0.46**
	Idem, stress in radial direction.	Table B.1, detail 3	100	**0.55**
			Sum:	**1.01**

Table E-10 Results fatigue calculation main load bearing element of the original Amalia bridge (Heijmans, 2015)

According to damage summation (rule of Palmgren-Miner, which can be found in Appendix A of NEN-EN-1-9) the above shown values can be added. This is done as follows:

$$\sum \frac{n_i}{N_i} = \frac{n_1}{N_1} + \frac{n_2}{N_2} + \frac{n_3}{N_3} + \frac{n_4}{N_4} \leq D_L$$

Equation E-1 Rule of Palmgren-Miner (NNI, 2012)

E.3.1.2.   Damage limit exceedance

When it comes to a fatigue check, the resulting damages should be below 1.00. As is illustrated in the figure above this is not the case for this governing detail, however the calculated damage is only slightly greater than 1.00. This exceedance is deemed to be acceptable.

$$k_s := \text{if}\left[\text{antw} = \text{"ja"}, \text{if}\left[t > 25\text{mm}, \left(\frac{25\text{mm}}{t}\right)^{0.2}, 1\right], 1\right]$$

$$\Delta\sigma_{c.d} := \frac{\Delta\sigma_c}{\gamma_{Mf}}$$

$$\Delta\sigma_D := k_s \cdot \left(\frac{2}{5}\right)^{\frac{1}{m}} \cdot \Delta\sigma_{c.d}$$

$$N_{cycles_i} := \begin{vmatrix} 2\cdot10^6 \cdot \left(\frac{\Delta\sigma_{c.d}}{\Delta\sigma_i}\right)^m & \text{if } \Delta\sigma_i \geq \Delta\sigma_D \\ 5\cdot10^6 \cdot \left(\frac{\Delta\sigma_D}{\Delta\sigma_i}\right)^5 & \text{if } \Delta\sigma_D > \Delta\sigma_i \geq \Delta\sigma_L \\ \infty & \text{otherwise} \end{vmatrix}$$

$$\Delta\sigma_L := \left(\frac{5}{100}\right)^{\frac{1}{5}} \cdot \Delta\sigma_D$$

$$D_i := \frac{n_i}{N_{cycles_i}}$$

Equation E-2 Damage calculation approach (Heijmans, 2015)

In the figure above the damage calculation is shown. One can see that in the calculation of the amount of governing cycles, it depends on a ratio, to the power of either m (3 - according to the slope of the Wöhler-line) or 5. In the case of having a slightly decreased fatigue stress difference, this results in a 1.5 to 2.5 times greater decrease in the damage. This means, that an exceedance of 1% can be reduced, to fulfil the damage criterium, by as little as 0.67 of a reduction in the fatigue stress difference. As a result, the acquired damages due to fatigue stress, are considered to be acceptable.

E.3.1.3. Built up

The governing damage due to fatigue loading consists of the summation of two damages, due to the fact they initiate the same crack pattern.

- The first is in the bottom flange of the main girder and is located below the rear girder. This is the last girder, as seen from the tip of the leaf.
- The second is in the flange of the main girder and is also located below the rear girder.

A wide range of different load models have been applied to the bridge to obtain the stresses at this location, which could possibly lead to fatigue damages. Below this has been illustrated for both of the governing locations, depicting which of these load models is governing.

E.3.1.4. Bottom flange – main girder

The following table has been taken from appendix D.2 (Heijmans, 2015), as has been illustrated in Equation E-2:

Voertuig:	n_i:	$\Delta\sigma_i$:	N_{cycles}:	D_i:
Wagen 1, Rijstrook 1	11.250.000	20,75	oneindig	0,000
Wagen 1, Rijstrook 1 & 2	1.250.000	23,88	oneindig	0,000
Wagen 2, Rijstrook 1	1.125.000	22,33	oneindig	0,000
Wagen 2, Rijstrook 1 & 2	125.000	27,11	oneindig	0,000
	125.000	27,13	oneindig	0,000
Wagen 3, Rijstrook 1	4.500.000	23,35	oneindig	0,000
Wagen 3, Rijstrook 1 & 2	500.000	29,12	oneindig	0,000
	500.000	29,14	oneindig	0,000
Wagen 4, Rijstrook 1	3.375.000	21,98	oneindig	0,000
Wagen 4, Rijstrook 1 & 2	375.000	26,39	oneindig	0,000
	375.000	26,40	oneindig	0,000
Wagen 5, Rijstrook 1	2.250.000	22,20	oneindig	0,000
Wagen 5, Rijstrook 1 & 2	250.000	26,85	oneindig	0,000
	250.000	26,86	oneindig	0,000
Trilling ballastkist	200.000.000	17,83	oneindig	0,000
Openen en sluiten	1.000.000	89,85	2,189E+06	0,457
			D_{totaal} =	0,46

Table E-11 Damage calculation bottom flange; category 125; detailed description (Heijmans, 2015)

NOTE: in this figure, the values smaller than 25% of the cut-off limit have not been depicted.

The above shown figure shows the amount of governing cycles; the stress difference; and the resulting damage for different situations. These considered situations are: five different kinds of trucks on either traffic lane 1 or traffic lane 1 and 2; the vibrations caused by the counterweight; the opening and closing cycle.

As one can clearly see, only the opening and closing cycle causes fatigue damage and is therefore the governing criterium.

The value of the stress difference, for this governing criterium, can be obtained when viewing the situation in which the bridge is FULLY opened, and in rest, as well as when the bridge is JUST opened. In the latter case, this means that the support at the tip of the leaf, will be removed, however the

bridge is still considered to be horizontal. Both situations and their corresponding values are shown next. The pictures illustrating this, are screenshots, obtained from the aforementioned document.

Since the values might be rather small, they have been written down below each screenshot.
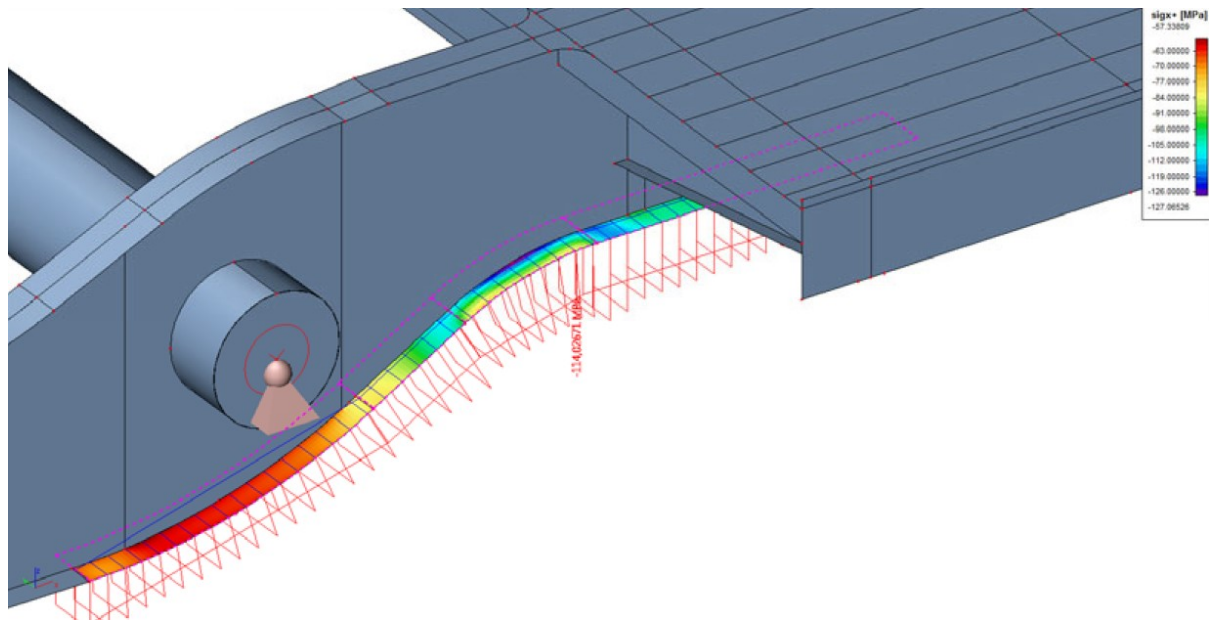

Figure E-4 S11, stress in length direction – just opened condition; Amalia bridge, SCIA (Heijmans, 2015)
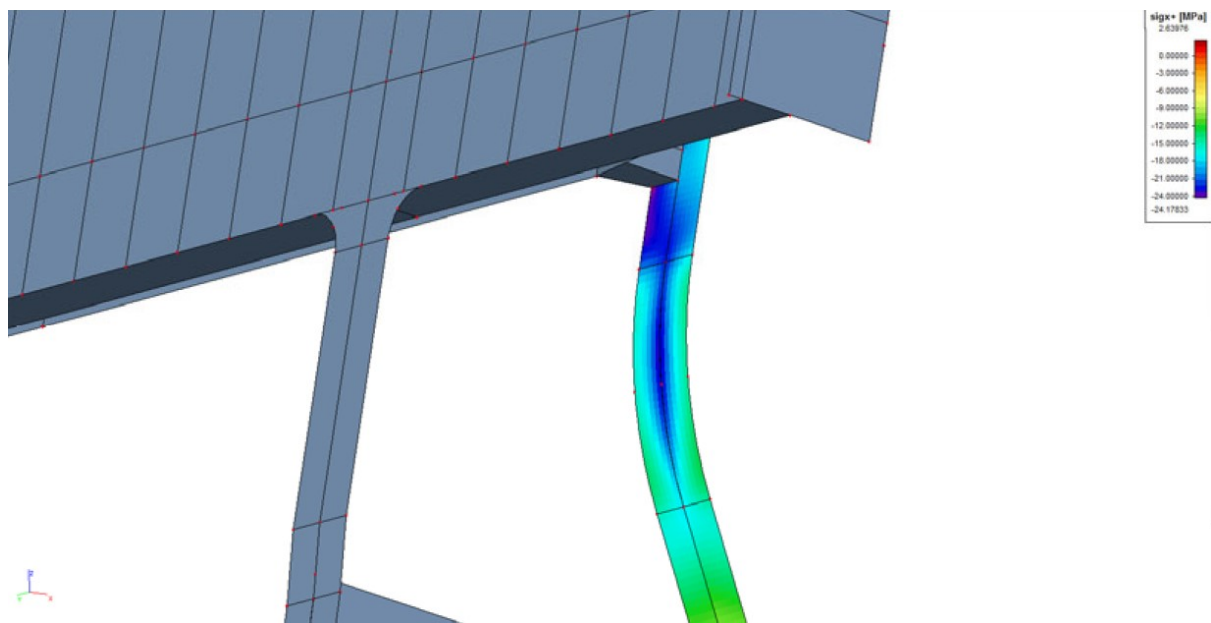
$$\sigma_{11, just\ opened} = -114.027\ MPa$$

Figure E-5 S11, stress in length direction – fully opened condition; Amalia bridge, SCIA (Heijmans, 2015)

$$\sigma_{11, fully\ opened} = -24.176\ MPa$$

Resulting in:

$$\Delta\sigma_i = \left|\sigma_{11, just\ opened} - \sigma_{11, fully\ opened}\right| = 89.85\ MPa$$

E.3.1.5.   Web – main girder

The following table has been taken from appendix D.2 (Heijmans, 2015), as has been illustrated in Equation E-2:

Voertuig:	n_i:	$\Delta\sigma_i$:	N_{cycles}:	D_i:
Wagen 1, Rijstrook 1	11.250.000	16,60	oneindig	0,000
Wagen 1, Rijstrook 1 & 2	1.250.000	17,06	oneindig	0,000
Wagen 2, Rijstrook 1	1.125.000	17,66	oneindig	0,000
Wagen 2, Rijstrook 1 & 2	125.000	18,28	oneindig	0,000
Wagen 3, Rijstrook 1	4.500.000	17,94	oneindig	0,000
Wagen 3, Rijstrook 1 & 2	500.000	18,60	oneindig	0,000
Wagen 4, Rijstrook 1	3.375.000	17,41	oneindig	0,000
Wagen 4, Rijstrook 1 & 2	375.000	17,97	oneindig	0,000
Wagen 5, Rijstrook 1	2.250.000	17,28	oneindig	0,000
Wagen 5, Rijstrook 1 & 2	250.000	17,81	oneindig	0,000
Trilling ballastkist	200.000.000	14,63	oneindig	0,000
Openen en sluiten	1.000.000	76,56	1,812E+06	0,552
			$D_{totaal}=$	0,55

Table E-12 Damage calculation web; category 100; detailed description (Heijmans, 2015)

NOTE: in this figure, the values smaller than 25% of the cut-off limit have not been depicted.

The same situations as were checked in the previous section, have been checked for the web. And as was the case for the bottom flange, for the web only the opening and closing cycle results in fatigue damages.

The difference here is that for the web, the radial stresses have been checked.

Since the values might not be readable, they have been written down below each screenshot.
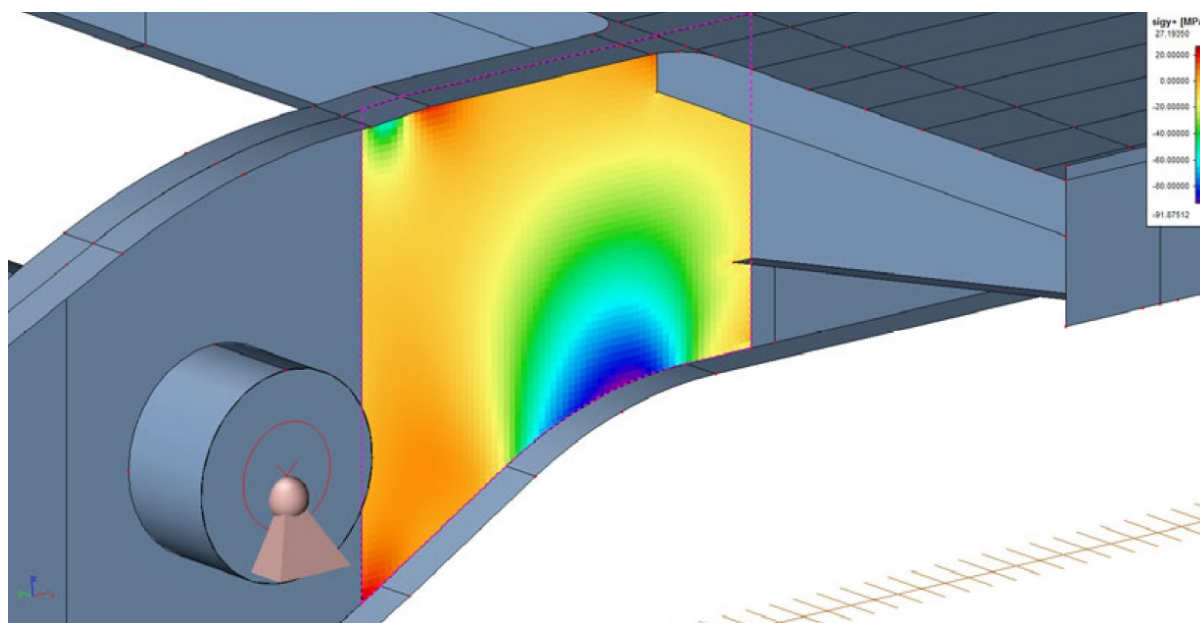

Figure E-6 S22, stress in radial direction – just opened condition; Amalia bridge, SCIA (Heijmans, 2015)
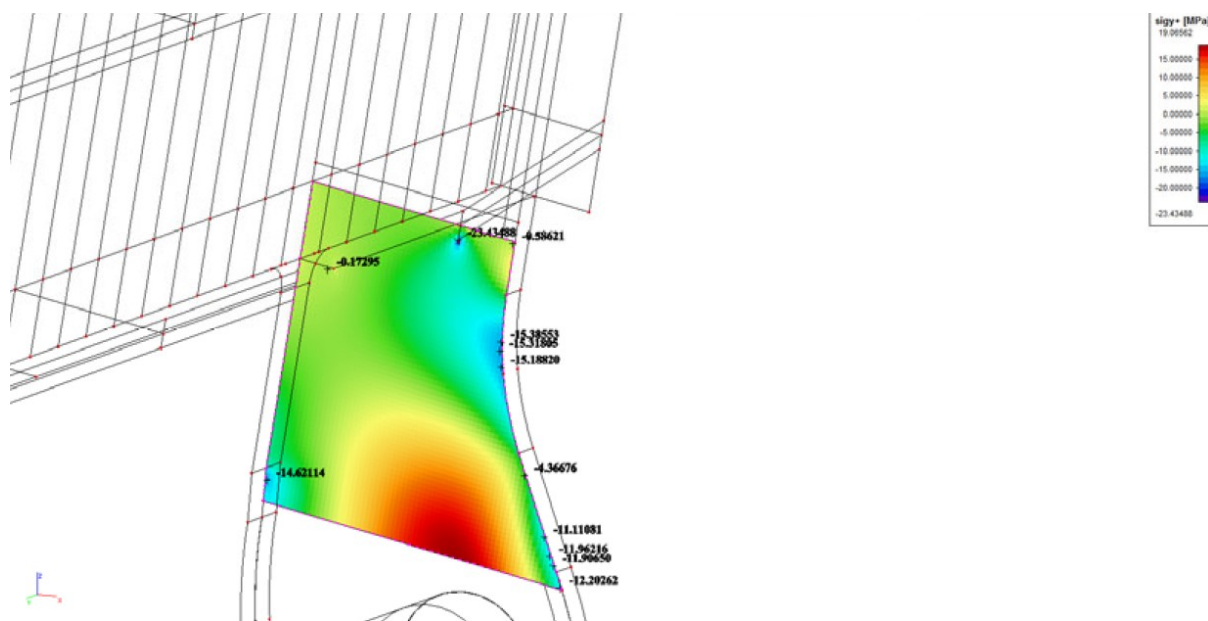
$$\sigma_{22,just\ opened} = -91.875\ MPa$$

Figure E-7 S22, stress in radial direction – fully opened condition; Amalia bridge, SCIA (Heijmans, 2015)

$$\sigma_{22,fully\ opened} = -15.318\ MPa$$

Resulting in:

$$\Delta\sigma_i = \left|\sigma_{22,just\ opened} - \sigma_{22,fully\ opened}\right| = 76.56\ MPa$$

E.3.2. Abaqus model

The same approach as used in obtaining the results from the SCIA-Engineer model (Heijmans, 2015), has been used for the Abaqus model. These steps are illustrated next.

E.3.2.1. Bottom flange – main girder

Applied load factors

γ_{Ff}	1.00	[-]	Load safety factor	NEN-EN 1993-2 art. 9.3
$\Delta\varphi_{fat}$	1.15	[-]	Impact factor near joint	NEN-EN 1991-2 art. 4.6.1
α_{user}	1.00	[-]	Additional multiplication factor on behalf of the user	

Table E-13 Applied load factors; bottom flange of the main girder (Heijmans, 2015)

Assumptions fatigue calculation

$\Delta\sigma_c$	125	[N/mm²]	Detail category
γ_{Mf}	1.35	[-]	Partial load factor for fatigue
t	100	[mm]	Plate thickness
k_s	1.00	[-]	Reduction factor for the plate thickness; not applied
m	3	[-]	Slope Wöhler-line
$\Delta\sigma_{c,d}$	92.59	[N/mm²]	Design value detail category
$\Delta\sigma_D$	68.22	[N/mm²]	Constant amplitude limit
$\Delta\sigma_L$	37.47	[N/mm²]	Cut-off limit

Table E-14 Assumptions fatigue calculation; bottom flange of the main girder (Heijmans, 2015)

The values in Table E-14 have been calculated using the formulas found in Equation E-2. Next the stress values , obtained from Abaqus have been combined to obtain the stress difference, from which the fatigue damage can be calculated. This is illustrated next:

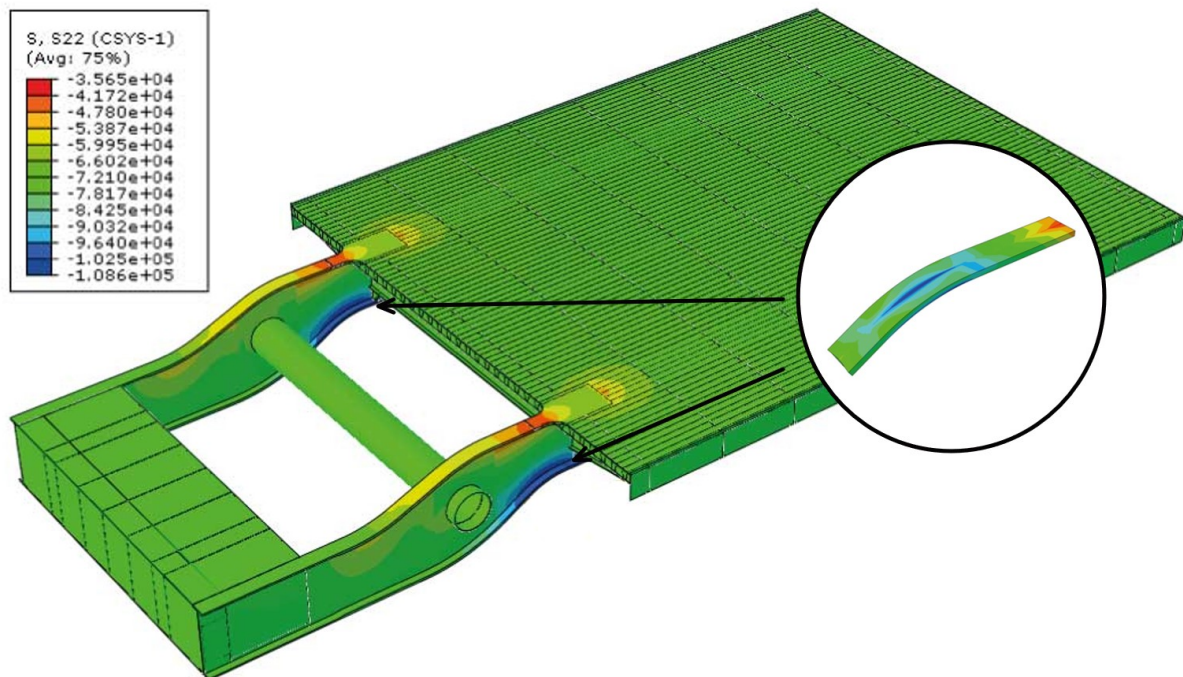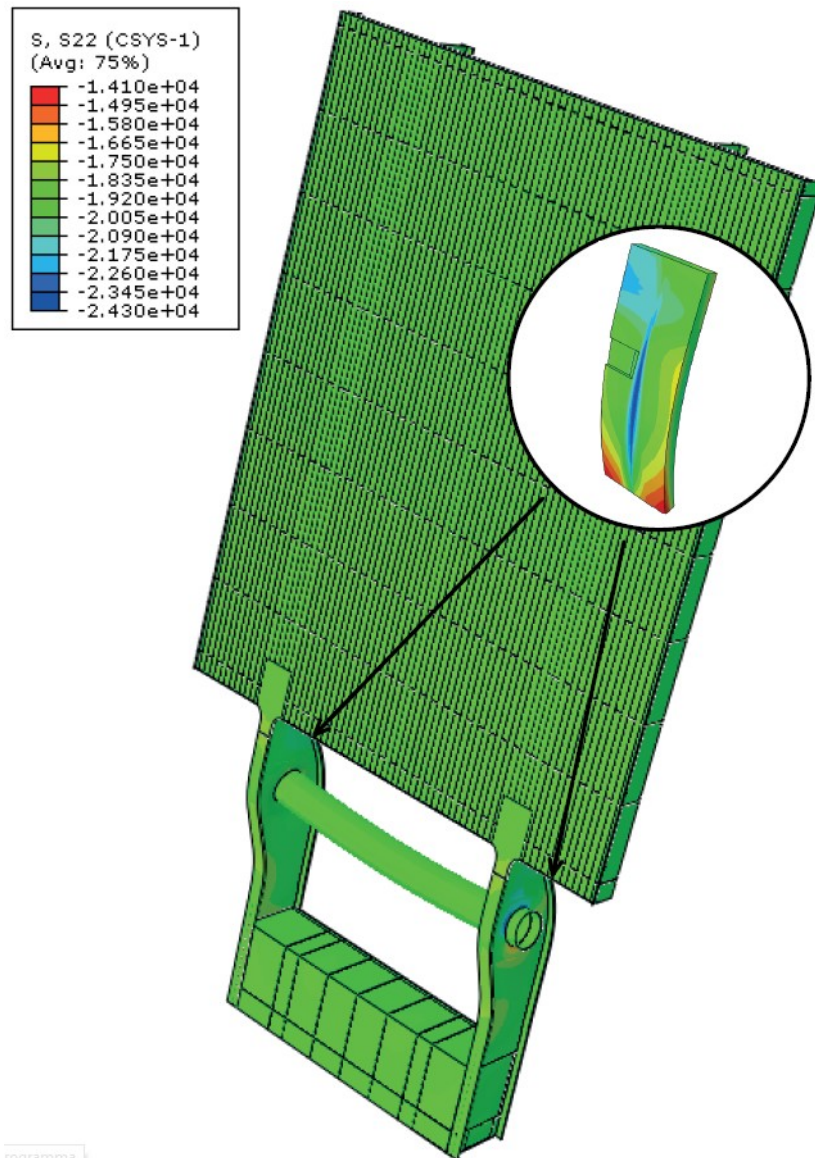### E.3.2.1.1.   Just opened condition

Figure E-8 S11, stress in length direction – just opened condition; Amalia bridge, Abaqus

$$\sigma_{11,just\ opened} = -1.086 \times 10^5 kPa \rightarrow -108.6\ MPa$$

NOTE1: The illustrations mention S22, while the equations mention S11, which is the requested stress value. A local coordinate system has been defined to extract the longitudinal stresses along the curvature of the bottom flange. This coincides with the tangential stresses for a circle at this location. Thus, S22 is shown in this illustration.

NOTE2: The stresses calculated above, have been defined by a local coordinate system, due to the curvature of the bottom flange. Thus, the name used in the legend, local S22 (csys-1), corresponds with the global primary direction.

NOTE3: For all the illustrations similar to the one illustrated above, the stresses in the legend correspond with the close-up section (shown in the circle). It does NOT correspond with the stresses in the bridge as a whole.

E.3.2.1.2.   Fully opened condition

Figure E-9 S11, stress in length direction – fully opened condition; Amalia bridge, Abaqus

$$\sigma_{11,fully\ opened} = -2.430 \times 10^4 kPa \rightarrow -24.30\ MPa$$

Resulting in a stress difference

$$\Delta\sigma_i = \left|\sigma_{22,just\ opened} - \sigma_{22,fully\ opened}\right| = 84.30\ MPa$$

This stress difference is considered to be comparable to the one obtained from SCIA. Both values differ, however not significantly. The found stress difference leads to a lower fatigue damage, which due to the powers in these calculations, result in a larger difference. This is noted and can be explained by the difference in the model built up, as stated in 8.3.1 – Comparing models

and the fatigue damage (according to Equation E-2 and Table E-14)

$$D_i = 0.377$$

E.3.2.2.   Web – main girder

The applied load factors are identical to the ones displayed in Table E-13.

Assumptions fatigue calculation

$\Delta\sigma_c$	100	[N/mm²]	Detail category
γ_{Mf}	1.35	[-]	Partial load factor for fatigue
t	100	[mm]	Plate thickness
k_s	1.00	[-]	Reduction factor for the plate thickness; not applied
m	3	[-]	Slope Wöhler-line
$\Delta\sigma_{c,d}$	74.07	[N/mm²]	Design value detail category
$\Delta\sigma_D$	54.58	[N/mm²]	Constant amplitude limit
$\Delta\sigma_L$	29.98	[N/mm²]	Cut-off limit

Table E-15 Assumptions fatigue calculation; web of the main girder (Heijmans, 2015)

The values in Table E-15 have been calculated using the formulas found in Equation E-2. Next the stress values , obtained from Abaqus have been combined to obtain the stress difference, from which the fatigue damage can be calculated. This is illustrated below:

E.3.2.2.1.   Just opened condition
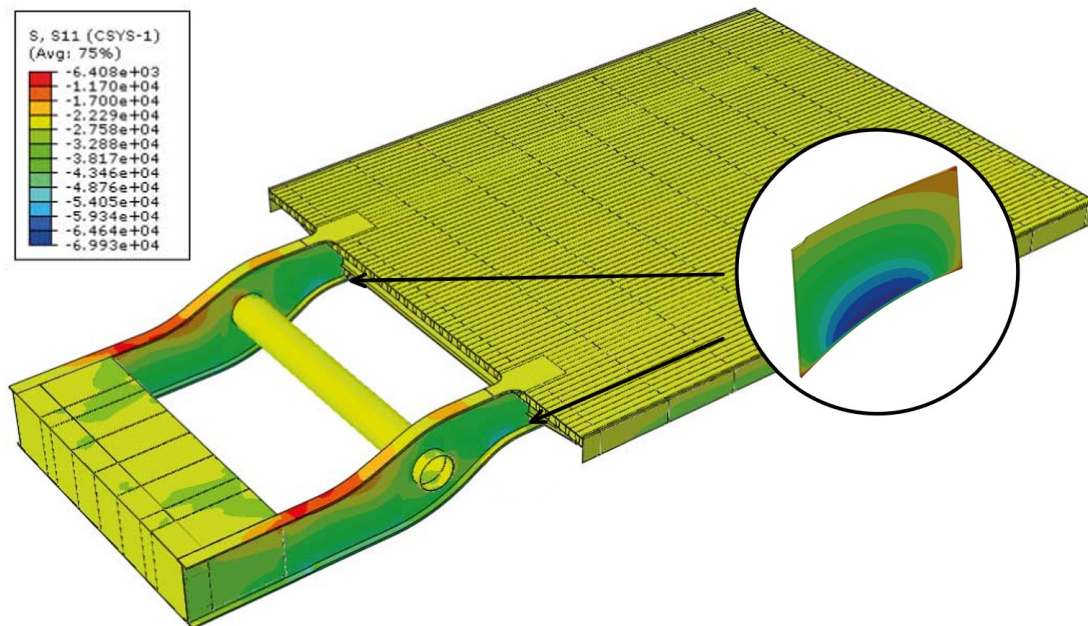
Figure E-10 S22, stress in radial direction – just opened condition; Amalia bridge, Abaqus

$$\sigma_{22, just\ opened} = -6.993 \times 10^4 kPa \rightarrow -69.93\ MPa$$

E.3.2.2.2.   Fully opened condition
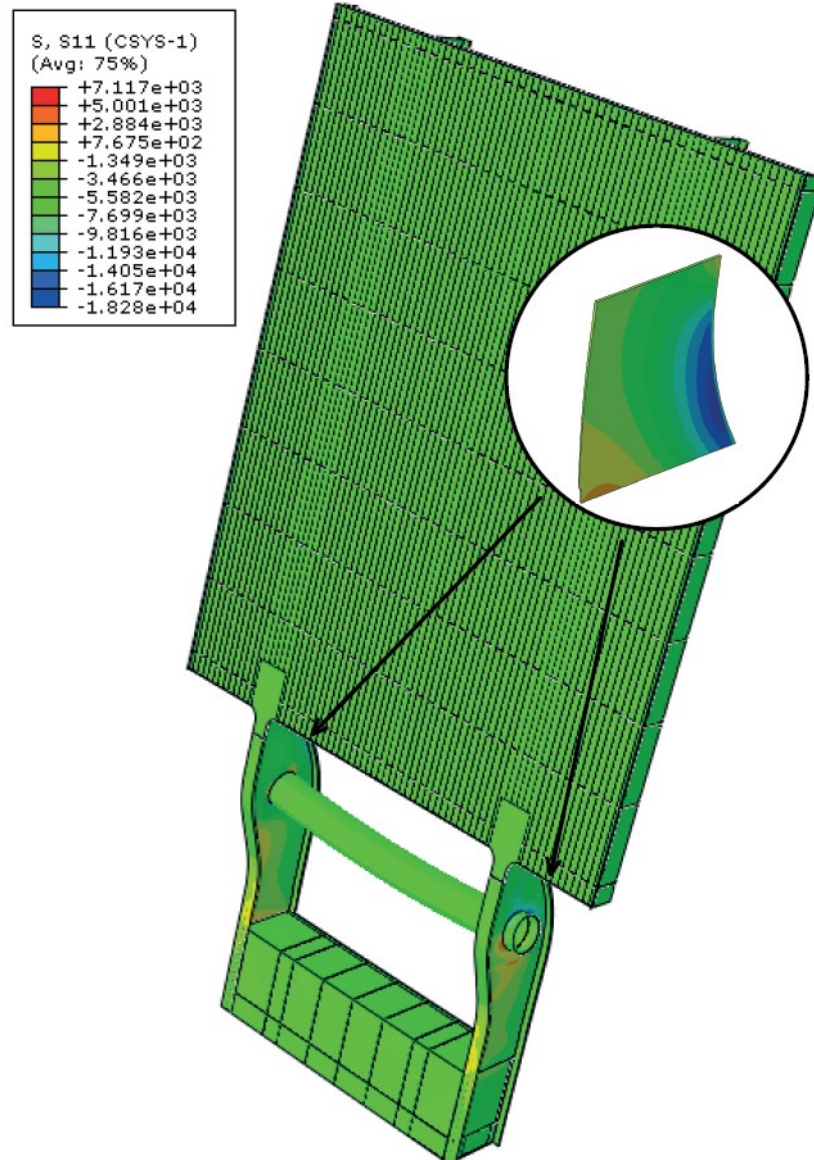
Figure E-11 S22, stress in radial direction – fully opened condition; Amalia bridge, Abaqus

NOTE: The illustrations mention S11, while the equations mention S22, which is the requested stress value. A local coordinate system has been defined to extract the longitudinal stresses along the curvature of the bottom flange. This coincides with the radial stresses for a circle at this location.

The value found for fatigue damage differs significantly from the value obtained in SCIA. Due to the lower radial stresses found in the just opened condition.

This stress difference can be explained due to the difference in programs. The values obtained from the bottom flange, are rather straight forward, since they hail from countering the cantilevering effect. Whereas the values obtained from the web, hail from the inward bending of both of the main girders. This is a much less straight forward calculation method. Thus, in this difference in this approach between the programs could account for the difference in these values.

$$\sigma_{22, fully\ opened} = -1.828 \times 10^4 kPa \rightarrow -18.28\ MPa$$

Resulting in a stress difference

$$\Delta\sigma_i = \left|\sigma_{22,just\ opened} - \sigma_{22,fully\ opened}\right| = 51.65\ MPa$$

In this case, the value in the just opened condition differs more, than the value in the fully opened condition. These stress difference can be explained due the difference in the model built up, as stated in 8.3.1 – Comparing models. In this case the calculation of the stresses is not as straightforward as was the case mentioned earlier. Due to the complexity is these stresses, combined with the difference in code used between the FEM-programs, as stated in 8.3.1 – Comparing models, this makes sense.

and the fatigue damage (according to Equation E-2 and Table E-15)

$$D_i = 0.379$$

E.3.2.2.3. Combined – main girder

For the total fatigue damage, the damage obtained from the bottom flange, needs to be combined with the damage obtained from the web. This results in:

$$D_{i,total} = D_{i,bottom,flange} + D_{i,web} = 0.757$$

This value differs from the value obtained in SCIA-engineer. This has been addressed for the individual values.

Appendix F. Details of Design 1 – Non-hybrid

This appendix contains more detailed information regarding the non-hybrid design. It contains the following topics:

- Bridge built up
- Weight calculation
- Fatigue verification
- Design verifications
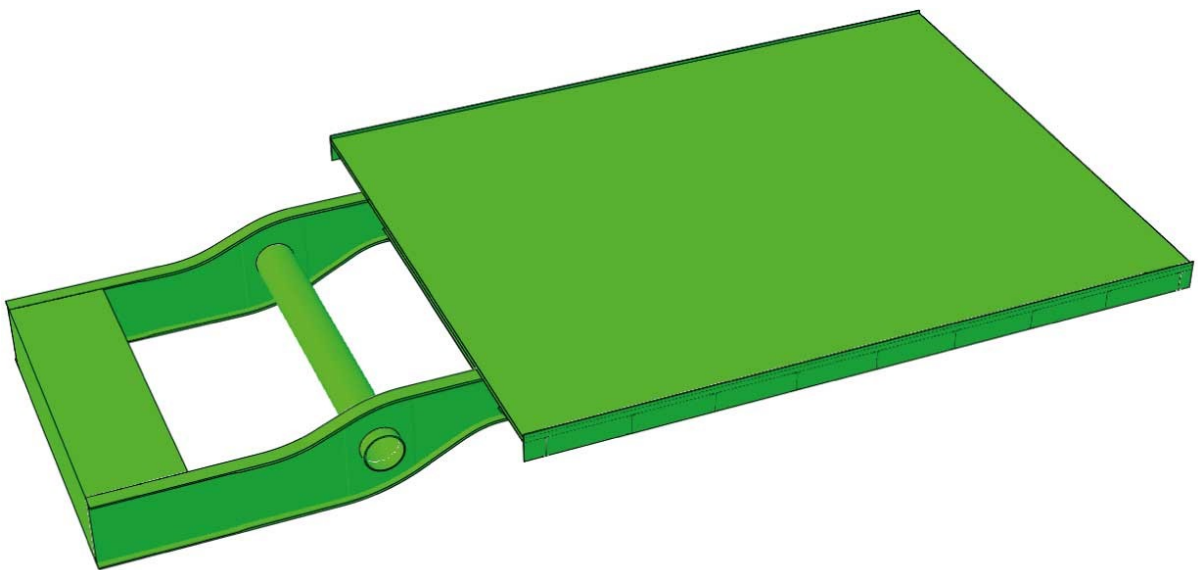
Figure F-1 3D-impression of the non-hybrid design

NOTE: The calculations for this design are from a version with slimmer top, bottom flanges of the main girder and webs of the deck. Since these suffice and thicker sections have been applied, these should to suffice as well. The 'old' calculations are displayed on the following pages. The exception to this is the weight-based calculations and LM2.

F.1. Bridge built up

F.1.1. FRP-deck

The FRP deck used in this design is based upon the redundancy principal of FiberCore, by making use of Z-shaped shells. In the model this has been simplified to a horizontal top and bottom layer and vertical webs, allowing for the height required in the design. In the fabrication of this deck, foam blocks are used to ensure the proper placement and alignment of fibres. These foam cores have been assumed NOT to contribute to the structural strength and stiffness of the deck as a whole. Thus, they have not been modelled in the FEM-programming. An impression of this deck can be seen in Figure 10-1.

F.1.2. Main and cross girder cross sections
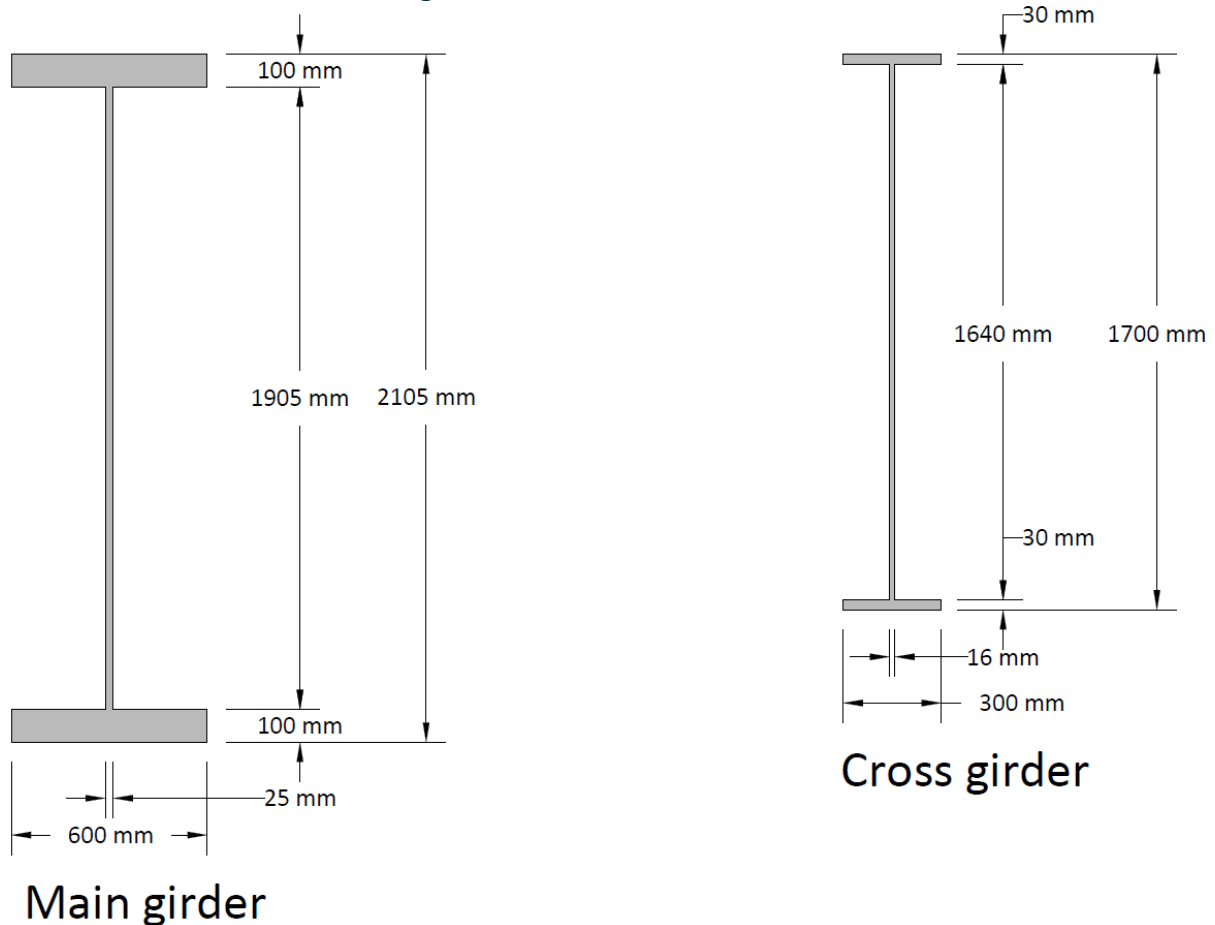
Figure F-2 Cross sections of the main and cross girders of the non-hybrid design

F.1.3. Cross section of the movable bridge section
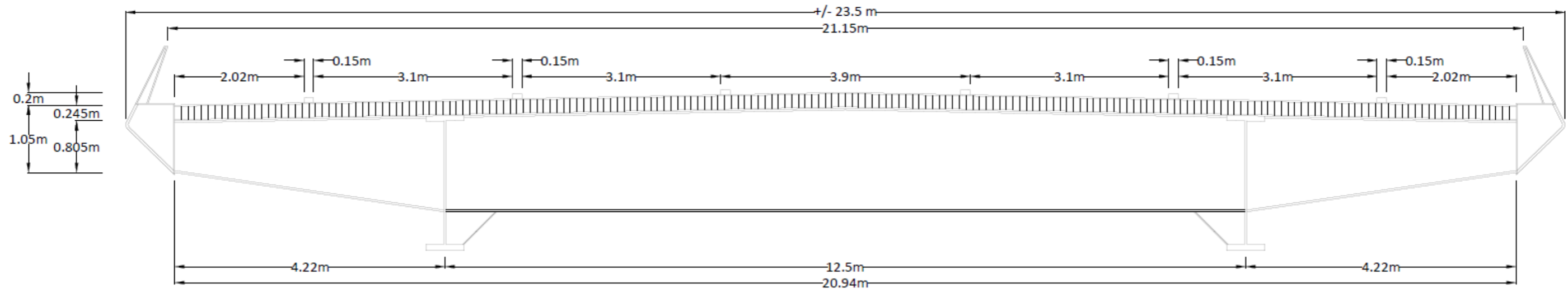
Figure F-3 Cross section of the non-hybrid design

F.1.4. Length section of the movable bridge section

Figure F-4 Length section of the non-hybrid design
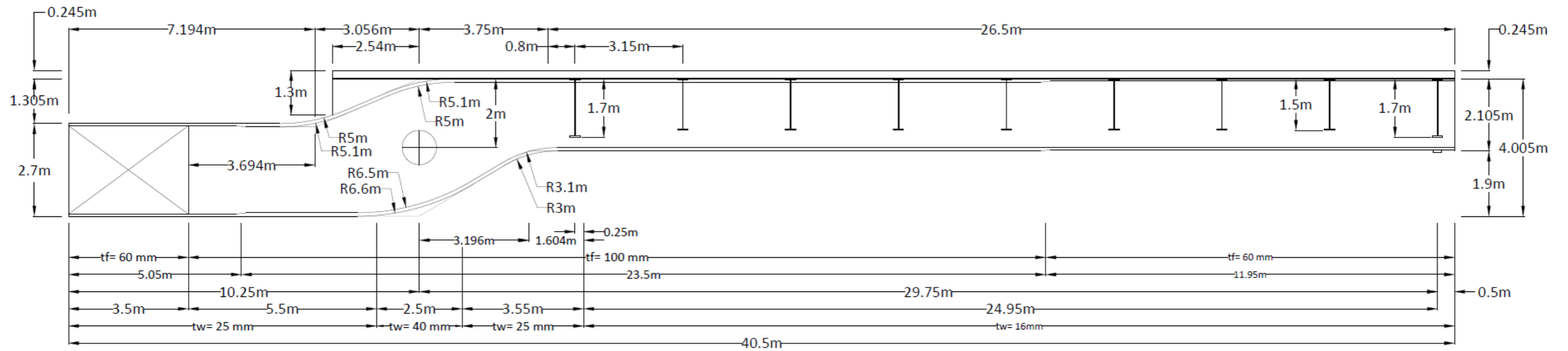
F.2. Weight calculation

In this section the calculation, mentioned in chapter 10.3, has been shown. In essence the bridge's length section is split into two; one left and one right section. For all the existing elements an approximation of the volume, combined with the location of the centre of gravity and the modelled counterweight, using only steel. The weight can also be taken from the Abaqus model, however to gain more insight into the effects of the different elements on the weight distribution this excel-based calculations were made.

F.2.1. Input parameters

Here the different parameters used in these calculations have been displayed.

General		
width deck	20940	mm
length deck	26500	mm
distance rotation centre – start deck	3750	mm
c.t.c. main girders	12500	mm
number of cross girders	9	[-]
distance rotation centre – top deck	2245	mm

Table F-2 General input parameters defining of the non-hybrid design

Densities		
rho,steel	78.5	kN/m3
rho, conc.	40.5	kN/m3
rho,frp,fac	16.7	kN/m3
hro,frp,web	14.6	kN/m3

Table F-1 Desity definitions regarding the materials of the non-hybrid design

Deck			Deck (facing, web, facing)			Main girder			Cross girder		
t,deck	20	mm	t,f,top	20	mm	h,girder	2105	mm	h,girder-1,9	1700	mm
						t,w	16	mm	h,girder-2-8	1500	mm
Front cover			h,w	205	mm	t,f,1,top	100	mm	t,w	16	mm
t,w	8	mm	t,w	8	mm	t,f,2,top	60	mm	t,f,top	30	mm
h,w	245	mm	# of webs	201	[-]	t,f,1,bot	100	mm	t,f,bot	30	mm
			c.t.c.	104.70	mm	t,f,2,bot	60	mm	b,bot	300	mm
Side cover						b,bot	600	mm	c.t.c.	3.15	m
t,w	20	mm	t,f,bot	20	mm	c.t.c.	12.5	m	offset,l	800	mm
h,w	1150	mm				l,thin,R	11950	mm	offset,r	500	mm
						l,thin,L	5050	mm	h,side	805	mm

Table F-3 Detailed input parameters, per component, defining of the non-hybrid design

F.2.2. Leaf calculation

Below is the table containing the values used for the weight calculation. This is regarding the section on the right side of the rotation centre, as is shown in Figure F-4.

Description	b1	b2	t	L	Horizontal centre of gravity X	Vertical centre of gravity Y (above is +)	Amount	Volume	Weight	Moment X	Centre of Gravity X	Moment Y	Centre of Gravity Y
Deck system									702 kN	11936 kNm	17. m	1445 kNm	2.06 m
Deck - top facing	20940mm	20940mm	20mm	26500mm	17000mm	2235mm	1	11.1 m3	185kN	3151 kNm		414 kNm	
Deck - webs (incl. lost core)	205mm	205mm	8mm	26500mm	17000mm	2123mm	201	8.74 m3	235kN	3987 kNm		498 kNm	
Deck - bottom facing	20940mm	20940mm	20mm	26500mm	17000mm	2010mm	1	11.1 m3	185kN	3151 kNm		373 kNm	
Side cover	1150mm	1150mm	20mm	26500mm	17000mm	1648mm	2	1.22 m3	96kN	1627 kNm		158 kNm	
Front cover (tip leaf)	20940mm	20940mm	8mm	245mm	30250mm	2123mm	1	.04 m3	1kN	18 kNm		1 kNm	
Back cover (base leaf)	20940mm	20940mm	8mm	245mm	3750mm	2123mm	1	.04 m3	1kN	2 kNm		1 kNm	
Main girder									653 kN	8719 kNm	13.36 m	488 kNm	.75 m
Web-1 (t=40mm)	3805mm	2648mm	40mm	1250mm	1046mm	80mm	2	.25 m3	20kN	21 kNm		2 kNm	
Web-2 (t= 25mm)	2648mm	1905mm	25mm	1946mm	2223mm	588mm	2	.22 m3	17kN	39 kNm		10 kNm	
Web-3 (t=25mm)	1905mm	1905mm	25mm	1604mm	3998mm	948mm	2	.15 m3	12kN	48 kNm		11 kNm	
Web-4 (t=16mm)	1905mm	1905mm	16mm	13500mm	11550mm	948mm	2	.82 m3	65kN	746 kNm		61 kNm	
Web-5 (t=16mm)	1965mm	1965mm	16mm	11950mm	24275mm	958mm	2	.75 m3	59kN	1432 kNm		56 kNm	
Bottom-flange-1	600mm	600mm	100mm	3196mm	1598mm	-1005mm	2	.38 m3	30kN	48 kNm		-30 kNm	
Bottom-flange-2	600mm	600mm	100mm	15104mm	10748mm	-427mm	2	1.81 m3	142kN	1529 kNm		-61 kNm	
Bottom-flange-3	600mm	600mm	60mm	11950mm	24275mm	-427mm	2	.86 m3	68kN	1640 kNm		-29 kNm	
Top-flange-1	600mm	600mm	100mm	18300mm	9150mm	1950mm	2	2.2 m3	172kN	1577 kNm		336 kNm	
Top-flange-2	600mm	600mm	60mm	11950mm	24275mm	1930mm	2	.86 m3	68kN	1640 kNm		130 kNm	

Cross girder-1 (front girder)									**68 kN**	**2016 kNm**	**29.75 m**	**82 kNm**	**1.2 m**
Web-centre	1640mm	1640mm	16mm	12484mm	29750mm	1150mm	1	.33 m3	26kN	765 kNm		30 kNm	
Web-side	1640mm	745mm	16mm	4204mm	29750mm	1374mm	2	.16 m3	13kN	375 kNm		17 kNm	
Top -flange	300mm	300mm	30mm	19740mm	29750mm	1985mm	1	.18 m3	14kN	415 kNm		28 kNm	
Flange-centre	300mm	300mm	30mm	12484mm	29750mm	315mm	1	.11 m3	9kN	262 kNm		3 kNm	
Flange-side	300mm	300mm	30mm	4298mm	29750mm	763mm	2	.08 m3	6kN	181 kNm		5 kNm	
Support-web	292mm	597mm	16mm	305mm	29750mm	-667mm	2	. m3	kN	10 kNm		kNm	
Support-flange	300mm	200mm	16mm	431mm	29750mm	-667mm	2	. m3	kN	8 kNm		kNm	
Cross girder-9 (rear girder)									**68 kN**	**308 kNm**	**4.55 m**	**82 kNm**	**1.2 m**
Web-centre	1640mm	1640mm	16mm	12475mm	4550mm	1150mm	1	.33 m3	26kN	117 kNm		30 kNm	
Web-side	1640mm	745mm	16mm	4195mm	4550mm	1374mm	2	.16 m3	13kN	57 kNm		17 kNm	
Top -flange	300mm	300mm	30mm	19740mm	4550mm	1985mm	1	.18 m3	14kN	63 kNm		28 kNm	
Flange-centre	300mm	300mm	30mm	12484mm	4550mm	315mm	1	.11 m3	9kN	40 kNm		3 kNm	
Flange-side	300mm	300mm	30mm	4298mm	4550mm	763mm	2	.08 m3	6kN	28 kNm		5 kNm	
Support-web	292mm	597mm	16mm	305mm	4550mm	-667mm	2	. m3	kN	2 kNm		kNm	
Support-flange	300mm	200mm	16mm	431mm	4550mm	-667mm	2	. m3	kN	1 kNm		kNm	
Cross girder-2-4 (h=1500)									**194 kN**	**3941 kNm**	**20.3 m**	**244 kNm**	**1.26 m**
Web-centre	1470mm	1470mm	16mm	12484mm	20300mm	1235mm	3	.88 m3	69kN	1404 kNm		85 kNm	
Web-side	1470mm	745mm	16mm	4204mm	20300mm	1416mm	6	.45 m3	35kN	712 kNm		50 kNm	
Top -flange	300mm	300mm	30mm	19740mm	20300mm	1985mm	3	.53 m3	42kN	849 kNm		83 kNm	
Flange-centre	300mm	300mm	30mm	12484mm	20300mm	485mm	3	.34 m3	26kN	537 kNm		13 kNm	
Flange-side	300mm	300mm	30mm	4298mm	20300mm	848mm	6	.23 m3	18kN	370 kNm		15 kNm	
Support-web	292mm	797mm	16mm	505mm	20300mm	-730mm	6	.03 m3	2kN	42 kNm		-2 kNm	
Support-flange	300mm	200mm	16mm	714mm	20300mm	-730mm	6	.02 m3	1kN	26 kNm		-1 kNm	
Cross girder-5-8 (h=1500)									**259 kN**	**2401 kNm**	**9.28 m**	**325 kNm**	**1.26 m**
Web-centre	1470mm	1470mm	16mm	12484mm	9275mm	1235mm	4	1.17 m3	92kN	855 kNm		114 kNm	
Web-side	1470mm	745mm	16mm	4204mm	9275mm	1416mm	8	.6 m3	47kN	434 kNm		66 kNm	
Top -flange	300mm	300mm	30mm	19740mm	9275mm	1985mm	4	.71 m3	56kN	517 kNm		111 kNm	
Flange-centre	300mm	300mm	30mm	12484mm	9275mm	485mm	4	.45 m3	35kN	327 kNm		17 kNm	
Flange-side	300mm	300mm	30mm	4298mm	9275mm	848mm	8	.31 m3	24kN	225 kNm		21 kNm	
Support-web	292mm	797mm	16mm	505mm	9275mm	-730mm	8	.04 m3	3kN	26 kNm		-2 kNm	
Support-flange	300mm	200mm	16mm	714mm	9275mm	-730mm	8	.02 m3	2kN	16 kNm		-1 kNm	
Axle									**97 kN**	**kNm**	**. m**	**kNm**	**. m**
Axle (R=750)		750mm	40mm	13500mm	mm	mm	1	1.24 m3	97kN	kNm		kNm	
Addition									**14 kN**	**190 kNm**	**13.26 m**	**27 kNm**	**1.86 m**
Welding/ conservation (steel)				1.00%					14kN	190kN		27kN	
Road equipment & wear layer									**471 kN**	**8005 kNm**	**17. m**	**1035 kNm**	**2.2 m**
Wear layer 22,5 kN/m³	20940mm	20940mm	8mm	26500mm	17000mm	2249mm	1	4.44 m3	100kN	1698 kNm		225 kNm	
Edge elements 4,0 kN/m				26500mm	17000mm	1949mm	2		212kN	3604 kNm		413 kNm	
Mid-section 3,0 kN/m				26500mm	17000mm	2249mm	1		80kN	1352 kNm		179 kNm	
Road equipment 1,5 kN/m				26500mm	17000mm	2745mm	2		80kN	1352 kNm		218 kNm	
Total									**2526 kN**	**37515 kNm**	**14854 mm**	**3726 kNm**	**1475 mm**

Table F-4 Weight calculation of the right side of the non-hybrid design

F.2.3. Counterweight Calculation

Below is the table containing the values used for the weight calculation. This is regarding the section on the left side of the rotation centre, as is shown in Figure F-4.

Description	b1	b2	t	L	Horizontal centre of gravity X	Vertical centre of gravity Y (down is +)	Amount	Volume	Weight	Moment X	Centre of Gravity X	Moment Y	Centre of Gravity Y
Main girder									**265 kN**	**1244 kNm**	**4.69 m**	**21 kNm**	**.08 m**
Web-1 (t=40mm)	3805mm	3510mm	40mm	1250mm	625mm	-111mm	2	.34 m3	26kN	17 kNm		-3 kNm	
Web-2 (t= 25mm)	2540mm	3510mm	25mm	1802mm	2151mm	-428mm	2	.27 m3	21kN	46 kNm		-9 kNm	
Web-3 (t=25mm)	2540mm	2540mm	25mm	2148mm	4126mm	870mm	2	.27 m3	21kN	88 kNm		19 kNm	
Web-4 (t=25mm)	2640mm	2640mm	25mm	5050mm	7725mm	920mm	2	.67 m3	52kN	404 kNm		48 kNm	
Bottom-flange-1	600mm	600mm	60mm	5050mm	7725mm	1197mm	2	.36 m3	29kN	220 kNm		34 kNm	
Bottom-flange-2	600mm	600mm	100mm	5200mm	2600mm	100mm	2	.62 m3	49kN	127 kNm		5 kNm	
Top-flange-1	600mm	600mm	60mm	5050mm	7725mm	-1448mm	2	.36 m3	29kN	220 kNm		-41 kNm	
Top-flange-2	600mm	600mm	100mm	1802mm	2151mm	-845mm	2	.22 m3	17kN	37 kNm		-14 kNm	
Top-flange-3	600mm	600mm	100mm	2148mm	4126mm	-845mm	2	.26 m3	20kN	83 kNm		-17 kNm	
Counterweight (steel box)									**507 kN**	**4464 kNm**	**8.81 m**	**218 kNm**	**.43 m**
Top cover	11900mm	11900mm	25mm	3000mm	8750mm	-928mm	1	.89 m3	70kN	613 kNm		-65 kNm	
Bottom cover	11900mm	11900mm	25mm	3000mm	8750mm	1760mm	1	.89 m3	70kN	613 kNm		123 kNm	
Front cover	12475mm	12475mm	25mm	2650mm	7263mm	435mm	1	.83 m3	65kN	471 kNm		28 kNm	
Back cover	12475mm	12475mm	25mm	2650mm	10238mm	435mm	1	.83 m3	65kN	664 kNm		28 kNm	
Width separators	12475mm	12475mm	25mm	2650mm	9230mm	435mm	1	.83 m3	65kN	599 kNm		28 kNm	
Length separators	2950mm	2950mm	40mm	2650mm	8750mm	435mm	7	2.19 m3	172kN	1504 kNm		75 kNm	
Axle									**97 kN**	**kNm**	**. m**	**kNm**	**. m**
Axle (R=750)		750mm	40mm	13500mm	mm	mm	1	1.24 m3	97kN	kNm		kNm	
Addition									**17 kN**	**114 kNm**	**6.57 m**	**5 kNm**	**.27 m**
Welding/ conservation				2.00%					17kN	114kN		5kN	
Counterweight (content)									**3681 kN**	**30801 kNm**	**8.37 m**	**2989 kNm**	**.81 m**
Front counterweight	12195mm	12195mm	2350mm	2475mm	7988mm	805mm	1	70.93 m3	2873kN	22945 kNm		2312 kNm	
Rear counterweight	1625mm	1625mm	2350mm	975mm	9738mm	805mm	2	7.45 m3	302kN	2937 kNm		243 kNm	
Rear counterweight	760mm	760mm	2350mm	975mm	9738mm	805mm	2	3.48 m3	141kN	1373 kNm		114 kNm	
Adjustable (50 kN/m3)	1600mm	1600mm	1094mm	900mm	9700mm	876mm	2	3.15 m3	158kN	1528 kNm		138 kNm	
Adjustable (50 kN/m3)	2113mm	2113mm	1094mm	900mm	9700mm	876mm	2	4.16 m3	208kN	2017 kNm		182 kNm	
Total									**4567 kN**	**36622 kNm**	**-8019 mm**	**3232 kNm**	**-708 mm**

Table F-5 Weight calculation of the left side of the non-hybrid design

F.2.4. Balance Calculation

The counterweight of the bridge has been designed based upon **Moment X** (as is shown in Table F-6). Here Moment X in the closed condition is the closing pressure of 30 kN over the total span of the bridge., whereas Moment X in the opened condition is the overpressure required to keep the bridge opened, which is 1/3 of the closing pressure. From the closing pressure the adjustable counterweights were designed and from the overpressure the placement of these adjustable counterweights were calculated. This however is theoretical. To achieve this is reality, the counterweight will be filled until the aforementioned closing pressure is achieved, thus balancing the bridge manually at site. Which could differ from these calculated values. This is based on the Dutch code :NEN6787 VOBB:2001 article 8.4.2.5.2.

Description	Element angle [°]	Distance between total & elemental Centre of Gravity	Horizontal centre of gravity X	Vertical centre of gravity Y (above is +)			Weight	Moment X	Centre of Gravity X	Moment Y	Centre of Gravity Y
Closed condition							**7092 kN**	**892.5 kNm**	**126 mm**	**494 kNm**	**70 mm**
Leaf section	5.67	14927 mm	14854 mm	1475 mm			2526 kN	37515 kNm		3726 kN	
Counterweight section	5.04	8050 mm	-8019 mm	-708 mm			4567 kN	-36622 kNm		-3232 kN	
Opened condition							**7092 kN**	**-297.5 kNm**	**-42 mm**	**-976 kNm**	**-138 mm**
Leaf section	83.67	14927 mm	1645 mm	14836 mm			2526 kN	4155 kNm		-37470 kNm	
Counterweight section	83.04	8050 mm	975 mm	7991 mm			4567 kN	-4452 kNm		36494 kNm	

Table F-6 Balancing calculation of the non-hyrbid design

NOTE: In the opened condition the rotation angle of the bridge is set at 78 degrees.

F.2.5. Weight division

Below insight is given into the weight division of the non-hybrid bridge and its sections. This is illustrated in three tables; each illustration their respective components with their corresponding contribution to the total weight.

	Whole bridge	
	[kN]	
Deck-system	702	10%
Main girders	918	13%
Cross girders	588	8%
Counterweight	4187	59%
Axle	194	3%
Rest	503	7%
Total bridge	**7092**	**100%**

Table F-8 Weight division of the non-hyrbid design

	Leaf	
	[kN]	
Deck-system	702	28%
Main girders	653	26%
Cross girders	588	23%
Axle	97	4%
Conservation	14	0.6%
Road equipment	471	19%
Total bridge	**2526**	**100%**

Table F-9 Weight division of the leaf of the non-hybrid design

	Counterweight	
	[kN]	
Main girders	265	6%
Axle	97	2%
CW-box	507	11%
CW-content	3681	81%
Conservation	17	0.4%
Total bridge	**4567**	**100%**

Table F-7 Weight division of the counterweight of the non-hybrid design

F.2.6.   Fatigue verification

F.2.7. Bottom flange – main girder

The same formulas, load factors and calculation assumptions as have been used in the original Amalia bridge fatigue calculations. This can been seen in Appendix E – Fatigue verification (Bottom flange – main girder) The stress values , obtained from Abaqus have been combined to obtain the stress difference, from which the fatigue damage can be calculated. This is illustrated next:

F.2.7.1.   Just opened condition
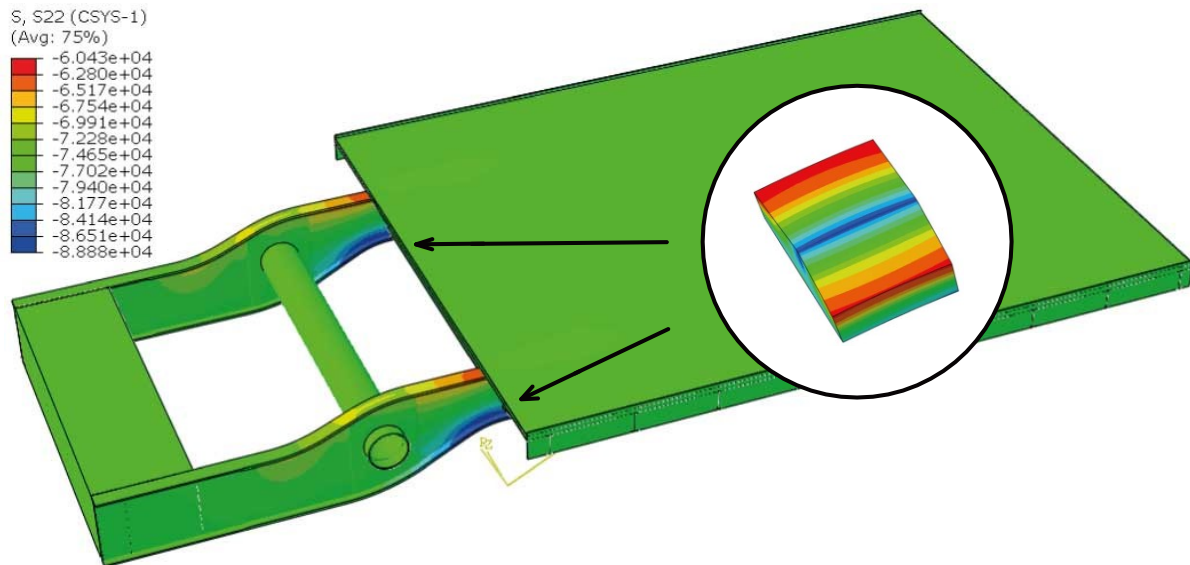
Figure F-5 S11, stress in length direction – just opened condition; design 1 – non-hybrid

$$\sigma_{11, just\ opened} = -8.888 \times 10^4 kPa \rightarrow -88.88\ MPa$$

NOTE: due to the choice of the coordinate system such that the longitudinal stresses coincides with the curvature of the bottom flange, the stress in the illustration is noted as S22. This is the same as global S11.

F.2.7.2.   Fully opened condition
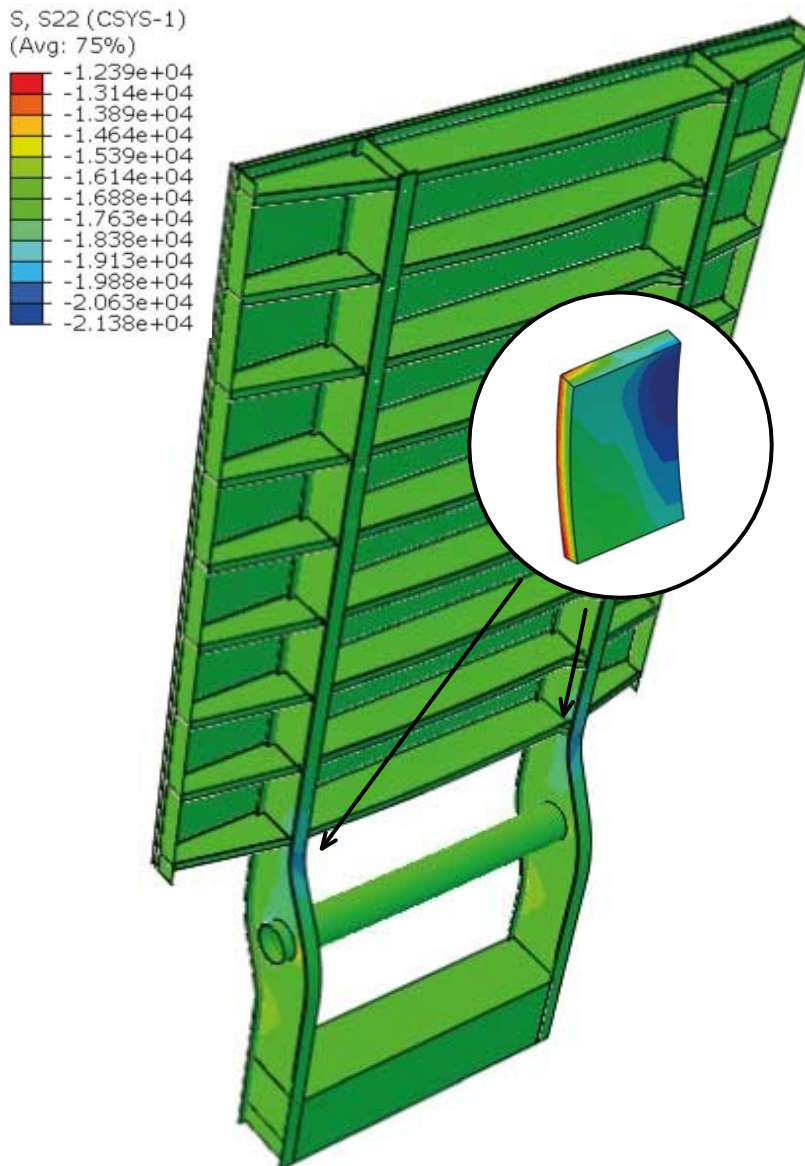
Figure F-6 S11, stress in length direction – fully opened condition; design 1 – non-hybrid

The stress value located at the same location as has been found for the just opened condition is:

$$\sigma_{11,fully\ opened} = -2.138 \times 10^4 kPa \rightarrow -21.38\ MPa$$

Resulting in a stress difference

$$\Delta\sigma_i = \left|\sigma_{22,just\ opened} - \sigma_{22,fully\ opened}\right| = 67.50\ MPa$$

and the fatigue damage (according to Equation E-2 and Table E-14)

$$D_i = 0.378$$

NOTE: due to the choice of the coordinate system such that the longitudinal stresses coincides with the curvature of the bottom flange, the stress in the illustration is noted as S22. This is the same as global S11.

The obtained stress difference with its corresponding damage value are deemed to be comparable with the values found for the Amalia bridge calculated in Abaqus (See section: E.3.2 – Abaqus model).

F.2.8. Web – main girder

The same formulas, load factors and calculation assumptions as have been used in the original Amalia bridge fatigue calculations. This can been seen in Appendix E – Fatigue verification (Web – main girder)The stress values , obtained from Abaqus have been combined to obtain the stress difference, from which the fatigue damage can be calculated. This is illustrated below:

F.2.8.1. Just opened condition
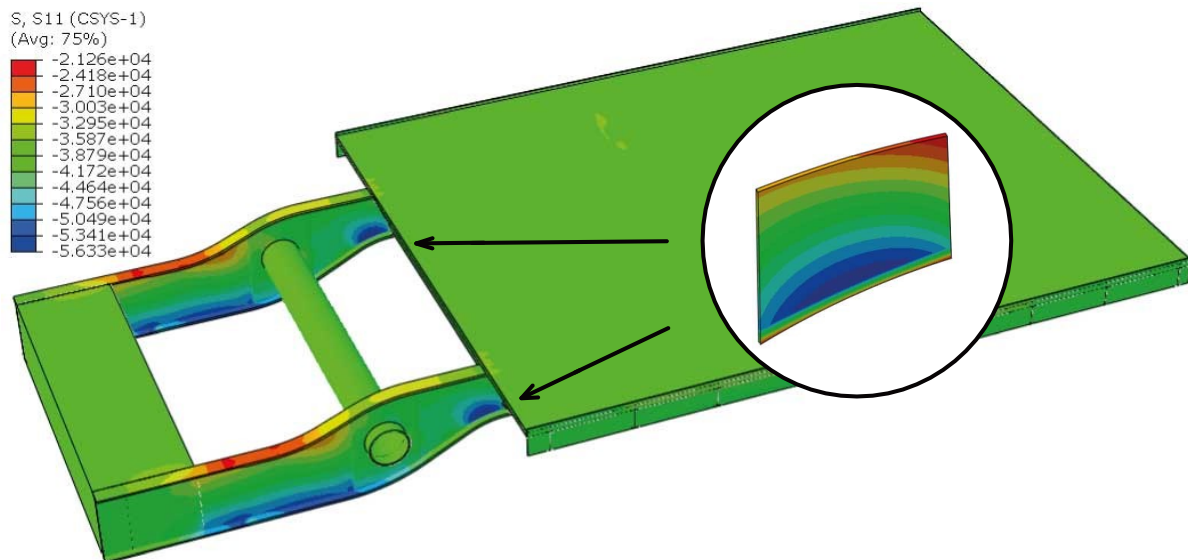
Figure F-7 S22, stress in radial direction – just opened condition; design 1 – non-hybrid

$$\sigma_{22,just\ opened} = -5.633 \times 10^4 kPa \rightarrow -56.33\ MPa$$

The difference between the value above and the corresponding value obtained for the Amalia bridge calculated in Abaqus can be explained due to the reduction in the weight of the leaf of the bridge, while maintaining the same thickness of the web. A lower load divided over a similar area, resulting lower stresses.

F.2.8.2.   Fully opened condition
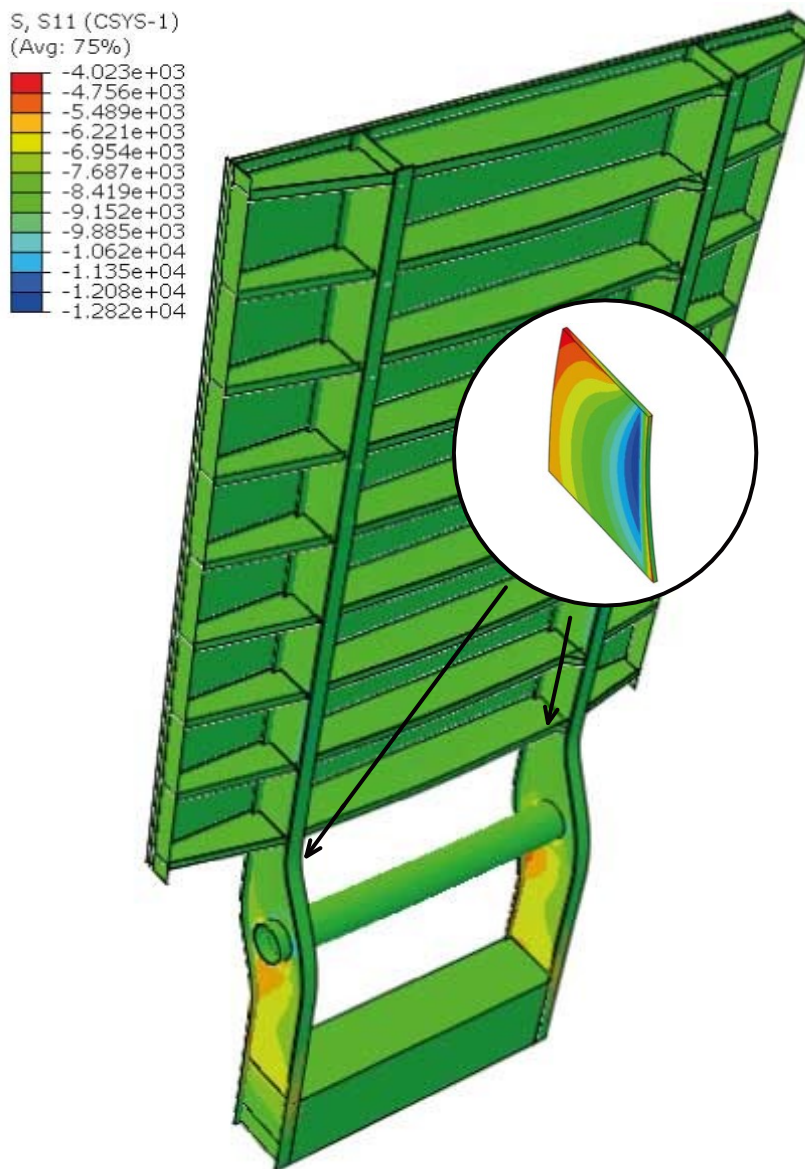
Figure F-8 S22, stress in radial direction – fully opened condition; design 1 – non-hybrid

The stress value located at the same location as has been found for the just opened condition is:

$$\sigma_{22,fully\ opened} = -1.282 \times 10^4 kPa \rightarrow -12.82\ MPa$$

Resulting in a stress difference

$$\Delta\sigma_i = \left|\sigma_{22,just\ opened} - \sigma_{22,fully\ opened}\right| = 43.51\ MPa$$

and the fatigue damage (according to Equation E-2 and Table E-15)

$$D_i = 0.539$$

NOTE: due to the choice of the coordinate system such that the radial stresses coincides with the curvature of the bottom flange, the stress in the illustration is noted as S11. This is the same as global S22.

The obtained stress difference with its corresponding damage value differ from the values found for the Amalia bridge calculated in Abaqus (See section: E.3.2 – Abaqus model). These lower values are a result of the weight reduction, resulting in lower forces, while the thickness of the web has been maintained, resulting in lower stresses.

F.2.8.3. Combined – main girder

For the total fatigue damage, the damage obtained from the bottom flange, should be combined with the damage obtained from the web. This results in:

$$D_{i,total} = D_{i,bottom,flange} + D_{i,web} = 0.102$$

The resulting combined fatigue damages are lower compared to the value found for the original Amalia bridge and result in a safe structure with regard to fatigue. Thus, since this scenario was governing in the original case and it has been assumed to be governing for this design, this design is deemed to be safe for fatigue damages. Please note, that for a full fatigue check, the fatigue resistance of the traffic loading and the vibration of the counterweight should be taken into account. This has not been covered in this thesis

NOTE: This calculation is very sensitive to slight variations in the stress differences. A slight difference in this stress difference can be the difference between fulfilling/ failing the 1.0 damage condition.

F.3. Design verifications

The loading has been applied according to the approach, as has been explained in chapter 8.4 – Design verification. For a more detailed explanation on the approach, please refer to Appendix D.

F.3.1. LM1

F.3.1.1. Deck

Even though strength is not the governing criterium for FRP, this still has been verified; along with deformation (deflection and buckling). The table below illustrates the strength values of the FRP used.

Layer	S11,d		S22,d		S12,d
	Stxx	Scxx	Styy	Scyy	Txy
	[MPa]	[MPa]	[MPa]	[MPa]	[MPa]
Top/ bottom facing	249.71	-230.46	76.97	-97.56	19.69
Webs	116.66	-99.93	84.67	-93.65	29.04

Table F-10 FiberCore laminate design strength properties in case of strength check

F.3.1.1.1. Top facing

The top facing has been checked on strength using LM1 for the primary as well as their shear stresses. The applied load placement is illustrated in Appendix D – Figure D-2.

F.3.1.1.1.1. Longitudinal stress – S11
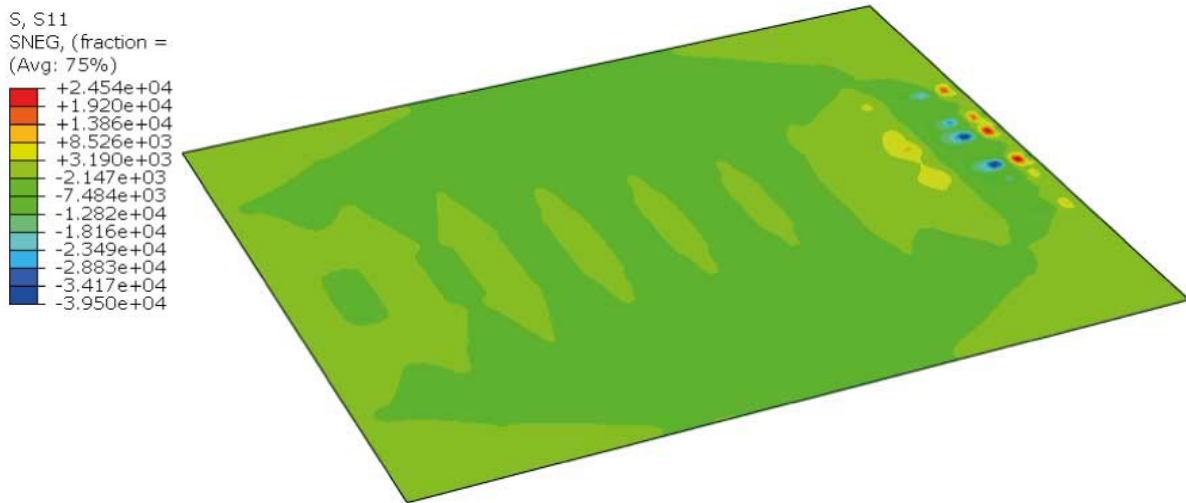
Figure F-9 Non-hybrid; LM1; ULS; deck, top facing – S11

This loading resulted in the following UC's at the location, as illustrated in Figure F-9:

$$UC_{tension} = 0.098 \qquad UC_{compression} = 0.171$$
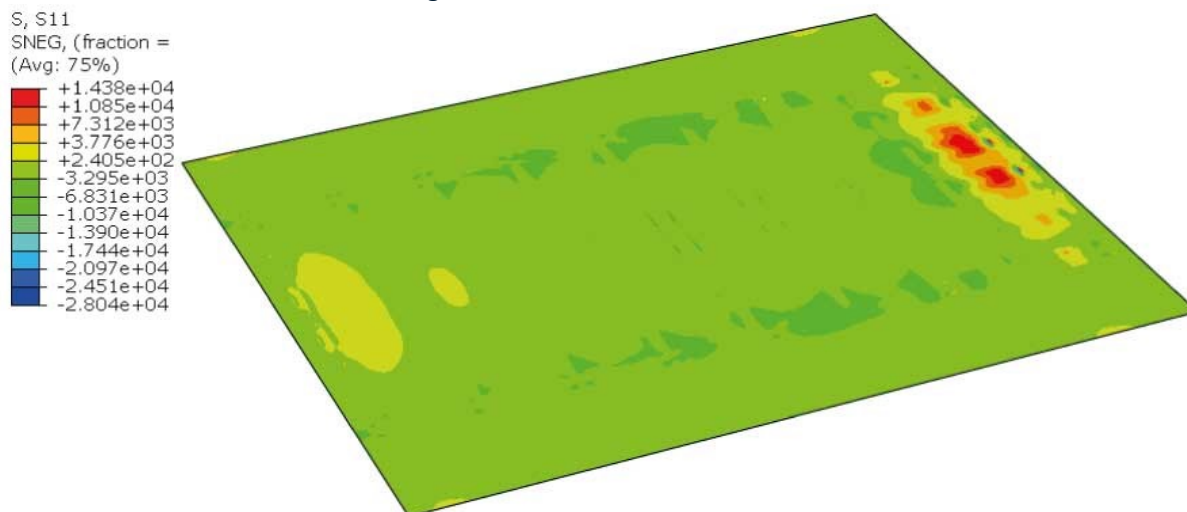
F.3.1.1.1.2. Transverse stress – S22
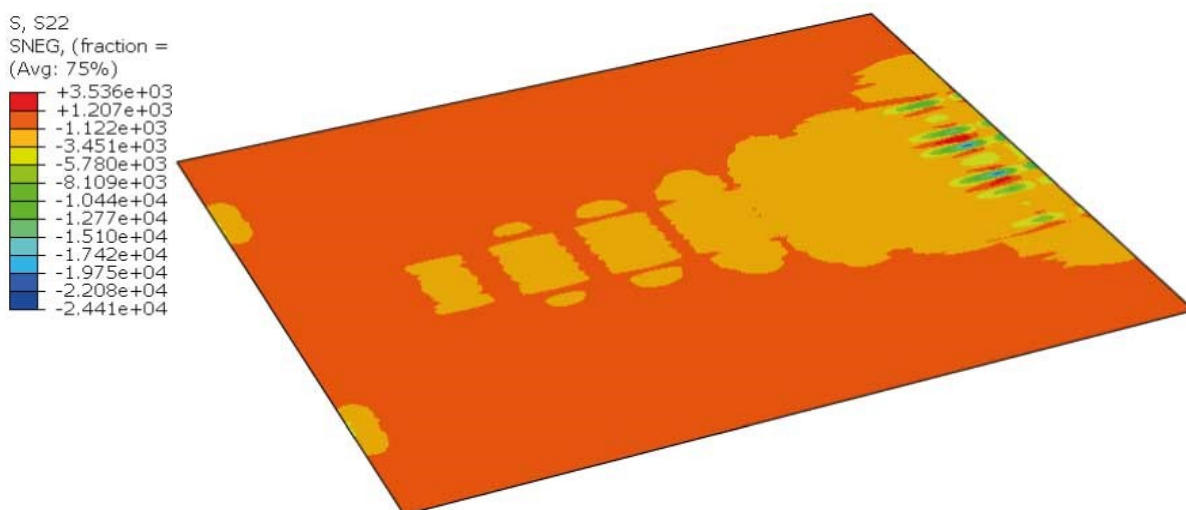
Figure F-10 Non-hybrid; LM1; ULS; deck, top facing – S22

This loading resulted in the following UC at the location, as illustrated in Figure F-10:

$$UC_{tension} = 0.046 \qquad UC_{compression} = 0.250$$
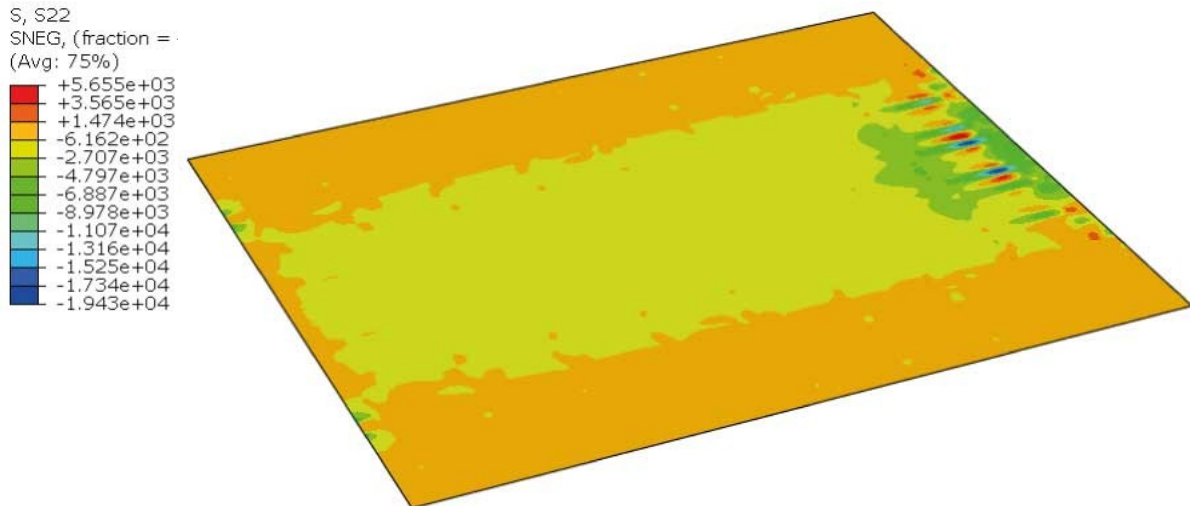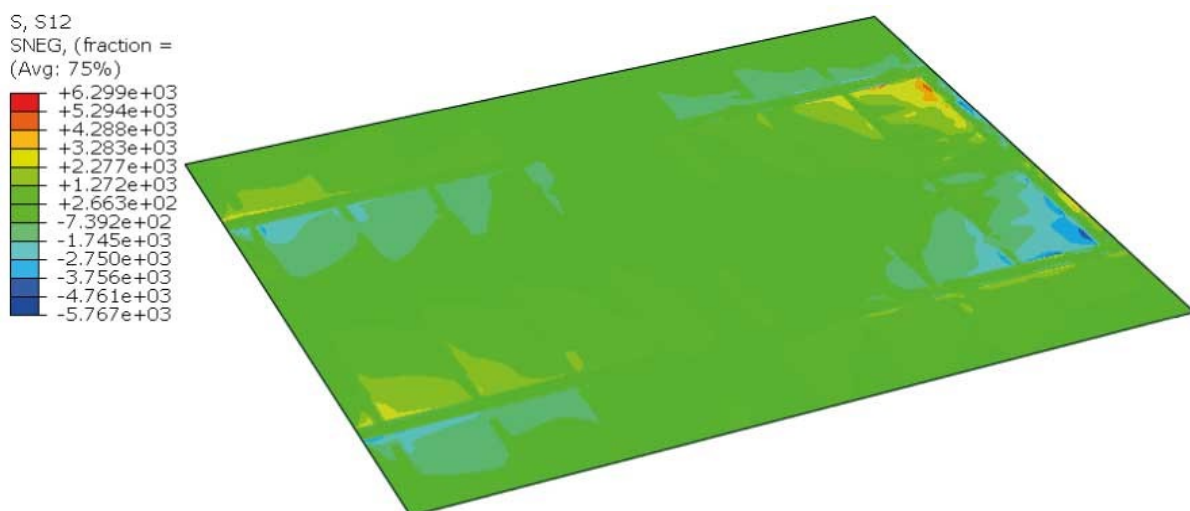
F.3.1.1.1.3. Shear stress – S12
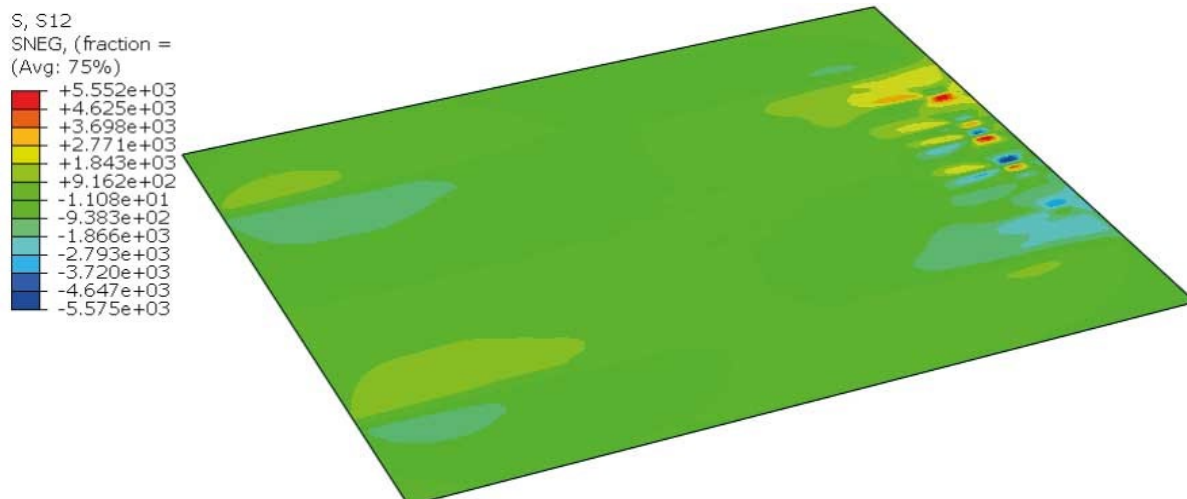
Figure F-11 Non-hybrid; LM1; ULS; deck, top facing – S12

This loading resulted in the following UC at the location, as illustrated in Figure F-11:

$$UC = 0.283$$

F.3.1.1.1.4. Combination

According to the CUR 96+ section 6.3.1 a combined stress criterium must suffice the following equation, where aforementioned stresses have been applied, resulting in a unity check:

$$\left(\frac{\sigma_{1,Ed}}{\sigma_{1,Rd}}\right)^2 + \left(\frac{\sigma_{2,Ed}}{\sigma_{2,Rd}}\right)^2 + \left(\frac{\tau_{12,Ed}}{\tau_{12,Rd}}\right)^2 - \frac{\sigma_{1,Ed} \cdot \sigma_{2,Ed}}{\sigma_{1,Rd}^2} = 0.154 \leq 1.0$$

F.3.1.1.1.5. Vertical Deflection
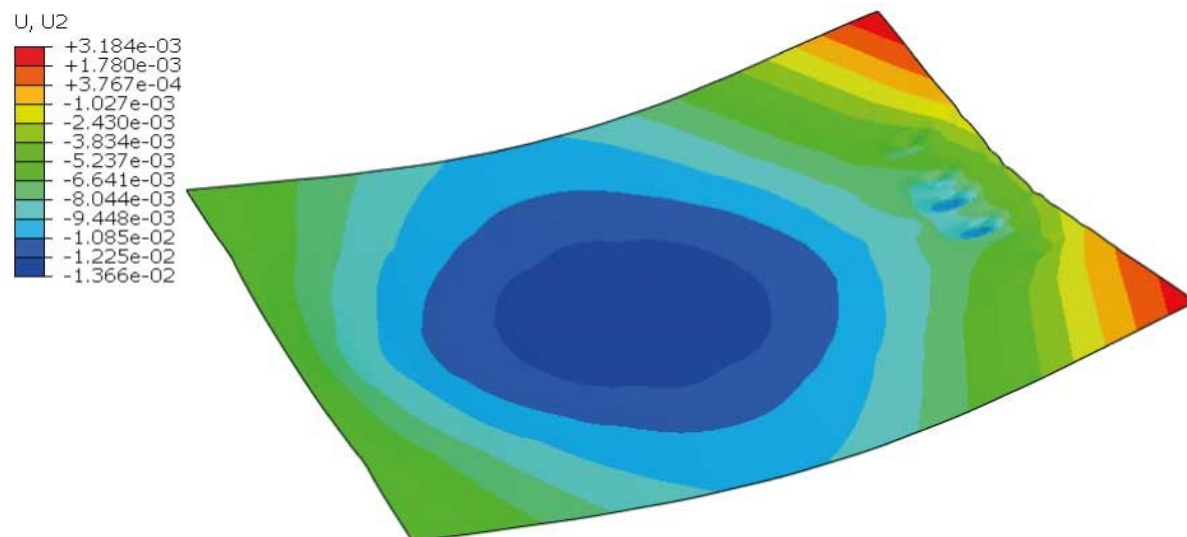
Figure F-12 Non-hybrid; LM1; SLS; deck, top facing – vertical deflection

The governing location with regard to the vertical 5 mm limit, is located on the far left and right of the deck, as illustrated in Figure F-12. The deflection on the right (both up and downward) stay within the limit. (**3.2** and **4.1 mm** respectively) The deflection on the left, has a maximum downward value of **5.0 mm**. This is on the limit and still considered to be tolerable, since its smaller compared to the values found by Movares, as stated in section D.1.1.1.

F.3.1.1.2.   Webs

The webs have been checked both on strength, as well as buckling. The applied load placement is illustrated in Appendix D – Figure D-1. This load placement differs from the one used for the top facing, since the previous placement doesn't result in a proper calculation for the buckling of the webs.

F.3.1.1.2.1. Longitudinal stress – S11
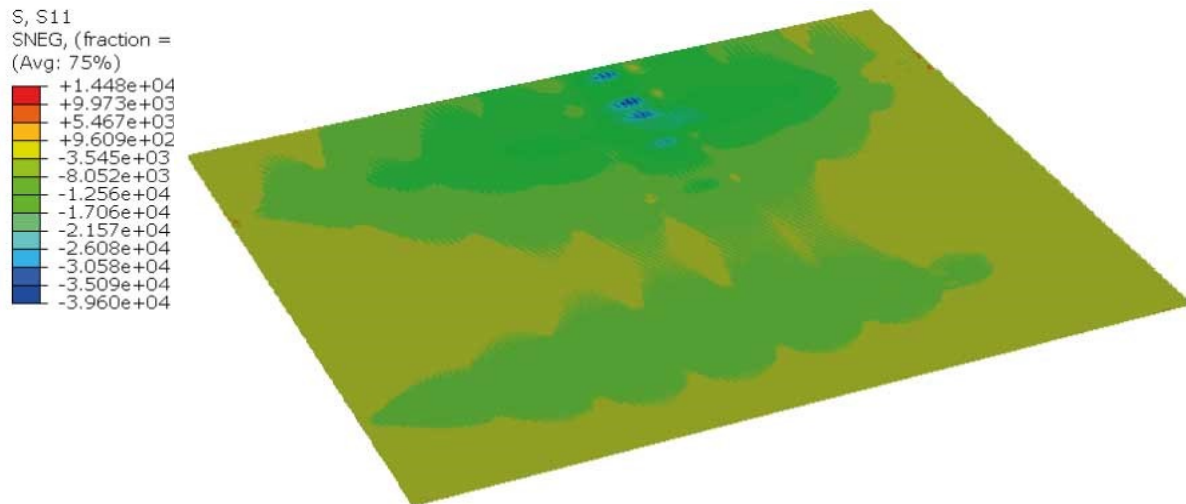
Figure F-13 Non-hybrid; LM1; ULS; deck, webs – S11

This loading resulted in the following UC at the location, as illustrated in Figure F-13:

$$UC_{tension} = 0.124 \qquad UC_{compression} = 0.396$$
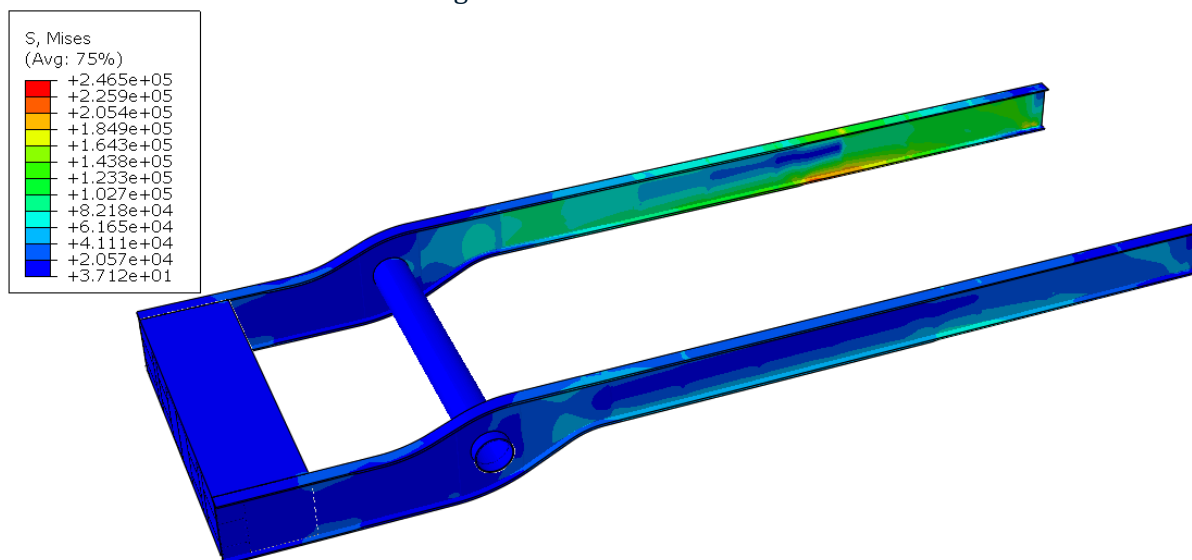
F.3.1.1.2.2. Transverse stress – S22
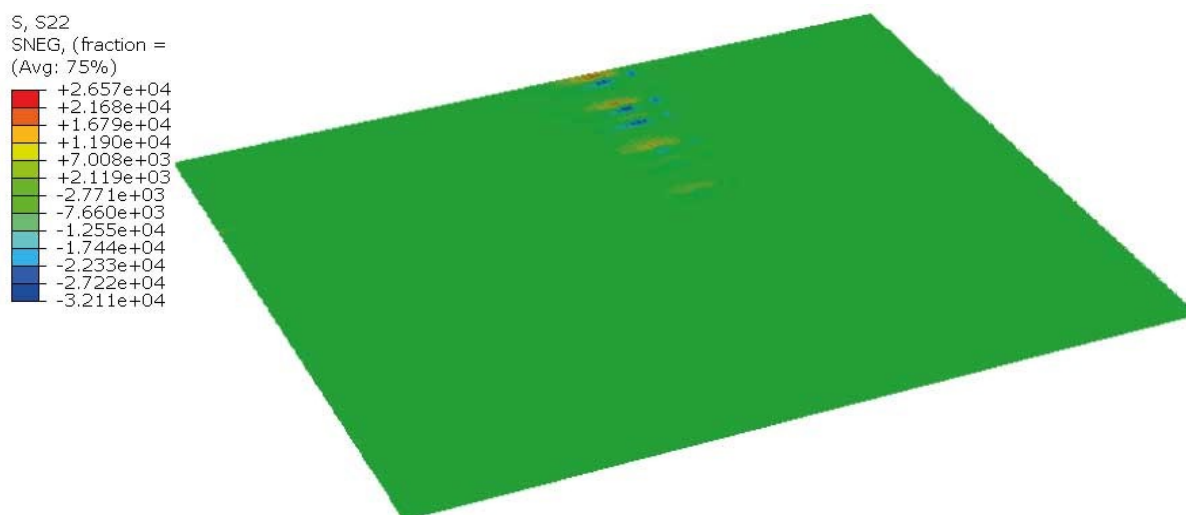
Figure F-14 Non-hybrid; LM1; ULS; deck, webs – S22

This loading resulted in the following UC at the location, as illustrated in Figure F-14:

$$UC_{tension} = 0.314 \qquad UC_{compression} = 0.343$$
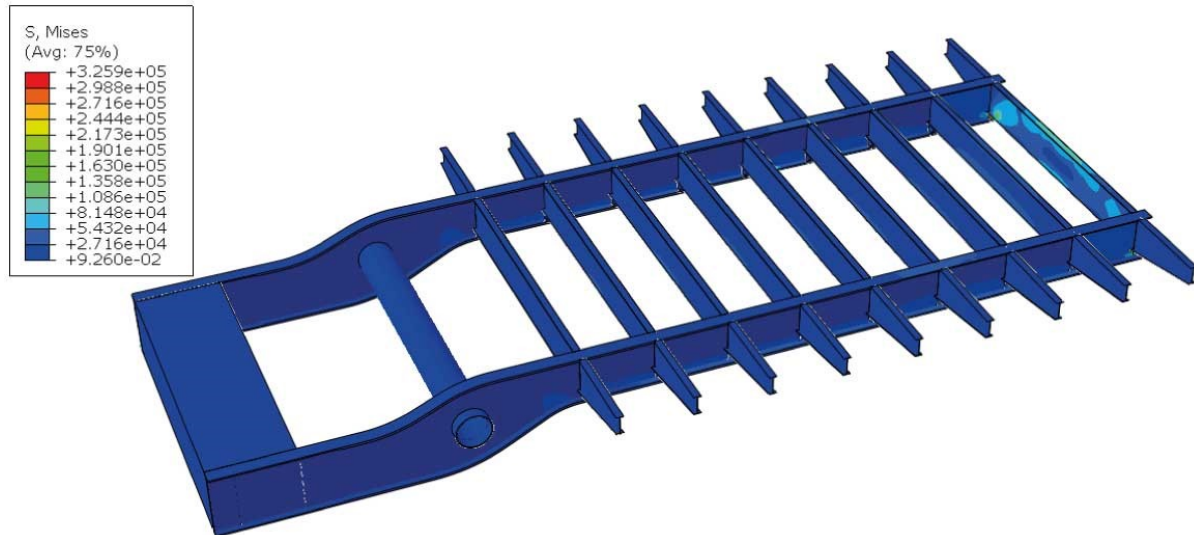
F.3.1.1.2.3. Shear stress – S12
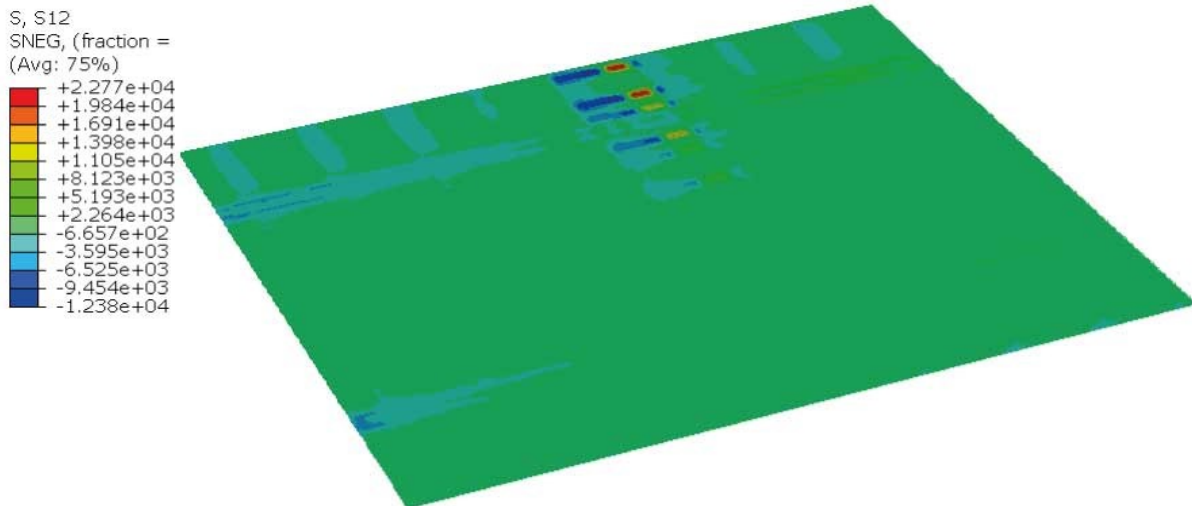
Figure F-15 Non-hybrid; LM1; ULS; deck, webs – S12

This loading resulted in the following UC at the location, as illustrated in Figure F-15:

$$UC = 0.784$$

F.3.1.1.2.4. Combination

According to the CUR 96+ section 6.3.1 a combined stress criterium must suffice the following equation, where aforementioned stresses have been applied, resulting in a unity check:

$$\left(\frac{\sigma_{1,Ed}}{\sigma_{1,Rd}}\right)^2 + \left(\frac{\sigma_{2,Ed}}{\sigma_{2,Rd}}\right)^2 + \left(\frac{\tau_{12,Ed}}{\tau_{12,Rd}}\right)^2 - \frac{\sigma_{1,Ed} \cdot \sigma_{2,Ed}}{\sigma_{1,Rd}^2} = 0.762 \leq 1.0$$

F.3.1.1.2.5. Buckling

A critical buckling stress has been obtained from Abaqus. This is compared with the transverse stress in the web. This stress distribution can be found in Figure F-14, where the max compression stress is:

$$\sigma_{22,max} = -32.11 \, MPa$$

When viewing the web with this max compressive stress, the stress along the length of this web, is as follows, with the **stresses** displayed in **MPa** and the **distance** in **m**:
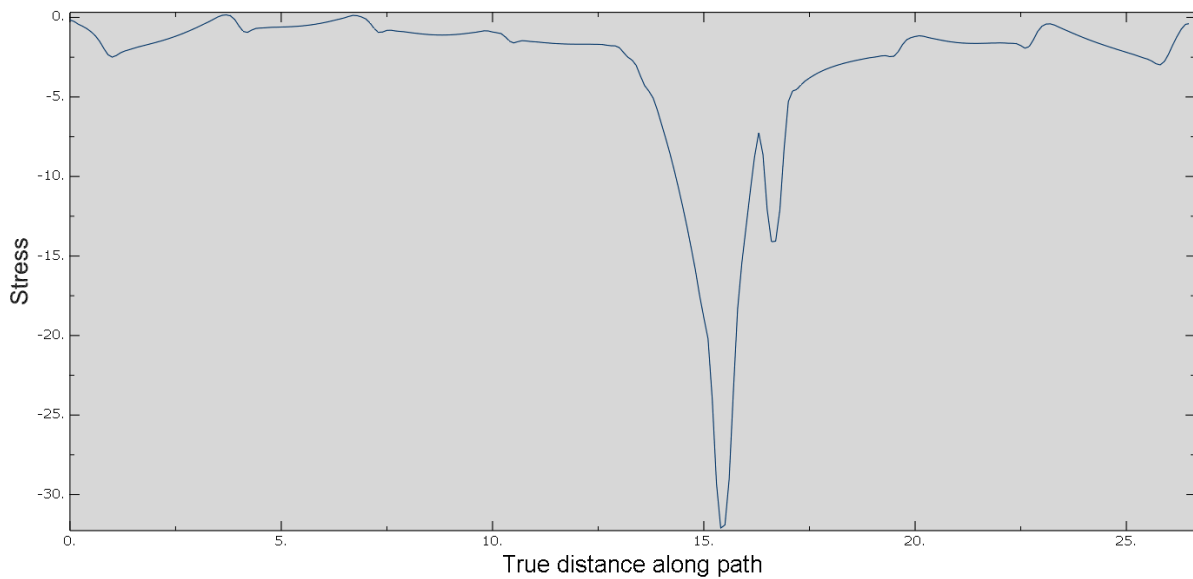
Figure F-16 Development of S22 over the length of the web

Next the integral of the vertical stress of the entire web is used to obtain the total capacity of the web. Resulting in:
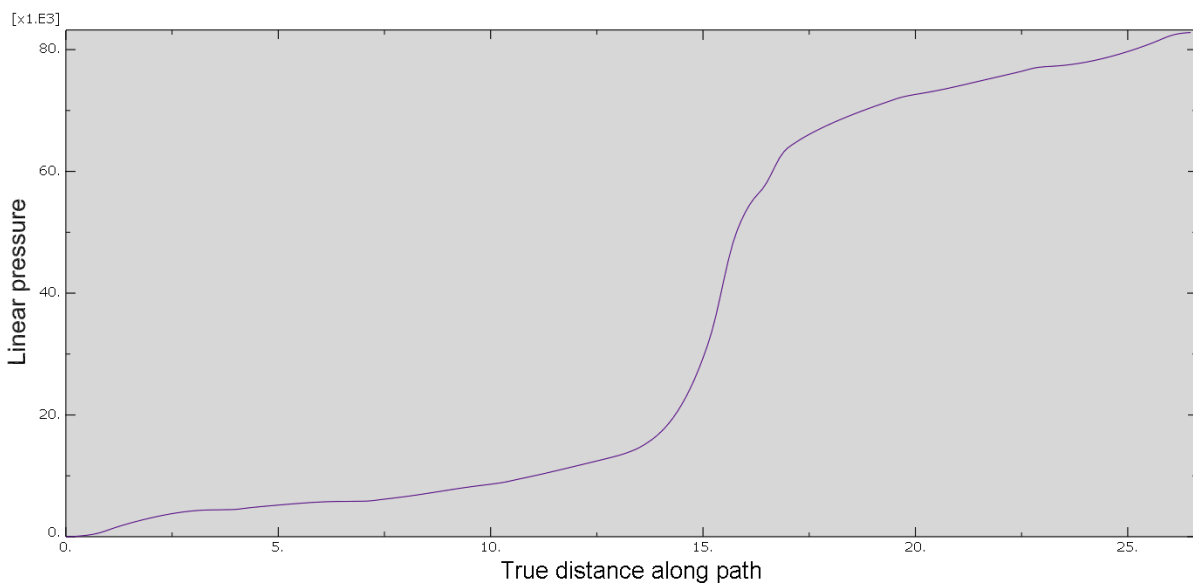
Figure F-17 Integral of S22 over the length of the web

$$\sigma_{22,int} = 82800 \, MPa \cdot mm$$

Dividing this integral by the maximum stress, an effective width is found. This effective width is used in the buckling check as the width of the web:

$$b_{eff} = \frac{\sigma_{22,int}}{\sigma_{22,max}} \rightarrow 2500 \, mm$$
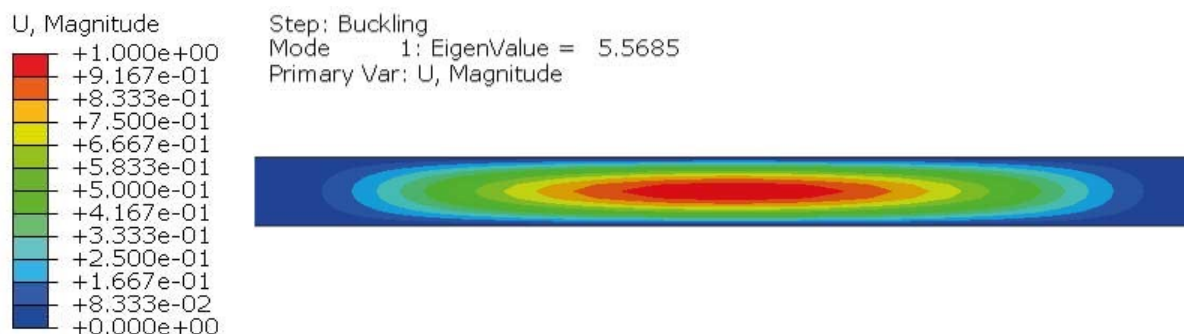
Figure F-18 Non-hybrid; LM1; ULS; deck, webs – buckling

Applying maximum stress value ($\sigma_{22,max}$) to the effective width (b_{eff}), results in the deformed shape, illustrated in Figure F-18. Here due to the deformation shape a clear indication of plate effects is visible. It has led to the following eigenvalue:

$$\alpha_{cr} = 5.5685$$

To find the critical stress value the applied stress value is multiplied with the eigenvalue:

$$\sigma_{22,cr} = \alpha_{cr} \cdot \sigma_{22,max} \rightarrow -184 \; MPa$$

Since the critical stress is greater than the acting stress, the webs will not buckle. (This can be also concluded from the eigenvalue being greater than 1.0) Thus no buckling will occur. (see section 6.4.5 of (CUR, 2013)

F.3.1.1.3.   Bottom facing

The bottom facing has been checked on strength using LM1 for the primary as well as their shear stresses.

F.3.1.1.3.1. Longitudinal stress – S11

Figure F-19 Non-hybrid; LM1; ULS; deck, bottom facing – S11

This loading resulted in the following UC's at the location, as illustrated in Figure F-9:

$$UC_{tension} = 0.058 \qquad UC_{compression} = 0.122$$

F.3.1.1.3.2. Transverse stress – S22

Figure F-20 Non-hybrid; LM1; ULS; deck, bottom facing – S22

This loading resulted in the following UC at the location, as illustrated in Figure F-10:

$$UC_{tension} = 0.073 \qquad UC_{compression} = 0.199$$

F.3.1.1.3.3. Shear stress – S12

Figure F-21 Non-hybrid; LM1; ULS; deck, bottom facing – S12

This loading resulted in the following UC at the location, as illustrated in Figure F-11:

$$UC = 0.320$$

F.3.1.1.3.4. Combination

According to the CUR 96+ section 6.3.1 a combined stress criterium must suffice the following equation, where aforementioned stresses have been applied, resulting in a unity check:

$$\left(\frac{\sigma_{1,Ed}}{\sigma_{1,Rd}}\right)^2 + \left(\frac{\sigma_{2,Ed}}{\sigma_{2,Rd}}\right)^2 + \left(\frac{\tau_{12,Ed}}{\tau_{12,Rd}}\right)^2 - \frac{\sigma_{1,Ed} \cdot \sigma_{2,Ed}}{\sigma_{1,Rd}^2} = 0.147 \leq 1.0$$

F.3.1.1.3.5. Vertical Deflection

The deflections of the bottom flange of the deck are not governing. It is the top flange, which has a governing criterium. This has been addressed earlier in section F.3.1.1.1.5 – Vertical Deflection.

F.3.1.2. Main girders

The main girders have been designed to have a comparable stress level for this load case. In the case of the original Amalia bridge, the tensile stress in the bottom flange is under 200 MPa.

The main girders have been checked both on strength and deformation:
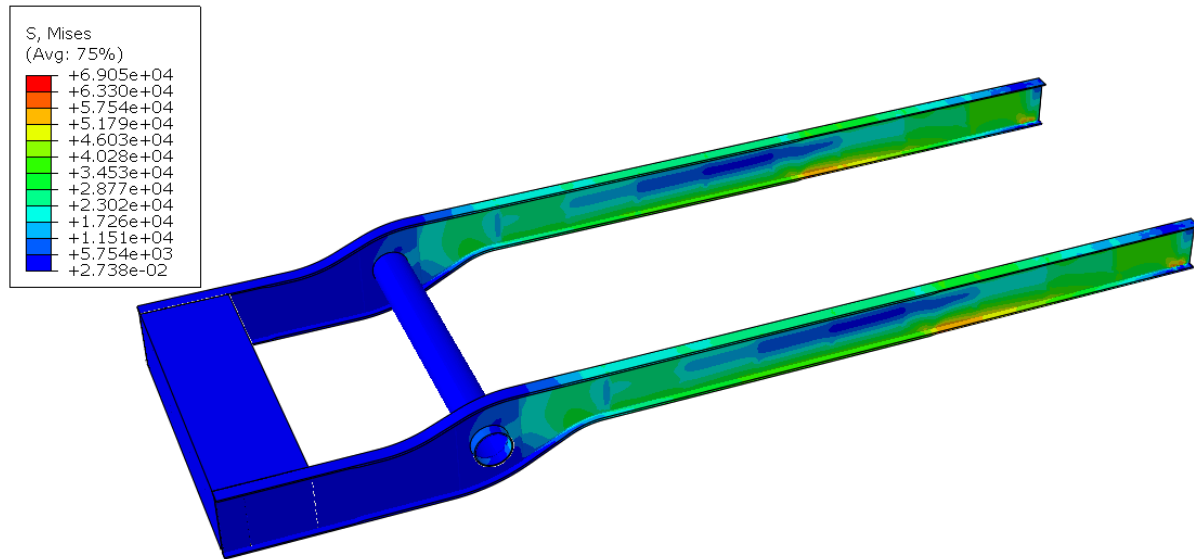
F.3.1.2.1. Strength

Figure F-22 Non-hybrid; LM1; ULS; main girder – S, Mises

This loading resulted in the following UC at the location, as illustrated in Figure F-22. The flange thickness has resulted in a lower yield stress. This has been applied in the UC:

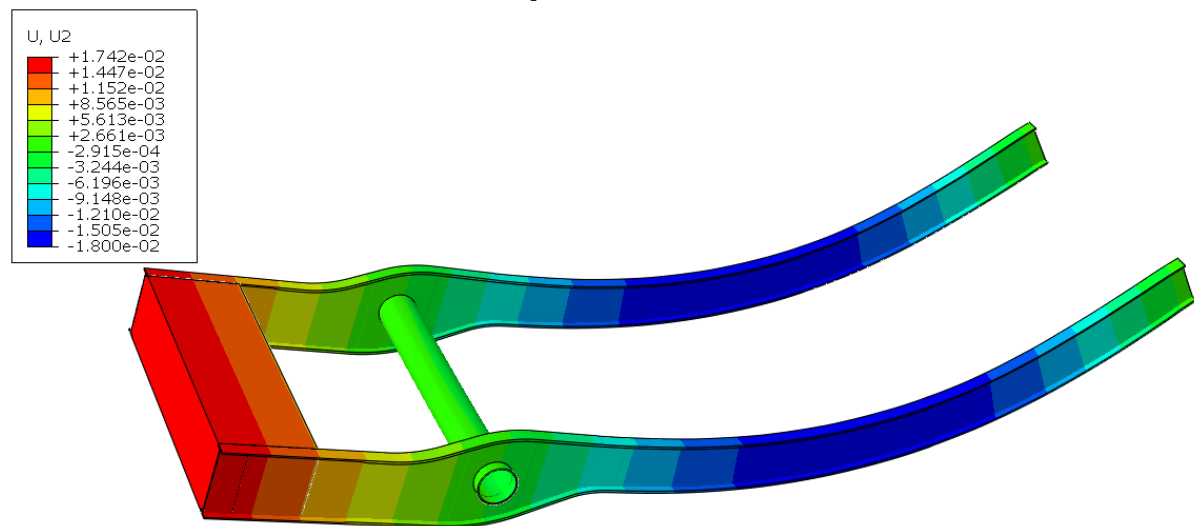$$UC = 0.836$$

F.3.1.2.2. Vertical Deflection
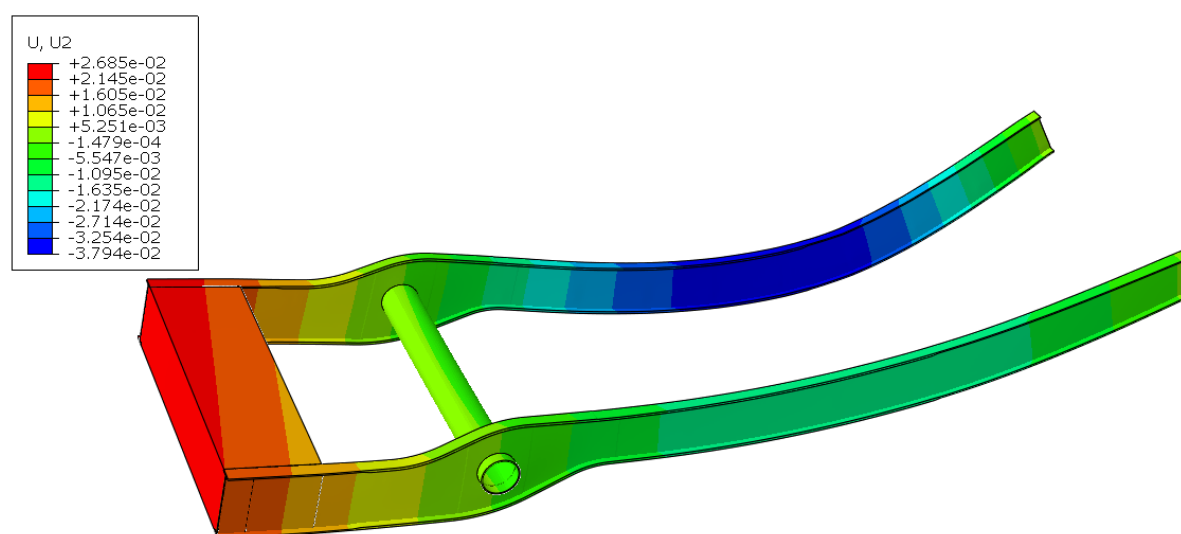
Figure F-23 Non-hybrid; LM1; SLS; main girders – U2 (vertical displacement)

This loading resulted in the following UC at the location, as illustrated in Figure F-23:

$$U = 37.94\ mm \leq 59.5\ mm$$

F.3.1.3.   Cross girders

The cross girders have been checked both on strength and deformation:

F.3.1.3.1.   Strength

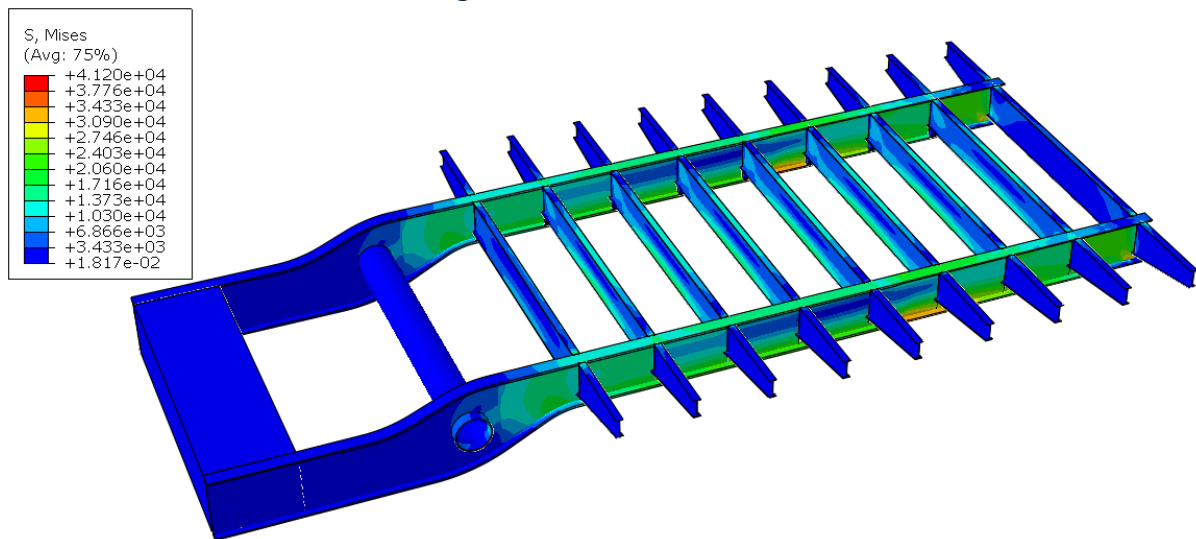**Figure F-24 Non-hybrid; LM1; ULS; cross girders – S, Mises**

This loading resulted in the following UC at the location, as illustrated in Figure F-24:

$$UC_{CrossGirder} = 0.576 \qquad UC_{support} = 0.918$$

Here a distinction has been made between the supports and the cross girders, due to the additional stress concentration found in the supports.
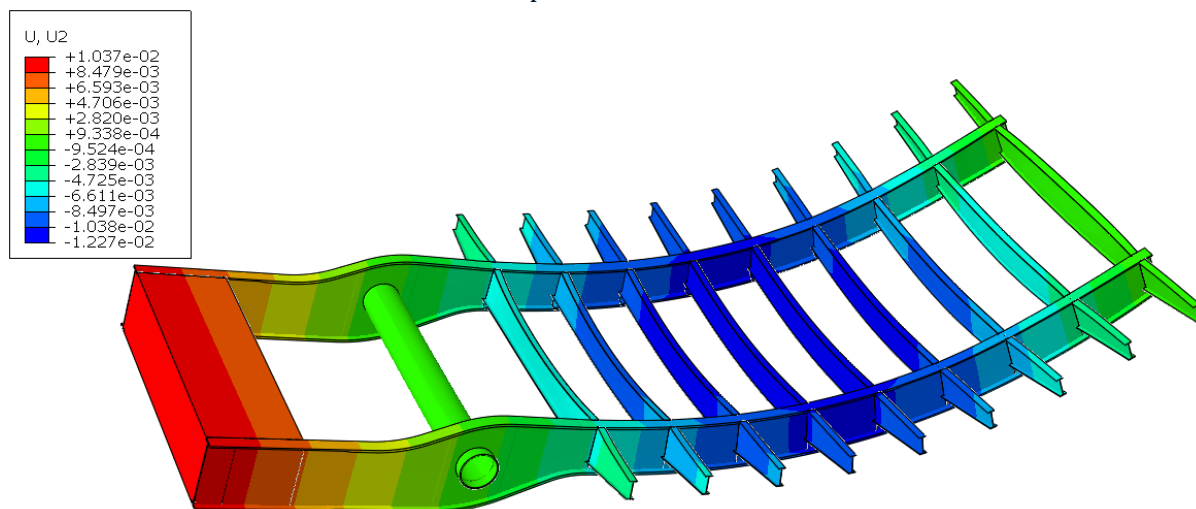
F.3.1.3.2.   Vertical Deflection
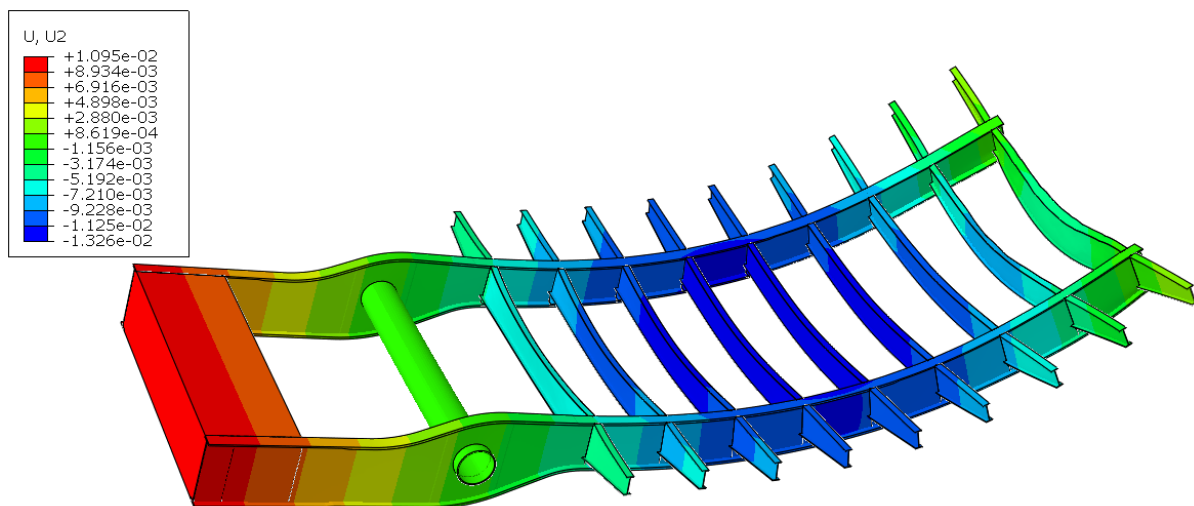
Figure F-25 Non-hybrid; LM1; ULS; cross girders – U2 (vertical displacement)

This loading resulted in the following UC at the location, as illustrated in Figure F-25:

$$U = 13.26\ mm \leq 25\ mm$$

F.3.2. LM2

This load case has only been used to check the webs of the deck for stability. This has resulted in the following stress distribution:
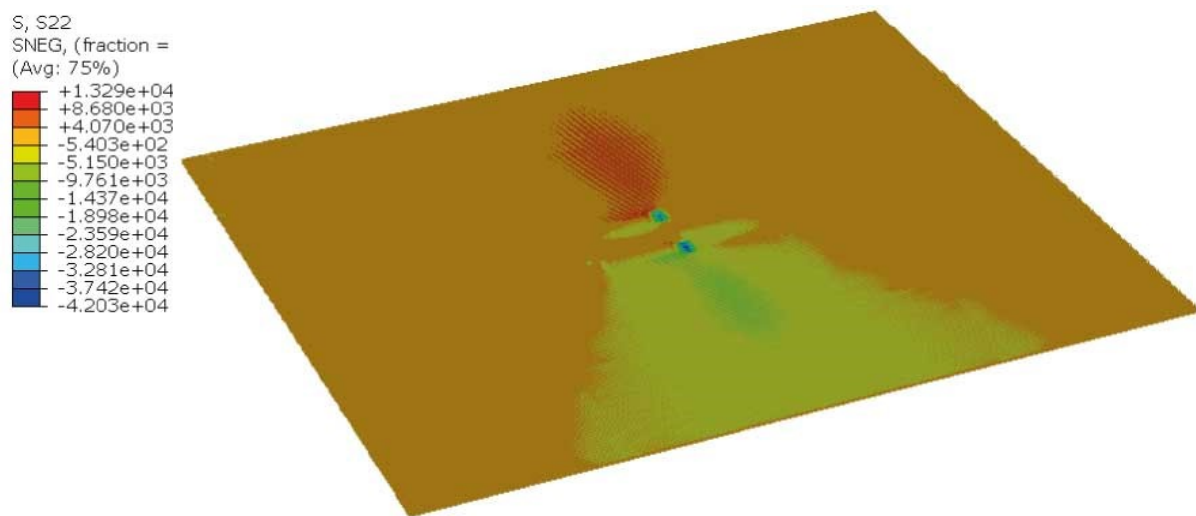
Figure F-26 Non-hybrid; LM2; ULS; deck, webs – S22

This loading resulted in the following UC at the location, as illustrated in Figure F-26:

$$UC_{tension} = 0.086 \qquad UC_{compression} = 0.472$$

F.3.2.1.   Buckling

A critical buckling stress has been obtained from Abaqus. This is compared with the transverse stress in the web. This stress distribution can be found in Figure F-26, where the max compression stress is:

$$\sigma_{22,max} = -42.03 \, MPa$$

When viewing the web with this max compressive stress, the stress along the length of this web, is as follows, with the **stresses** displayed in **MPa** and the **distance** in **m**:
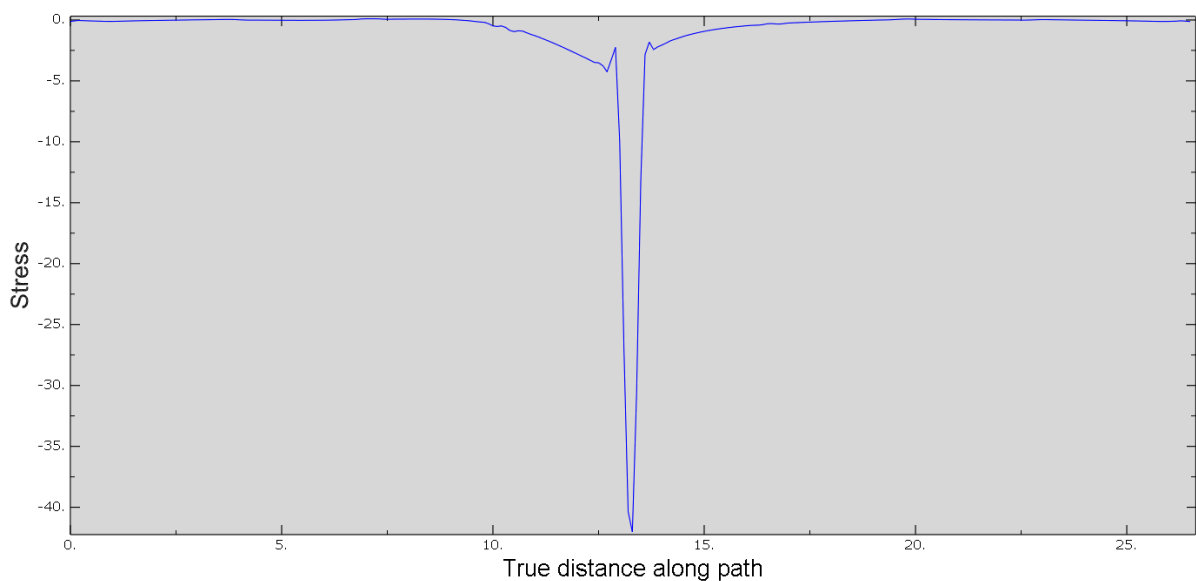
Figure F-27 Development of S22 over the length of the web

Next the integral of the vertical stress of the entire web is used to obtain the total capacity of the web. Resulting in:
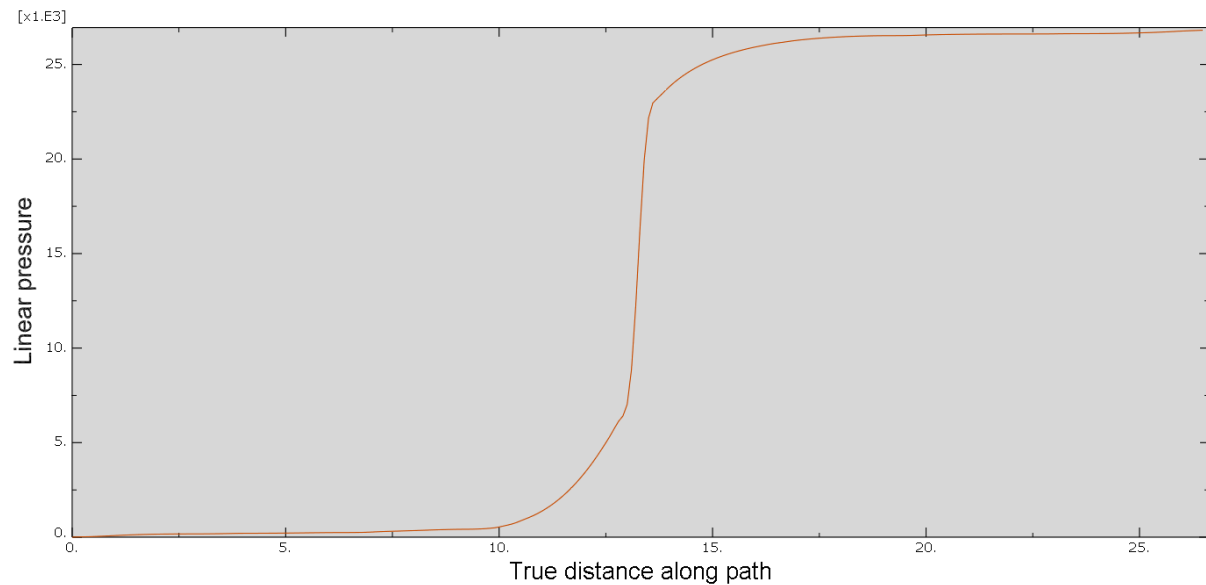
Figure F-28 Integral of S22 over the length of the web

$$\sigma_{22,int} = 26815 \, MPa \cdot mm$$

Dividing this integral by the maximum stress, an effective width is found. This effective width is used in the buckling check as the width of the web:

$$b_{eff} = \frac{\sigma_{22,int}}{\sigma_{22,max}} \rightarrow 638 \, mm$$
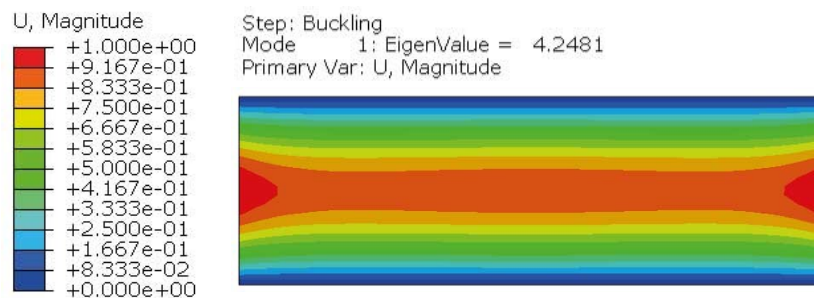
Figure F-29 Non-hybrid; LM1; ULS; deck, webs – buckling

Applying maximum stress value ($\sigma_{22,max}$) to the effective width (b_{eff}), results in the deformed shape, illustrated in Figure F-29. Here due to the deformation shape a clear indication of plate effects is visible. It has led to the following eigenvalue:

$$\alpha_{cr} = 4.2481$$

To find the critical stress value the applied stress value is multiplied with the eigenvalue:

$$\sigma_{22,cr} = \alpha_{cr} \cdot \sigma_{22,max} \rightarrow -179 \, MPa$$

Since the critical stress is greater than the acting stress, the webs will not buckle. (This can be also concluded from the eigenvalue being greater than 1.0) Thus no buckling will occur. (see section 6.4.5 of (CUR, 2013)

F.3.3. LM4

F.3.3.1.   Main girders

F.3.3.1.1.   Strength

Figure F-30 Non-hybrid; LM4; SLS; main girders – S, Mises

This loading resulted in the following UC at the location, as illustrated in Figure F-30:

$$UC = 0.195$$

F.3.3.1.2.   Vertical displacement

Figure F-31 Non-hybrid; LM4; SLS; main girders – U2 (vertical displacement)

This loading resulted in the following UC at the location, as illustrated in Figure F-31:

$$U = 17.42 \ mm \leq 59.5 \ mm$$

F.3.3.2.   Cross girders (centre span)

F.3.3.2.1.   Strength

Figure F-32 Non-hybrid; LM4; SLS; cross girders (centre span) – S, Mises

This loading resulted in the following UC at the location, as illustrated in Figure F-32:

$$UC = 0.116$$

F.3.3.2.2.   Vertical displacement

Figure F-33 Non-hybrid; LM4; SLS; cross girders (centre span) – U2 (vertical displacement)

This loading resulted in the following UC at the location, as illustrated in Figure F-33:

$$U = 12.27\ mm \le 25\ mm$$

F.3.3.3.　　　Cross girders (side span)

F.3.3.3.1.　　　Strength
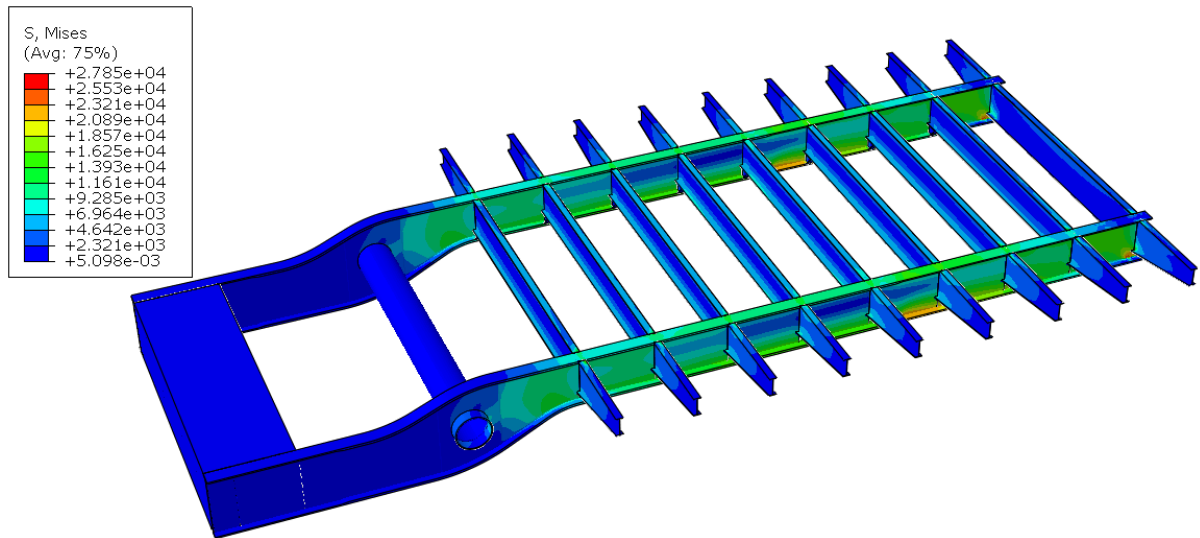
Figure F-34 Non-hybrid; LM4; SLS; cross girders (side span) – S, Mises

This loading resulted in the following UC at the location, as illustrated in Figure F-34:

$$UC = 0.078$$

F.3.3.3.2.　　　Vertical displacement
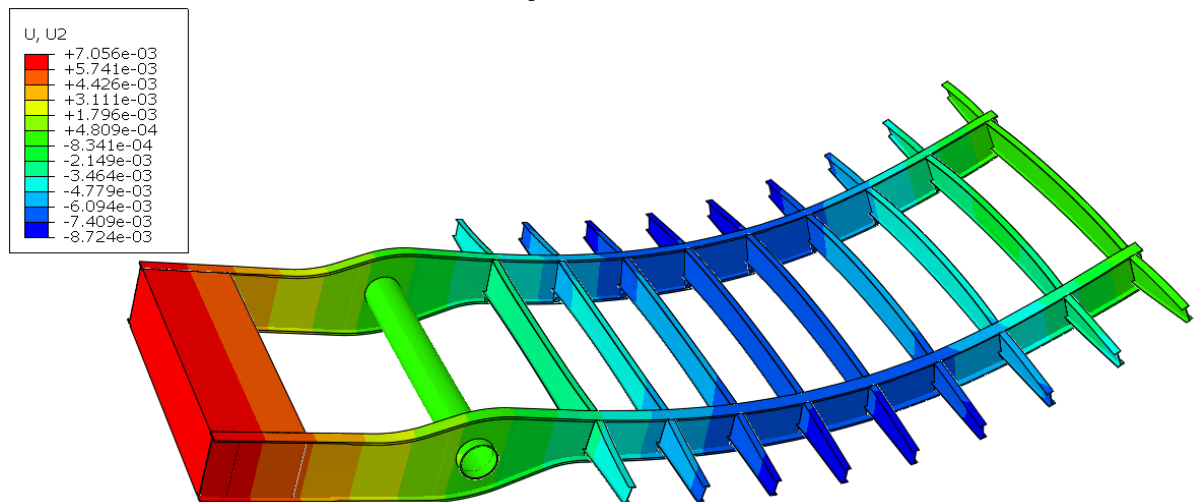
Figure F-35 Non-hybrid; LM4; SLS; cross girders (side span) – U2 (vertical displacement)

This loading resulted in the following UC at the location, as illustrated in Figure F-35:

$$U = 8.7\ mm \leq 25\ mm$$

Appendix G. Details of Design 2 – Hybrid

This appendix contains more detailed information regarding the hybrid design. It contains the following topics:

- Bridge built up
- Weight calculation
- Fatigue verification
- Design verifications
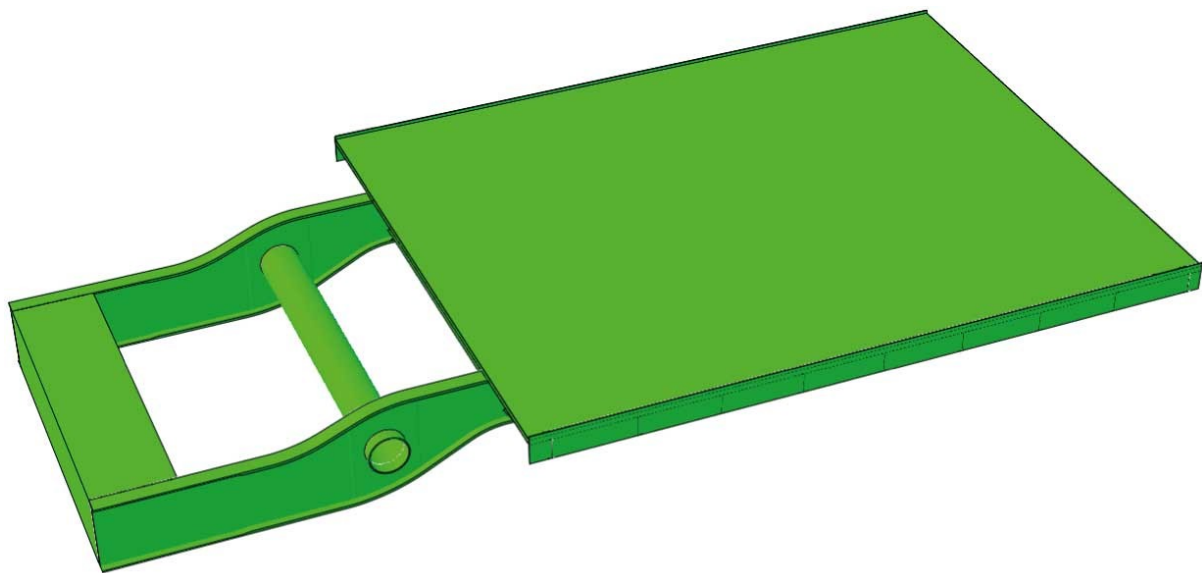
Figure G-1 3D-impression of the hybrid design

G.1. Bridge built up

G.1.1. FRP-deck

The FRP deck used in this design is based upon the redundancy principal of FiberCore, by making use of Z-shaped shells. In the model this has been simplified to a horizontal top and bottom layer and vertical webs, allowing for the height required in the design. In the fabrication of this deck, foam blocks are used to ensure the proper placement and alignment of fibres. These foam cores have been assumed NOT to contribute to the structural strength and stiffness of the deck as a whole. Thus, they have not been modelled in the FEM-programming. An impression of this deck can be seen in Figure 10-1.

G.1.2. Hybrid interaction

The FRP deck functions as the top flange of both the main and cross girders, this increase in area of the top flange, allows for a reduction of the steel section in this section. The same approach as used for the orthotropic deck, can be used here, taking into account the difference in stiffness properties between the two materials used.

G.1.3. Main and cross girder cross sections
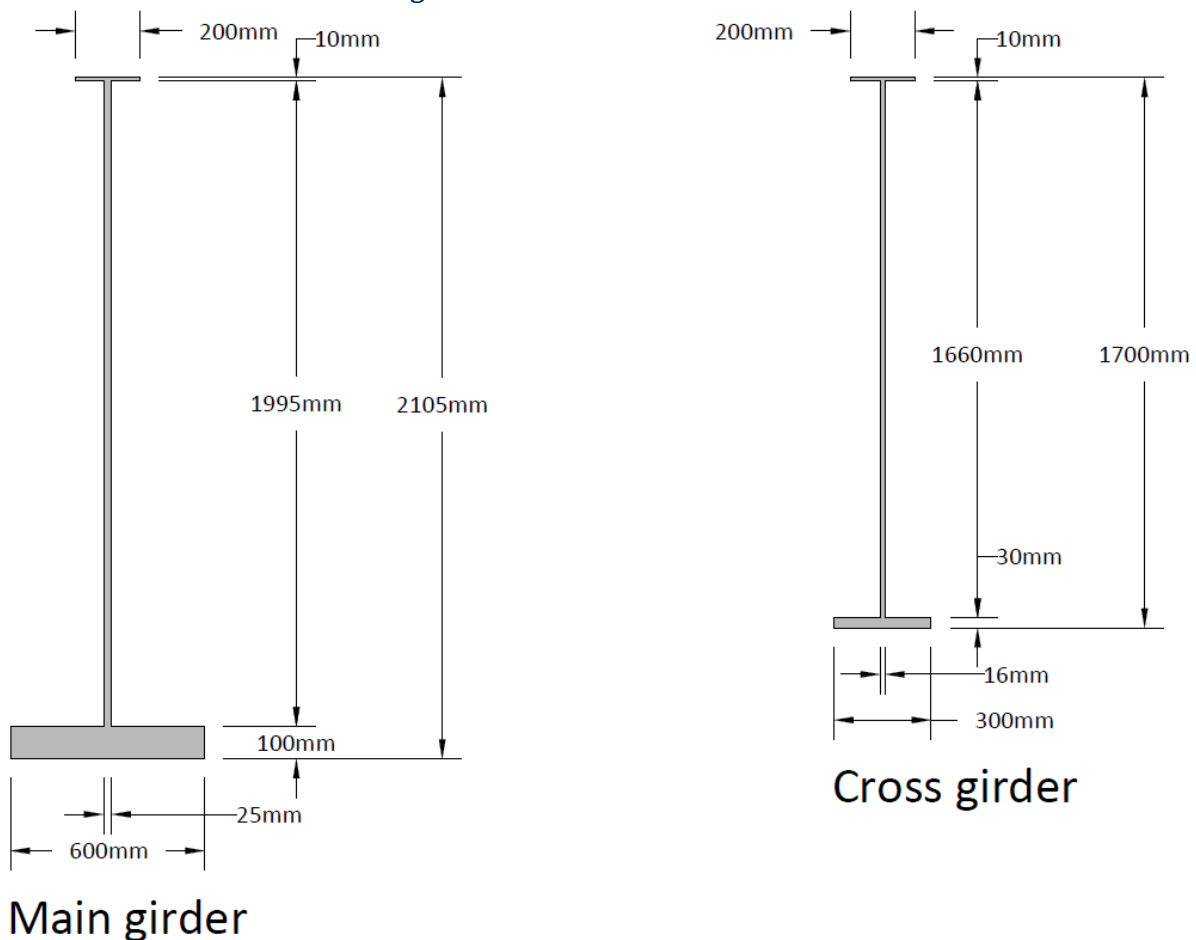
Figure G-2 Cross sections of the main and cross girders of the hybrid design

G.1.4. Cross section of the movable bridge section
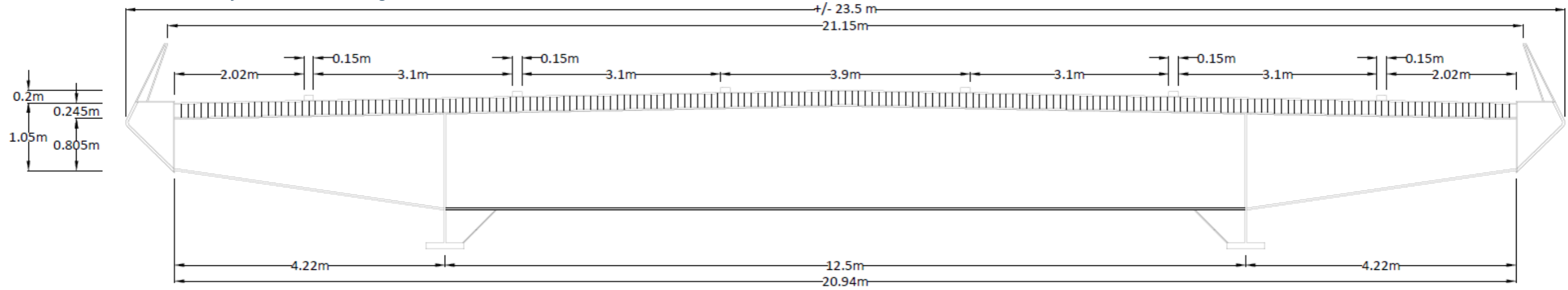
Figure G-3 Cross section of the hybrid design

G.1.5. Length section of the movable bridge section
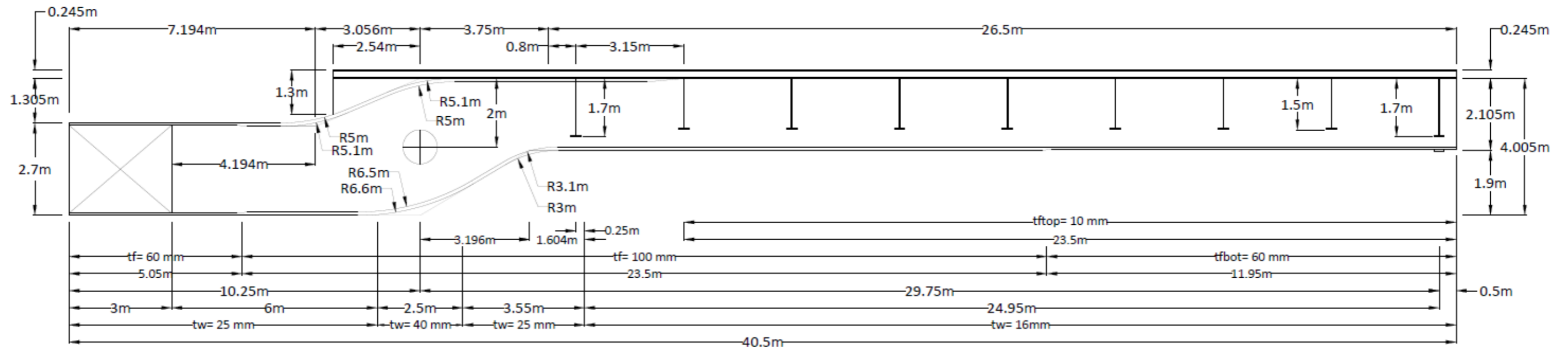
Figure G-4 Length section of the hybrid design

G.2. Weight calculation

In this section the calculation, mentioned in chapter …, has been shown. In essence the bridge's length section is split into two; one left and one right section. For all the existing elements an approximation of the volume, combined with the location of the centre of gravity and the modelled counterweight, using only steel.

G.2.1. Input Parameters

Here the different parameters used in these calculations have been displayed.

General		
width deck	20940	mm
length deck	26500	mm
distance rotation centre – start deck	3750	mm
c.t.c. main girders	12500	mm
number of cross girders	9	[-]
distance rotation centre – top deck	2245	mm

Table G-2 General input parameters defining of the hybrid design

Densities		
rho,steel	78.5	kN/m3
rho, conc.	40.5	kN/m3
rho,frp,fac	16.7	kN/m3
hro,frp,web	14.6	kN/m3

Table G-1 Desity definitions regarding the materials of the hybrid design

Deck			Deck (facing, web, facing)			Main girder			Cross girder		
t,deck	20	mm	t,f,top		20	mm	h,girder	2105	mm	h,girder-1,9	1700	mm
							t,w	16	mm	h,girder-2-8	1500	mm
Front cover			h,w		205		t,f,1,top,thick	100	mm	t,w	16	mm
t,w	8	mm	t,w		8	mm	t,f,2,top,thin	10	mm	t,f,top	10	mm
h,w	245	mm	# of webs		201	[-]	t,f,1,bot,thick	100	mm	t,f,bot	30	mm
			c.t.c.		104.70	mm	t,f,2,bot,thin	60	mm	b,top	200	mm
Side cover							b,top,thin	200	mm	b,bot	300	mm
t,w	20	mm	t,f,bot		20	mm	b,top/b,bot	600	mm	c.t.c.	3.15	m
h,w	1150	mm					c.t.c.	12.5	m	offset,l	800	mm
							l,thin,R	11950	mm	offset,r	800	mm
							l,thin,L	5050	mm	h,side	805	mm

Table G-3 Detuilled input parameters, per component, defining of the hybrid design

G.2.2. Leaf Calculation

Below is the table containing the values used for the weight calculation. This is regarding the section on the right side of the rotation centre, as is shown in Table G-4.

Description	b1	b2	t	L	Horizontal centre of gravity X	Vertical centre of gravity Y (above is +)	Amount	Volume	Weight	Moment X	Centre of Gravity X	Moment Y	Centre of Gravity Y
Deck system									**702 kN**	**11936 kNm**	**17. m**	**1445 kNm**	**2.06 m**
Deck - top facing	20940mm	20940mm	20mm	26500mm	17000mm	2235mm	1	11.1 m3	185kN	3151 kNm		414 kNm	
Deck - webs (incl. lost core)	205mm	205mm	8mm	26500mm	17000mm	2123mm	201	8.74 m3	235kN	3987 kNm		498 kNm	
Deck - bottom facing	20940mm	20940mm	20mm	26500mm	17000mm	2010mm	1	11.1 m3	185kN	3151 kNm		373 kNm	
Side cover	1150mm	1150mm	20mm	26500mm	17000mm	1648mm	2	1.22 m3	96kN	1627 kNm		158 kNm	
Front cover (tip leaf)	20940mm	20940mm	8mm	245mm	30250mm	2123mm	1	.04 m3	1kN	18 kNm		1 kNm	
Back cover (base leaf)	20940mm	20940mm	8mm	245mm	3750mm	2123mm	1	.04 m3	1kN	2 kNm		1 kNm	
Main girder									**594 kN**	**7333 kNm**	**12.35 m**	**374 kNm**	**.63 m**
Web-1 (t=40mm)	3805mm	2648mm	40mm	1250mm	1046mm	80mm	2	.25 m3	20kN	21 kNm		2 kNm	
Web-2 (t= 25mm)	2648mm	1905mm	25mm	1946mm	2223mm	588mm	2	.22 m3	17kN	39 kNm		10 kNm	
Web-3 (t=25mm)	1905mm	1905mm	25mm	1604mm	3998mm	948mm	2	.15 m3	12kN	48 kNm		11 kNm	
Web-4 (t=16mm)	1905mm	1905mm	16mm	13500mm	11550mm	948mm	2	.82 m3	65kN	746 kNm		61 kNm	
Web-5 (t=16mm)	2015mm	2015mm	16mm	11950mm	24275mm	983mm	2	.77 m3	60kN	1468 kNm		59 kNm	
Bottom-flange-1	600mm	600mm	100mm	3196mm	1598mm	-1005mm	2	.38 m3	30kN	48 kNm		-30 kNm	
Bottom-flange-2	600mm	600mm	100mm	15104mm	10748mm	-427mm	2	1.81 m3	142kN	1529 kNm		-61 kNm	
Bottom-flange-3	600mm	600mm	60mm	11950mm	24275mm	-427mm	2	.86 m3	68kN	1640 kNm		-29 kNm	
Top-flange-1	600mm	600mm	100mm	18300mm	9150mm	1950mm	2	2.2 m3	172kN	1577 kNm		336 kNm	
Top-flange-2	200mm	200mm	10mm	23150mm	29875mm	1905mm	2	.09 m3	7kN	217 kNm		14 kNm	

Cross girder-1 (front girder)									**57 kN**	**1697 kNm**	**29.75 m**	**61 kNm**	**1.08 m**
Web-centre	1640mm	1640mm	16mm	12484mm	29750mm	1170mm	1	.33 m3	26kN	765 kNm		30 kNm	
Web-side	1640mm	745mm	16mm	4204mm	29750mm	1394mm	2	.16 m3	13kN	375 kNm		18 kNm	
Top -flange	200mm	200mm	10mm	20540mm	29750mm	1995mm	1	.04 m3	3kN	96 kNm		6 kNm	
Flange-centre	300mm	300mm	30mm	12484mm	29750mm	335mm	1	.11 m3	9kN	262 kNm		3 kNm	
Flange-side	300mm	300mm	30mm	4298mm	29750mm	783mm	2	.08 m3	6kN	181 kNm		5 kNm	
Support-web	292mm	597mm	16mm	305mm	29750mm	-647mm	2	. m3	kN	10 kNm		kNm	
Support-flange	300mm	200mm	16mm	431mm	29750mm	-647mm	2	. m3	kN	8 kNm		kNm	
Cross girder-9 (rear girder)									**57 kN**	**259 kNm**	**4.55 m**	**61 kNm**	**1.07 m**
Web-centre	1640mm	1640mm	16mm	12475mm	4550mm	1170mm	1	.33 m3	26kN	117 kNm		30 kNm	
Web-side	1640mm	745mm	16mm	4195mm	4550mm	1394mm	2	.16 m3	13kN	57 kNm		18 kNm	
Top -flange	200mm	200mm	10mm	19740mm	4550mm	1995mm	1	.04 m3	3kN	14 kNm		6 kNm	
Flange-centre	300mm	300mm	30mm	12484mm	4550mm	335mm	1	.11 m3	9kN	40 kNm		3 kNm	
Flange-side	300mm	300mm	30mm	4298mm	4550mm	783mm	2	.08 m3	6kN	28 kNm		5 kNm	
Support-web	292mm	597mm	16mm	305mm	4550mm	-647mm	2	. m3	kN	2 kNm		kNm	
Support-flange	300mm	200mm	16mm	431mm	4550mm	-647mm	2	. m3	kN	1 kNm		kNm	
Cross girder-2-4 (h=1500)									**162 kN**	**3288 kNm**	**20.3 m**	**183 kNm**	**1.13 m**
Web-centre	1470mm	1470mm	16mm	12484mm	20300mm	1255mm	3	.88 m3	69kN	1404 kNm		87 kNm	
Web-side	1470mm	745mm	16mm	4204mm	20300mm	1436mm	6	.45 m3	35kN	712 kNm		50 kNm	
Top -flange	200mm	200mm	10mm	20540mm	20300mm	1995mm	3	.12 m3	10kN	196 kNm		19 kNm	
Flange-centre	300mm	300mm	30mm	12484mm	20300mm	505mm	3	.34 m3	26kN	537 kNm		13 kNm	
Flange-side	300mm	300mm	30mm	4298mm	20300mm	868mm	6	.23 m3	18kN	370 kNm		16 kNm	
Support-web	292mm	797mm	16mm	505mm	20300mm	-710mm	6	.03 m3	2kN	42 kNm		-1 kNm	
Support-flange	300mm	200mm	16mm	714mm	20300mm	-710mm	6	.02 m3	1kN	26 kNm		-1 kNm	
Cross girder-5-8 (h=1500)									**216 kN**	**2003 kNm**	**9.28 m**	**244 kNm**	**1.13 m**
Web-centre	1470mm	1470mm	16mm	12484mm	9275mm	1255mm	4	1.17 m3	92kN	855 kNm		116 kNm	
Web-side	1470mm	745mm	16mm	4204mm	9275mm	1436mm	8	.6 m3	47kN	434 kNm		67 kNm	
Top -flange	200mm	200mm	10mm	20540mm	9275mm	1995mm	4	.16 m3	13kN	120 kNm		26 kNm	
Flange-centre	300mm	300mm	30mm	12484mm	9275mm	505mm	4	.45 m3	35kN	327 kNm		18 kNm	
Flange-side	300mm	300mm	30mm	4298mm	9275mm	868mm	8	.31 m3	24kN	225 kNm		21 kNm	
Support-web	292mm	797mm	16mm	505mm	9275mm	-710mm	8	.04 m3	3kN	26 kNm		-2 kNm	
Support-flange	300mm	200mm	16mm	714mm	9275mm	-710mm	8	.02 m3	2kN	16 kNm		-1 kNm	
Axle									**97 kN**	**kNm**	**. m**	**kNm**	**. m**
Axle (R=750)		750mm	40mm	13500mm	mm	mm	1	1.24 m3	97kN	kNm		kNm	
Addition									**13 kN**	**162 kNm**	**12.68 m**	**24 kNm**	**1.85 m**
Welding/ conservation (steel)				1.00%					13kN	162kN		24kN	
Road equipment & wear layer									**471 kN**	**8005 kNm**	**17. m**	**1035 kNm**	**2.2 m**
Wear layer 22,5 kN/m³	20940mm	20940mm	8mm	26500mm	17000mm	2249mm	1	4.44 m3	100kN	1698 kNm		225 kNm	
Edge elements 4,0 kN/m				26500mm	17000mm	1949mm	2		212kN	3604 kNm		413 kNm	
Mid-section 3,0 kN/m				26500mm	17000mm	2249mm	1		80kN	1352 kNm		179 kNm	
Road equipment 1,5 kN/m				26500mm	17000mm	2745mm	2		80kN	1352 kNm		218 kNm	
Total									**2369 kN**	**34682 kNm**	**14642 mm**	**3427 kNm**	**1447 mm**

Table G-4 Weight calculation of the right side of the hybrid design

G.2.3. Counterweight Calculation

Below is the table containing the values used for the weight calculation. This is regarding the section on the left side of the rotation centre, as is shown in Table G-5.

Description	b1	b2	t	L	Horizontal centre of gravity X	Vertical centre of gravity Y (down is +)	Amount	Volume	Weight	Moment X	Centre of Gravity X	Moment Y	Centre of Gravity Y
Main girder									**265 kN**	**1244 kNm**	**4.69 m**	**21 kNm**	**.08 m**
Web-1 (t=40mm)	3805mm	3510mm	40mm	1250mm	625mm	-111mm	2	.34 m3	26kN	17 kNm		-3 kNm	
Web-2 (t= 25mm)	2540mm	3510mm	25mm	1802mm	2151mm	-428mm	2	.27 m3	21kN	46 kNm		-9 kNm	
Web-3 (t=25mm)	2540mm	2540mm	25mm	2148mm	4126mm	870mm	2	.27 m3	21kN	88 kNm		19 kNm	
Web-4 (t=25mm)	2640mm	2640mm	25mm	5050mm	7725mm	920mm	2	.67 m3	52kN	404 kNm		48 kNm	
Bottom-flange-1	600mm	600mm	60mm	5050mm	7725mm	1197mm	2	.36 m3	29kN	220 kNm		34 kNm	
Bottom-flange-2	600mm	600mm	100mm	5200mm	2600mm	100mm	2	.62 m3	49kN	127 kNm		5 kNm	
Top-flange-1	600mm	600mm	60mm	5050mm	7725mm	-1448mm	2	.36 m3	29kN	220 kNm		-41 kNm	
Top-flange-2	600mm	600mm	100mm	1802mm	2151mm	-845mm	2	.22 m3	17kN	37 kNm		-14 kNm	
Top-flange-3	600mm	600mm	100mm	2148mm	4126mm	-845mm	2	.26 m3	20kN	83 kNm		-17 kNm	
Counterweight (steel box)									**507 kN**	**4464 kNm**	**8.81 m**	**218 kNm**	**.43 m**
Top cover	11900mm	11900mm	25mm	3000mm	8750mm	-928mm	1	.89 m3	70kN	613 kNm		-65 kNm	
Bottom cover	11900mm	11900mm	25mm	3000mm	8750mm	1760mm	1	.89 m3	70kN	613 kNm		123 kNm	
Front cover	12475mm	12475mm	25mm	2650mm	7263mm	435mm	1	.83 m3	65kN	471 kNm		28 kNm	
Back cover	12475mm	12475mm	25mm	2650mm	10238mm	435mm	1	.83 m3	65kN	664 kNm		28 kNm	
Width separators	12475mm	12475mm	25mm	2650mm	9230mm	435mm	1	.83 m3	65kN	599 kNm		28 kNm	
Length separators	2950mm	2950mm	40mm	2650mm	8750mm	435mm	7	2.19 m3	172kN	1504 kNm		75 kNm	
Axle									**97 kN**	**kNm**	**. m**	**kNm**	**. m**
Axle (R=750)		750mm	40mm	13500mm	mm	mm	1	1.24 m3	97kN	kNm		kNm	
Addition									**17 kN**	**114 kNm**	**6.57 m**	**5 kNm**	**.27 m**
Welding/ conservation				2.00%					17kN	114kN		5kN	
Counterweight (content)									**3176 kN**	**27968 kNm**	**8.81 m**	**2690 kNm**	**.85 m**
Front counterweight	12195mm	12195mm	2000mm	1975mm	8238mm	980mm	1	48.17 m3	1951kN	16070 kNm		1912 kNm	
Rear counterweight	1625mm	1625mm	2600mm	975mm	9738mm	680mm	2	8.24 m3	334kN	3249 kNm		227 kNm	
Rear counterweight	760mm	760mm	2600mm	975mm	9738mm	680mm	2	3.85 m3	156kN	1520 kNm		106 kNm	
Adjustable (50 kN/m3)	1600mm	1600mm	2199mm	900mm	9700mm	606mm	2	6.33 m3	317kN	3072 kNm		192 kNm	
Adjustable (50 kN/m3)	2113mm	2113mm	2199mm	900mm	9700mm	606mm	2	8.36 m3	418kN	4056 kNm		253 kNm	
Total									**4062 kN**	**33789 kNm**	**-8319 mm**	**2934 kNm**	**-722 mm**

Table G-5 Weight calculation of the left side of the hybrid design

G.2.4. Balance Calculation

The counterweight of the bridge has been designed based upon **Moment X** (as is shown in Table G-6). Here Moment X in the closed condition is the closing pressure of 30 kN over the total span of the bridge., whereas Moment X in the opened condition is the overpressure required to keep the bridge opened, which is 1/3 of the closing pressure. From the closing pressure the adjustable counterweights were designed and from the overpressure the placement of these adjustable counterweights were calculated. This however is theoretical. To achieve this is reality, the counterweight will be filled until the aforementioned closing pressure is achieved, thus balancing the bridge manually at site. Which could differ from these calculated values. This is based on the Dutch code :NEN6787 VOBB:2001 article 8.4.2.5.2.

Description	Element angle [°]	Distance between total & elemental Centre of Gravity	Horizontal centre of gravity X	Vertical centre of gravity Y (above is +)			Weight	Moment X	Centre of Gravity X	Moment Y	Centre of Gravity Y
Closed condition							**6430 kN**	**892.5 kNm**	**139 mm**	**494 kNm**	**77 mm**
Leaf section	5.64	14714 mm	14642 mm	1447 mm			2369 kN	34682 kNm		3427 kN	
Counterweight section	4.96	8350 mm	-8319 mm	-722 mm			4062 kN	-33789 kNm		-2934 kN	
Opened condition							**6430 kN**	**-297.5 kNm**	**-46 mm**	**-976 kN**	**-152 mm**
Leaf section	83.64	14714 mm	1629 mm	14623 mm			2369 kN	3858 kNm		-34636 kNm	
Counterweight section	82.96	8350 mm	1023 mm	8288 mm			4062 kN	-4156 kNm		33661 kNm	

Table G-6 Balancing calculation of the hybrid design

NOTE: In the opened condition the rotation angle of the bridge is set at 78 degrees.

G.2.5. Weight division

Below insight is given into the weight division of the non-hybrid bridge and its sections. This is illustrated in three tables; each illustration their respective components with their corresponding contribution to the total weight.

	Whole bridge	
	[kN]	
Deck-system	702	11%
Main girders	859	13%
Cross girders	492	8%
Counterweight	3682	57%
Axle	194	3%
Rest	501	8%
Total bridge	**6430**	**100%**

Table G-8 Weight division of the hyrbid design

	Leaf	
	[kN]	
Deck-system	702	30%
Main girders	594	25%
Cross girders	492	21%
Axle	97	4%
Conservation	13	0.5%
Road equipment	471	20%
Total bridge	**2369**	**100%**

Table G-9 Weight division of the leaf of the hybrid design

	Counterweight	
	[kN]	
Main girders	265	7%
Axle	97	2%
CW-box	507	12%
CW-content	3176	78%
Conservation	17	0.4%
Total bridge	**4062**	**100%**

Table G-7 Weight division of the counterweight of the hybrid design

G.3.   Fatigue verification

G.3.1. Bottom flange – main girder

The same formulas, load factors and calculation assumptions as have been used in the original Amalia bridge fatigue calculations. This can be seen in Appendix E – Fatigue verification (Bottom flange – main girder). The stress values , obtained from Abaqus have been combined to obtain the stress difference, from which the fatigue damage can be calculated. This is illustrated next:
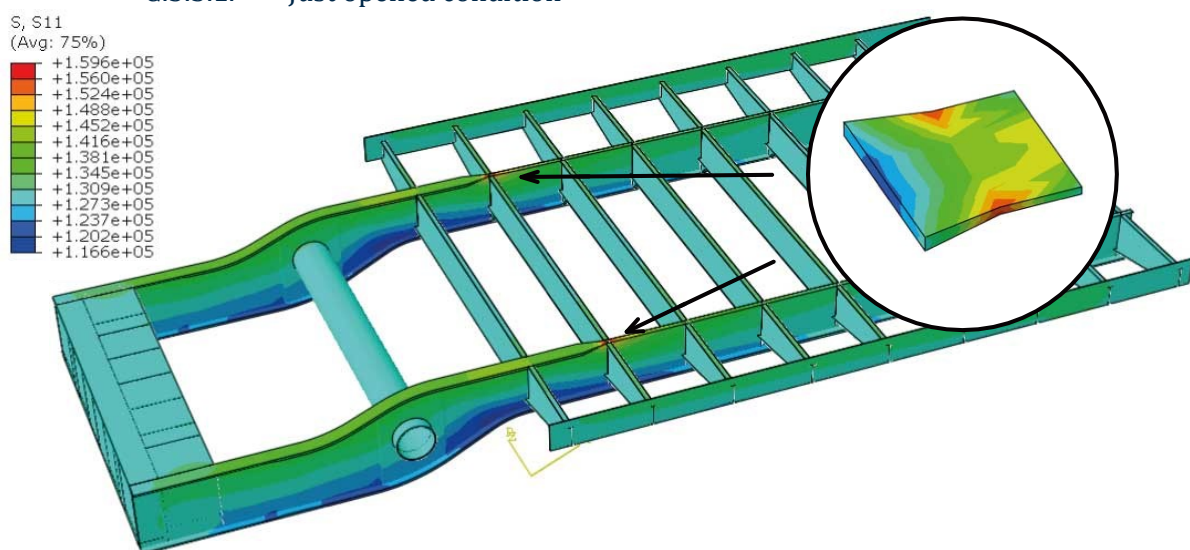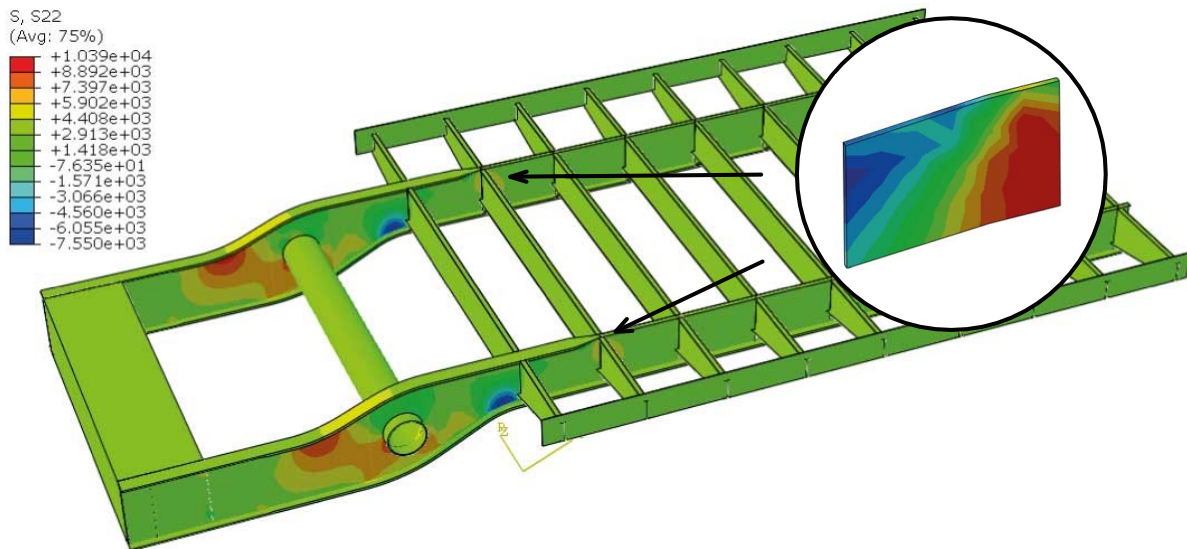
G.3.1.1.   Just opened condition
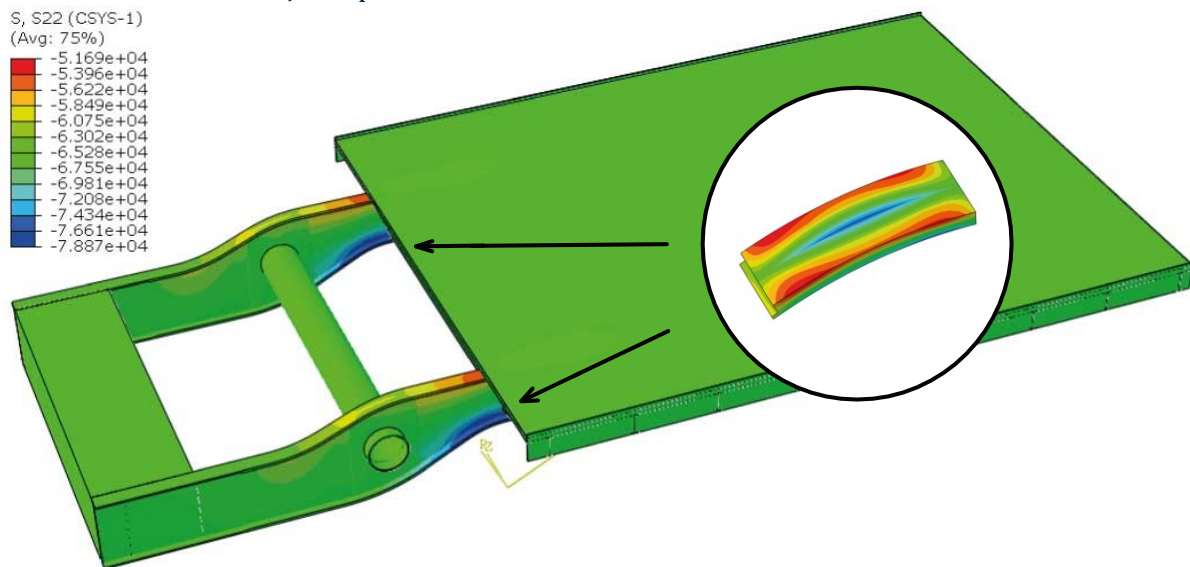
Figure G-5 S11, stress in length direction – just opened condition; design 2 – hybrid

$$\sigma_{11, just\ opened} = -7.887 \times 10^4 kPa \rightarrow -78.87\ MPa$$

NOTE: due to the choice of the coordinate system such that the longitudinal stresses coincides with the curvature of the bottom flange, the stress in the illustration is noted as S22. This is the same as global S11.

NOTE: (regarding the legends in the figures illustrating stresses resulting from Abaqus in this chapter) If a zoomed in section has been used, these legends corresponds with this zoomed section, which is shown in a circle, NOT the whole bridge picture.

G.3.1.2.   Fully opened condition
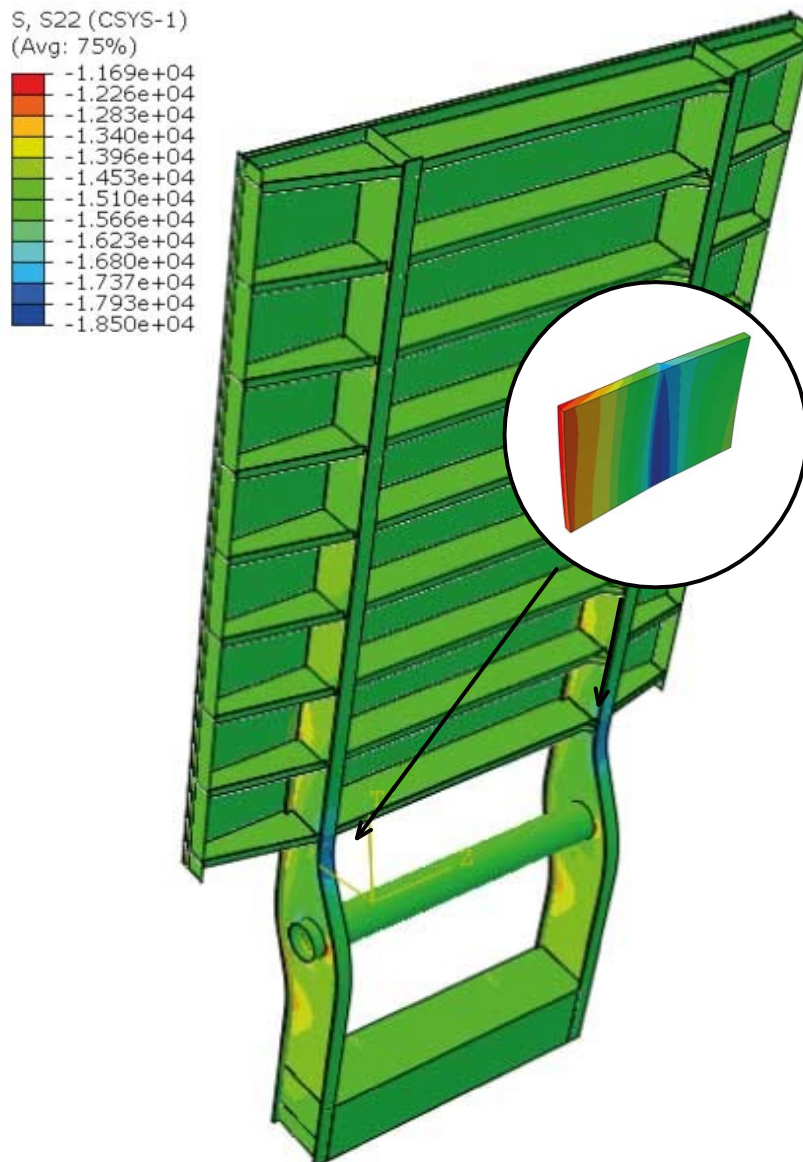
Figure G-6 S11, stress in length direction – fully opened condition; design 2 – hybrid

The stress value located at the same location as has been found for the just opened condition is:

$$\sigma_{11,fully\ opened} = -1.850 \times 10^4 kPa \rightarrow -18.50 MPa$$

Resulting in a stress difference

$$\Delta\sigma_i = \left|\sigma_{22,just\ opened} - \sigma_{22,fully\ opened}\right| = 60.37\ MPa$$

and the fatigue damage (according to Equation E-2 and Table E-14)

$$D_i = 0.271$$

NOTE: due to the choice of the coordinate system such that the longitudinal stresses coincides with the curvature of the bottom flange, the stress in the illustration is noted as S22. This is the same as global S11.

The obtained stress difference with its corresponding damage value are deemed to be comparable with the values found for the Amalia bridge calculated in Abaqus (See section: E.3.2 – Abaqus model).

G.3.2. Web – main girder 1

The same formulas, load factors and calculation assumptions as have been used in the original Amalia bridge fatigue calculations. This can be seen in Appendix E – Fatigue verification (Web – main girder). The stress values , obtained from Abaqus have been combined to obtain the stress difference, from which the fatigue damage can be calculated. This is illustrated below:

G.3.2.1.　　Just opened condition
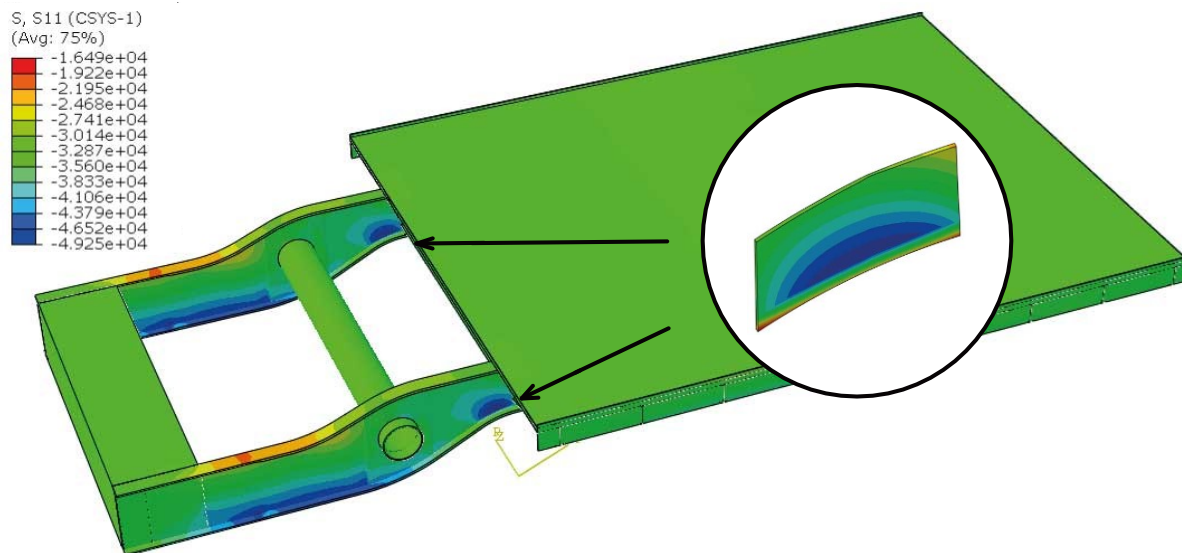
Figure G-7 S22, stress in radial direction – just opened condition; design 2 – hybrid

$$\sigma_{22, just\ opened} = -4.925 \times 10^4 kPa \rightarrow -49.25\ MPa$$

NOTE: due to the choice of the coordinate system such that the longitudinal stresses coincides with the curvature of the bottom flange, the stress in the illustration is noted as S11. This is the same as global S22.

G.3.2.2.   Fully opened condition
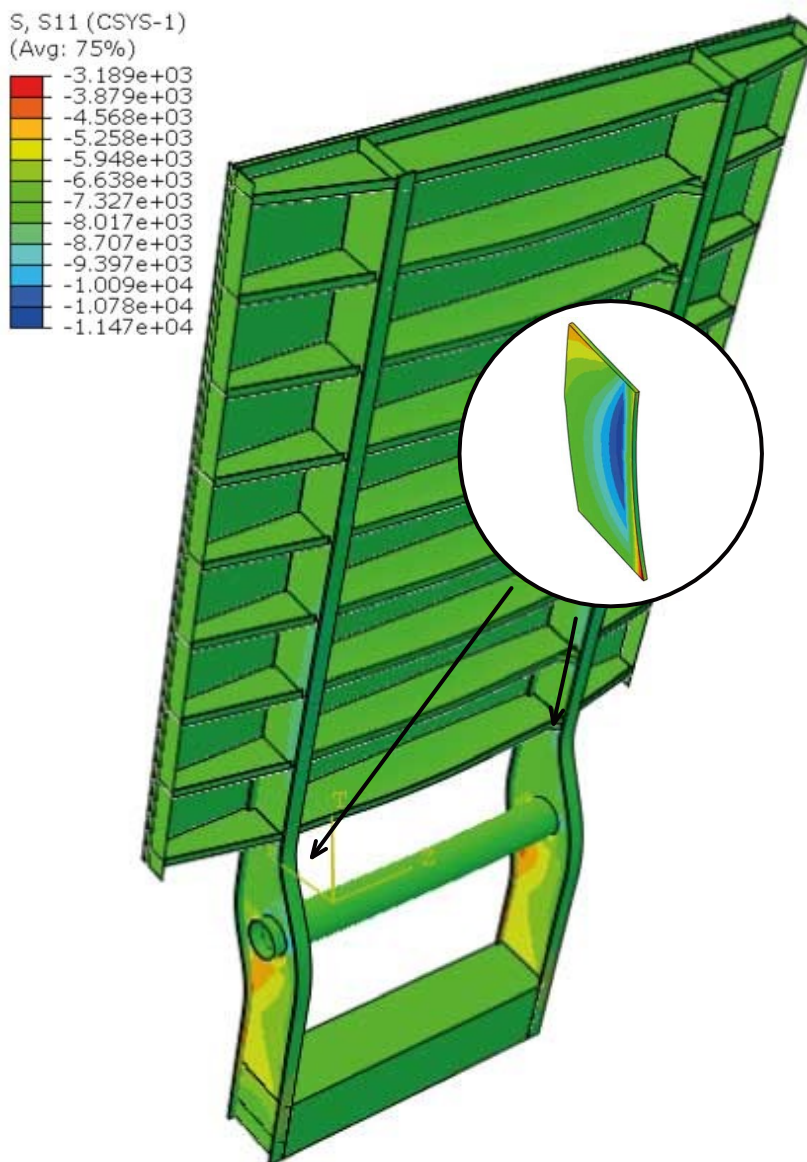
Figure G-8 S22, stress in radial direction – fully opened condition; design 2 – hybrid

The stress value located at the same location as has been found for the just opened condition is:

$$\sigma_{22,fully\ opened} = -1.147 \times 10^4 kPa \rightarrow -11.47\ MPa$$

Resulting in a stress difference

$$\Delta\sigma_i = \left|\sigma_{22,just\ opened} - \sigma_{22,fully\ opened}\right| = 37.78\ MPa$$

and the fatigue damage (according to Equation E-2 and Table E-15)

$$D_i = 0.079$$

NOTE: due to the choice of the coordinate system such that the longitudinal stresses coincides with the curvature of the bottom flange, the stress in the illustration is noted as S11. This is the same as global S22.

The obtained stress difference with its corresponding damage value differ from the values found for the Amalia bridge calculated in Abaqus (See section: E.3.2 – Abaqus model). These lower values are a result of the weight reduction, resulting in lower forces, while the thickness of the web has been maintained, resulting in lower stresses.

G.3.2.3.   Combined – main girder 1

For the total fatigue damage, the damage obtained from the bottom flange, should be combined with the damage obtained from the web. This results in:

$$D_{i,total} = D_{i,bottom,flange} + D_{i,web} = 0.351$$

The resulting combined fatigue damages are lower compared to the value found for the original Amalia bridge and result in a safe structure with regard to fatigue. Thus, since this scenario was governing in the original case and it has been assumed to be governing for this design, this design is deemed to be safe for fatigue damages. Please note, that for a full fatigue check, the fatigue resistance of the traffic loading and the vibration of the counterweight should be taken into account. This has not been covered in this thesis

NOTE: This calculation is very sensitive to slight variations in the stress differences. A slight difference in this stress difference can be the difference between fulfilling/ failing the 1.0 damage condition.

G.3.3. Top flange – main girder

Due to the reduction of the top flanges, an increase in the stresses is found. This section has been checked on the same fatigue criterium as the bottom flange, with the same exception that the traffic induced fatigue loading has NOT been taken into account. For inclusion, this should be done!

The same formulas, load factors and calculation assumptions as have been used in the original Amalia bridge fatigue calculations. This can be seen in Appendix E – Fatigue verification (Bottom flange – main girder). The stress values , obtained from Abaqus have been combined to obtain the stress difference, from which the fatigue damage can be calculated. This is illustrated next:

G.3.3.1.   Just opened condition

Figure G-9 S11, stress in length direction – just opened condition; design 2 – hybrid

$$\sigma_{11,just\ opened} = +1.166 \times 10^5 kPa \rightarrow +116.6\ MPa$$

G.3.3.2.   Fully opened condition
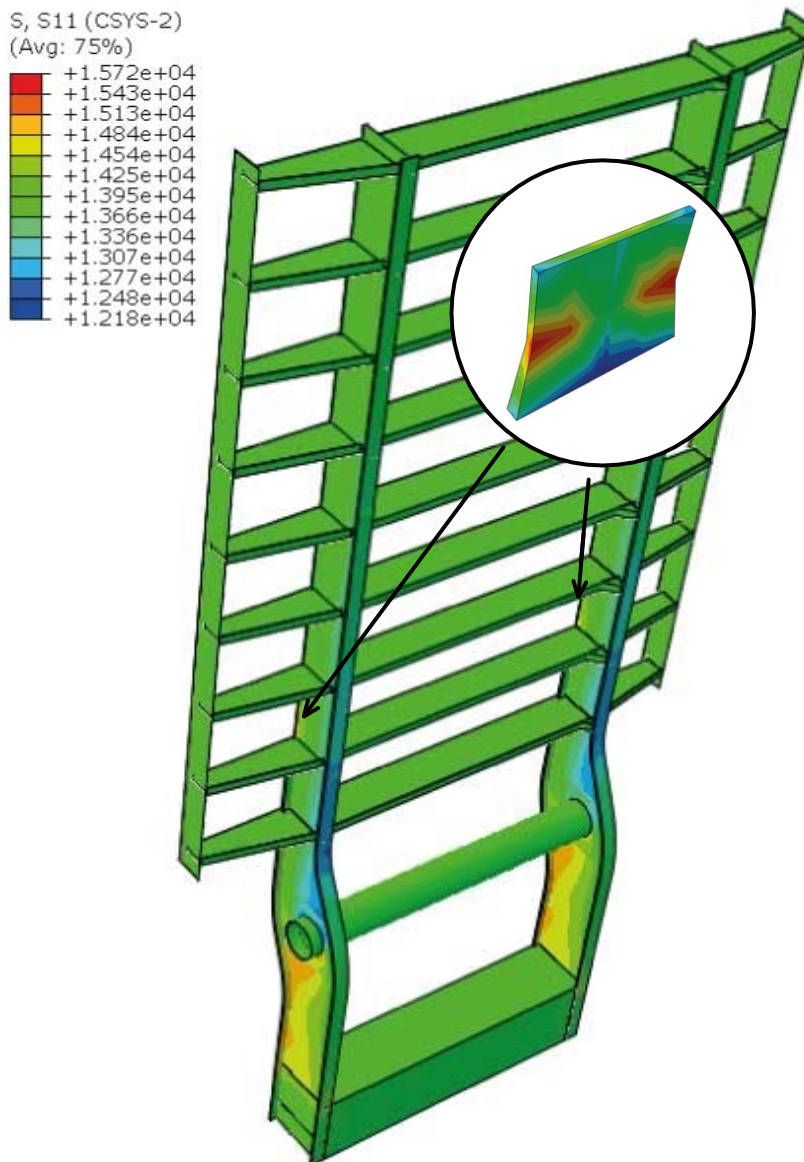
Figure G-10 S11, stress in length direction – fully opened condition; design 2 – hybrid

The stress value located at the same location as has been found for the just opened condition is:

$$\sigma_{11,fully\ opened} = +1.218 \times 10^4 kPa \rightarrow +12.18\ MPa$$

Resulting in a stress difference

$$\Delta\sigma_i = \left|\sigma_{22,just\ opened} - \sigma_{22,fully\ opened}\right| = 104.42\ MPa$$

and the fatigue damage (according to Equation E-2 and Table E-14)

$$D_i = 0.717$$

The obtained stress difference is below 1.0, thus should be safe.

G.3.4. *Web – main girder 2*

The same formulas, load factors and calculation assumptions as have been used in the original Amalia bridge fatigue calculations. This can been seen in Appendix E – Fatigue verification (Web – main girder).The stress values , obtained from Abaqus have been combined to obtain the stress difference, from which the fatigue damage can be calculated. This is illustrated below:

G.3.4.1.   Just opened condition

Figure G-11 S22, stress in radial direction – just opened condition; design 2 – hybrid

$$\sigma_{22,just\ opened} = -7.550 \times 10^3 kPa \rightarrow -7.55\ MPa$$

G.3.4.2.   Fully opened condition
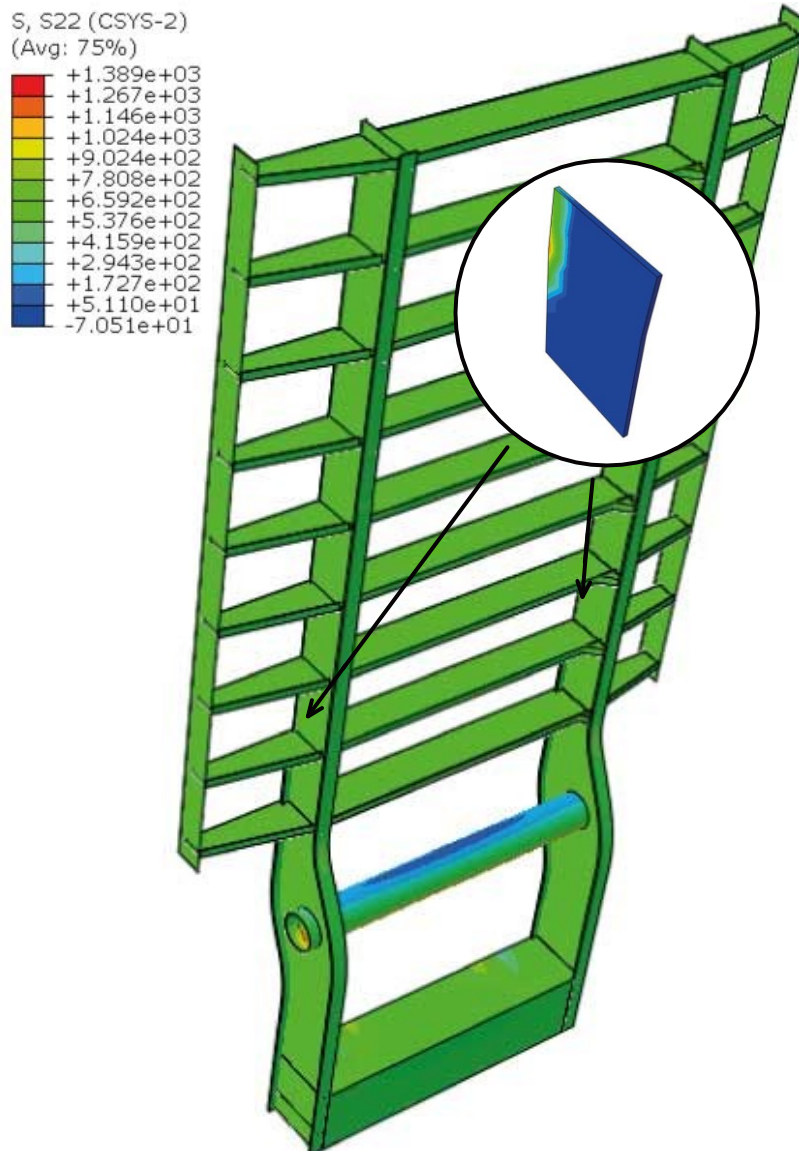
Figure G-12 S22, stress in radial direction – fully opened condition; design 2 – hybrid

$$\sigma_{22,fully\ opened} = 1.389 \times 10^3 kPa \rightarrow +1.389\ MPa$$

Resulting in a stress difference

$$\Delta\sigma_i = \left|\sigma_{22,just\ opened} - \sigma_{22,fully\ opened}\right| = 8.939\ MPa$$

and the fatigue damage (according to Equation E-2 and Table E-15) is none existent, since the stress difference is below the cut off limit.

$$D_i = 0.0$$

NOTE: due to the choice of the coordinate system such that the longitudinal stresses coincides with the curvature of the bottom flange, the stress in the illustration is noted as S11. This is the same as global S22.

G.3.4.3.   Combined – main girder 2

For the total fatigue damage, the damage obtained from the bottom flange, needs to be combined with the damage obtained from the web. This results in:

$$D_{i,total} = D_{i,top,flange} + D_{i,web} = 0.697$$

This combined value is lower than 1.0. Thus, it is assumed to be safe for fatigue damages. However, it must be noted that fatigue damages due to traffic is not included in this thesis. For a full inclusion this should be checked. Thus, additional calculations are required.

NOTE: This calculation is very sensitive to slight variations in the stress differences. A slight difference in this stress difference can be the difference between fulfilling/ failing the 1.0 damage condition.

G.4.   Design verifications

The loading has been applied according to the approach, as has been explained in chapter 8.4 – Design verification. For a more detailed explanation on the approach, please refer to Appendix D.

G.4.1. LM1

G.4.1.1.   Deck

Even though strength is not the governing criterium for FRP, this still has been verified; along with deformation (deflection and buckling). Table F-10 illustrates the strength values of the FRP used.

G.4.1.1.1.   Top Facing

The top facing has been checked on strength using LM1 for the primary as well as their shear stresses. The applied load placement is illustrated in Appendix D – Figure D-2.

G.4.1.1.1.1. Longitudinal stress – S11
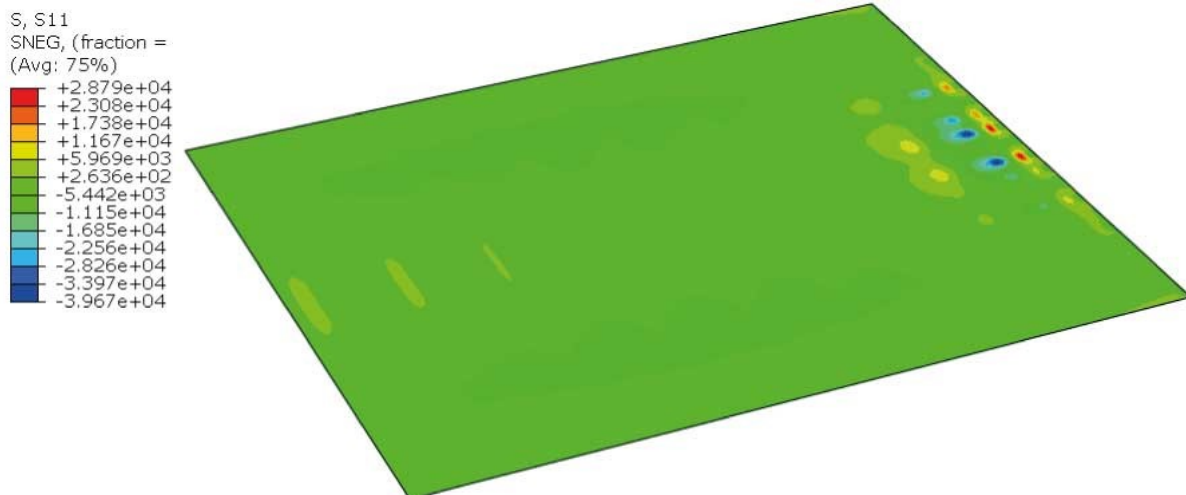
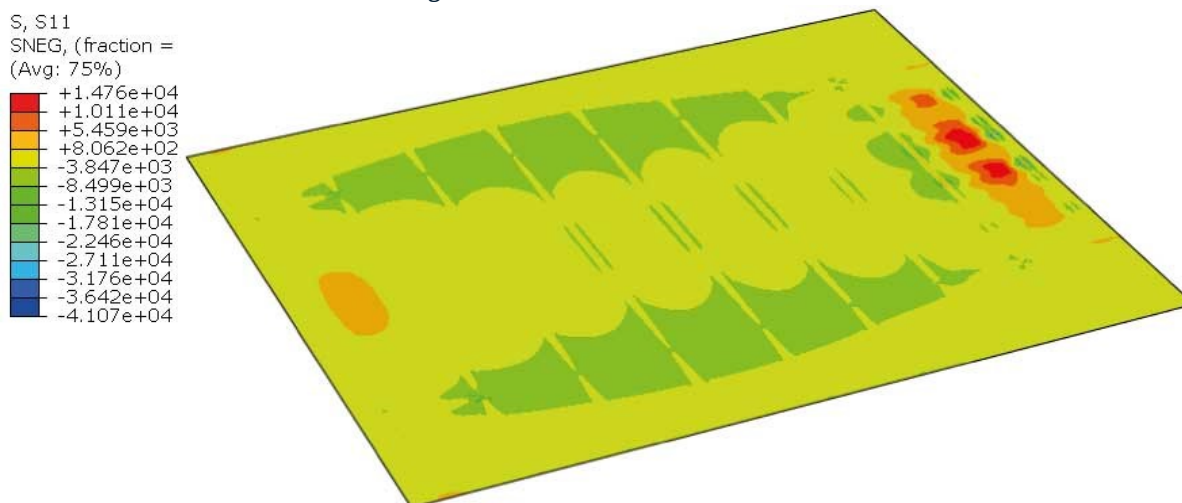**Figure G-13 Hybrid; LM1; ULS; deck, facing – S11**

This loading resulted in the following UC's at the location, as illustrated in Figure G-13:

$$UC_{tension} = 0.115 \qquad UC_{compression} = 0.172$$

G.4.1.1.1.2. Transverse stress – S22
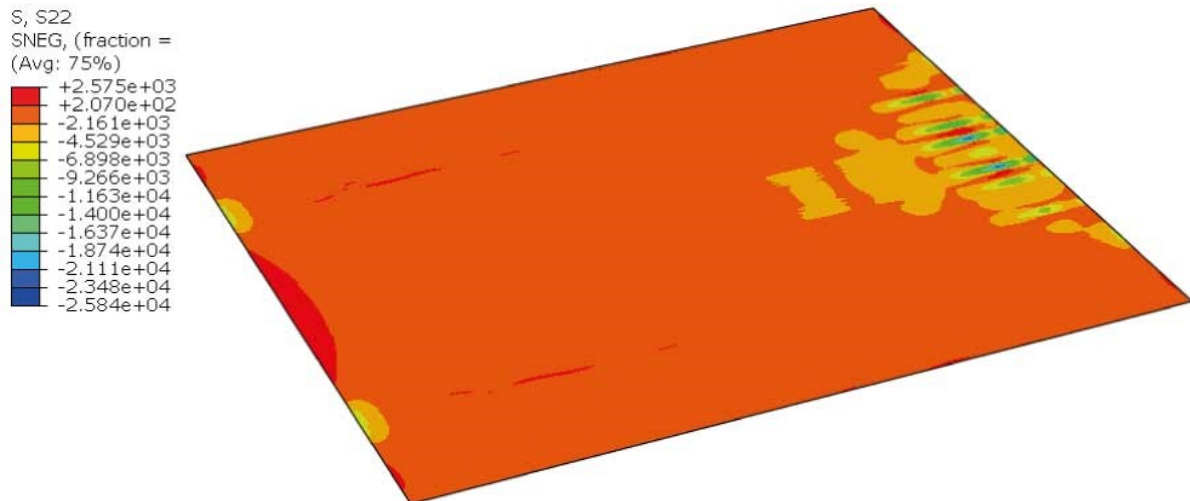
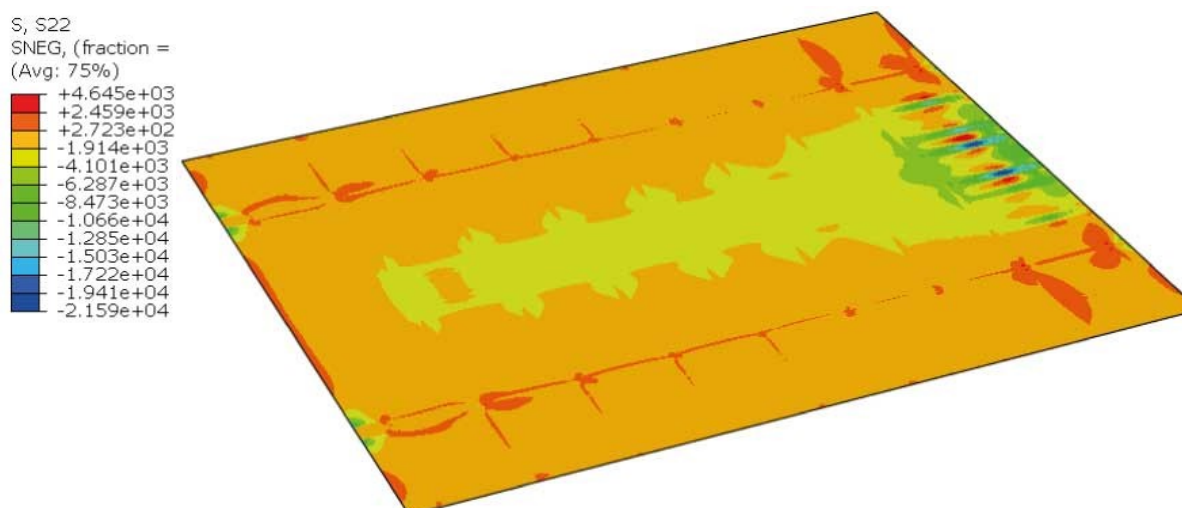**Figure G-14 Hybrid; LM1; ULS; deck, facing – S22**

This loading resulted in the following UC at the location, as illustrated in Figure G-14:

$$UC_{tension} = 0.033 \qquad UC_{compression} = 0.265$$

G.4.1.1.1.3. Shear stress – S12
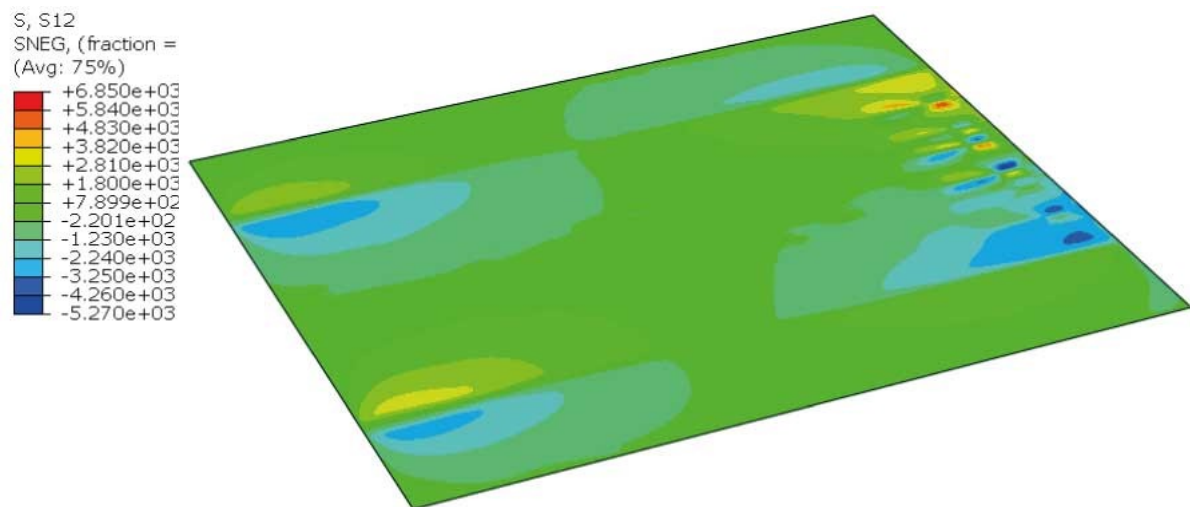
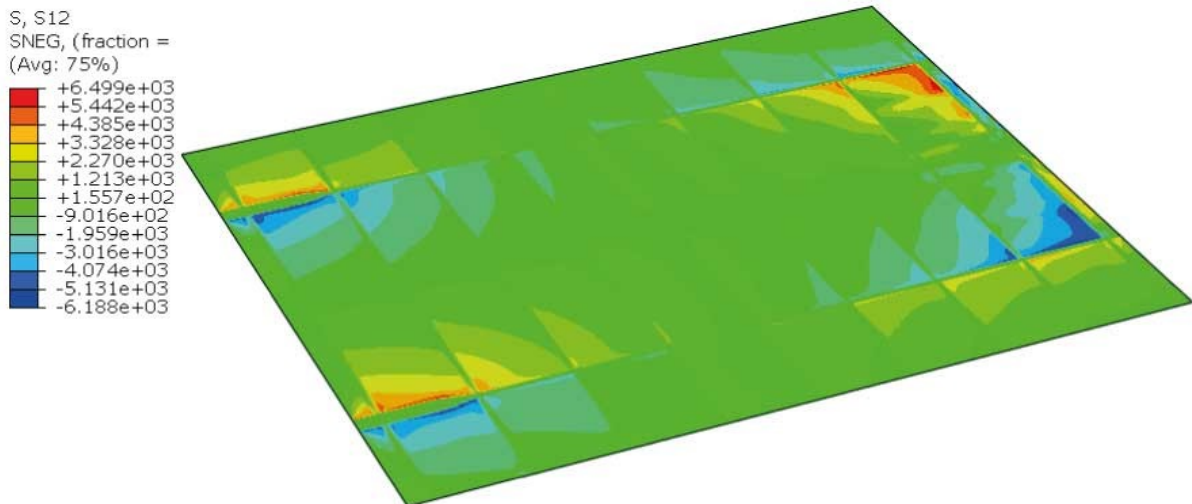**Figure G-15 Hybrid; LM1; ULS; deck, facing – S12**

This loading resulted in the following UC at the location, as illustrated in Figure G-15:

$$UC = 0.300$$

G.4.1.1.1.4. Combination

According to the CUR 96+ section 6.3.1 a combined stress criterium must suffice the following equation, where aforementioned stresses have been applied, resulting in a unity check:

$$\left(\frac{\sigma_{1,Ed}}{\sigma_{1,Rd}}\right)^2 + \left(\frac{\sigma_{2,Ed}}{\sigma_{2,Rd}}\right)^2 + \left(\frac{\tau_{12,Ed}}{\tau_{12,Rd}}\right)^2 - \frac{\sigma_{1,Ed} \cdot \sigma_{2,Ed}}{\sigma_{1,Rd}^2} = 0.202 \leq 1.0$$

G.4.1.1.1.5. Vertical deflection
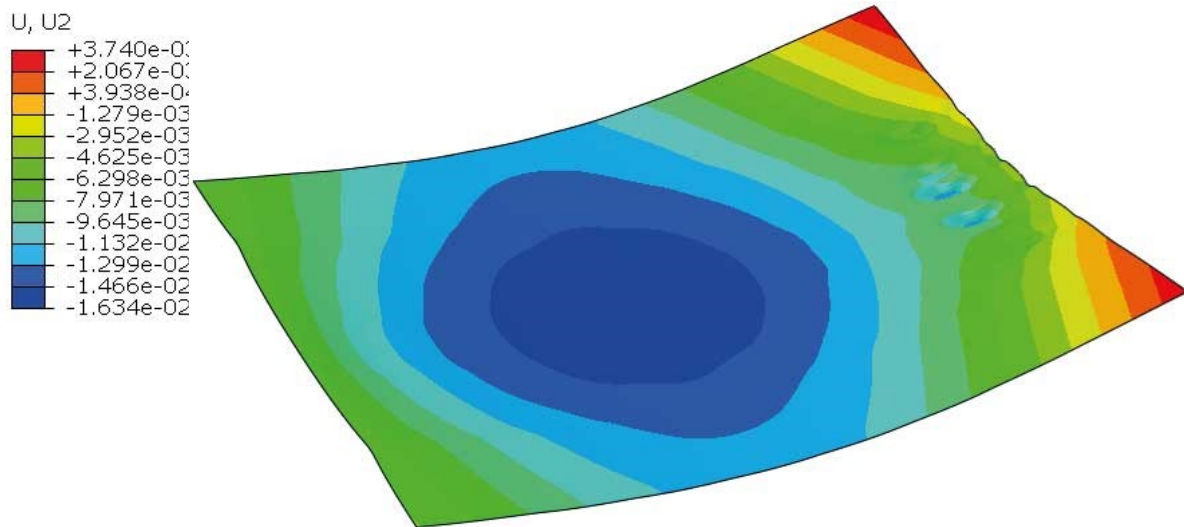
Figure G-16 Hybrid; LM1; SLS; deck, facing – U2 (vertical displacement)

The governing location with regard to. the vertical 5 mm limit, is located on the far left and right of the deck, as illustrated in Figure G-16. The upward deflection on the right falls inside the limit (**3.7 mm**), whereas the downward deflection falls just outside the limit (**5.3 mm**) The deflection on the left has a maximum downward value of **5.9 mm**. This exceeds the limit, however both exceeding values are still considered to be tolerable, since they are smaller compared to the values found by Movares, as stated in section D.1.1.1. The location of the value exceeding the aforementioned comparison is such that it is very unlikely that a vehicle would ever be present at. Thus, this also is deemed tolerable.

G.4.1.1.2.   Webs
The webs have been checked both on strength, as well as buckling.

G.4.1.1.2.1. Longitudinal stress – S11
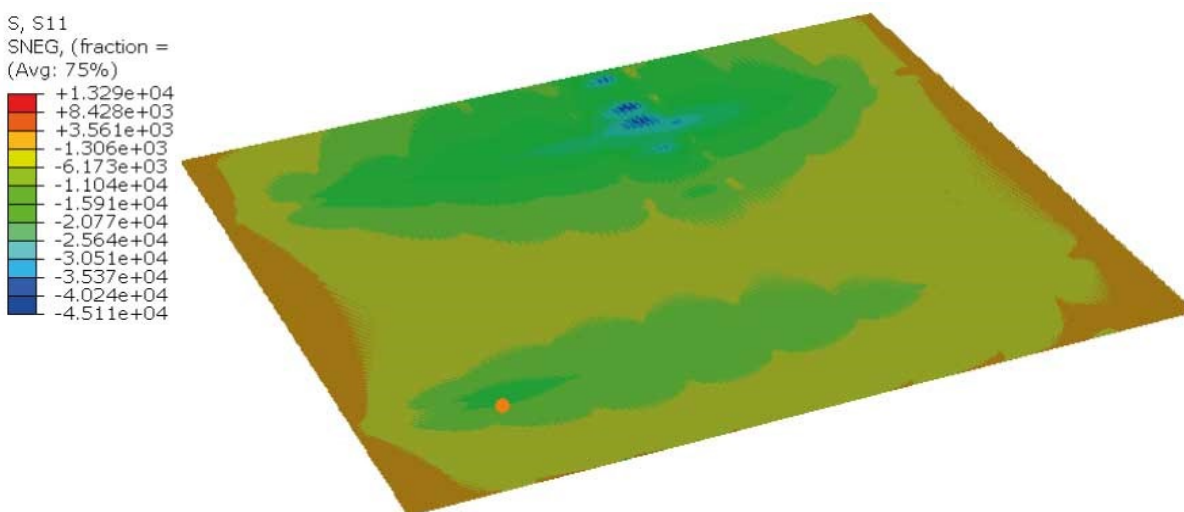
Figure G-17 Hybrid; LM1; ULS; deck, webs – S11

This loading resulted in the following UC at the location, as illustrated in Figure G-17:

$$UC_{tension} = 0.114 \qquad UC_{compression} = 0.451$$

G.4.1.1.2.2. Transverse stress – S22
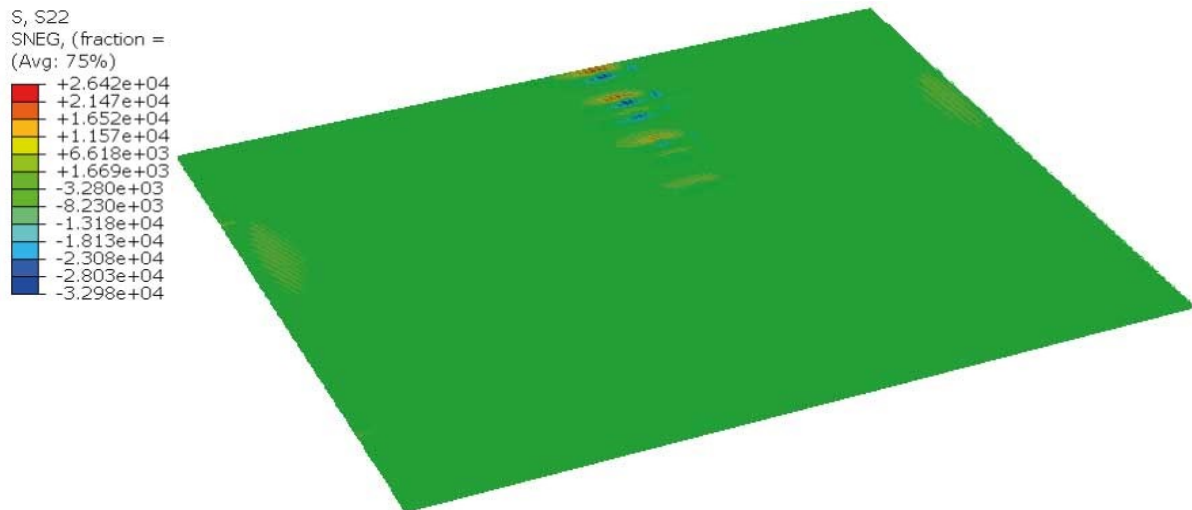
Figure G-18 Hybrid; LM1; ULS; deck, webs – S22

This loading resulted in the following UC at the location, as illustrated in Figure G-18:

$$UC_{tension} = 0.312 \qquad UC_{compression} = 0.352$$

G.4.1.1.2.3. Shear stress – S12
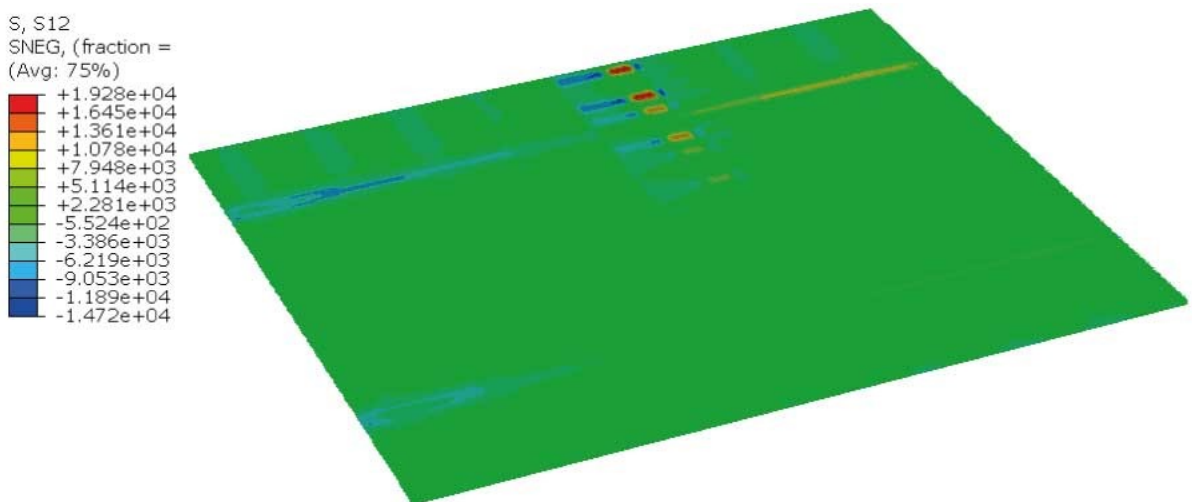
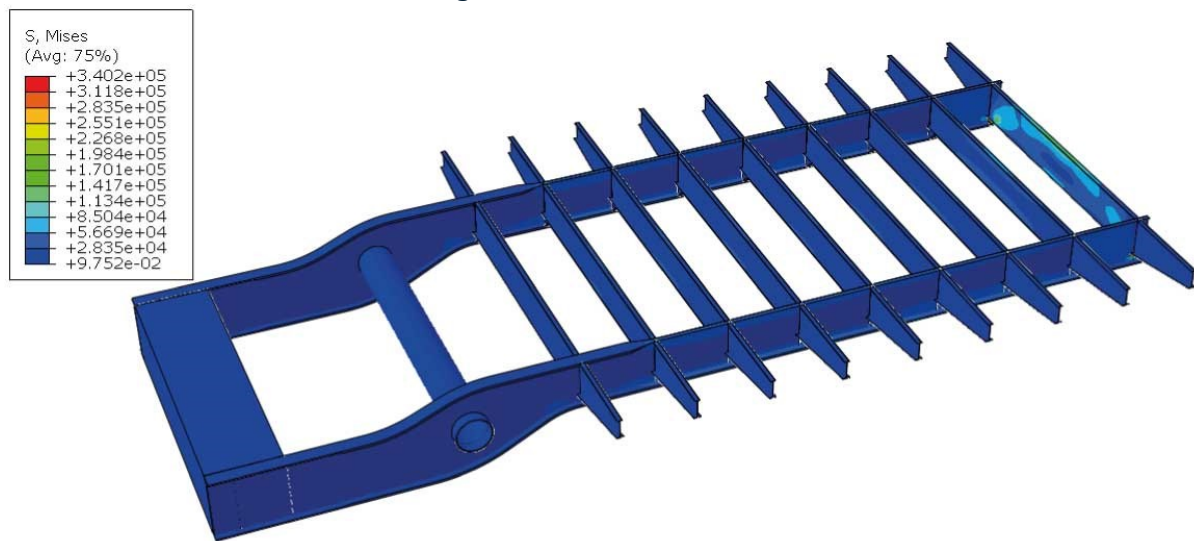**Figure G-19 Hybrid; LM1; ULS; deck, webs – S12**

This loading resulted in the following UC at the location, as illustrated in Figure G-19:

$$UC = 0.664$$

G.4.1.1.2.4. Combination

According to the CUR 96+ section 6.3.1 a combined stress criterium must suffice the following equation, where aforementioned stresses have been applied, resulting in a unity check:

$$\left(\frac{\sigma_{1,Ed}}{\sigma_{1,Rd}}\right)^2 + \left(\frac{\sigma_{2,Ed}}{\sigma_{2,Rd}}\right)^2 + \left(\frac{\tau_{12,Ed}}{\tau_{12,Rd}}\right)^2 - \frac{\sigma_{1,Ed} \cdot \sigma_{2,Ed}}{\sigma_{1,Rd}^2} = 0.620 \leq 1.0$$

G.4.1.1.2.5. Buckling

A critical buckling stress has been obtained from Abaqus. This is compared with the transverse stress in the web. This stress distribution can be found in Figure G-18 Where the max compression stress is:

$$\sigma_{22,max,top} = -32.98 \, MPa$$

When viewing the web with this max compressive stress, the stress along the length of this web, is as follows, with the stresses displayed in **MPa** and the **distance** in **m**:
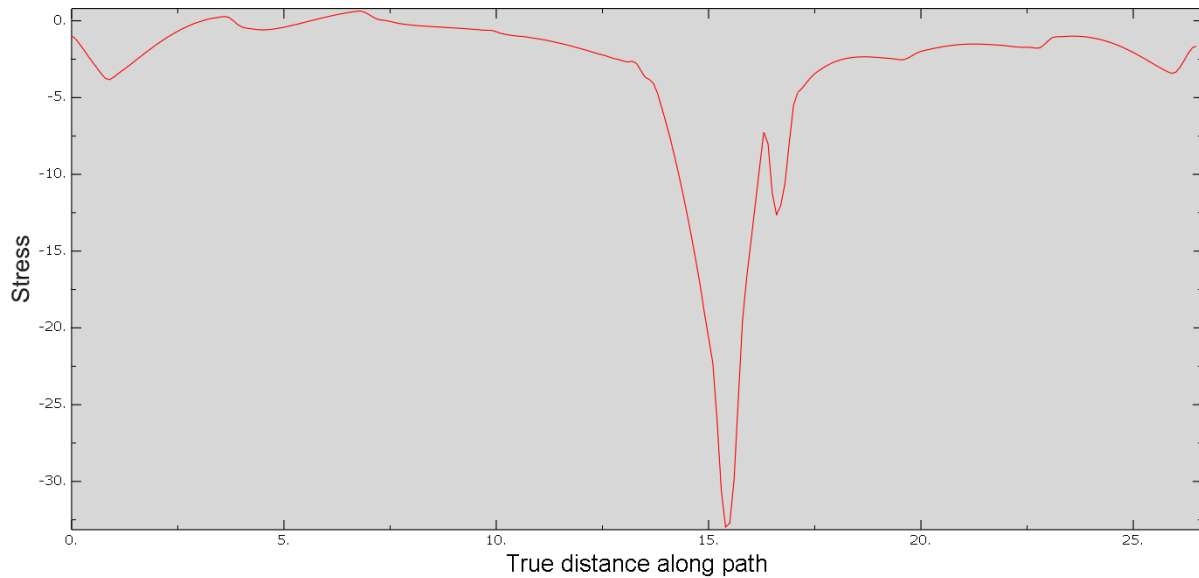
Figure G-20 Development of S22 over the length of the web

Comparing this stress diagram to the values found for the non-hybrid design, one can see tensile stresses. This is the result of the interaction properties between the deck and the girders. In the hybrid case, the TIE connection resulting in moment carrying connections, since the TIE-constraint is applied over an area. Thus, resulting in tensile stresses in the top of the webs.

Next the integral of the vertical stress of the entire web is used to obtain the total capacity of the web. Resulting in:
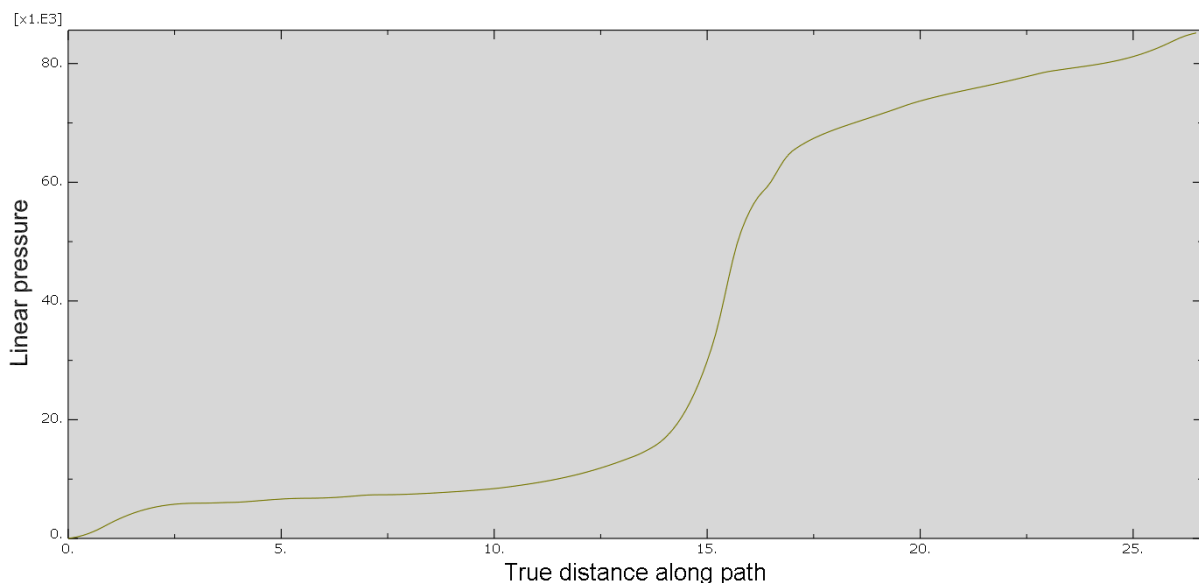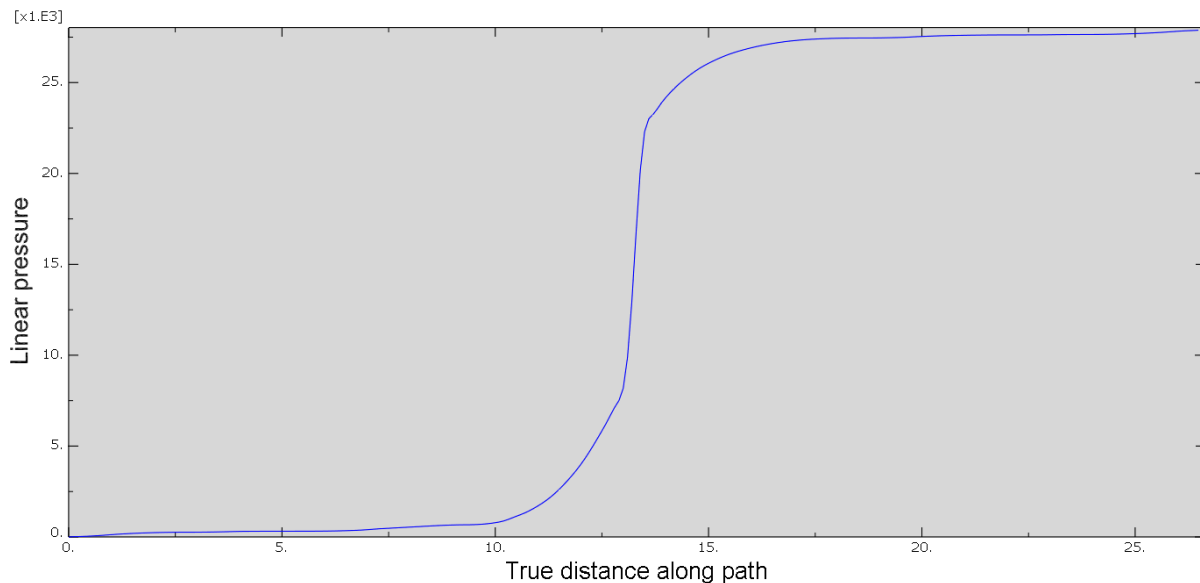

Figure G-21 Integral of S22 over the length of the web

$$\sigma_{22,int} = 85200 \; MPa \cdot mm$$

Dividing this integral, by the max found stress an effective width is found. This is used in the buckling check as the width of the web:

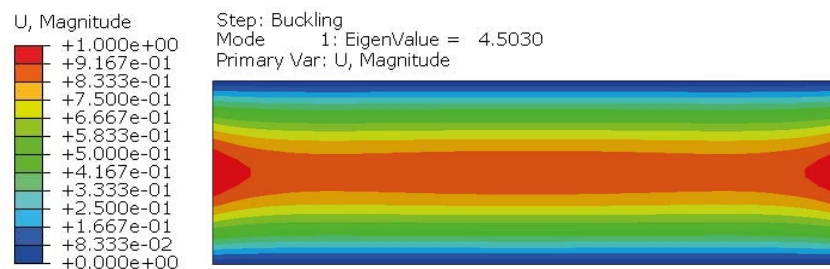$$b_{eff,FEM} = \frac{\sigma_{22,int}}{\sigma_{22,max}} \rightarrow 2583 \; mm$$
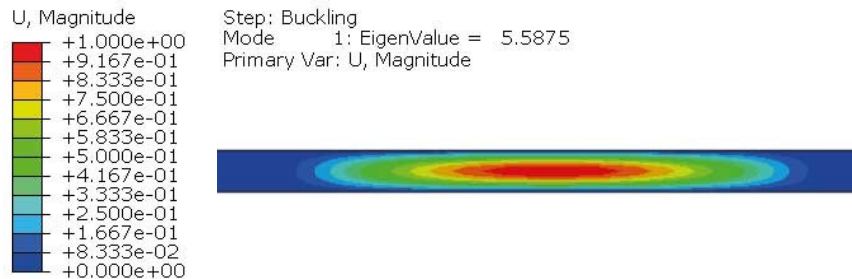
Figure G-22 Hybrid; LM1; ULS; deck, webs – buckling

Applying maximum stress value ($\sigma_{22,max}$) to the effective width (b_{eff}),results in the deformed shape, illustrated in Figure G-22. Here due to the deformation shape a clear indication of plate effects is visible. It has led to the following eigenvalue:

$$\alpha_{cr} = 5.5875$$

This results in the same critical stress value, as found for the non-hybrid design:

$$\sigma_{22,cr} = \alpha_{cr} \cdot \sigma_{22,max} \rightarrow -184 MPa$$

Since the critical stress is greater than the acting stress, the webs will not buckle. (This can be also concluded from the eigenvalue being greater than 1.0) Thus no buckling will occur. (see section 6.4.5 of (CUR, 2013)

NOTE: The critical stress value is identical to the value found for the non-hybrid design. Since the decks are identical, the webs of the deck should have the same buckling values. This is confirmed by calculation above, together with the respective calculation from the non-hybrid design.

G.4.1.1.3.   Bottom facing

The bottom facing has been checked on strength using LM1 for the primary as well as their shear stresses.

G.4.1.1.3.1. Longitudinal stress – S11

Figure G-23 Non-hybrid; LM1; ULS; deck, bottom facing – S11

This loading resulted in the following UC's at the location, as illustrated in Figure F-9:

$$UC_{tension} = 0.059 \qquad UC_{compression} = 0.178$$

G.4.1.1.3.2. Transverse stress – S22

Figure G-24 Non-hybrid; LM1; ULS; deck, bottom facing – S22

This loading resulted in the following UC at the location, as illustrated in Figure F-10:

$$UC_{tension} = 0.060 \qquad UC_{compression} = 0.221$$

G.4.1.1.3.3. Shear stress – S12

Figure G-25 Non-hybrid; LM1; ULS; deck, bottom facing – S12

This loading resulted in the following UC at the location, as illustrated in Figure F-11:

$$UC = 0.330$$

G.4.1.1.3.4. Combination

According to the CUR 96+ section 6.3.1 a combined stress criterium must suffice the following equation, where aforementioned stresses have been applied, resulting in a unity check:

$$\left(\frac{\sigma_{1,Ed}}{\sigma_{1,Rd}}\right)^2 + \left(\frac{\sigma_{2,Ed}}{\sigma_{2,Rd}}\right)^2 + \left(\frac{\tau_{12,Ed}}{\tau_{12,Rd}}\right)^2 - \frac{\sigma_{1,Ed} \cdot \sigma_{2,Ed}}{\sigma_{1,Rd}^2} = \mathbf{0.173 \le 1.0}$$

G.4.1.1.3.5. Vertical Deflection

The deflections of the bottom flange of the deck are not governing. It is the top flange, which has a governing criterium. This has been addressed earlier in section F.3.1.1.1.5 – Vertical Deflection.

G.4.1.2.   Main girder

The cross girders have been checked both on strength and deformation:
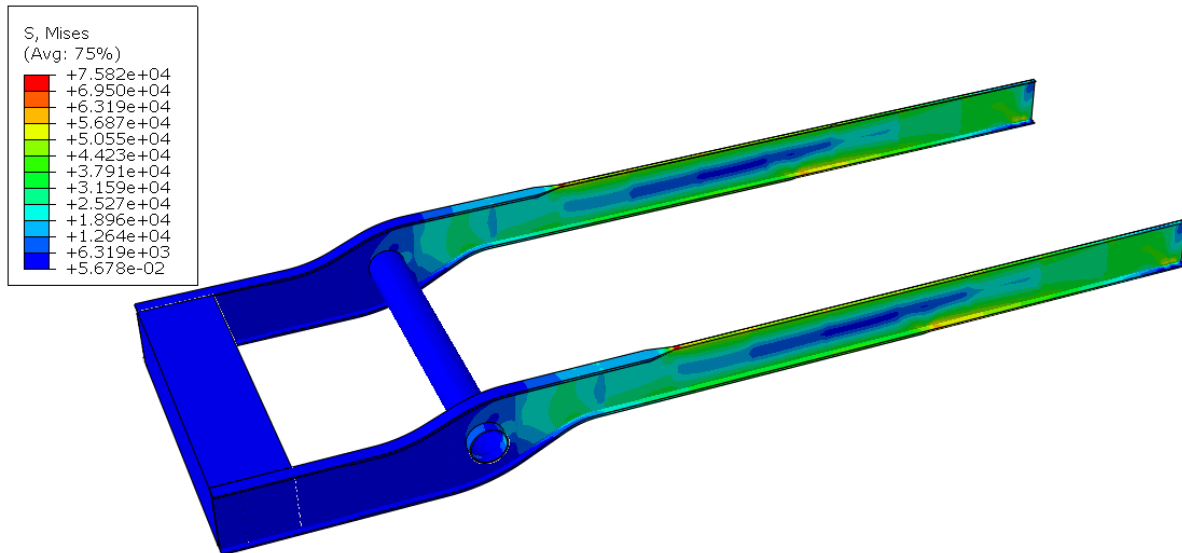
G.4.1.2.1.   Strength
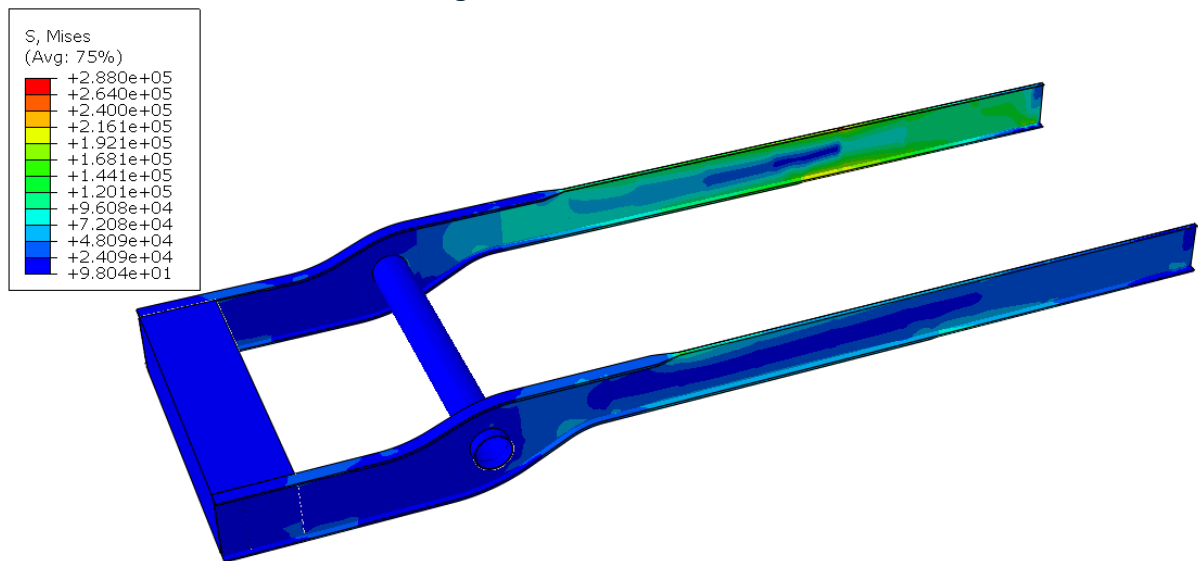
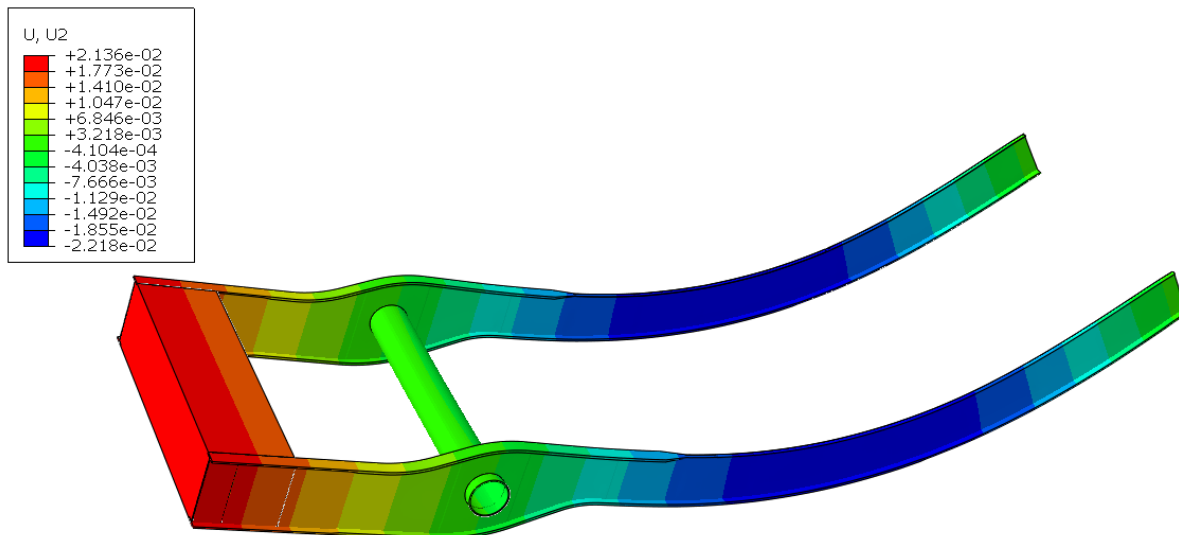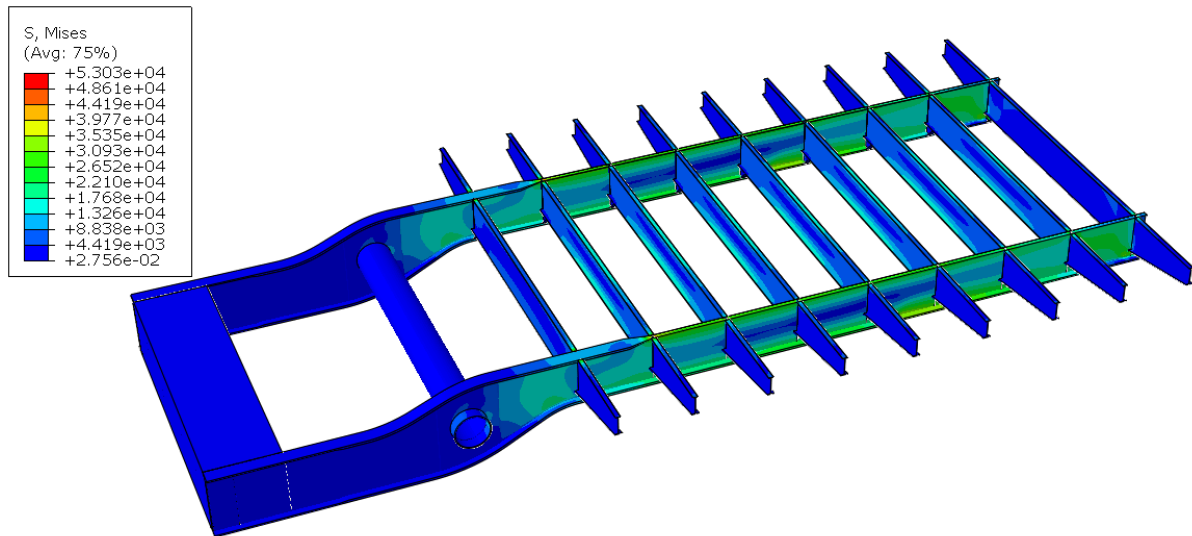**Figure G-26 Hybrid; LM1; ULS; main girder – S, Mises**

This loading resulted in the following UC at the location, as illustrated in Figure G-26. The flange thickness has resulted in a lower yield stress. This has been applied in the UC:

$$UC = 0.976$$

G.4.1.2.2.   Deformation
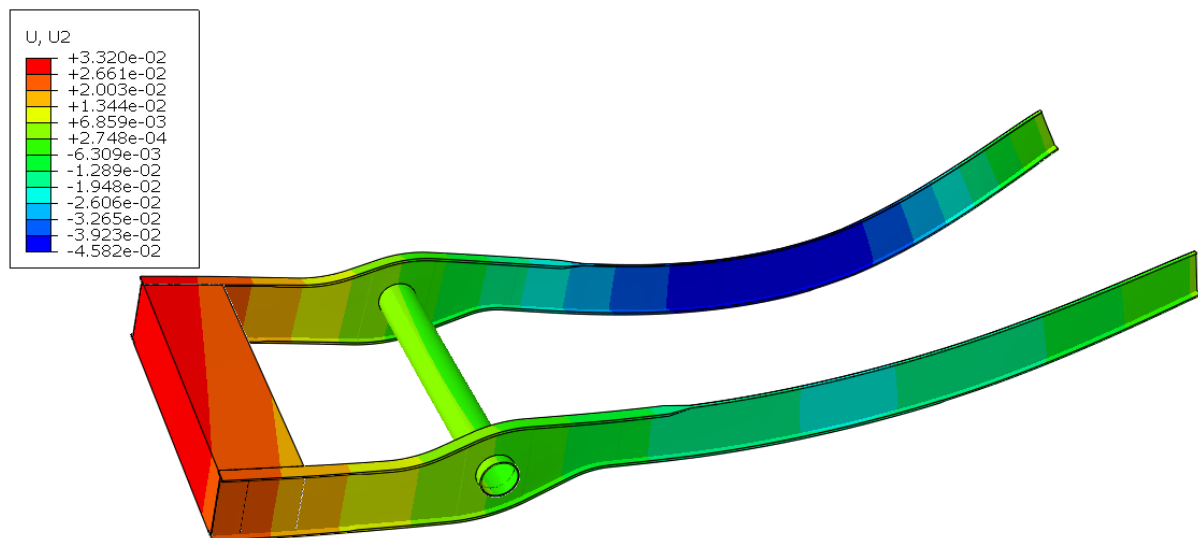
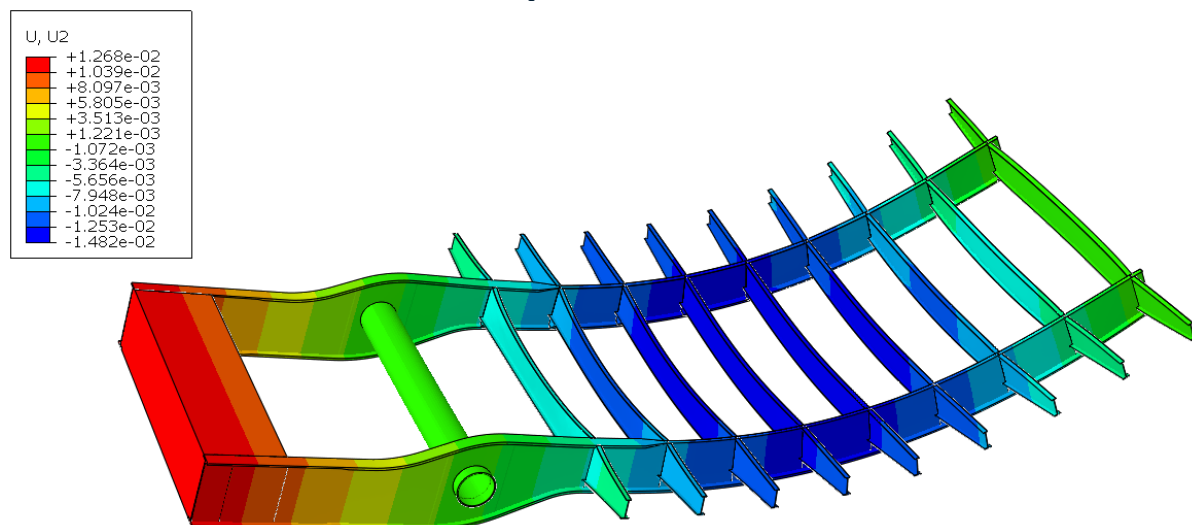**Figure G-27 Hybrid; LM1; SLS; main girder – U2 (vertical displacement**

This loading resulted in the following UC at the location, as illustrated in Figure G-27:

$$U = 45.82\ mm \leq 59.5\ mm$$

G.4.1.3. Cross girder

The cross girders have been checked both on strength and deformation:

G.4.1.3.1. Strength

Figure G-28 Hybrid; LM1; ULS; cross girder – S, Mises

This loading resulted in the following UC at the location, as illustrated in Figure G-28:

$$UC_{CrossGirder} = 0.669 \qquad UC_{support} = 0.958$$

Here a distinction has been made between the supports and the cross girders, due to the additional stress concentration found in the supports.
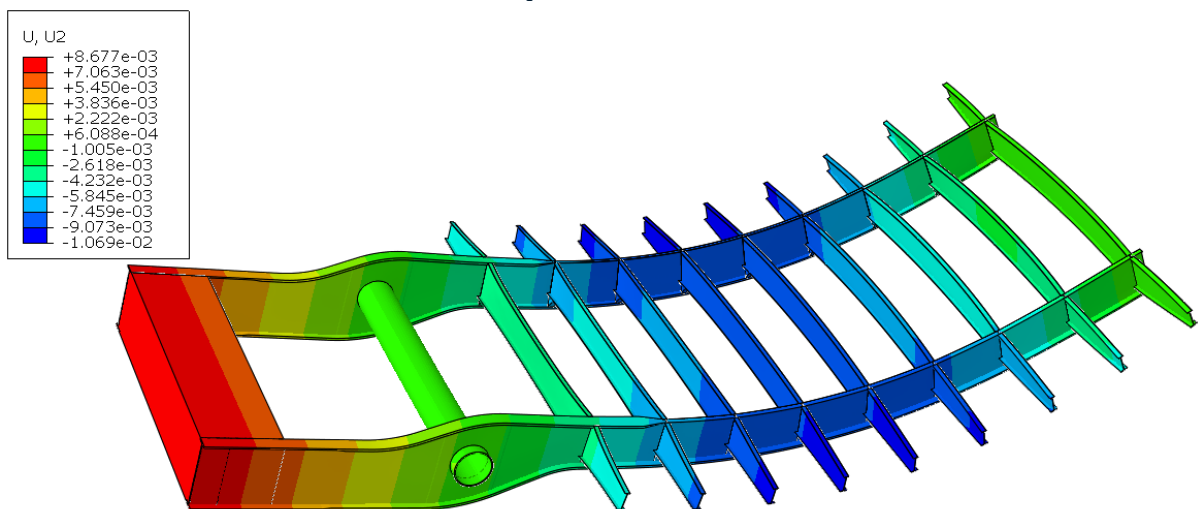
G.4.1.3.2. Deformation
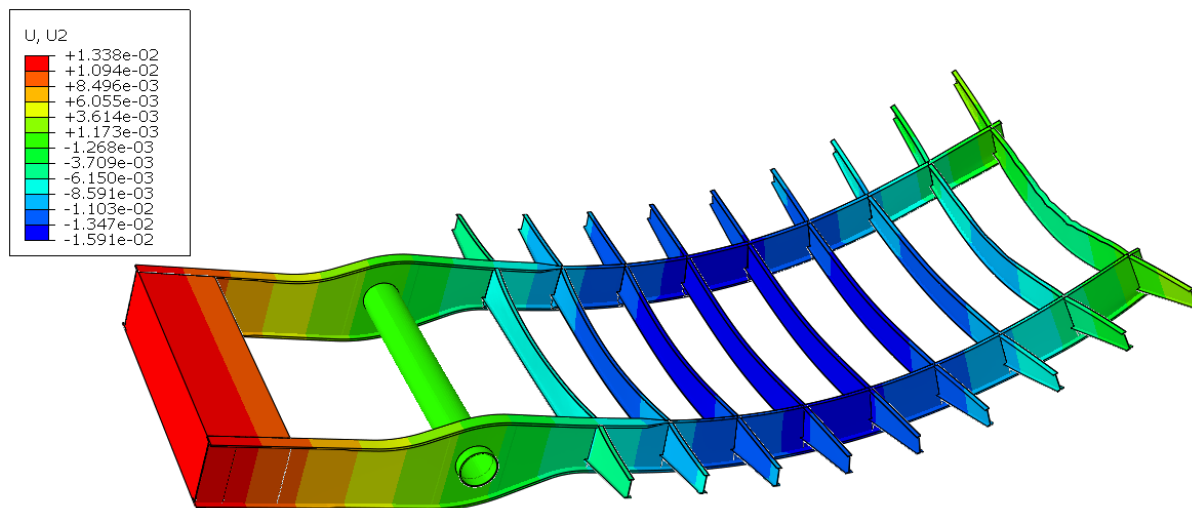
Figure G-29 Hybrid; LM1; SLS; cross girder – U2 (vertical displacement)

This loading resulted in the following UC at the location, as illustrated in Figure G-29:

$$U = 15.91 \; mm \leq 25 \; mm$$

G.4.2. LM2

This load case has only been used to check the webs of the deck for stability. This has resulted in the following stress distribution:
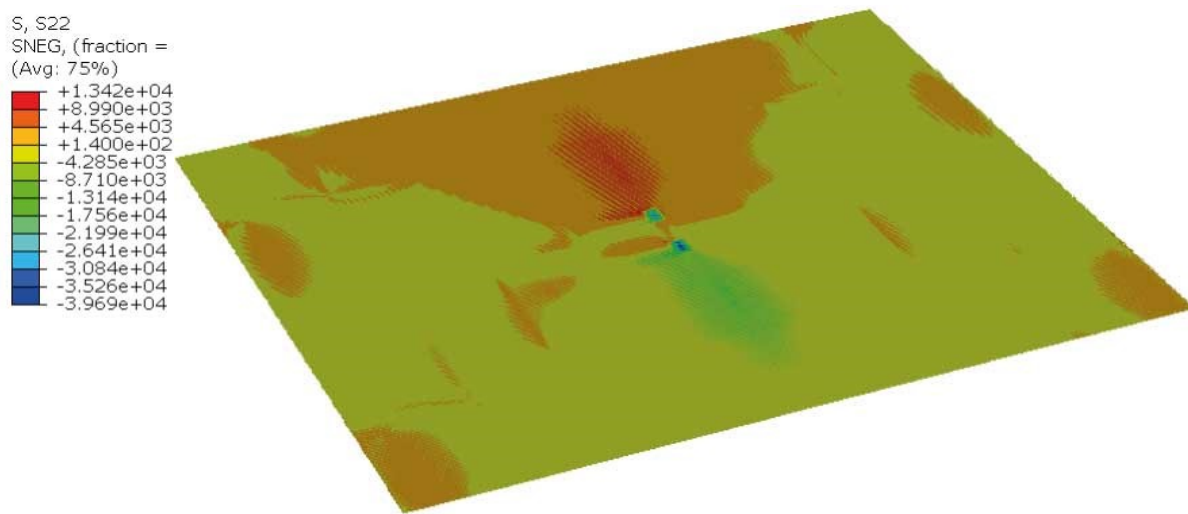
Figure G-30 Non-hybrid; LM2; ULS; deck, webs – S22

This loading resulted in the following UC at the location, as illustrated in Figure G-30:

$$UC_{tension} = 0.087 \qquad UC_{compression} = 0.445$$

G.4.2.1. Buckling

A critical buckling stress has been obtained from Abaqus. This is compared with the transverse stress in the web. This stress distribution can be found in Figure G-30, where the max compression stress is:

$$\sigma_{22,max} = -39.69 \, MPa$$

When viewing the web with this max compressive stress, the stress along the length of this web, is as follows, with the **stresses** displayed in **MPa** and the **distance** in **m**:
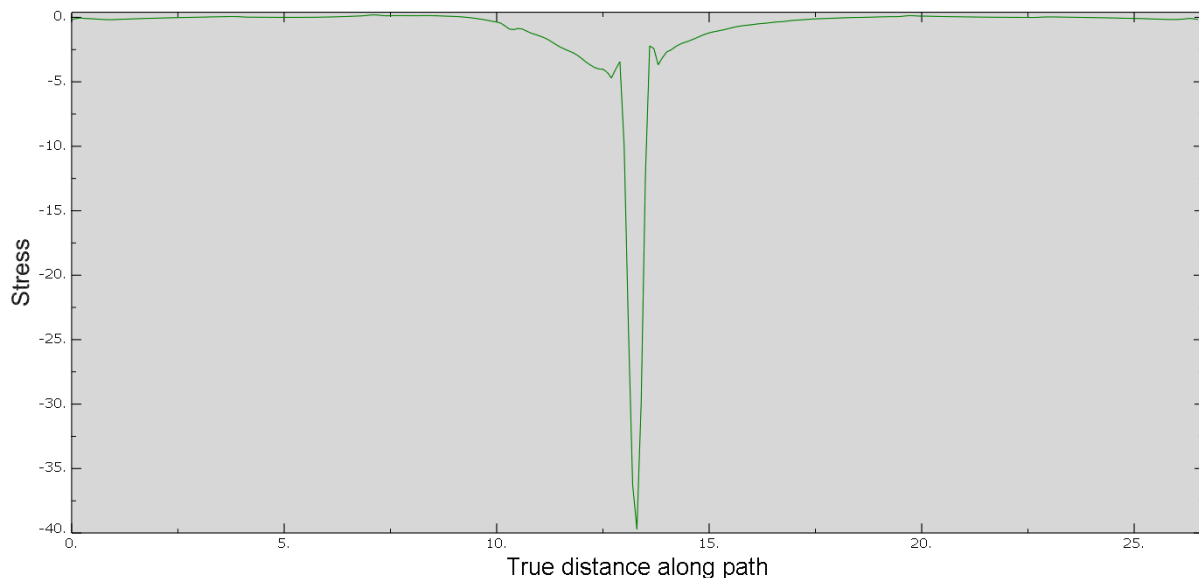
Figure G-31 Development of S22 over the length of the web

Next the integral of the vertical stress of the entire web is used to obtain the total capacity of the web. Resulting in:

Figure G-32 Integral of S22 over the length of the web

$$\sigma_{22,int} = 27900 \ MPa \cdot mm$$

Dividing this integral by the maximum stress, an effective width is found. This effective width is used in the buckling check as the width of the web:

$$b_{eff} = \frac{\sigma_{22,int}}{\sigma_{22,max}} \rightarrow 703 \ mm$$

Figure G-33 Non-hybrid; LM1; ULS; deck, webs – buckling

Applying maximum stress value ($\sigma_{22,max}$) to the effective width (b_{eff}),results in the deformed shape, illustrated in Figure G-33. Here due to the deformation shape a clear indication of plate effects is visible. It has led to the following eigenvalue:

$$\alpha_{cr} = 4.5030$$

This results in the same critical stress value, as found for the non-hybrid design:

$$\sigma_{22,cr} = \alpha_{cr} \cdot \sigma_{22,max} \rightarrow -179 \ MPa$$

Since the critical stress is greater than the acting stress, the webs will not buckle. (This can be also concluded from the eigenvalue being greater than 1.0) Thus no buckling will occur. (see section 6.4.5 of (CUR, 2013)

NOTE: The critical stress value is identical to the value found for the non-hybrid design. Since the decks are identical, the webs of the deck should have the same buckling values. This is confirmed by calculation above, together with the respective calculation from the non-hybrid design.

G.4.3. LM4
G.4.3.1. Main girders
G.4.3.1.1. Strength

Figure G-34 Hybrid; LM4; SLS; main girders – S, Mises

This loading resulted in the following UC at the location, as illustrated in Figure G-34:

$$UC = 0.214$$

G.4.3.1.2. Vertical displacement

Figure G-35 Hybrid; LM4; SLS; main girders – U2 (vertical displacement)

This loading resulted in the following UC at the location, as illustrated in Figure G-35:

$$U = 22.18\ mm \leq 59.5\ mm$$

G.4.3.2. Cross girders (centre span)
G.4.3.2.1. Strength

Figure G-36 Hybrid; LM4; SLS; cross girders (centre span) – S, Mises

This loading resulted in the following UC at the location, as illustrated in Figure G-36:

$$UC = 0.149$$

G.4.3.2.2. Vertical displacement

Figure G-37 Hybrid; LM4; SLS; cross girders (centre span) – U2 (vertical displacement)

This loading resulted in the following UC at the location, as illustrated in Figure G-37:

$$U = 14.82 \ mm \leq 25 \ mm$$

G.4.3.3. Cross girders (side span)

G.4.3.3.1. Strength
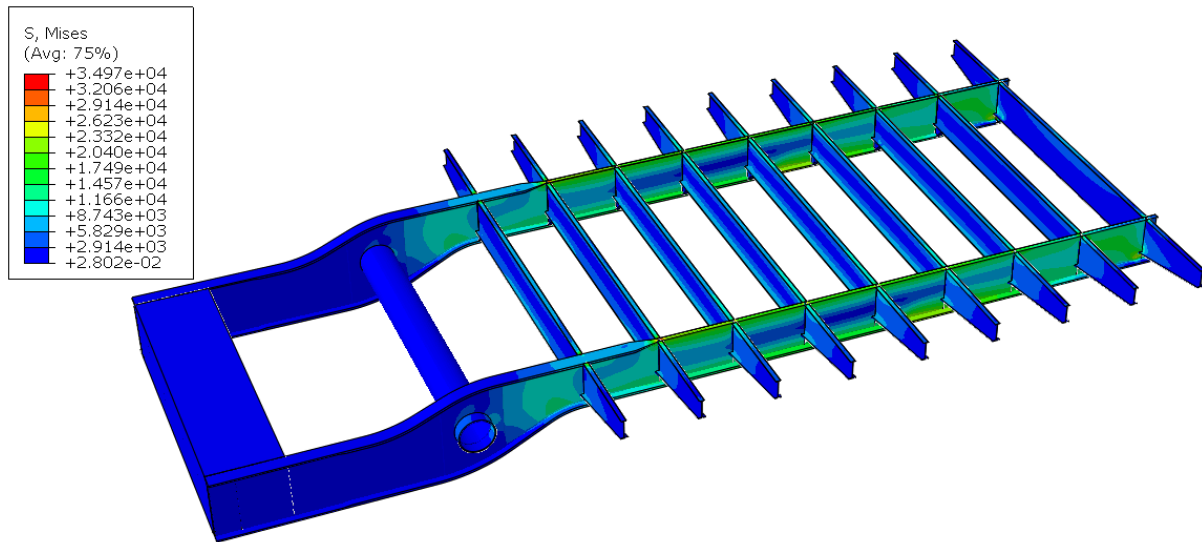
Figure G-38 Hybrid; LM4; SLS; cross girders (side span) – S, Mises

This loading resulted in the following UC at the location, as illustrated in Figure G-38:

$$UC = 0.099$$

G.4.3.3.2. Vertical displacement

Figure G-39 Hybrid; LM4; SLS; cross girders (side span) – U2 (vertical displacement)

This loading resulted in the following UC at the location, as illustrated in Figure G-39:

$$U = 10.69 \; mm \leq 25 \; mm$$

Appendix H. Weight Comparison

This appendix illustrates the weight differences of the different designs. A view into the built-up of each element has been depicted. The bridges can be divided into two section:

- Leaf of the bridge (direct weight saving)
- Counterweight of the bridge (indirect weight saving)

Next a closeup view of the bridge elements has been made to zoom in on the influence each element has on the total. The division is as follows:

- Deck-system
- Main girders
- Cross girders
- Axle
- Counterweight

On the following pages an exposition on the influence of the different elements is shown for each bridge design, related to each section of the bridge as well as to the bridge as a whole.

The weight of each element is related in two different manners: relative and absolute. The relative comparison relates each element to their corresponding counterpart from the original design; and the absolute comparison relates each element to their corresponding portion of their respective designs.

H.1. Full bridge

Original Amalia bridge

The original Amalia bridge is an orthotropic steel deck bridge. This deck functions as the top flange of the main and cross girders.
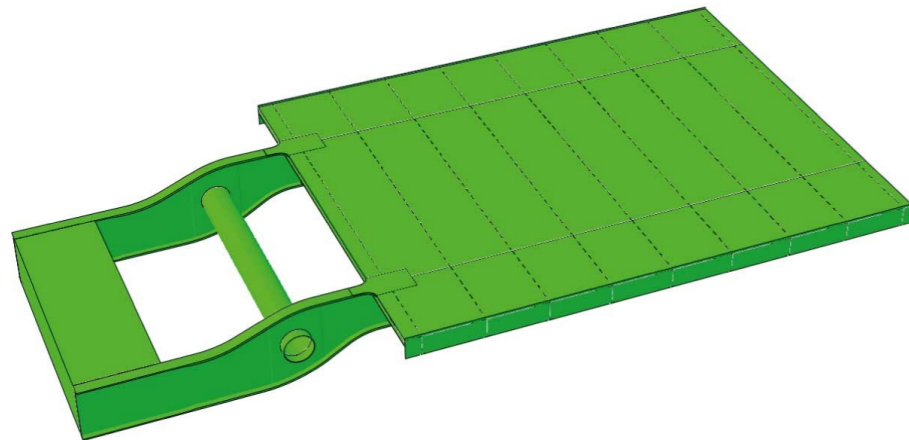
Figure H-1 Amalia bridge

Related to		Amalia bridge	
		[kN]	
Whole bridge	Relative	8472	100%
	Absolute	8472	100%

Table H-1 Weight comparison of the Amalia bridge
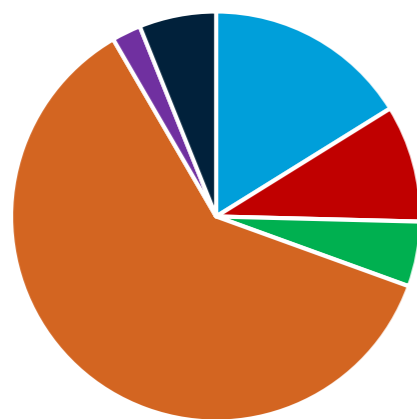
Figure H-4 Pie chart: weight division of the Amalia bridge

Non-hybrid design

The non-hybrid design is an FRP sandwich deck (FiberCore based Z-shells), placed on top of balanced I-profile main and cross girders, without allowing hybrid interaction between the FRP-deck and the girders.
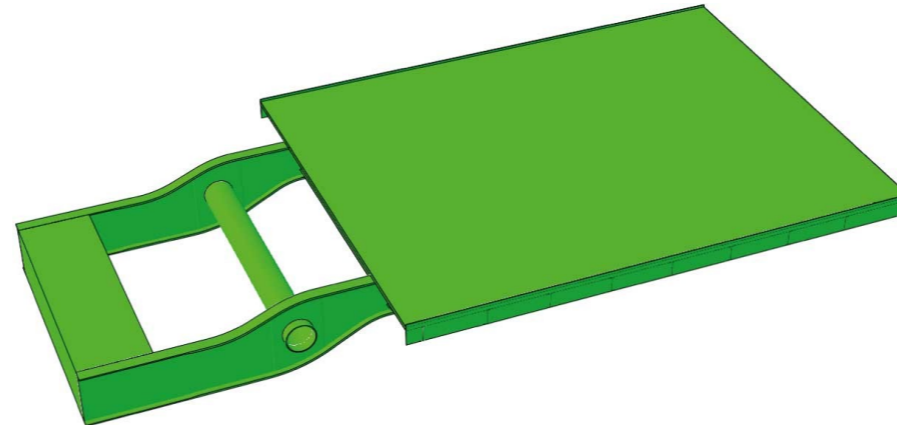
Figure H-2 Non-hybrid design

Related to		Non-hybrid	
		[kN]	
Whole bridge	Relative	7092	84%
	Absolute	7092	100%

Table H-2 Weight comparison of the non-hybrid design

Difference 16%
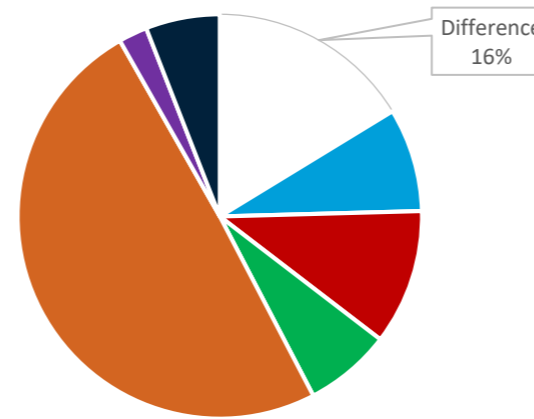
Figure H-5 Pie chart: weight division of the non-hybrid design

Hybrid design

The hybrid design is an FRP sandwich deck (FiberCore based Z-shells) placed on top of non-balanced I-profile main and cross girders, which does allow for hybrid interaction between the deck and the girders, such that the FRP-deck functions as the top flange of the main and cross girders.
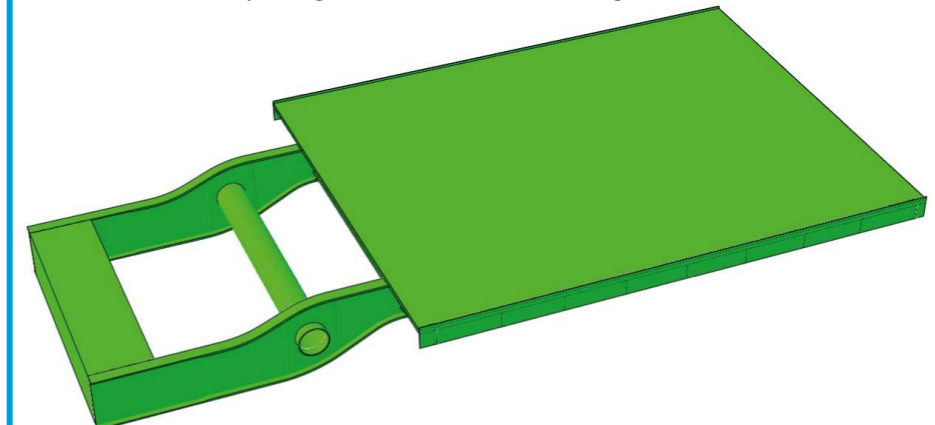
Figure H-3 Hybrid design

Related to		Hybrid	
		[kN]	
Whole bridge	Relative	6430	76%
	Absolute	6430	100%

Table H-3 Weight comparison of the hybrid design

Difference 24%

- ☐ Difference
- ☐ Deck-system
- ☐ Main girders
- ☐ Cross girders
- ☐ Counterweight
- ☐ Axle
- ☐ Rest
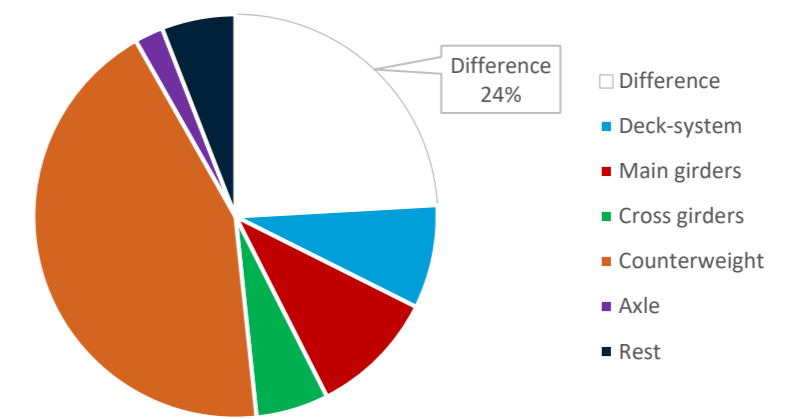
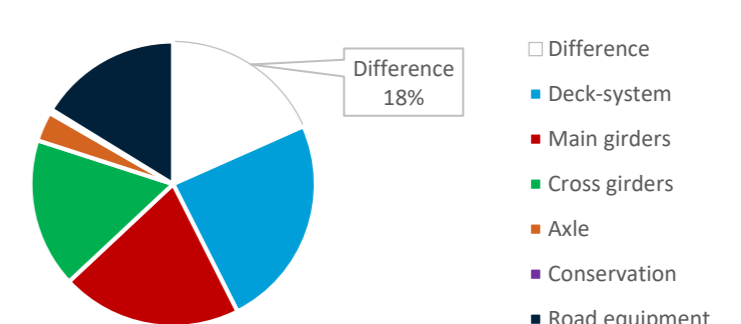**Figure H-6 Pie chart: weight division of the hybrid design**

For an explanation on the percentages found in the tables shown above, please review the bold text found in Appendix H.

A clear weight reduction is achieved, by implementing an FRP-deck instead of an orthotropic steel deck. Even when the FRP-deck is not considered to be structurally contributing, in the sense that hybrid interaction will NOT take place, a reduction in the total weight is found. By extension, when hybrid interaction IS considered, an additional weight saving is achieved. The weight saved has been illustrated visually in the pie charts above. They illustrate the weight division of all elements in each bridge, along with the weight difference compared to the original Amalia bridge.

H.2.　　Bridge sections

H.2.1.　Leaf of the bridge

The leaf of the bridge is the section where it is favourable to save weight. Therefore, this is the section which is examined first:

Original Amalia bridge	*Non-hybrid design*	*Hybrid design*
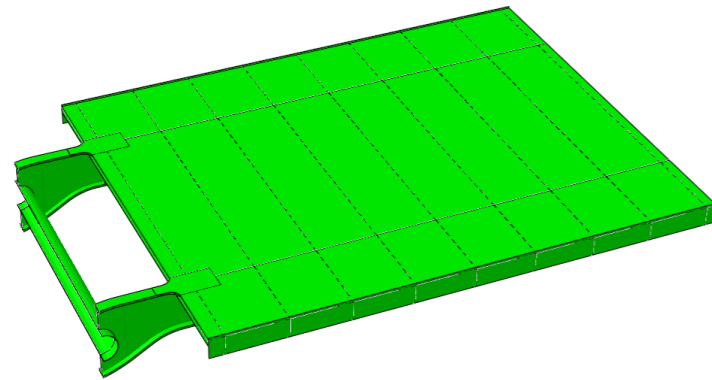
Figure H-7 Leaf section of the Amalia bridge

	Amalia bridge	
	[kN]	
Deck-system	1369	47%
Main girders	505	17%
Cross girders	435	15%
Axle	97	3%
Conservation	24	0.8%
Road equipment	471	16%
Total bridge	**2901**	**100%**

Table H-4 Weight devision of the leaf of the Amalia bridge
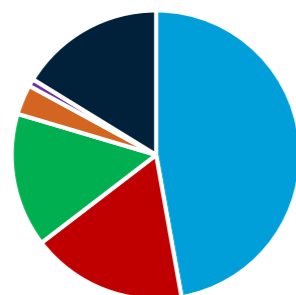
Figure H-10 Pie chart: weight division of the leaf section of the Amalia bridge
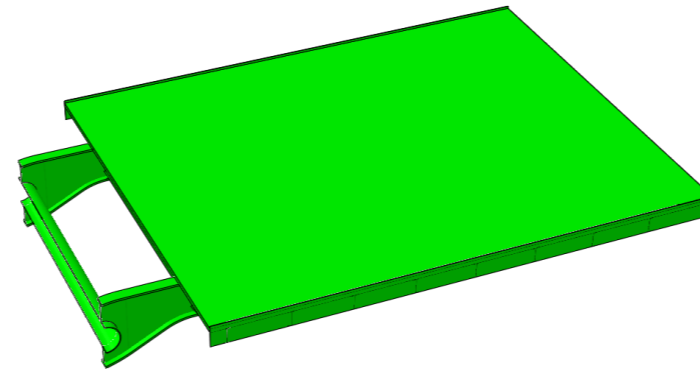
Figure H-8 Leaf section of the Non-hybrid design

	Non-hybrid	
	[kN]	
Deck-system	702	28%
Main girders	653	26%
Cross girders	588	23%
Axle	97	4%
Conservation	14	0.6%
Road equipment	471	19%
Total bridge	**2525**	**100%**

Table H-5 Weight devision of the leaf of the non-hybrid design
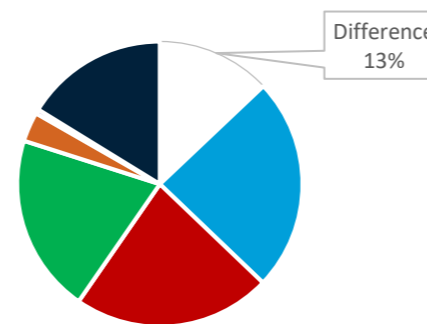
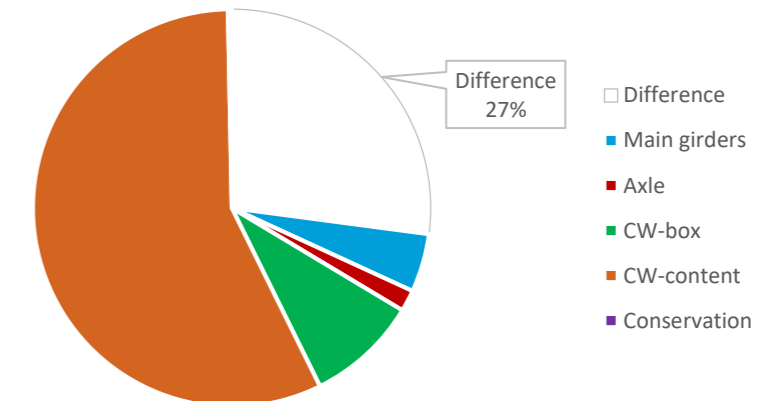**Figure H-11 Pie chart: weight division of the leaf section of the Non-hybrid design**
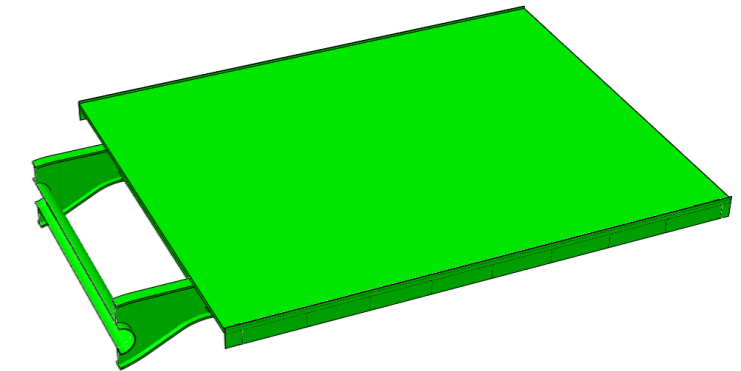
Figure H-9 Leaf section of the Hybrid design

	Hybrid	
	[kN]	
Deck-system	702	30%
Main girders	594	25%
Cross girders	492	21%
Axle	97	4%
Conservation	13	0.5%
Road equipment	471	20%
Total bridge	**2368**	**100%**

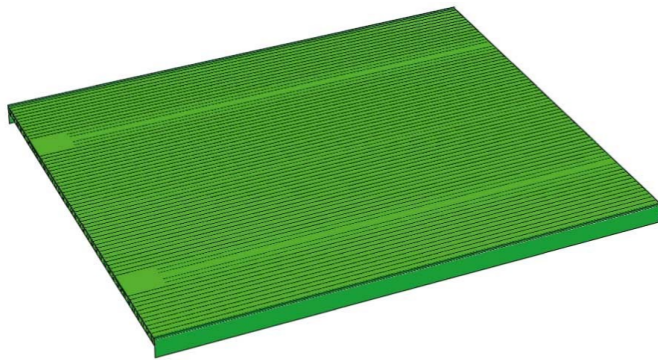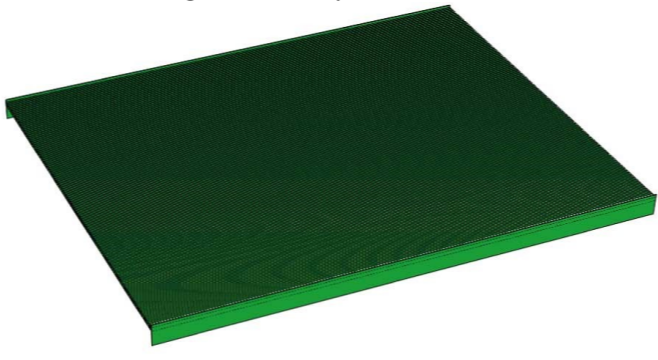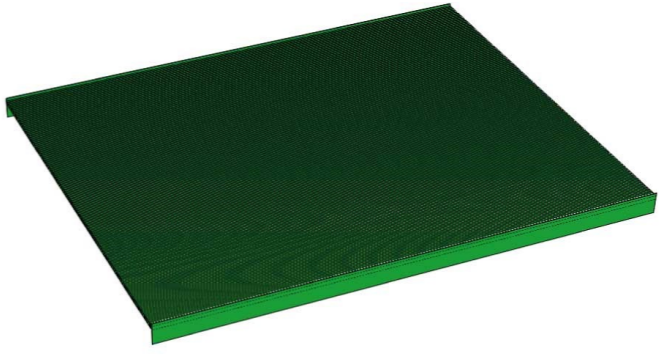**Table H-6 Weight devision of the leaf of the hybrid design**

Figure H-12 Pie chart: weight division of the leaf section of the Hybrid design

For an explanation on the percentages found in the tables shown above, please review the bold text found in Appendix H.

The tables shown above illustrate the weight division of each bridge's leaf, with each bridge making a sum of 100%. The graphs differ slightly from these. Here the total sum of each graph is related to the weight of the original bridge's leaf. Resulting in a difference value for the leaf of both the non-hybrid and the hybrid bridge. This illustrates clearly the weight savings as well as an absolute comparison between the elements.

H.2.2. Counterweight of the bridge

The leaf of the bridge is the section where it is favourable to save weight. Therefore, this is the section which is examined first:

Original Amalia bridge	*Non-hybrid design*	*Hybrid design*
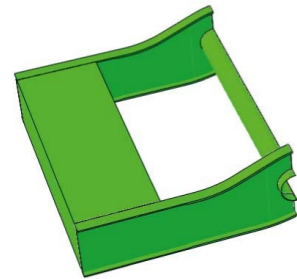
Figure H-13 Counterweight section of the Amalia bridge

	Amalia bridge	
	[kN]	
Main girders	278	5%
Axle	97	2%
CW-box	640	11%
CW-content	4535	81%
Conservation	20	0.4%
Total bridge	**5571**	**100%**

Table H-7 Weight devision of the counterweight of the Amalia bridge
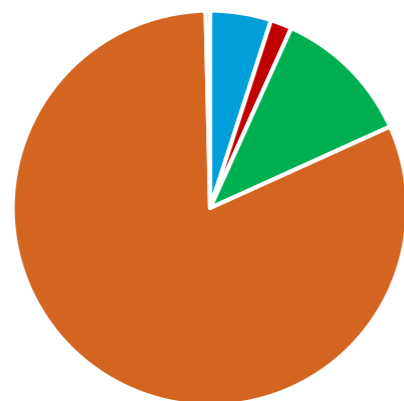
Figure H-16 Pie chart: weight division of the counterweight section of the Amalia bridge
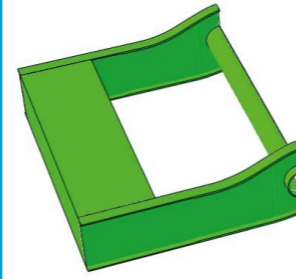
Figure H-14 Counterweight section of the Non-hybrid design

	Non-hybrid	
	[kN]	
Main girders	265	6%
Axle	97	2%
CW-box	507	11%
CW-content	3680	81%
Conservation	17	0.4%
Total bridge	**4566**	**100%**

Table H-8 Weight devision of the counterweight of the non-hybrid design
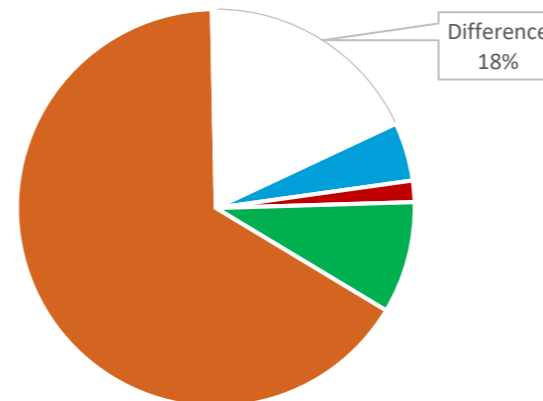
Figure H-17 Pie chart: weight division of the counterweight section of the Non-hybrid design
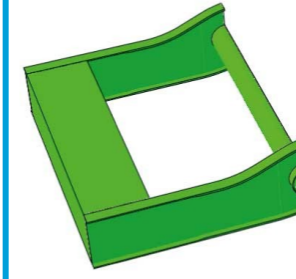
Figure H-15 Counterweight section of the Hybrid design

	hybrid	
	[kN]	
Main girders	265	7%
Axle	97	2%
CW-box	507	12%
CW-content	3175	78%
Conservation	17	0.4%
Total bridge	**4061**	**100%**

Table H-9 Weight devision of the counterweight of the hybrid design

Figure H-18 Pie chart: weight division of the counterweight section of the Hybrid design

For an explanation on the percentages found in the tables shown above, please review the bold text found in Appendix H.

The tables shown above illustrate the weight division of each bridge's counterweight, with each bridge making a sum of 100%. The graphs differ slightly from these. Here the total sum of each graph is related to the weight of the original bridge's counterweight. Resulting in a difference value for the counterweight of both the non-hybrid and the hybrid bridge. This illustrates clearly the weight savings as well as an absolute comparison between the elements.

H.3.   Bridge elements

H.3.1. Deck-system

Original Amalia bridge	Non-hybrid design	Hybrid design
This deck system consists of: - A steel deck plate of 20 mm; - 35 steel troughs; - A steel front and back cover, both 20 mm thick; - And two steel side covers of 20 mm.	This deck system consists of an FRP-sandwich deck built up of Z-shape shells. It has been modelled as: - An FRP top-facing of 20 mm; - 201 FRP webs of 8 mm each; - An FRP bottom-facing of 20 mm; - An FRP front and back cover of 8 mm; - And two steel side covers of 20 mm.	This deck-system is identical to the non-hybrid system, explained on the left.
The troughs are 'sunk' into the main girders, to reduce structural height and the deck system doubles as the top flange of the main and cross girders.	The FRP-deck is placed upon the main and cross girders. This results in a lower maximum height for the main and cross girders. It is considered separately from the main and cross girders: no hybrid interaction.	The FRP-deck is still placed on top of the main and cross girders, however now it is considered to function as the top flange of the main and cross girders: hybrid interaction.

Figure H-19 Deck system of the Amalia bridge

Figure H-20 Deck system of the non-hybrid design

Figure H-21 Deck system of the hybrid design

Related to		Amalia bridge	
		[kN]	
Leaf section	Relative	1369	100%
	Absolute	1369	47%
Whole bridge	Relative	1369	100%
	Absolute	1369	16%

Table H-10 Weight comparison of the deck system of the Amalia bridge

Related to		Non-hybrid	
		[kN]	
Leaf section	Relative	702	51%
	Absolute	702	28%
Whole bridge	Relative	702	51%
	Absolute	702	10%

Table H-11 Weight comparison of the deck system of the non-hybrid design

Related to		Hybrid	
		[kN]	
Leaf section	Relative	702	51%
	Absolute	702	30%
Whole bridge	Relative	702	51%
	Absolute	702	11%

Table H-12 Weight comparison of the deck system of the hybrid design

For an explanation on the percentages found in the tables shown above, please review the bold text found in Appendix H.

In this thesis the implemented deck **weighs about half** of the deck of the original bridge. The above tables clearly illustrate the use of implementing FRP and the goal of this thesis. Whereas the deck of the original Amalia bridge is almost half of the weight of the leaf of the bridge, this contribution is reduced drastically for both designs. Thus, **implementing FRP can result in weight reduction, regardless of the degree of hybrid interaction**.

H.3.2. Main girders

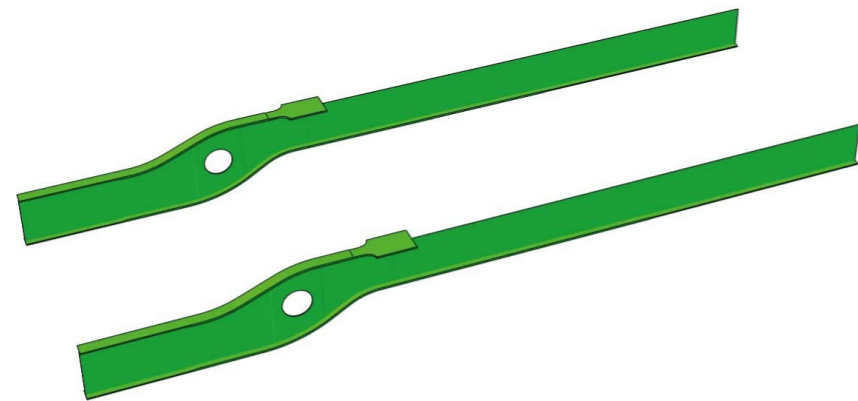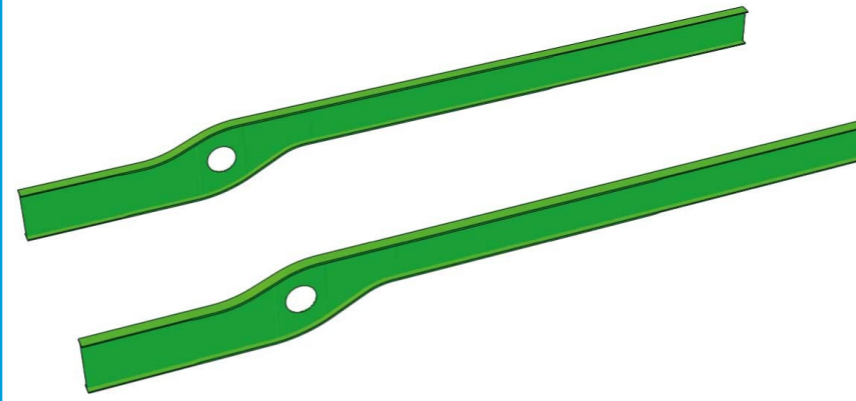| Original Amalia bridge	Non-hybrid design	Hybrid design
The main girders are shaped as an upside-down T, underneath the deck and as a balanced I-profile everywhere else. - The flanges are 100 mm thick, which are reduced towards both ends. - The flanges are 600 mm wide. - The web varies in thickness from 16 until 40 mm.	The main girders are balanced I-profiles throughout the entire bridge, since no hybrid interaction is considered. - The bottom flanges are identical to those of the original design. - Top flanges have the same cross section as the bottom flanges, whereas the curvature is identical to those of the original design. - The web varies, identical to those of the original design.	The main girders are non-balanced I-profiles; the top flanges are reduced compared to the bottom flanges. - The girders are, reductions aside, identical to those of the non-hybrid design. - The top flanges are reduced to a thickness of 10 mm and a width of 200 mm. This is only underneath the deck.

Figure H-22 Main girders of the Amalia bridge

Figure H-23 Main girders of the non-hybrid design
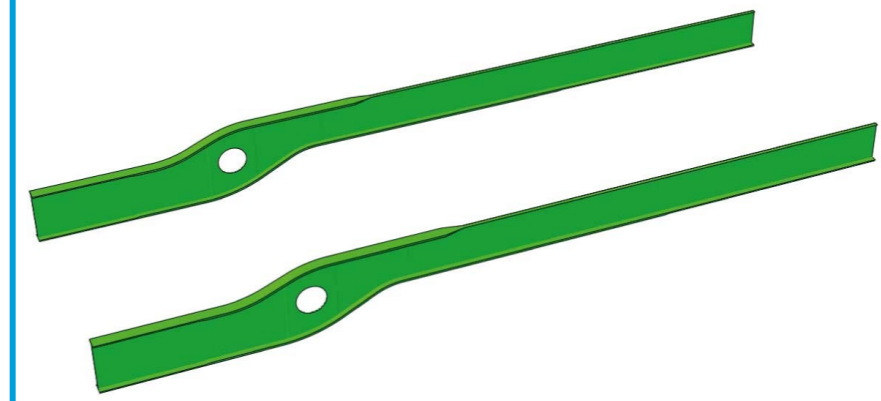
Figure H-24 Main girders of the hybrid design

Related to		Amalia bridge	
		[kN]	
Leaf section	Relative	505	100%
	Absolute	505	17%
Counterweight section	Relative	278	100%
	Absolute	278	5%
Whole bridge	Relative	783	100%
	Absolute	783	9%

Table H-13 Weight comparison of the main girders of the Amalia bridge

Related to		Non-hybrid	
		[kN]	
Leaf section	Relative	653	129%
	Absolute	653	26%
Counterweight section	Relative	265	95%
	Absolute	265	6%
Whole bridge	Relative	918	117%
	Absolute	918	13%

Table H-14 Weight comparison of the main girders of the non-hybrid design

Related to		Hybrid	
		[kN]	
Leaf section	Relative	594	118%
	Absolute	594	25%
Counterweight section	Relative	265	95%
	Absolute	265	7%
Whole bridge	Relative	859	110%
	Absolute	859	13%

Table H-15 Weight comparison of the main girders of the hybrid design

For an explanation on the percentages found in the tables shown above, please review the bold text found in Appendix H.

Both the hybrid and non-hybrid design have an increase of the weight of the main girders. This is due to the addition of the top flange, even though the height is slightly reduced. Reviewing the main girders' contribution to the whole bridge, the non-hybrid design has a larger contribution, compared to the other designs. When reviewing the contribution in the counterweight section, a reduction is visible for both created designs. This is due to a reduction in the height of the girders. This means: due to the weight reduction, less counterweight is required; such that a reduction in height of the girders is possible. A next step here is to see is a reduction of the length of the main girders, in the counterweight section is possible. This has NOT been dealt with in this thesis, but it shows promise for future investigation.

H.3.3. Cross girders

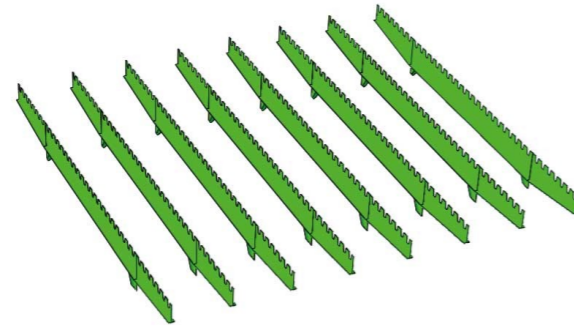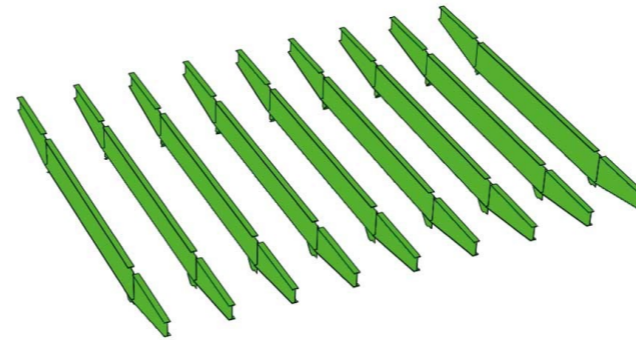| Original Amalia bridge	Non-hybrid design	Hybrid design
The cross girders are upside down T-shaped sections with two different heights of 1500 and 1700 mm in the centre span. In the side spans, these heights are reduced gradually. They are resting on the main girders' bottom flange by mean of supports with an angle of 60 degrees.	The cross girders are balanced I-shaped sections with two different heights of 1500 and 1700 mm in the centre span. In the side spans, these heights are reduced gradually. They are resting on the main girders' bottom flange by mean of supports with an angel of 45 degrees.	The cross girders are non-balanced I-shaped sections with two different heights of 1500 and 1700 mm in the centre span. In the side spans, these heights are reduced gradually. They are resting on the main girders' bottom flange by mean of supports with an angel of 45 degrees.
Some measurements of the cross giders are: - The bottom flange is 300 time 30 mm. - The webs are 16 mm thick.	Some measurements of the cross giders are: - The flanges are 300 times 30 mm. - The webs are 16 mm thick.	Some measurements of the cross giders are: - The bottom flange is 300 time 30 mm. - The top flange is 200 times 10 mm. - The webs are 16 mm thick.

Figure H-25 Cross girders of the Amalia bridge

Figure H-26 Cross girders of the non-hybrid design
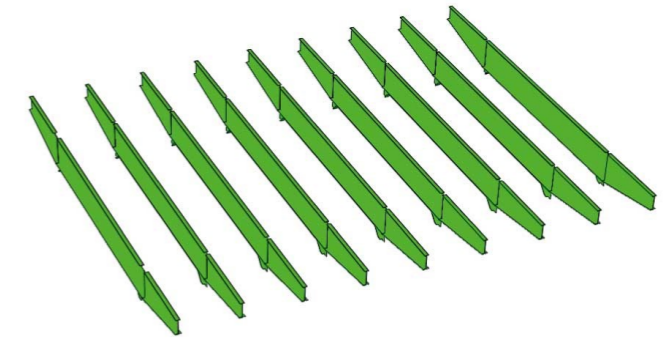
Figure H-27 Cross girders of the hybrid design

Related to		Amalia bridge	
		[kN]	
Leaf section	Relative	435	100%
	Absolute	435	15%
Whole bridge	Relative	435	100%
	Absolute	435	5%

Table H-16 Weight comparison of the cross giders of the Amalia bridge

Related to		Non-hybrid	
		[kN]	
Leaf section	Relative	588	135%
	Absolute	588	23%
Whole bridge	Relative	588	135%
	Absolute	588	8%

Table H-17 Weight comparison of the cross girders of the non-hybrid design

Related to		Hybrid	
		[kN]	
Leaf section	Relative	492	113%
	Absolute	492	21%
Whole bridge	Relative	492	113%
	Absolute	492	8%

Table H-18 Weight comparison of the cross girders of the hybrid design

For an explanation on the percentages found in the tables shown above, please review the bold text found in Appendix H.

The cross girders have an increase in weight, compared to the original design, resulting in a larger contribution to the total weight. This is due to the required stiffness in opened condition. Fortunately, this increase in weight, does not outweigh the weight saved in other areas. Thus, still allowing for a weight reduction.

H.3.4. Axle

Original Amalia bridge	Non-hybrid design	Hybrid design
The axle has a thickness of 40 mm and a radius of 750 mm. It spans approximately 13.5 m, such not to interfere with e main girders.	The axle has the same measurements are in the original design.	The axle has the same measurements are in the original design.

Figure H-28 Axle of the Amalia bridge

Figure H-29 Axle of the non-hybrid design

Figure H-30 Axle of the hybrid design

Related to		Amalia bridge	
		[kN]	
Whole bridge	Relative	194	100%
	Absolute	194	2%

Table H-19 Weight comparison of the axle of the Amalia bridge

Related to		Non-hybrid	
		[kN]	
Whole bridge	Relative	194	100%
	Absolute	194	3%

Table H-20 Weight comparison of the axle of the non-hybrid design

Related to		Hybrid	
		[kN]	
Whole bridge	Relative	194	100%
	Absolute	194	3%

Table H-21 Weight comparison of the axle of the hybrid design

For an explanation on the percentages found in the tables shown above, please review the bold text found in Appendix H.

No changes have been made to the axle. The weight remains the same, however the contribution to the total weight for the **non-hybrid** and **hybrid** design is increased by **20** respectively **30**%, due to the reduction in the total weight. Regarding the balancing of the bridge, the axle does not have an influence, since the balancing is done around the centre of the axle.

H.3.5. Counterweight

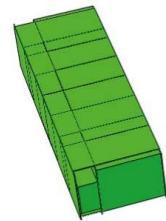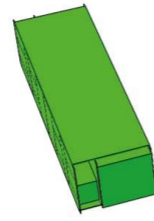| Original Amalia bridge	Non-hybrid design	Hybrid design
The counterweight has been determined based on the overpressure required in the closed condition. The height and width based on the height of and the distance between the main girders respectively. The length is set to 4.0 m. Within steel counterweight structure, concrete elements are placed, to obtain the required moment.	The counterweight has been determined based on the overpressure required in the closed condition. The height and width based on the height of and the distance between the main girders respectively. The length is set to 3.5 m.	The counterweight is reduced even further to the counterweight in the non-hybrid design. Here the length is only 3.0 m. In concrete elements inside differ as well. These have been adjusted to reach the required moments.

Figure H-31 Counterweight of the Amalia bridge

Figure H-32 Counterweight of the non-hybrid design
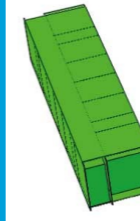
Figure H-33 Counterweight of the hybrid design

Related to		Amalia bridge	
		[kN]	
Counterweight section	Relative	5176	100%
	Absolute	5176	46%
Whole bridge	Relative	5176	100%
	Absolute	5176	61%

Table H-22 Weight comparison of the counterweight of the Amalia bridge

Related to		Non-hybrid	
		[kN]	
Counterweight section	Relative	4187	80%
	Absolute	4187	46%
Whole bridge	Relative	4187	81%
	Absolute	4187	59%

Table H-23 Weight comparison of the counterweight of the non-hybrid design

Related to		Hybrid	
		[kN]	
Counterweight section	Relative	3682	75%
	Absolute	3682	45%
Whole bridge	Relative	3682	71%
	Absolute	3682	57%

Table H-24 Weight comparison of the counterweight of the hybrid design

For an explanation on the percentages found in the tables shown above, please review the bold text found in Appendix H.

The weight saved in the counterweight is directly linked to the amount of weight saved in the leaf of the bridge. Due to the amount of weight saved in the **non-hybrid** design the length of the counterweight was reduced by **500 mm**. For the **hybrid** design, an additional **500 mm** of length was saved. This led to the possibility of reducing the length of the main girders in this section. This has not been examined in this thesis. It is considered to be the next step. To be applied in future research when reviewing the bridge for an optimisation.